Search for Electroweakly Produced Supersymmetric Particles in Final States Including Two Charged Leptons with the ATLAS Experiment at the LHC

Dissertation der
Fakultät für Physik
der
Ludwig-Maximilians-Universität München

vorgelegt von

Josephine Verena Laura Wittkowski
München
2014

Erstgutachterin: Prof. Dr. Dorothee Schaile
Zweitgutachter: Prof. Dr. Martin Faessler
Datum der mündlichen Prüfung: 19. November 2014

ZUSAMMENFASSUNG

Es werden drei Analysen vorgestellt, die nach elektroschwach produzierten supersymmetrischen Teilchen in Proton-Proton-Kollisionen suchen. Die Kollisionen wurden mit dem ATLAS-Experiment am Large Hadron Collider aufgenommen. Zwei Leptonen (Elektronen oder Myonen), Jets und fehlende transversale Energie werden im Endzustand erwartet. 'Simplified Models' werden genauso wie das 'phenomenological Minimal Supersymmetric Standard Model' (pMSSM) verwendet, um die Produktion und den Zerfall von Gaugino-Paaren, also Paaren aus Charginos und Neutralinos, zu untersuchen.

Die erste Analyse wird mit ATLAS Daten, die einer integrierten Luminosität von 4.7 fb^{-1} entsprechen und im Jahr 2011 bei einer Schwerpunktenergie von $\sqrt{s}$=7 TeV aufgenommen wurden, durchgeführt. Die direkte Produktion von Sleptonen sowie drei weitere Szenarien, in denen Gaugino-Paare über zwischenzeitliche Sleptonen zerfallen, werden untersucht. Besonders hervorgehoben wird die Triggerstrategie. Da kein Überschuss an Ereignissen in den ATLAS Daten beobachtet wird, können beispielsweise die Massen linkshändiger Sleptonen im Bereich von 85 bis 195 GeV mit 95% Konfidenzniveau ausgeschlossen werden. Hierfür wird ein Simplified Model, das die direkte Produktion von Sleptonen annimmt, verwendet, und das Neutralino besitzt eine Masse von 20 GeV.

In einer zweiten Analyse werden 20.3 fb^{-1} ATLAS Daten benutzt, die im Jahr 2012 mit $\sqrt{s} = 8$ TeV aufgenommen wurden. Sieben Signalregionen zielen auf supersymmetrische Zerfallsketten ab, in denen zwei Leptonen mit entgegengesetztem Ladungsvorzeichen im Endzustand erwartet werden. Der dominante Standardmodelluntergrund besteht, analog zu der Analyse der 2011er Daten, aus $t\bar{t}$-, $Z/\gamma^* + jets$- und zwei-Boson-Prozessen. Zwei-Lepton-Trigger werden kombiniert um die Ereignisse auszuwählen. Die Ergebnisse entsprechen den Erwartungen des Standardmodells und werden im Rahmen des pMSSM interpretiert. Massen des $\tilde{\chi}_1^{\pm}$ können zwischen 100 und 105 GeV, 120 und 135 GeV sowie zwischen 145 und 160 GeV mit 95% Konfidenzniveau für ein masseloses $\tilde{\chi}_1^0$ ausgeschlossen werden. Das Simplified Model für den Prozess $\tilde{\chi}_1^+\tilde{\chi}_1^- \rightarrow W^+\tilde{\chi}_1^0 W^-\tilde{\chi}_1^0 \rightarrow l^+\nu\tilde{\chi}_1^0 l^-\bar{\nu}\tilde{\chi}_1^0$ wird dazu verwendet. Mit der Simulation der direkten Produktion von Sleptonen in einem weiteren Simplified Model können Sleptonmassen zwischen 90 und 325 GeV ausgeschlossen werden ($m_{\tilde{\chi}_1^0} < 30$ GeV).

Die dritte Analyse wird ebenfalls mit 2012er Daten durchgeführt. Es wird ein Szenario betrachtet, in dem ein Chargino-Neutralino-Paar über ein W- und ein Higgsboson in einen Endzustand mit zwei gleichnamig geladenen Leptonen, zwei Quarks und zwei leichtesten Neutralinos zerfällt. Der Hauptuntergrund beruht auf Leptonen, die nicht vom primären Zerfallsvertex stammen, und wird mit Hilfe von ATLAS Daten bestimmt. Der Beitrag durch Standardmodell-Prozesse mit zwei Boso-

nen wird z.B. durch Schnitte auf die invariante Masse der Zerfallsprodukte des Higgsbosons und auf die effektive Masse, das ist die skalare Summe der Transversalimpulse der Leptonen, Jets und der fehlenden Transversalenergie, unterdrückt. Die Ergebnisse dieser Analyse sind noch nicht veröffentlicht. Man erwartet, dass die drei Massenpunkte mit Neutralinomassen unter 10 GeV und Charginomassen unter 150 GeV mit 95% Konfidenzniveau ausgeschlossen werden können.

ABSTRACT

Three analyses searching for electroweakly produced supersymmetric particles in proton-proton collisions are presented. The collisions were recorded by the ATLAS experiment at the Large Hadron Collider. Two leptons (electrons or muons), jets and missing transverse energy are expected in the final states. Simplified models as well as the phenomenological Minimal Supersymmetric Standard Model (pMSSM) are used to study the production and decay of pairs of gauginos, i.e. charginos and neutralinos.

The first analysis is performed with an integrated luminosity of 4.7 fb^{-1} of ATLAS data, recorded in 2011 at a centre-of-mass energy of $\sqrt{s}$ =7 TeV. Direct slepton production and three scenarios in which pairs of gauginos decay via intermediate sleptons are addressed. Particular attention is paid to the trigger strategy. No excess is observed in the number of data events. In the simplified model that assumes the direct slepton production, left-handed slepton masses between 85 and 195 GeV are excluded at 95% confidence level for a 20 GeV neutralino.

The second analysis uses 20.3 fb^{-1} of ATLAS data recorded in 2012 at $\sqrt{s} = 8$ TeV. Seven signal regions address supersymmetric decay scenarios with two oppositely charged leptons in the final state. The dominating Standard Model background processes are, analogously to the 2011 analysis, $t\bar{t}$, $Z/\gamma^* + jets$ and diboson processes. A combination of dilepton triggers is used to select the events. The results are in agreement with the Standard Model expectations and are interpreted in the context of the pMSSM. $\tilde{\chi}_1^{\pm}$ masses between 100 and 105 GeV, 120 and 135 GeV and 145 and 160 GeV can be excluded at 95% confidence level for $m_{\tilde{\chi}_1^0} = 0$ GeV in the simplified model for which $\tilde{\chi}_1^+\tilde{\chi}_1^- \rightarrow W^+\tilde{\chi}_1^0 W^-\tilde{\chi}_1^0 \rightarrow l^+\nu\tilde{\chi}_1^0 l^-\bar{\nu}\tilde{\chi}_1^0$. Slepton masses between 90 and 325 GeV can be excluded at 95% CL for a neutralino mass of less than 30 GeV when the direct slepton production is simulated in a simplified model.

A third analysis is also performed on the 2012 data addressing a scenario in which a chargino-neutralino pair decays via a W- and a Higgs boson into a final state with two same-sign leptons, two quarks and two lightest neutralinos. The dominating background is due to non-prompt leptons and is estimated by a data-driven method. The contribution due to diboson background is suppressed e.g. by cuts on the invariant mass of the decay products of the Higgs boson and on the effective mass, which is the scalar sum of the p_T of the leptons, jets and of the missing transverse energy. The results for this analysis are not yet published. The three mass points with the neutralino masses of less than 10 GeV and chargino masses of less than 150 GeV are expected to be excluded at 95% CL.

Nobody in the game of football should be called a genius. A genius is somebody like Norman Einstein.

(Joe Theismann, former quarterback)

Raj: Can you believe it! He watched me work for 10 minutes and than he tried to build a little piece of software that could replace me!

Leonard: Is that really possible?

Raj: As it turned out, yes.

(from *The Big Bang Theory*, C. Lorre / B. Prady)

Contents

1. Introduction

CERN, the Large Hadron Collider and the two experiments ATLAS and CMS were mentioned in the news world-wide in the summer of 2012. On July 4th, the day which is sometimes now referred to as the Higgs-dependence day, both experiments announced the discovery of a Higgs-like particle. The Higgs mechanism had been predicted already almost fifty years earlier (see e.g. [1]) and the discovery of the particle can be seen as a proof of the mechanism being realised in nature.

The Standard Model of particle physics can be mathematically described by Lagrangian densities; the interactions of the particle fields can be read off from the individual terms. Although there is clearly some beauty in the simplicity of the mathematical equations, extreme fine-tuning is needed to bring the experimental results in agreement with the theoretical framework. Many parameters cannot be predicted but only measured. The discovery of the Higgs boson means undoubtedly a great scientific achievement and a relief because it is now theoretically explained why some elementary particles are massive. But the Standard Model still has more open issues. For example the fundamental force of gravity can not be included.

A possible solution of several problems is presented with the idea of Supersymmetry as an extension to the Standard Model. Supersymmetric Lagrangians describe the interactions between even more particles than the ones predicted by the Standard Model. Some of the additional particles like the neutralinos or gravitinos may be candidates for the Dark Matter. The Higgs boson can also be included in the Supersymmetry models and four more Higgs particles are expected in the 'Higgs sector'.

In this thesis, three analyses searching for supersymmetric particles that are produced by electroweak interactions in proton-proton collisions at the LHC will be presented. ATLAS data which was recorded in the years of 2011 or 2012 is analysed, looking for final states with exactly two leptons (electrons or muons).

In the first two chapters, the Standard Model as well as the idea of Supersymmetry will be introduced. In Chapter 3 it will be explained how a supersymmetric model is assumed to be discovered or excluded in terms of statistics. The Large Hadron Collider, the ATLAS experiment, particle identification as well as the trigger system are introduced in Chapters 4 and 5. The analysis of 2011 data is presented in Chapter 6, and 2012 data is analysed in Chapter 7. The Higgs boson is included in

the analysis of 2012 data regarding a scenario in which supersymmetric particles decay via a Higgs boson. This analysis is shown in Chapter 8.

2. The Standard Model and Its Supersymmetric Extension

2.1. The Standard Model of Elementary Particle Physics

The well-established Standard Model (SM) of particle physics is described in this Chapter. The theoretical framework as well as the consequences for the measurable physical effects are explained based on [2], [3], [4].

The variable action S which describes the evolution of a physical system must fulfil the equation

$$\frac{\delta S}{\delta \mathbf{q}(t)} = 0, \tag{2.1}$$

where $\mathbf{q}$ are the N generalised coordinates (q_1, q_2, ..., q_N) and $\mathbf{q}(t)$ is the true trajectory. This is called the Hamilton's principle.

Lagrangian Mechanics S is the integral over a time-dependent function $L(t)$, called the Lagrange function:

$$S = \int_{-\infty}^{+\infty} dt L(t) = \int dx^4 \mathscr{L}(\phi, \partial_\mu \phi). \tag{2.2}$$

The Lagrange function L is the space-integral of the Lagrange density or Lagrangian $\mathscr{L}$ which depends on the real or complex field $\phi(\mathbf{x})$ with $\mathbf{x}$=$(t, \vec{x})$, and the derivatives $\partial_\mu \phi = \frac{\partial \phi}{\partial x^\mu}$ with $\partial_\mu = (\frac{\partial}{\partial t}, \vec{\nabla})$. The Lagrange function summarises the dynamics of the physical system which it describes. In classical mechanics it can be interpreted as the difference between the kinetic energy T and the potential energy V, $L = T - V$. The basic equations of motion of the system are given by the Euler-Lagrange equations. They are obtained by minimising the action with respect to the field:

$$\frac{\delta \mathscr{L}}{\delta \phi} = \partial_\mu \frac{\delta \mathscr{L}}{\delta \partial_\mu \phi}. \tag{2.3}$$

If the Lagrangian remains invariant under a group of transformations where a local phase difference is created, it is called locally gauge invariant.

2.1.1. Electroweak Interactions

The interactions of particle fields are described by Lagrangians. The quantum field theory of **Q**uantum **E**lectro-**D**ynamics (QED) describes the interactions which are mediated by the electromagnetic force. Electromagnetism can be unified with the weak force for energies higher than $\mathcal{O}$ (100 GeV)[1]. Although the weak force is 10^{-11} times less strong than the electromagnetic force, both should be seen as two aspects of the electroweak interaction. The mathematical description of electroweak interactions is based on the group $SU(2)_L \otimes U(1)_Y$, i.e. $\mathscr{L}_{electroweak}$ is local gauge invariant. The interactions can be read from the Lagrangian

$$\mathscr{L}_{electroweak} = \sum_k \bar{\psi}_k i\gamma^\mu D_\mu \psi_k - \frac{1}{4} B_{\mu\nu} B^{\mu\nu} - \frac{1}{4} \vec{W}_{\mu\nu} \vec{W}^{\mu\nu} \tag{2.4}$$

with the covariant derivatives for left-handed and right-handed fermions

$$D^\mu := \partial^\mu + \frac{1}{2} i g' Y_L B_\mu(x) + \frac{1}{2} i g \vec{\tau} \vec{W}_\mu(x) \tag{2.5}$$

and

$$D^\mu := \partial^\mu + \frac{1}{2} i g' Y_R B_\mu(x), \tag{2.6}$$

respectively. A fermion is a particle with a half-integer spin quantum number; particles with integer spin are called bosons. The helicity expresses the orientation of the momentum vector and the spin vector of a particle: $h = \vec{S} \cdot \hat{p} = +\frac{1}{2}$ for right-handed fermions, and $h = -\frac{1}{2}$ for left-handed fermions. $\hat{p}$ is the momentum unit vector. Y_L denotes the weak hypercharge for left-handed isospin doublets and Y_R for right-handed singlets. The components of $\vec{\tau}$ are the Pauli matrices. The field strength tensors

$$B^{\mu\nu} = \partial^\mu B^\nu - \partial^\nu B^\mu \tag{2.7}$$

and

$$\vec{W}^{\mu\nu} = \partial^\mu \vec{W}^\nu - \partial^\nu \vec{W}^\mu - g \vec{W}^\mu \times \vec{W}^\nu \tag{2.8}$$

are based on the fields of $\vec{W}_\mu$ (which couple with the strength g of $SU(2)_L$) and B_μ (which couple with the strength g' of $U(1)_Y$). The coupling strengths can be converted

[1] 1 eV = 1.6022^{-19} J is the amount of energy gained by an electron which moves across an electric potential difference of 1 V.

with the help of the electroweak mixing angle Θ_w:

$$gsin(\Theta_w) = g'cos(\Theta_w) = e. \tag{2.9}$$

e denotes the elementary charge of 1.6022×10^{-19} C [5]. The fields can be combined to form the mass eigenstates of the electroweak interactions by using the electroweak mixing angle.

$$A_\mu = B_\mu cos(\Theta_w) + W^3_\mu sin(\Theta_w) \tag{2.10}$$

corresponds to the electrically neutral and massless photon which mediates the electroweak force and

$$Z_\mu = -B_\mu sin(\Theta_w) + W^3_\mu cos(\Theta_w) \tag{2.11}$$

corresponds to the electrically neutral Z-boson. The latter as well as the charged $W^\pm$ bosons also mediate the electroweak force. The observed existence of these massive excitations of the electroweak gauge fields can only be explained if spontaneous breaking of the electroweak symmetry is assumed.

2.1.2. Higgs Mechanism

The spontaneous breaking of the electroweak symmetry is described theoretically by the ABEGHHK'tH mechanism (for **A**nderson, **B**rout, **E**nglert, **G**uralnik, **H**agen, **H**iggs, **K**ibble and **'t H**ooft). Spontaneous symmetry breaking occurs when the ground state of a field has a non-zero vacuum expectation value, $|\phi_0| \neq 0$. The 'wine bottle' or 'Mexican hat' potential is defined as

$$V(\phi) = -\mu^2 |\phi|^2 + \lambda^2 |\phi|^4 \tag{2.12}$$

with $\lambda, \mu \in \mathbb{R}$, $\lambda > 0$, $\mu^2 > 0$. The Higgs field ϕ is a complex scalar field, $\phi(x) = \frac{1}{\sqrt{2}}(\phi_1(x) + i\phi_2(x))$. The potential $V(\phi)$ is depicted in Figure 2.1. It is invariant under phase transformations, i.e. rotations in the plane spanned by ϕ_1 and ϕ_2. Choosing a single specific phase means breaking the electroweak symmetry.

When the Higgs field is expanded around its vacuum expectation value, $\phi(x) = \frac{1}{\sqrt{2}}(v + \eta(x) + i\zeta(x))$ with two real fields $\eta(x)$ and $\zeta(x)$ and $v \in \mathbb{R}$, the first two terms in the Lagrangian $\mathscr{L}_{Higgs}$ explain the mass acquisition of the weak gauge bosons:

$$\mathscr{L}_{Higgs} = \frac{1}{2}(D_\mu \phi)^\dagger (D^\mu \phi) - V(\phi) - g_f(\bar{R}\phi^\dagger L + \bar{L}\phi R). \tag{2.13}$$

The covariant derivative of ϕ is

$$D^\mu \phi = [\partial^\mu + \frac{1}{2} i g' Y B_\mu(x) + \frac{1}{2} i g \vec{\tau} \vec{W}_\mu(x)]\phi. \tag{2.14}$$

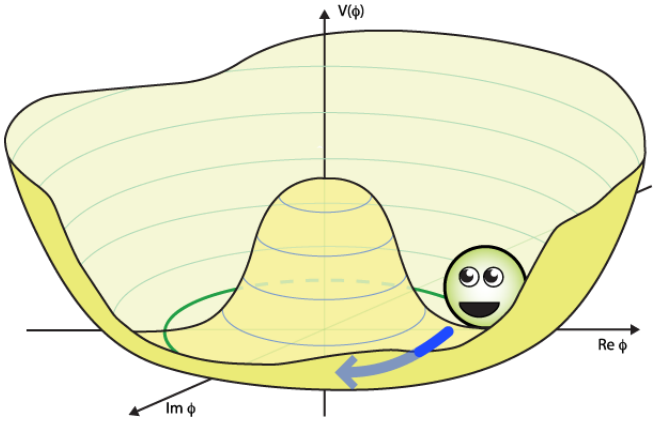

FIGURE 2.1.: *The 'Mexican hat' or 'wine bottle' potential and the excitation in radial direction depicted as a smiley [6].*

R and L are the right-handed and left-handed projections of the fermion field, respectively. They also describe the mass of the Higgs boson itself as well as the self-couplings of H.

If the Lagrangian describing the system has an exact continuous global symmetry which the ground state ϕ_0 does not possess, the Goldstone theorem states that the theory must contain massless particles. This is the case for $\mathscr{L}_{Higgs}$. Three of those four so-called Nambu-Goldstone bosons which are introduced by the massless field $\zeta(x)$ vanish in the transformed Higgs field. They give mass to the W and Z bosons. The fourth boson corresponds to an excitation of the Higgs field in the radial direction of the potential. This is the massive Higgs boson H which is illustrated as a smiley in Figure 2.1.

The Higgs field does not only affect the weak force carriers. The coupling of the scalar Higgs field to the fermions with strength g_f is called Yukawa coupling. The third term in equation 2.13 yields the interaction of the Higgs field with fermions. After the symmetry breaking it provides the fermion mass terms.

2.1.3. STRONG INTERACTIONS

The strong force is about one hundred times stronger than the electromagnetic force. It is mediated by the massless and electrically neutral gluons which are bosonic states. They can be interpreted as excitations of the strong gauge field.

COLOUR CHARGE Quarks cannot exist isolated but only as composed hadrons. A quark and an anti-quark form a meson; three quarks form a baryon.

The Pauli exclusion principle states that two fermionic particles cannot occupy the same quantum state. As a consequence, the wave functions have to be anti-symmetric in respect to exchanging the particles. The eight gluons interact with six spin-$\frac{1}{2}$ quarks which have different flavour, mass and electric charge. Since baryons

can also contain three of the same quarks, an additional way to distinguish quarks is needed. Therefore the attribute of colour charge was postulated. Quarks carry red, green or blue colour. Anti-quarks carry anti-red, anti-green or anti-blue colour. Hadrons have to be colourless. Therefore two quarks carry one unit of colour and the corresponding unit of anti-colour to form a meson, and three quarks carry three different units of (anti-)colour to form a baryon. Gluons carry one unit of colour and one unit of anti-colour. They can be combined to eight linearly independent states.

Interactions involving gluons are described by the Lagrangian for **Q**uantum **C**hromo-**D**ynamics (QCD),

$$\mathscr{L}_{QCD} = \bar{\psi}(i\gamma_\mu D^\mu - m)\psi - \frac{1}{4}\vec{G}_{\mu\nu}\vec{G}^{\mu\nu}. \tag{2.15}$$

The QCD field strength tensor

$$\vec{G}^{\mu\nu} = \partial^\mu \vec{G}^\nu - \partial^\nu \vec{G}^\mu - g_s \vec{G}^\mu \times \vec{G}^\nu \tag{2.16}$$

is composed from the gluon fields $\vec{G}_\mu$ and the SU(3) vector product. QCD is based on the local gauge group SU(3). The covariant derivative is defined as

$$D^\mu = \partial^\mu + \frac{1}{2} i g_s \vec{\lambda} \vec{G}^\mu \tag{2.17}$$

with $\vec{\lambda}$ denoting the Gell-Mann matrices.

2.1.4. Gravity

The fourth fundamental force is gravity. It is 10^{-42} times weaker than the electromagnetic force and cannot be included in the Standard Model. No mediator like a graviton was observed up to now.

2.1.5. Particle Content

The two tables 2.1 and 2.2 in this Section list the particles of the SM and their measured properties. The latest data from high energy physics experiments is used to determine especially the masses with higher accuracy. The most recent measurements are given in e.g. [5].

Fermions Table 2.1 lists the fermions which take part in the strong interactions (quarks) and electroweak interactions (both quarks and leptons). They are grouped in three categories or families with similar structures. All have spin $\frac{1}{2}$. The masses of the particles are all different. The charges are given in units of the elementary charge

of an electron, e, and the masses are given in units of eV which corresponds to 1.783×10^{-36} kg. In this thesis, the speed of light c and the reduced Planck constant $\hbar$ are set to unity. For each fermion an anti-particle exists which has the same mass but opposite electric charge.

BOSONS The bosons, their charges, their masses and the forces which they are mediating are listed in table 2.2. The Higgs boson is an exception since it is not a force carrier but the measurable excitation of the Higgs field. Its existence was proven by measurements published in the year 2012 with a significance of 5.9 standard deviations [7], [8] and has since been confirmed by numerous additional measurements.

TABLE 2.1.: *The three generations of fermions and their attributes [5].*

Leptons			Quarks		
Flavour	Mass	Charge	Flavour	Mass	Charge
electron e^-	0.510998928 $\pm$ 0.000000011 MeV	-1	up	2.3 $^{+0.7}_{-0.5}$ MeV	$+\frac{2}{3}$
e-neutrino ν_e	< 2 eV	0	down	4.8 $^{+0.7}_{-0.3}$ MeV	$-\frac{1}{3}$
muon μ^-	105.6583715 $\pm$ 0.0000035 MeV	-1	charm	1.275 $\pm$ 0.025 GeV	$+\frac{2}{3}$
μ-neutrino ν_μ	< 0.19 MeV	0	strange	95 $\pm$ 5 MeV	$-\frac{1}{3}$
tau τ^-	1776.82 $\pm$ 0.16 MeV	-1	top	173.5 $\pm$ 0.6 $\pm$ 0.8 GeV	$+\frac{2}{3}$
τ-neutrino ν_τ	< 18.2 MeV	0	bottom	4.18 $\pm$ 0.03 GeV	$-\frac{1}{3}$

TABLE 2.2.: *The attributes of the bosons [5], [9], [10].*

Mediator	Spin	Charge	Mass	Force
photon γ	1	0	0	electromagnetic (electroweak)
gluon g	1	0	0	strong
$W^\pm$	1	± 1	80.385 $\pm$ 0.015 GeV	charged weak (electroweak)
Z^0	1	0	91.188 $\pm$ 0.002 GeV	neutral weak (electroweak)
H	0	0	125.6 $\pm$ 0.3 GeV	–

2.1.6. LIMITATIONS OF THE STANDARD MODEL

The theory of the SM has 18 free parameters. These are the masses of the massive particles, the weak mixing parameters, the coupling constants of the fundamental interactions and a parameter for the strong CP violation. They need to be determined by experimental measurements which seems ad hoc and inelegant. To ex-

plain the neutrino masses, seven more free parameters possibly need to be taken into account.

After the Big Bang, matter and antimatter are expected to have been produced in equal amounts. Today, matter clearly dominates over antimatter in our Universe. The SM does not give an obvious reason.

The strengths or coupling constants of the weak, electromagnetic and strong interactions depend on the squared momentum transfer $|q|^2$ in an interaction. In Figure 2.2 it is illustrated how they 'run' with $|q|^2$. It is expected that they become

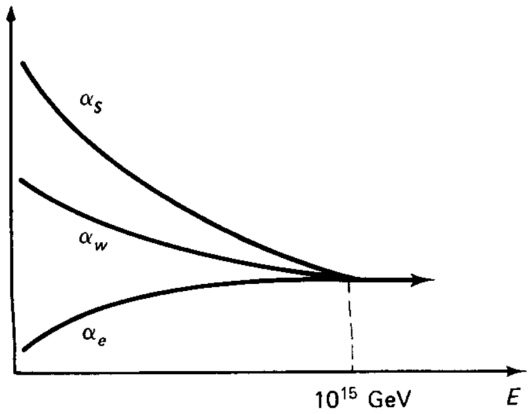

FIGURE 2.2.: *Evolution of the weak (α_w), electromagnetic (α_e) and strong coupling constants (α_s) with the energy E [2].*

comparable at $\mathcal{O}(10^{15}$ GeV). For processes occurring at the energies of the Planck scale, $\mathcal{O}(10^{19}$ GeV), the strength of the gravitational force is also expected to become significant. Grand unifying theories (GUTs) combining the three fundamental forces or theories 'of everything', which also include gravity, are being developed.

HIERARCHY PROBLEM The mass of the Higgs boson was measured to be 125.6 $\pm$ 0.3 GeV [9], which is much smaller than the Planck mass. The enormous difference between these two parameters is referred to as the hierarchy problem. It is contradictory to the aim for naturalness where physical constants should take relative values of $\mathcal{O}(1)$.

FINE-TUNING The third term in the Lagrangian $\mathscr{L}_{Higgs}$ in equation 2.13 describes the coupling of a Higgs boson to fermions. Taking into account second order loop diagrams (as depicted in Figure 2.3 (a)) leads to correction terms for the mass of the Higgs boson like

$$\Delta m_H^2 = -\frac{|\lambda_f|^2}{8\pi^2}\Lambda_{UV}^2 + ... \tag{2.18}$$

with the ultraviolet momentum cut-off Λ_{UV}. E.g. for the top-quarks, $\lambda_f \sim 1$ and Λ_{UV} should be set to a value where the gravitational force becomes comparable

in strength, thus again the Planck scale. These values make Δm_H many orders of magnitudes higher than the nominal measured value of 125.6 GeV, and Δm_H needs to be cancelled by an unnatural amount of fine-tuning [11].

(a) (b)

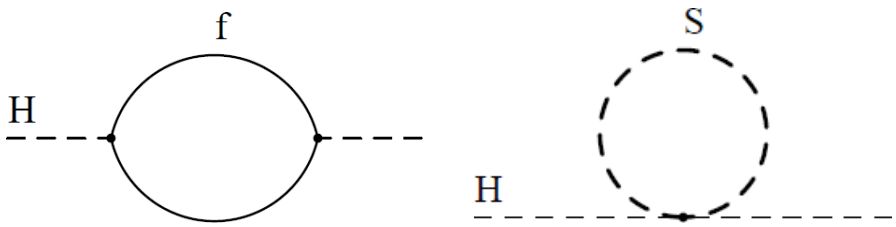

FIGURE 2.3.: *One-loop corrections of second order to the squared Higgs mass due to a fermion f (a) and a scalar S (b) [12].*

DARK MATTER To explain the differences between observed physical effects and possible effects caused by visible (i.e. measurable) matter, the existence of Dark Matter (DM) was hypothesised. It was observed that galaxies like the Coma Cluster cannot be held together only by the gravitational forces between the visible constituents [13]. The existence of DM was further proven indirectly by other physical effects. The SM cannot provide a candidate in form of an elementary or compound particle.

2.2. SUPERSYMMETRY

When theories are developed which extend the SM framework the constraints mentioned in the last Section are addressed. In this Section the fundamentals of Supersymmetry (SUSY) are discussed based on [10], [11] and [12].

2.2.1. PRINCIPLES

The idea of Supersymmetry is that a superpartner degree of freedom (d.o.f.) is allocated to each SM particle d.o.f. and to each anti-particle d.o.f., introducing a symmetry between fermions and bosons. The operator $\hat{Q}$ turns fermionic states into bosonic states and vice versa,

$$\hat{Q}|fermion>=|boson> \tag{2.19}$$

$$\hat{Q}|boson>=|fermion>. \tag{2.20}$$

For the operator $\hat{Q}$ it must hold that

$$\{\hat{Q},\hat{Q}^\dagger\}=P^\mu, \tag{2.21}$$

$$\{\hat{Q},\hat{Q}\}=\{\hat{Q}^\dagger,\hat{Q}^\dagger\}=0 \tag{2.22}$$

and

$$[P^\mu,\hat{Q}]=[P^\mu,\hat{Q}^\dagger]=0, \tag{2.23}$$

with $\hat{Q}^\dagger$ being the Hermitian adjoint of $\hat{Q}$, and P^μ being the four-momentum generator of space-time translations.

The superpartners or 'sparticles' have the same quantum numbers as their partners except for the spin which is different by $\frac{1}{2}$. In analogy to the SM framework a Lagrangian $\mathscr{L}_{SUSY}$ can be derived for which the fields are invariant under a supersymmetric transformation. The interactions and coupling strengths for the various particles can be read off from the Lagrangian.
A supermultiplet is the reducible representation of the SUSY algebra. Each supermultiplet contains the same number of fermions and bosons that are the superpartners of each other. In an unbroken symmetry the superpartners should have the same masses as their SM partners. However since no sparticles have been observed as of this writing, their masses have to be higher than the ones of their SM partners and SUSY must be a spontaneously broken symmetry. This necessity is taken into account by adding a term to the Lagrangian, $\mathscr{L}_{soft}$. The breaking of the symmetry should be soft, i.e. hardly modify the theory at high energies not to create any new divergent contributions to e.g. the mass of the SM Higgs boson.

2.2.2. Motivation for Supersymmetric Extensions

One of the main motivations to consider SUSY concerns the unnatural fine-tuning of the Higgs mass correction in the SM. The heavy complex scalar particles S with the mass m_S that are introduced by SUSY couple to the Higgs field as depicted in Figure 2.3 (b). They give corrections to the Higgs mass like

$$\Delta m_H^2=\frac{|\lambda_S|}{16\pi^2}[\Lambda_{UV}^2-2m_S^2\ln\frac{\Lambda_{UV}}{m_S}+...] \tag{2.24}$$

with the coupling constant λ_S [11]. For $\lambda_f=2\cdot\lambda_S^2$ the two contributions of equations 2.18 and 2.24 cancel out and no fine-tuning is needed.

In the SM it is assumed that the baryon number B, defined as $B=\frac{1}{3}(n_q-n_{\bar{q}})$ with n_q and $n_{\bar{q}}$ being the numbers of quarks and anti-quarks, respectively, is conserved

in each process. The conservation of the lepton number L, defined as $L = n_l - n_{\bar{l}}$ with n_l and $n_{\bar{l}}$ being the numbers of leptons and anti-leptons, respectively, is also always assumed. A variable which is defined by B, L and the spin quantum number s is the 'R-parity', P_R,

$$P_R = (-1)^{3(B-L)+2s}. \tag{2.25}$$

In most SUSY models it is required that P_R is conserved to forbid the violation of B and L. The consequences of this new symmetry are - since SM particles always have $P_R = +1$ while sparticles have $P_R = -1$ - that the lightest supersymmetric particle (LSP) must be stable and that all heavier sparticles must decay into a state with an odd number of LSPs. Furthermore, sparticles can only be produced in pairs. The LSP is a promising candidate for Dark Matter.

Another motivation to consider the supersymmetric extension to the SM is that SUSY predicts that the gauge coupling constants merge at $\mathcal{O}(10^{16}$ GeV) with higher accuracy than solely with the SM particle content.

2.2.3. Minimal Supersymmetric Standard Model

The minimal Supersymmetric SM (MSSM) is the supersymmetric extension of the SM with the smallest particle yield and is therefore often tested in experiments. The superpartners of the SM particles have names which are similar to the SM particles. For the supersymmetric partners of the fermions, 's-' is prepended to the fermion name as abbreviation for 'scalar', and for the partners of the bosons, '-ino' is appended. For example the superpartner of the left-handed electron e_L is the left-handed selectron $\tilde{e}_L$ (the handedness of a slepton actually indicates the handedness of the leptonic superpartner since sleptons are no fermions). The superpartner of the gluon g is the gluino $\tilde{g}$. The symbols of the sparticles are denoted with a tilde.

Supermultiplets Left- and right-handed particles have to be sorted into different supermultiplets since they act differently in weak interactions. The chiral supermultiplets of the MSSM are shown in Table 2.3 together with the number of colours, the third component of the weak isospin I_3 and the weak hypercharge $Y = 2(q - I_3)$ which can be computed from the electromagnetic charge q and from I_3. The SM fermions have spin $\frac{1}{2}$, the bosonic superpartners have spin 0.
The gauge supermultiplets together with the attributes of the particles and sparticles are shown in Table 2.4. The SM gauge bosons have spin 1, the fermionic superpartners have spin $\frac{1}{2}$.

TABLE 2.3.: *The chiral supermultiplet of the MSSM.*

Supermultiplets	Bosons	Fermions	SU(3) (N_{colour})	SU(2) ($N_{Isospin\,states}$)	U(1) ($Weak\,Hypercharge$)
slepton/lepton	$(\tilde{\nu},\tilde{e}^-)_L$	$(\nu,e^-)_L$	1	2	$-\frac{1}{2}$
	$\tilde{e}^-_R$	e^-_R	1	1	1
squark/quark	$(\tilde{u}_L,\tilde{d}_L)$	$(u,d)_L$	3	2	$\frac{1}{6}$
	$\tilde{u}_R$	u_R	3	1	$-\frac{2}{3}$
	$\tilde{d}_R$	d_R	3	1	$\frac{1}{3}$
Higgs/Higgsino	(H^0_d,H^-_d)	$(\tilde{H}^0_d,\tilde{H}^-_d)$	1	2	$-\frac{1}{2}$
	(H^+_u,H^0_u)	$(\tilde{H}^+_u,\tilde{H}^0_u)$	1	2	$\frac{1}{2}$

TABLE 2.4.: *The gauge supermultiplet of the MSSM.*

Supermultiplets	Bosons	Fermions	SU(3) (N_{colour})	SU(2) ($N_{Isospin\,states}$)	U(1) ($Weak\,Hypercharge$)
gluon/gluino	g	$\tilde{g}$	8	1	0
gauge/gaugino	$W^\pm,W^0$	$\tilde{W}^\pm,\tilde{W}^0$	1	3	0
	B	$\tilde{B}$	1	1	0

HIGGS SECTOR The Higgs sector of the MSSM has two complex Higgs doublets, $H_u=(H^+_u,H^0_u)$ and $H_d=(H^0_d,H^-_d)$, i.e. eight degrees of freedom. They generate mass for the 'up'-type and 'down'-type fermions After the breaking of the electroweak symmetry which is explained by a mechanism similar to the one in the SM, the Higgs sector is reduced to five mass states. Two are CP-even[2] Higgs particles, H and h, one is CP-odd, A, and two are electrically charged, H^+ and H^-.

NEUTRALINOS AND CHARGINOS The supersymmetric winos, binos and Higgsinos as given in Tables 2.3 and 2.4 are only expected to be realised as mixed mass eigenstates. The charged gauginos, namely the $\tilde{W}^+$ and $\tilde{W}^-$ as well as the charged Higgsinos $\tilde{H}^+_u$ and $\tilde{H}^-_d$, are combined to the 'charginos' $\tilde{\chi}^\pm_1$ and the heavier $\tilde{\chi}^\pm_2$. Depending on the size of the contributions, they can be more Higgsino- or more wino-like. The electrically neutral gauginos and Higgsinos $\tilde{W}^0$, $\tilde{B}$, $\tilde{H}^0_u$ and $\tilde{H}^0_d$ mix to four states which are called 'neutralinos', $\tilde{\chi}^0_i$, with $i=1,2,3,4$. By convention it is hereafter assumed for the masses of the neutralinos that $m_{\tilde{\chi}^0_4}\geq m_{\tilde{\chi}^0_3}\geq m_{\tilde{\chi}^0_2}\geq m_{\tilde{\chi}^0_1}$. In many SUSY models the lightest neutralino $m_{\tilde{\chi}^0_1}$ is the LSP.

[2]The charge conjugation operator $\hat{C}$ turns matter into anti-matter and vice versa. The parity operator $\hat{P}$ flips the signs of spatial coordinates. 'CP-even' means that after applying both $\hat{C}$ and $\hat{P}$ to a state, the eigenvalue is $+1$, while for 'CP-odd' states it is -1.

2.2.4. Phenomenological MSSM

Since the MSSM contains 105 new free parameters, further theoretical assumptions are made to reduce them and to make SUSY experimentally accessible.

One of the restricted models is called 'phenomenological MSSM' (pMSSM). The restrictions are: no new source of CP violation is added to the known SM sources, no flavour changing neutral currents are allowed just as in the SM, and the first and second generation sparticles are mass-degenerate.

As a consequence, the 19 free parameters which are left in addition to the 18 parameters of the SM are [14]:

- three gaugino masses M_1, M_2 and M_3 for the binos, winos and gluinos,
- two Higgs sector parameters: m_A, the mass of the CP-odd Higgs, and $\tan\beta = \frac{v_u}{v_d}$ with the vacuum expectation values v_u (v_d) of the neutral components of the Higgs field H_u (H_d) that couples exclusively to up-type (down-type) quarks and leptons;
- the Higgsino mass parameter μ,
- five squark and slepton squared mass parameters for the degenerate first and second generations $M^2_{\tilde{Q}1}$, $M^2_{\tilde{U}1}$, $M^2_{\tilde{D}1}$, $M^2_{\tilde{L}1}$ and $M^2_{\tilde{E}1}$,
- five squark and slepton squared-mass parameters for the third generation $M^2_{\tilde{Q}3}$, $M^2_{\tilde{U}3}$, $M^2_{\tilde{D}3}$, $M^2_{\tilde{L}3}$ and $M^2_{\tilde{E}3}$ and
- three third-generation trilinear couplings A_t, A_b and $A\tau$ which are used to factor out the Yukawa couplings.

It is expected that Supersymmetry breaking occurs in a 'hidden sector' in contradiction to the 'visible sector' of the chiral MSSM supermultiplets. The breaking could e.g. occur via effects of gravitational strength which would make it gravity-mediated or via gauge forces, making it gauge-mediated. No such assumptions are made for the pMSSM.

2.2.5. Simplified Models

The phase space spanned by the free SUSY parameters is huge. This makes it necessary to develop more general models, making SUSY experimentally accessible. So-called 'simplified models' make it possible to find out about the general sensitivity of recorded data with respect to SUSY models and to set limits on SUSY parameters. Simplified models only contain a small set of parameters like the masses of sparticles, their production cross sections and their branching ratios for the various decay modes. Nevertheless do the observables depend strongly on the variation of these parameters. Decay chains are assumed to be as short as possible and only very few

interactions between the particles are assumed in simplified models. Normally only one production process and one decay mode are assumed with 100% branching ratio (BR). Simplified models do not describe a complete SUSY model but are based on a phenomenology which is typical for SUSY [15], [16].
An example is the simplified model which is used for the interpretation of the results of the analysis that is described in Chapter 7. The direct production of a pair of $\tilde{\chi}_1^+\tilde{\chi}_1^-$ via electroweak interactions is assumed. The pair then decays via intermediate sleptons, $\tilde{\chi}_1^+\tilde{\chi}_1^- \rightarrow (\tilde{l}^+\nu)/(l^+\tilde{\nu}) + (\tilde{l}^-\bar{\nu})/(l^-\tilde{\bar{\nu}}) \rightarrow l^+\bar{\nu}\tilde{\chi}_1^0 l^-\nu\tilde{\chi}_1^0$. The masses of $\tilde{\chi}_1^0$, $\tilde{\chi}_1^\pm$, $\tilde{\chi}_2^0$, $\tilde{\nu}$ and $\tilde{l}$ are the only free parameters with $m_{\tilde{\nu}} = m_{\tilde{l}}$. Furthermore $m_{\tilde{l}_R} = (m_{\tilde{\chi}_1^0} + m_{\tilde{\chi}_1^\pm,\chi_2^0})/2$ with $\tilde{\chi}_1^\pm$ and χ_2^0 being wino-like and mass degenerate. The squark masses are set to $\mathcal{O}$ (100 TeV).

2.3. Electroweak Production of Supersymmetry

Motivation for LHC Searches Figure 2.4 shows the production cross sections of SUSY particles as a function of the average mass of the outgoing massive sparticles at a centre-of-mass energy of $\sqrt{s} = 8$ TeV for a proton-proton collider such as the Large Hadron Collider (LHC) at the Conseil Européen pour la Recherche Nucléaire (CERN). The cross sections are calculated with the Prospino2 software [17]. They depend on the parameters of the underlying SUSY model. The production of strongly interacting sparticles such as squarks and gluinos clearly dominates for low masses. The search for bottom and top squarks in a simplified model in [18] excludes gluinos with masses below 1.34 TeV. Therefore the search for the electroweak production of gauginos and sleptons which can be light over a large parameter space also becomes important. As carried out in [19], charginos and neutralinos are foreseen to be light at $\mathcal{O}$ (100 GeV) for naturalness reasons. The analyses presented in this thesis focus on the search for electroweakly produced sparticles.

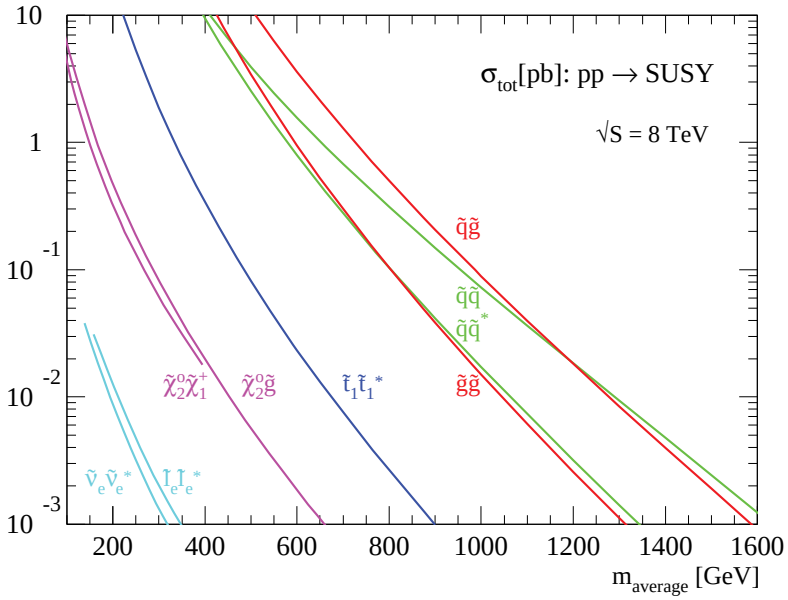

FIGURE 2.4.: *The cross section for the production of sparticles depending on the average mass of the outgoing massive sparticle. The plot is generated with the Prospino2 software [17].*

PRODUCTION OF SPARTICLES A proton-proton collider such as the LHC is able to produce electroweakly interacting sparticles via $q\bar{q} \to \tilde{\chi}_i^+ \tilde{\chi}_j^-$, $q\bar{q} \to \tilde{\chi}_i^0 \tilde{\chi}_j^0$, $q\bar{q} \to \tilde{l}_i^+ \tilde{l}_j^-$, $q\bar{q} \to \tilde{\nu}_l \tilde{\nu'}_l$, $q\bar{q'} \to \tilde{\chi}_i^\pm \tilde{\chi}_j^0$ and $q\bar{q'} \to \tilde{l}_L^\pm \tilde{\nu}_l$, where for the last two processes q must be an up- or down-type quark and $\bar{q'}$ must be a down- or up-type quark.

DECAY OF SPARTICLES The neutralinos $\tilde{\chi}_i^0$ decay via electroweak interactions in $Z\tilde{\chi}_j^0$, $W^\pm \tilde{\chi}_j^\mp$, $l\tilde{l}$, $\nu\tilde{\nu}$, $H^\pm \tilde{\chi}_j^\mp$ or $\Phi\tilde{\chi}_j^0$ with $\Phi = h, H, A$, $i > j$. The charginos $\tilde{\chi}_i^\pm$ decay into $W^\pm \tilde{\chi}_j^0$, $Z\tilde{\chi}_j^\pm$, $l\tilde{\nu}$, $\nu\tilde{l}$, $H^\pm \tilde{\chi}_j^0$ or $\Phi\tilde{\chi}_j^\pm$ with $\Phi = h, H, A$, $i > j$.

Also possible are three-body decays such as $\tilde{\chi}_i^0 \to f\bar{f}\tilde{\chi}_j^0$, $f\bar{f}'\tilde{\chi}_j^\pm$ or $\tilde{\chi}_i^\pm \to f\bar{f}'\tilde{\chi}_j^0$.

Charged sleptons can subsequently further decay into $l\tilde{\chi}_i^0$ or $\nu\tilde{\chi}_i^\pm$ and sneutrinos into $\nu\tilde{\chi}_i^0$ or $l\tilde{\chi}_i^\pm$ [20].

The typical detector signature for electroweakly produced sparticles contains one or more charged leptons in the final state, missing energy due to the invisible neutrinos and neutralinos, and possibly one or more jets.

2.4. CURRENT ATLAS RESULTS IN THE SEARCH FOR SUPERSYMMETRY

The most recent results from SUSY analyses performed with data taken by the ATLAS detector at the LHC (see Section 4.2) are shown in Figure 2.5. These results

were presented at the International Conference for High Energy Physics (ICHEP) 2014 and depict the excluded sparticle mass ranges in coloured bars for a selection of analyses.

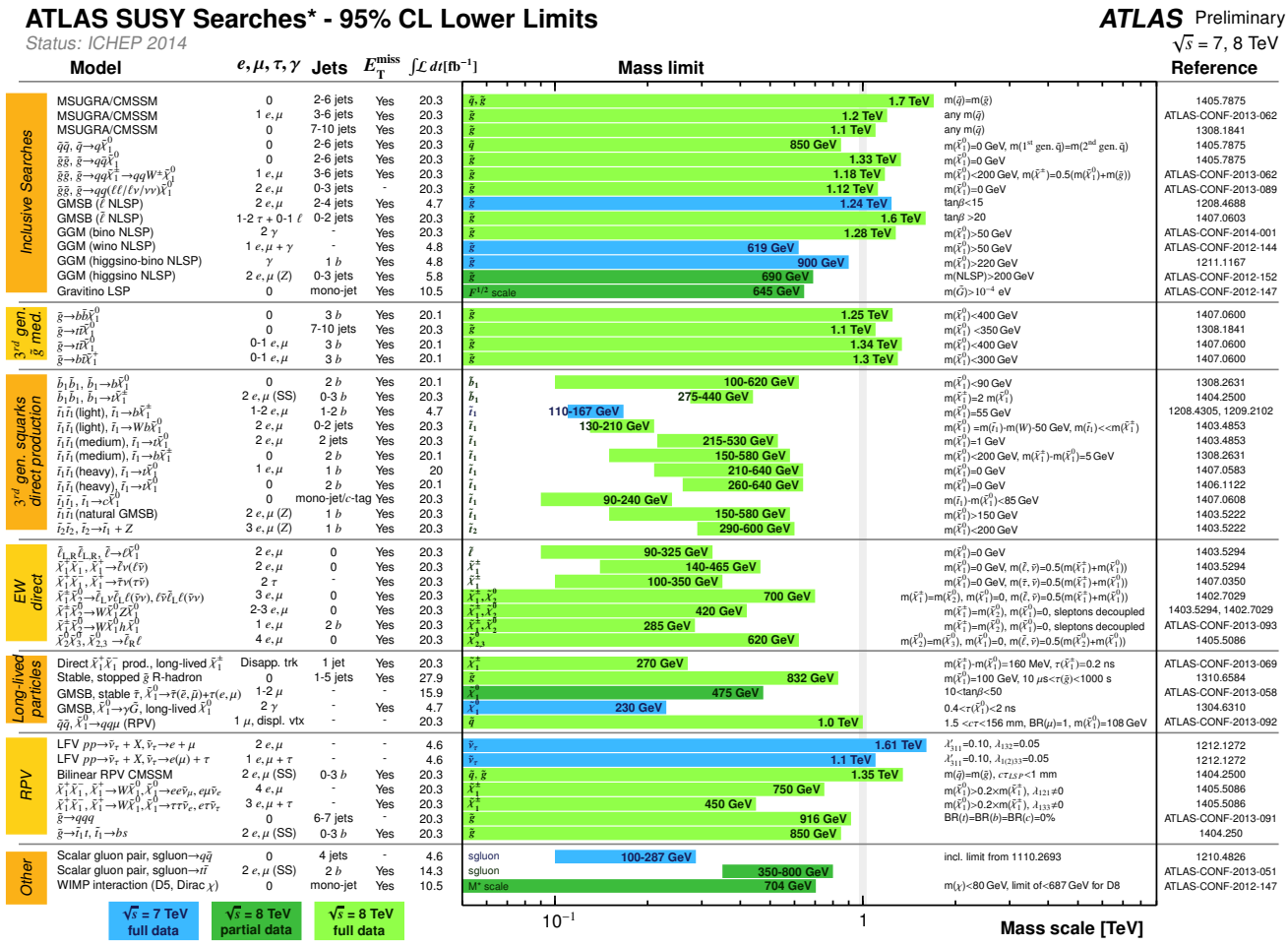

*Only a selection of the available mass limits on new states or phenomena is shown. All limits quoted are observed minus 1σ theoretical signal cross section uncertainty.

FIGURE 2.5.: *Selection of analyses looking for supersymmetric particles and the mass ranges of sparticles excluded as a result. The analyses are performed with data taken by the ATLAS detector at $\sqrt{s}$ =7 (turquoise), 8 TeV (light green; partial data: dark green) [21].*

Figure 2.6 shows the exclusion lines of the SUSY searches for sparticles produced via electroweak interactions, presented at ICHEP 2014. A simplified model is assumed where the only non-fixed parameters are the degenerate masses of the $\tilde{\chi}_1^{\pm}$ and $\tilde{\chi}_2^0$ (shown on the x-axis) and the mass of the $\tilde{\chi}_1^0$, which is the LSP (shown on the y-axis). The continuous lines are drawn around the points in the grid which are excluded at 95% confidence level using data recorded with ATLAS at $\sqrt{s} = 8$ GeV.

The dashed lines show the expected limits at 95% confidence level[3] only using the SM expectation. The different colours correspond to different analyses which address the various production and decay channels of electroweakly interacting sparticles. The four decay modes of the chargino and neutralino pairs are considered separately with 100% branching ratio each. As a result from the analysis which investigates the decay of $\tilde{\chi}_1^{\pm}\tilde{\chi}_2^0$ into a final state with three charged leptons via intermediate sleptons, chargino masses until 700 GeV and LSP masses until 250 GeV can be excluded. This is indicated by the continuous red line.

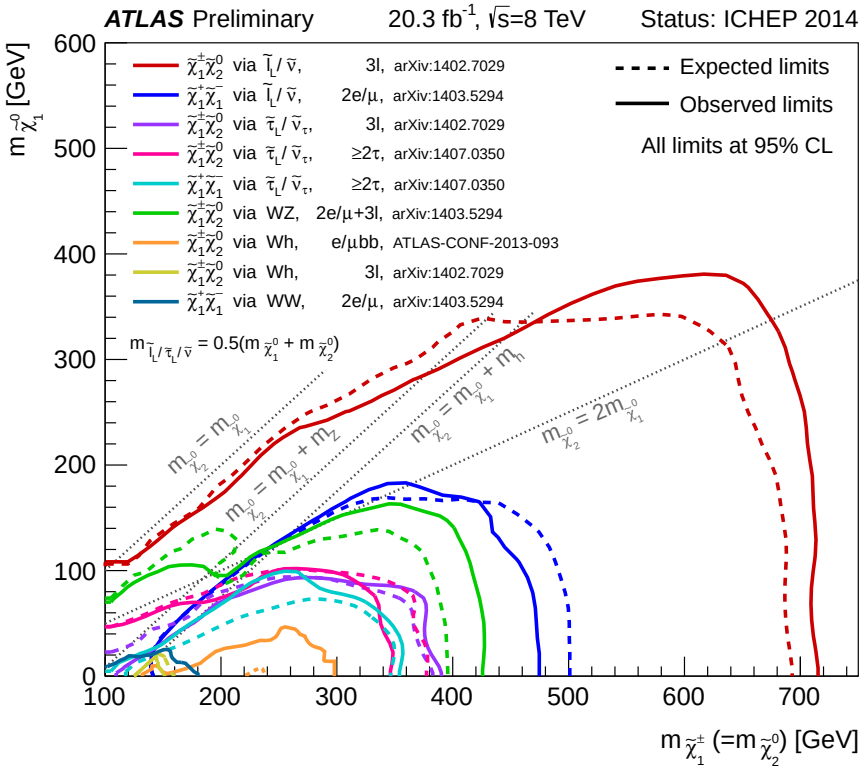

FIGURE 2.6.: *Summary of SUSY searches for electroweakly produced sparticles using ATLAS data recorded at $\sqrt{s} = 8$ GeV. The axes show the mass of the $\tilde{\chi}_1^0$ versus the degenerate masses of the $\tilde{\chi}_1^{\pm}$ and $\tilde{\chi}_2^0$. Contour lines are drawn at 95% confidence level, solid for the observed exclusion limits using ATLAS data and dashed for the expected limits using SM expectations [21].*

The exclusion lines for the analyses investigating the decay channels where a SM Higgs boson was produced in association with a W boson are indicated by an orange line for the final state with one charged lepton (electron or muon) and a $b\bar{b}$ pair. A yellow line shows the exclusion limit for the final state with three charged leptons (electrons or muons). $m_{\tilde{\chi}_1^{\pm},\tilde{\chi}_2^0}$ are excluded until almost 300 GeV (150 GeV) while $m_{\tilde{\chi}_1^0}$ is excluded for values higher than 20 GeV (about 5 GeV) for the $lb\bar{b}$ (3 lepton)

[3]The meaning of the confidence level will be explained in Section 3.

final state. Since the search with three leptons in the final state excludes $m_{\tilde{\chi}_1^\pm,\tilde{\chi}_2^0}$ at low values and the search for $lb\bar{b}$ excludes these masses at higher values, the two channels seem complementary.

3. Statistical Interpretation

To state how likely it is that a SUSY model exists or does not exist, for example a cut-and-count analysis is performed on the recorded ATLAS data. In this Chapter it is assumed that the expected event yield due to SM background is estimated only by MC simulation. Likewise the detector response can be simulated for a particular supersymmetric model - in this way a signal sample is provided. Recorded ATLAS data contains both SM background processes and potential SUSY signal. The number of events from the known SM background processes are assumed as null hypothesis. An alternative hypothesis which in addition contains events from new physics, namely the SUSY signal, is tested.

Profile Likelihood The expectation value of n events in a search region with a number of signal events s and a number of background events b_{tot} can be expressed as

$$E[n] = \mu s + b_{tot}. \tag{3.1}$$

The signal strength parameter μ is equal to 0 in a background-only hypothesis. μ equal to unity corresponds to the nominal signal rate as predicted from the tested SUSY model. b_{tot} is the expected total background which is computed from the N individual background components b_i for each process i, $b_{tot} = \sum_{i=1}^{N} b_i$.

For each background component b_i, M_i events are generated by Monte Carlo simulation, see Section 5.2, and from these, m_i events are selected in the search region. The expectation value of the Poisson distribution which models these measurements is

$$E[m_i] = \tau_i b_i. \tag{3.2}$$

τ_i is the ratio of the integrated luminosity of the ith Monte Carlo sample over the integrated luminosity of the recorded data, $\tau_i = \frac{\mathcal{L}_i^{MC}}{\mathcal{L}^{data}}$ [22]. A likelihood function for the parameter of interest μ and the nuisance parameters $\boldsymbol{\Theta} = (\boldsymbol{\Theta}_s, \boldsymbol{\Theta}_b, b_{tot})$ is defined as a product of Poisson probabilities. The nuisance parameters - i.e. the statistical and the systematic uncertainties on the number of signal and background events - characterise the shapes of the probability density functions for signal and background. The measured number of signal events s and the number of background

events b_i depend on the uncertainties.

$$L(\mu, \boldsymbol{\Theta}) = \frac{(\mu s + b_{tot})^n}{n!} e^{-(\mu s + b_{tot})} \prod_{i=1}^{N} \frac{(\tau_i b_i)^{m_i}}{m_i!} e^{-\tau_i b_i} \tag{3.3}$$

For this likelihood function the known absolute signal and background rates enter and thus constrain the nuisance parameters. $\lambda(\mu)$ is then defined as the profile likelihood ratio of $L(\mu, \hat{\hat{\boldsymbol{\Theta}}})$ over $L(\hat{\mu}, \hat{\boldsymbol{\Theta}})$,

$$\lambda(\mu) = \frac{L(\mu, \hat{\hat{\boldsymbol{\Theta}}})}{L(\hat{\mu}, \hat{\boldsymbol{\Theta}})}. \tag{3.4}$$

$\hat{\hat{\boldsymbol{\Theta}}}$ refers to the conditional maximum-likelihood estimators, i.e. to the nuisance parameters that maximise L for the fixed value of μ.

$\hat{\mu}$ as well as $\hat{\boldsymbol{\Theta}}$ refer to the unconditional maximum-likelihood estimators, i.e. to the values of μ and $\boldsymbol{\Theta}$ that maximise L independently of each other [23].

If μ is found to be equal to zero, the null hypothesis is confirmed. If on the other hand $q_\mu = -2 \ln \lambda(\mu)$ is close to 0, i.e. $\lambda(\mu)$ is close to 1, this means that the hypothesised value of μ is describing the observed data very well. Nevertheless the higher the obtained value for q_μ becomes, the less compatible is the observed data with the alternative hypothesis.

P-VALUE AND SIGNIFICANCE Supposing that the observed data results in a value of $q_\mu = q_{obs}$, the p-value states how well the data and the hypothesis, i.e. μ, agree:

$$p = \int_{q_{obs}}^{\infty} f(q_\mu | \mu) dq_\mu. \tag{3.5}$$

$f(q_\mu|\mu)$ is the sampling distribution of q_μ under the assumption of μ. The p-value therefore gives the probability to obtain test statistics which are equal to or less compatible than the observed ones, assuming that the null hypothesis with $\mu = 0$ is true.

To optimise signal selections, the significance Z_N is used. It is related to the p-value by

$$p = \int_{Z_N}^{\infty} \frac{1}{\sqrt{2\pi}} e^{-\frac{x^2}{2}} dx = 1 - \Phi(Z_N). \tag{3.6}$$

Z_N is the number of standard deviations at which a standard Gaussian would give a one-sided tail area equal to p. Φ is the cumulative distribution for the standard Gaussian [22].

Let σ_b be the uncertainty on the number of background events. It is treated as being due to an auxiliary background-only observation that is also Poisson distributed. As a measure of the signal significance, in this thesis Z_N is computed from s, b_{tot} and σ_b with a function called 'BinomialExpZ' implemented in ROOT RooStats [24], [25], [26]. This variable is used to find an approximately optimal signal selection using regularised beta functions [27]. A significance of $Z_N > 1.64$ corresponds to a p-value of less than 5%.

CONFIDENCE LEVEL The signal strength μ can be excluded at a confidence level (CL) of (1 - α) if the p-value is found below a certain threshold α. For the analyses presented in this thesis, α is chosen to be 5%.

The confidence level for the signal plus background hypothesis is given by the probability that the test-statistics q_μ is less than or equal to the measured statistics q_{obs}:

$$CL_{s+b} = p_{s+b}(q_\mu \leq q_{obs}) = \int_{-\infty}^{q_{obs}} \frac{dp_{s+b}}{dq_\mu} dq_\mu \tag{3.7}$$

with $\frac{dp_{s+b}}{dq_\mu}$ being the probability distribution function of the test-statistics for signal plus background experiments. Small values of CL_{s+b} mean that the observed data is not in good agreement with the signal-plus-background hypothesis. It is more likely that the background-only hypothesis is true for CL_{s+b} close to 0. For values close to 1, on the other hand, the alternative hypothesis is confirmed.

In analogy, the confidence level in the background-only hypothesis is given by

$$CL_b = p_b(q_\mu \leq q_{obs}) = \int_{-\infty}^{q_{obs}} \frac{dp_b}{dq_\mu} dq_\mu \tag{3.8}$$

with $\frac{dp_b}{dq_\mu}$ being the probability density function of the test statistics for background only. If CL_b is close to unity this means that the background-only hypothesis can most likely be rejected and that the signal-plus-background hypothesis is favoured. For a value close to 0, the null hypothesis is confirmed.

CL_s is defined by

$$CL_s = \frac{CL_{s+b}}{CL_b}. \tag{3.9}$$

The usage of CL_s for statements about the confidence level is also referred to as the 'modified frequentist procedure'. It is motivated by the fact that the observed number of events can also underestimate the expected number of events which leads to unphysical estimators and an implausible background modelling. Therefore the signal hypothesis is considered excluded at confidence level CL when $1 - CL_s \leq CL$ [28]. In other words, for $CL_s \leq 0.05$, the signal-plus-background hypothesis is excluded at 95% confidence level.

4. Experimental Setup

To find out if supersymmetric particles exist, high energies need to be provided to make the production of elementary particles with high masses possible. This is based on the equivalence of mass and energy, $E = mc^2$. Subsequently the produced particles need to be identified. Therefore their interaction vertices and tracks are recorded in a detector. Information about their kinematics such as energy and momentum is provided.

In 1954, the European research centre for nuclear physics was founded, CERN. It is located close to Geneva, Switzerland, and spreads out across the Swiss-French border. It hosted and hosts numerous physical experiments, not least the Large Electron Positron collider (LEP) which was taking data from the years 1989 to 2000. Among many other accomplishments also the idea of the world wide web was developed in 1989 at CERN to facilitate access to data storage. 21 countries are official members of CERN and a large number of scientists is involved from many more guest states world wide [29].

4.1. LHC - Large Hadron Collider

The high energies for the production of the elementary particles are achieved by proton-proton collisions at centre-of-mass energies of up to 14 TeV. The protons are extracted from hydrogen gas which was ionised by an electron beam. They then enter a linear accelerator and pass several circular accelerators before being injected in the Large Hadron Collider (LHC) in opposite directions. Occasionally LHC is also used to accelerate lead ions for lead-proton or lead-lead collisions. These collisions are investigated by some experiments but are not addressed by the analyses presented in this thesis.

The pre-accelerators, the LHC and the connected experiments are shown on a map in Figure 4.1. LHC is installed $\sim$100 m below the surface in the same 26.7 km long tunnel as the previous e^+e^--collider LEP.

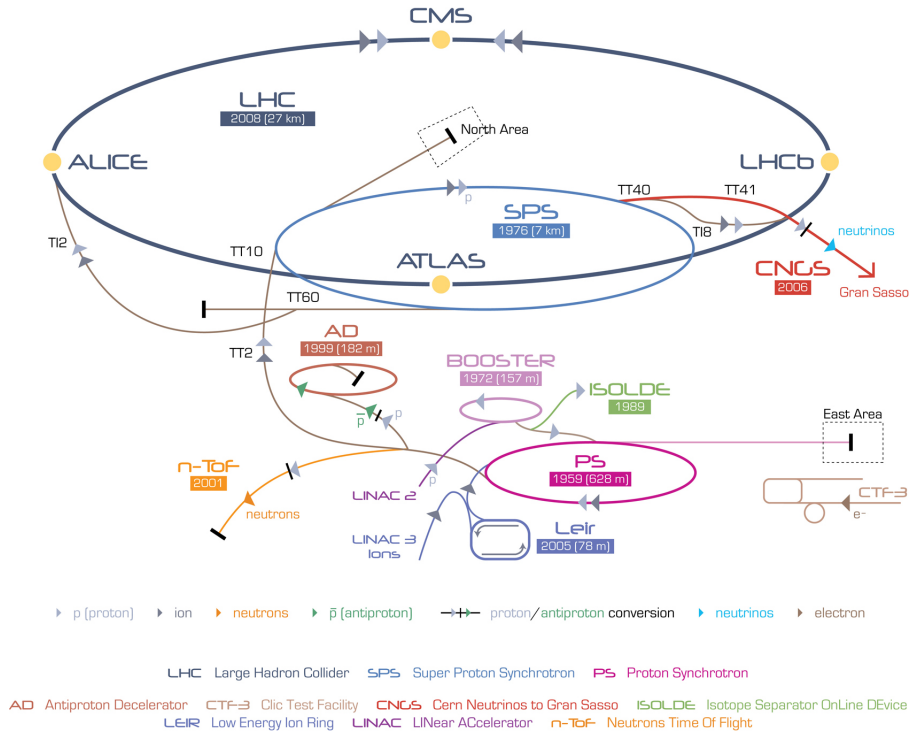

FIGURE 4.1.: *A map showing the pre-accelerators, the LHC and the connected experiments [30] (not to scale).*

The protons in the circular accelerators pass radio-frequency (RF) cavities which bring the protons to the required energies. For each of the two beam lines of the LHC, eight RF cavities are installed. The design-centre-of-mass energy is 14 TeV which means that in the LHC the protons travel at almost the speed of light.

The charged particles are forced on a circular path by magnetic fields of a strength of 8.33 T. The fields are provided by 1232 dipole magnets with a length of 15 m each. LHC magnets make use of superconducting cables made of a niobium-titanium alloy and they are cooled down to 1.9 K by liquid Helium. The proton beams are focused by quadrupole magnets of which in total 392 are installed in the tunnel.

There is no continuous proton flux in the beam pipes; the protons are bundled in 2808 bunches. These bunches are focused to a profile of 16 μm before they collide in one of the four collision points along the LHC [31].

At each collision point a particle detector is placed:

- One multi-purpose detector called the '**C**ompact **M**uon **S**olenoid' (CMS),
- one detector addressing ion collisions with ultra-high energy densities which are comparable to the ones at the time directly after the Big Bang, called '**A** **L**arge **I**on **C**ollider **E**xperiment' (ALICE),
- the '**L**arge **H**adron **C**ollider **b**eauty' (LHCb) experiment for b-physics and
- another multi-purpose detector called '**A** **T**orodoidal **L**HC **A**pparatu**S**' (ATLAS).

4.2. ATLAS - A Toroidal LHC Apparatus

The data recorded with the ATLAS detector is analysed to - among other purposes - study the possible substructure of particles, to address b-physics, to find supersymmetric particles, to find the Higgs boson and to measure particle masses and interaction strengths with high accuracy. Therefore ATLAS is demanded to provide precise low-momentum measurements, the possibility of particle tracking as well as the identification of electrons, photons, muons and hadrons.

The detector is composed from various subdetectors in an onion-skin structure. Each subdetector provides information about the passing particles and the information pieces are composed to identify the particles with high efficiency and to measure their kinematics. The information about ATLAS in this Section is based on [32], [33].

ATLAS measures 44 m in length and 25 m in height and weighs about 7000 t. It is depicted in Figure 4.2. The interaction point for the proton-proton collisions is in the very centre of the detector and the beam pipes enter from the left and from the right.

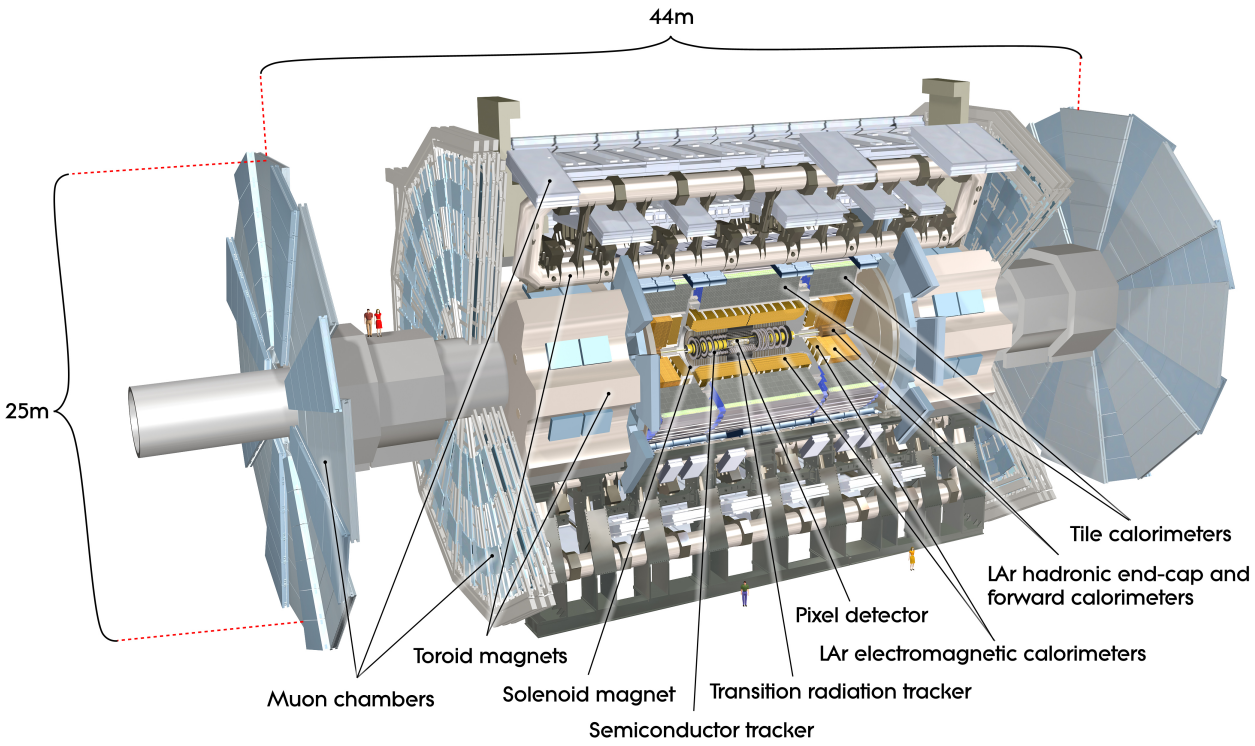

Figure 4.2.: *Depiction of ATLAS [34].*

4.2.1. ATLAS Coordinate System

To describe ATLAS, a right-handed Cartesian coordinate system is used. The detector is forward-backward symmetric. The origin is placed at the centre of the detector in the nominal bunch crossing point. The z-axis points along the beam axis and the x-axis points to the centre of the LHC ring. The transverse plane is defined by the x-y plane. The azimuth angle ϕ is measured around the z-axis and the polar angle θ is measured from the z-axis as indicated in Figure 4.3.

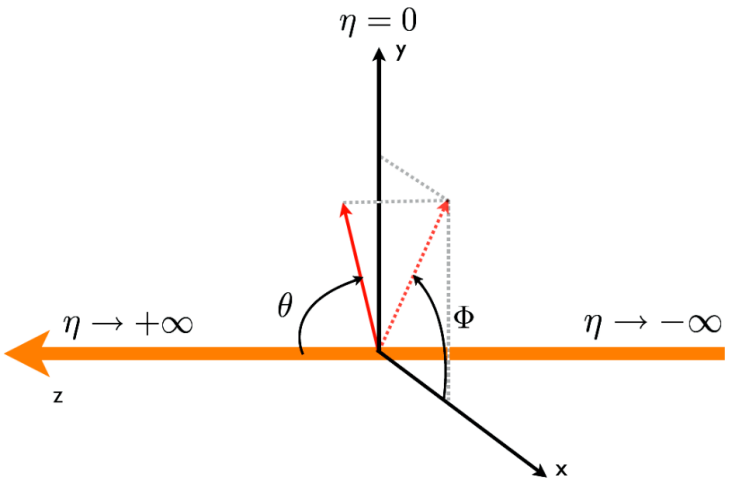

FIGURE 4.3.: *The ATLAS coordinate system [35].*

Instead of using the polar angle θ it is more common to use the pseudorapidity η to describe ATLAS. It is defined by

$$\eta = -\ln(\tan(\frac{\theta}{2})). \tag{4.1}$$

For a 'transverse' variable like e.g. the transverse momentum, the absolute value of the two dimensional vector in the x-y plane is computed, $p_T = \sqrt{p_x^2 + p_y^2}$.

The distance between two particle tracks, i.e. the distance of two axes in the η-ϕ plane, is given by $\Delta R = \sqrt{\Delta\eta^2 + \Delta\phi^2}$.

4.2.2. Inner Detector

The three tracking detectors in the centre of ATLAS form the Inner Detector (ID) which measures only 35 cm in length.

Pixel Detector The innermost part is the Pixel Detector (PD). It provides a spatial resolution of 12 μm [33] by the usage of 82 million silicon pixels.

SEMICONDUCTOR TRACKER The Semiconductor Tracker (SCT) also allows for high-precision track measurements. It relays the information about track points for the reconstruction of the flight paths of the passing particles. The 6 million channels make it possible to measure the particle tracks in this silicon microstrip tracker with an accuracy of 17 μm per layer in the direction transverse to the readout strips which are placed on the silicon, and with an accuracy of 580 μm [33] in longitudinal direction.

TRANSITION RADIATION TRACKER The outermost part of the ID is a transition radiation tracker (TRT) which allows to distinguish between passing electrons and hadrons. It consists of many layers of straw tubes which are filled with a xenon gas mixture and it has a spatial R-ϕ[1] resolution of 170 μm [33].

4.2.3. CALORIMETERS

In the calorimeters depicted in Figure 4.4 the passing particles are stopped by their interactions with the absorbing material. The entering particles cause shower cascades due to bremsstrahlung, ionisation, hadronisation and pair production of electrons and positrons. The energy which is deposited in the active material by the resulting particles, i.e. photons, is summed up to measure the energy of the initially entering particles.

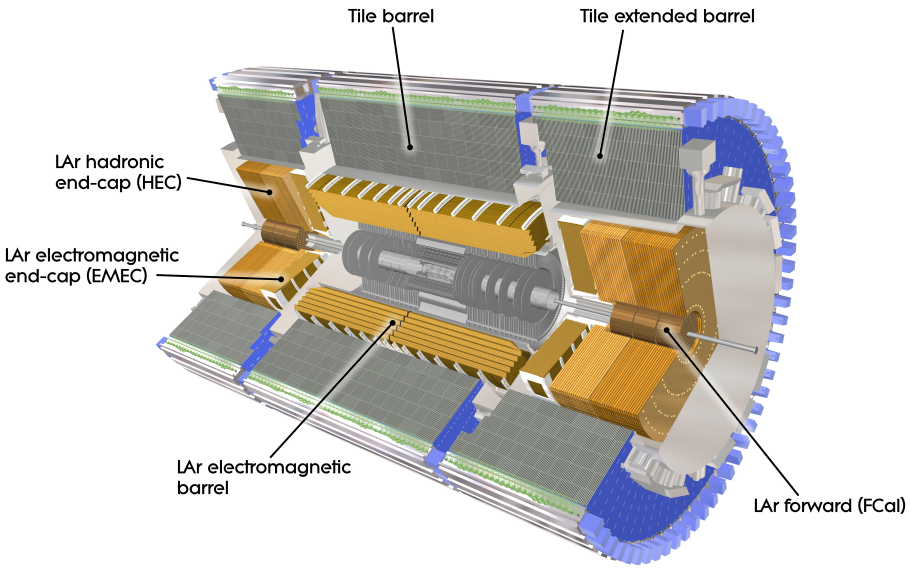

FIGURE 4.4.: *The combined calorimeters of ATLAS [34].*

[1] referring to cylindrical coordinates

Liquid Argon Calorimeters The electromagnetic calorimeters in the barrel part ($|\eta| < 1.475$) and in the two end-cap parts ($1.375 < |\eta| < 3.2$) use layers of liquid argon (LAr) at a temperature of -183 °C as active material. Electromagnetically interacting particles produce showers in the absorbing medium which is made from lead. The active and the absorbing calorimeter layers are arranged in accordion geometry for optimal coverage and read-out.

Hadronic Calorimeters The hadronic calorimeters use layers of steel as absorber and use scintillating tiles for the read-out. Both are arranged in a sampling structure. One hadronic calorimeter is placed directly outside the electromagnetic barrel calorimeter, covering $|\eta| < 1.0$. The energy of hadronically interacting particles escaping in $0.8 < |\eta| < 1.7$ is deposited in the two extended barrel calorimeters.
The LAr hadronic endcap calorimeters spatially overlap with the hadronic barrel calorimeter and the LAr forward calorimeters. For the latter a copper module is installed to measure the energy of electromagnetically interacting particles and two modules made of tungsten are provided to quantify the energy of hadrons. Since they both use LAr as active material, the hadronic as well as the electromagnetic endcap calorimeters share the same cryostats.

4.2.4. Muon Detector

Just as the neutrinos which are non-detectable in ATLAS at all, also the muons are not stopped or absorbed in the calorimeter system. Thus the outermost part of ATLAS consists of four different types of chambers for coordinate and momentum measurement of those electrically charged and relatively heavy particles. ~ 1 million channels can be read out in an area of 5500 m^2 and a spatial resolution of ≤ 50 μm is possible [33].
In the MS, monitored drift tubes (MDTs) and cathode strip chambers (CSCs) make precision tracking possible. Resistive plate chambers (RPCs) and thin gap chambers (TGCs) are used for triggering on muons, see Section 5.1.1.

4.2.5. Magnet System

To provide a magnetic field of 2 T for the ID, a superconducting solenoid is installed between the ID and the calorimeter system. It is 5.3 m long and measures 2.4 m in diameter. The solenoid shares a cryostat with the LAr barrel calorimeter to make the particles coming from the bunch crossing point pass as few absorbing material as possible before they enter the calorimeter system. Due to the magnetic field the tracks of charged particles are bent in the ID. Responsible for this is the Lorentz force $\vec{F}_{Lorentz} = q(\vec{v} \times \vec{B})$ which can be computed from the electric charge q and the velocity $\vec{v}$ of a particle as well as from the strength of the magnetic field $\vec{B}$ which the particle is passing. The momentum of the passing particles with mass m can

be determined from the sagitta of the bended track after equating the Lorentz force with the centripetal force.

The muons pass a magnetic field of 4 T before entering the MS. This field is created by eight toroids placed along the barrel region of the detector and by two toroidal systems located at the endcaps of the detector, outside the calorimeters. The direction of the deflection of the flight paths due to $\vec{F}_{Lorentz}$ gives indication of the sign of the charge, i.e. a muon being a particle or an anti-particle.

5. Data Taking and Reconstruction of Physics Objects

5.1. Trigger System

ATLAS detects 40 million events in one second, whereby an event means the collision of protons and the following scattering processes and decay chains. Such high data rate is not completely storable. Therefore at a very early stage, i.e. during data taking, it needs to be decided which events might contain interesting physics. These events are then kept for analysis and their data is written to disk. The decision making is done by the ATLAS trigger system.

Data is analysed according to the expected physics signature of the process of interest. Filters are applied selecting e.g. two leptons which are reconstructed with high quality and a certain amount of transverse momentum. The trigger signature is defined by interesting physics objects, i.e.electrons, photons, muons and hadrons.

First an event will be considered as interesting if it passes hardware-based criteria on Level 1 of the trigger system. Secondly it has to pass software-based filters (Level 2) and thirdly an online reconstruction procedure (Event Filter) is applied which is rather similar to the offline reconstruction algorithms, before the data is actually written to disk. Later the offline reconstruction algorithms can be re-run as often as needed. On each level, the rate of initially 40 MHz will be reduced as depicted in Figure 5.1 to finally storable $\mathcal{O}$ (100 Hz). During Run 1, i.e. data taking at $\sqrt{s}$=7 and 8 TeV in the years 2011 and 2012, respectively, the rate at Level 1 was restricted to 65 kHz. It will go up to 100 kHz for a luminosity of $\mathcal{L} = 3 \times 10^{34}\text{cm}^2\text{s}^{-1}$ during Runs 2 and 3 when $\sqrt{s}$ is increased to 14 TeV [36].

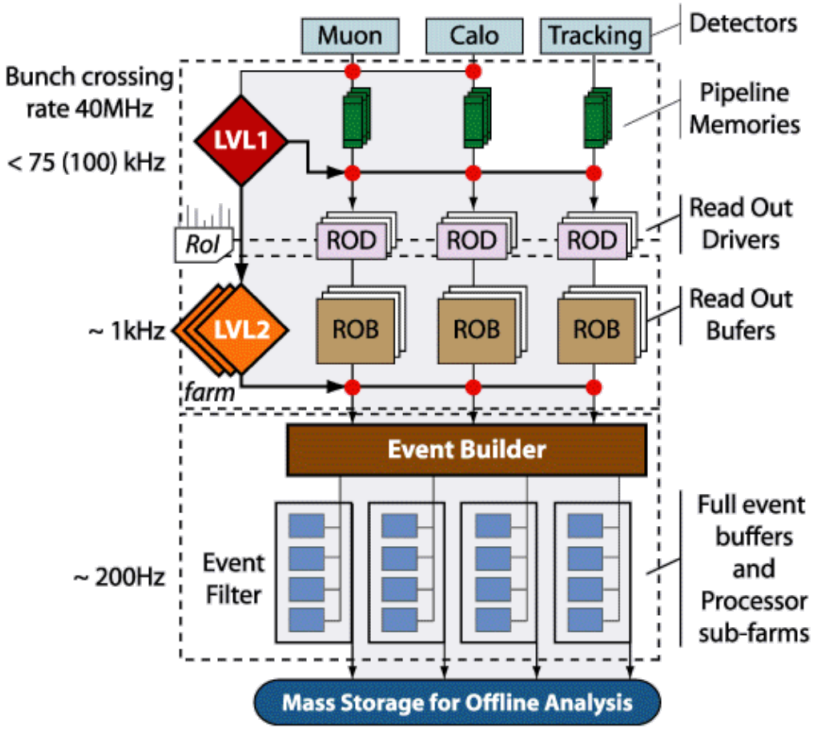

FIGURE 5.1.: *The ATLAS Trigger System [37].*

5.1.1. LEVEL 1

The first level of the ATLAS trigger system uses data from the detector with reduced granularity to decide whether an event passes the trigger criteria. The decision is based on information coming from the calorimeters or from the RPCs and TGCs in the Muon Spectrometer. Physical objects are then identified. The areas of the detector where the objects are recorded are treated as 'Regions of Interest' (RoIs).
Using the neighbouring cells in all samplings of the electromagnetic and hadronic calorimeters, trigger towers with a granularity of 0.1×0.1 in the $\eta \times \phi$ space are formed. They measure the transverse energy of the crossing particles from 1 GeV on. The Cluster Processor (CP) for example uses overlapping sliding windows for 2×2 clusters of electromagnetic trigger towers and the hadronic towers behind to identify electrons, photons and hadronically decaying taus. For an illustration see Figure 5.2.

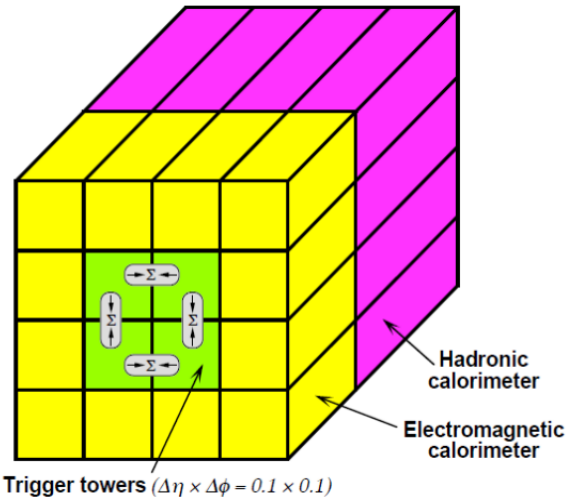

FIGURE 5.2.: *The trigger towers in the calorimeters. The green area corresponds to a window of size* $\Delta\eta \times \Delta\phi = 0.4 \times 0.4$ *[33]*

An object is identified and therefore fires the trigger when the local maximum transverse energy in a trigger-tower region exceeds a threshold. Requirements on the isolation of the object can also be part of the trigger criteria. An object is considered as being isolated when the energy deposit in a surrounding ring of trigger towers in the electromagnetic or hadronic calorimeters is less than a certain value.

Quarks can only exist as bounded hadrons due to the colour confinement described in Section 2.1.3. Because of the hadronisation effect they are not individually detectable, but they become measurable as cone shaped objects made from hadrons which generally move away from the production vertex. These objects are called jets and can be identified by the reconstruction algorithms.

The Jet/Energy Module (JEM) identifies jets at Level 1 when the energy depositions in trigger towers in the electromagnetic calorimeter added to the ones in the hadronic calorimeter fulfil a certain minimum criterion.

It is also possible to measure the total sums of E_x, E_y and E_T (the transverse energy) to trigger for example on events with high missing transverse energy[1] due to undetected particles like neutrinos.

The RPCs and TGCs have a time resolution of 1.5 and 4 ns, respectively. Each of the three RPC stations consists of two independent detector layers. Muon candidates are identified by hits in the first doublet of the RPC, the pivot plane. A scan is performed for more hits in the second RPC doublet. When the road whose centre is defined by the line of conjunction of the hit in the pivot plane with the interaction point has a certain maximum width, meaning a certain minimum p_T value, the cri-

[1] For the definition of the missing transverse energy see Section 5.3.5.

teria for a Level 1 muon candidate are fulfilled [33].

A prescale factor can be applied to the Level 1 trigger which means selecting only 1 out of N events. The prescale factor is adjusted during the data taking since the peak luminosity decreases over time. The trigger configuration however always remains the same during one luminosity block, which is the smallest subdivision of a data taking period [38]. Level 1 has a latency of 2.5μs until the information about the RoIs must be passed to the next trigger level [33].

5.1.2. High-Level Triggers: Level 2 and Event Filter

Level 2 requests information from all ATLAS subdetectors and is 'seeded' by Level 1, starting the algorithms and extrapolations at the RoIs which were passed by Level 1. Its purpose is to reduce the rate from the incoming $\mathcal{O}$ (100 kHz) to 3.5 kHz. The event processing time is 40 ms [38]. In the following will be briefly described how for example electron and muon candidates are processed at the software based high-level trigger.

Level 2 Electron Candidates For an electron candidate, which was passed as RoI to Level 2, the energy deposit in the calorimeter must be similar to the p_T of the matching track in the ID. Furthermore, it must fulfil requirements on the E_T of the considered electromagnetic calorimeter cluster, on the E_T in the first layer of the hadronic calorimeter (hadronic leakage), on the shower shape and on the ratio of the first and second energy maxima in the first measuring sampling of the electromagnetic calorimeter. In the ID the tracks are reconstructed using the area around the received RoI.

Level 2 Muon Candidates Two types of reconstructed muons can be considered as Level 2 muon candidates. First the so-called standalone muons are reconstructed using only the information from the MS. Secondly, combined muons are identified using also the information from the ID around the RoI which implies an improved resolution for soft particles which have low p_T.

Event Filter The hypothesis test - for example at least two leptons with a minimum p_T - must not fail or an event will not pass to the last level of the ATLAS trigger system, the Event Filter. Algorithms very close to the offline algorithms are used to further improve the identification of the passed objects. The Event Filter has a latency of 4 s [38].

The algorithms for electron identification use more shower shape and track quality cuts compared to Level 2. The physics objects can now already be reconstructed with loose, medium or tight quality [39]. A loose electron is more likely to be selected, but compared to a medium or tight electron the higher reconstruction efficiency also means a higher probability for misidentification.

To increase the identification quality for muons, two algorithms are implemented. One starts from the muon spectrometer and then extrapolates to the ID ('TrigMuonEF'), the other algorithm works reversely, starting from the ID ('TrigMuGirl') [40]. Both are seeded by the Level 2 objects.

5.1.3. Trigger Menu and Notation

Many event signatures corresponding to the wide ATLAS physics programme must be covered, but at the same time the data rate needs to be kept at a storable level. For these reasons the data stream is cut into slices, according to the trigger menu. Each slice corresponds to a particular trigger signature which has to balance the need for high statistics of events with soft objects and the requirement of the total bandwidth not to exceed $\mathcal{O}$ (100 Hz).
A trigger signature means that the hypothesis of at least a number of certain physics objects which are identified with a certain minimum transverse momentum is satisfied. The objects are labelled with

- *e* for electrons
- *mu* for muons
- *tau* for tauons
- *j* for jets
- *g* for photons and
- *xe* for missing transverse energy.

Followed by a number, such abbreviation indicates the minimum threshold on the transverse momentum of the object. Additional requirements on the isolation of the physics objects are indicated by the letter 'i' and leptons can be requested to be reconstructed with 'loose', 'medium' or 'tight' quality at trigger level. The label 'e24vhi_medium1' for example implies the hypothesis of at least one isolated electron with at least 24 GeV of transverse momentum which was reconstructed with the 'medium1' quality criterion (the quality criteria were tightened during several months of data taking, i.e. 'medium' became 'medium1'). The token 'vh' implies that the η-dependent E_T selections were applied at Level 1 and that the energy in the core of the hadronic calorimeter is required to be smaller than 1 GeV [41].

In this thesis, if not otherwise indicated, the trigger signature will always refer to the signature on the Event Filter level. To each signature on the Event Filter level corresponds a signature on Level 1 and one on Level 2 which seeded the Event Filter. For the above example of '24evhi_medium1', this would be e.g. 'EM18VH' on Level 1 where an object with at least 18 GeV E_T was requested in the electromagnetic calorimeter which also needed to fulfil the 'vh' criterion.

An event will only be considered for a physics analysis if a certain trigger or a combination of triggers is caused.

5.2. Data Acquisition and Monte Carlo Simulation

Data Formats After the trigger-based decision on which events to store on disk for later analysis, the data is still in a 'Byte-stream Data' format for all events which passed the high-level triggers. For simulated events the generated hits need to be translated into charges, light and the response of the readout electronics. After this step of digitisation and the conversion to 'Raw Data Object Data' (ROD) based on C++, the simulated data is similar to the recorded detector data. ROD contains all the information read out from the subdetectors, e.g. times and voltages. 'Event Summary Data' (ESD) is the next step during data handling for which the raw data is reconstructed into information about energy deposits and tracks. A summary of the ESD is the 'Analysis Object Data' (AOD) which contains the reconstructed physics objects. The data format which is finally used for most analyses is a n-tuple style representation of the AOD: the 'Derived Physics Data' (DPD) [42]. The DPD is processed for an analysis inside the 'ROOT' framework [43].

Monte Carlo Simulation To discover new physics or to exclude certain models, the recorded data needs to be compared to what is expected. It is not known what processes exactly lead to the recorded detector signature. Conclusions can be drawn only from applying cuts on the data and from comparisons with the theoretical expectation. This motivates the need for simulated data for which then not only the true process is known but also the consequent detector response.

The simulation is done by making use of 'Monte-Carlo (MC) methods': a statistical procedure many times repeats random experiments.

Pile-up During one bunch crossing more than one proton-proton collision can take place since a bunch contains $\mathcal{O}(10^{11})$ protons. The proton-proton collisions which happen in the same bunch crossing are called 'in-time pile-up'. It can happen that protons from a previous or following bunch crossing leave a detector signature. This is called 'out-of time pile-up'. The amount of pile-up is not always correctly estimated in the MC simulation. Therefore the MC events are reweighted depending on the number of inelastic interactions in data to reflect the detector response.

The underlying event means the collisions of the other constituents of the protons which are not part of the hard collision of the event primary vertex.

The following paragraph is based on information taken from [44]. The software used to simulate the complex hadronisation processes are 'PYTHIA' [45] and 'HERWIG' [46]. The latter also makes use of 'JIMMY' [47] which contains a multiple scattering model for the 'underlying event'.

Other examples for generator software are

- 'SHERPA' [48] which is a multipurpose event generator,
- 'MC@NLO' [49]- [51] which includes the full next-to-leading order QCD corrections in the computation of hard subprocesses,
- 'AlpGEN' [52] which is used for final states with high jet multiplicities and
- 'MadGraph' [53], a matrix element generator with automatic computation of the amplitudes for all relevant subprocesses.

The detector response for each generated event is simulated by the GEANT4 software [54]. The simulated data is then processed and provided in the same data formats, starting with ESD, as the data recorded by ATLAS.

5.3. Reconstruction and Definition of Physics Objects

5.3.1. Jets

Cone-shaped objects which are initiated by a hadron are detected in the calorimeters of ATLAS. For the definition and identification of the jets which are used in the analyses presented in this thesis, the 'anti-k_t jet clustering algorithm' [55] is used. It is therefore briefly summarised in the following. So-called topological clusters are used as input for the algorithm. Such a cluster is formed starting with a 'seed' cell in the calorimeter for which the signal is high compared to the noise. The neighbouring cells which still have a comparably high signal-to-noise ratio are then iteratively added. Finally, all surrounding cells which are direct neighbours to the cluster are added, independent of their signal [56].

The distance between two such entities i and j or the beam axis B is computed with the following formulae:

$$d_{ij} = min(\frac{1}{k_{Ti}^2}, \frac{1}{k_{Tj}^2})\frac{\Delta_{ij}^2}{R^2} \tag{5.1}$$

$$d_{iB} = \frac{1}{k_{Ti}^2}. \tag{5.2}$$

k_T denotes the transverse momentum, $y = \frac{1}{2}\ln\frac{E+p_z}{E-p_z}$ stands for the rapidity, $\Delta_{ij}^2 = (y_i - y_j)^2 + (\phi_i - \phi_j)^2$ defines a distance in the y-ϕ-plane and R is a radius parameter which is set to e.g. 0.4. For all clusters and the beam axis the distances are computed. If the smallest distance is d_{ij}, both entities i and j are combined and the algorithm starts all over again. If the smallest distance is d_{iB}, the cluster i is defined as a jet and no longer considered as an entity during the next run of the algorithm. In the anti-k_t jet clustering algorithm the soft entities, i.e. the ones with low p_T, will cluster

rather with the hard, i.e. high-p_T entities. Therefore the shape of the final jets is not depending much on the soft entities.

JET ENERGY SCALE AND RESOLUTION A calibration procedure is performed to make up for the difference of the energy of the measured jets compared to the energy of the truth jets which is referred to as 'Jet Energy Scale' (JES). Pile-up is one of the reasons why the reconstructed jets need to be calibrated to subtract the additional energy deposits in the calorimeters caused by other close-by proton-proton collisions. An offset correction is applied to the E_T of a jet which depends on the number of primary vertices for the proton-proton collisions, on the jet pseudorapidity and on the bunch spacing. Furthermore the direction of the jet is corrected to let it origin from the primary vertex and not from the geometrical centre of the detector. In a next step the energy of the jet is once more corrected using information from the comparison with truth jets in Monte Carlo simulation [56].

The jet energy resolution (JER) is determined from calorimeter observables, exploiting the transverse momentum balance in events which contain jets with large transverse momenta [57].

JET VERTEX FRACTION The 'Jet Vertex Fraction' (JVF) is the total transverse momentum of tracks in the ID which come from the primary vertex and which are associated to a jet. It is divided by the total transverse momentum of all tracks that are matched to the jet and which originate from any reconstructed vertex [58].

b-TAGGING A b-jet is assumed to be initiated by a b-quark, and hadrons containing a b-quark have a long life-time compared to other hadrons. Therefore the b-hadron can travel through the detector for some time before it decays. The travel path becomes visible because the secondary vertex of the b-decay-process is spatially displaced from the first production vertex. A possibility to classify these jets is the so-called 'b-tagging'. The 'ATLAS MV1 b-tagging algorithm' is a neural network which combines the information from three high-performance taggers which are called 'IP3D', 'SV1' and 'JetFitter'. To find out if a jet is most likely originating from a b-quark, they make use of its transverse and longitudinal impact parameter significances. They reconstruct the inclusive vertex which is formed by the decay products of the b-hadrons. The topology of the primary vertex and of the vertices of the b-decay as well as the flight length significance are parameters which are also taken into account.

The input variables are then compared to smoothed normalised distributions for the b-hadron hypothesis and the background hypothesis by using a likelihood ratio technique [59]. The efficiency for distinguishing between b-jets and other jets is different for data and for Monte Carlo simulation. Therefore scale factors depending on the transverse momentum and on the pseudorapidity of the jets are applied to all Monte Carlo samples to correct for small discrepancies in the b-tagging performance.

5.3.2. Electrons

Electrons interact with the detector material in the ID and in the electromagnetic calorimeter. A seeded calorimeter tower with $E_T > 3$ GeV must match to a track in the ID within a broad window of $\Delta\eta \times \Delta\phi = 0.05 \times 0.10$. At the same time the energy of the calorimeter cluster must not be more than ten times higher than the momentum of the matched track. This identifies electrons in the detector region with $|\eta| < 2.5$. Electrons with $2.5 < |\eta| < 3.7$ can only be reconstructed using the calorimeter clusters since the ID covers only $|\eta| < 2.5$. These electrons can then only be identified with high efficiency in specific processes such as $Z \to ee$ or $H \to eeee$ for which the decay products have e.g. a characteristic total invariant mass which is equal to the mass of the decaying boson.

Since jets also deposit energy in the electromagnetic calorimeter before they enter the outer hadronic calorimeter, it is important to find criteria which clearly distinguish between electron and jet candidates. The overlap removal procedure which is described in Section 5.3.6 rejects jets which are too close to electrons in the meaning of ΔR and and for which most likely the same calorimeter clusters are used to reconstruct a jet and an electron.

Quality Criteria A summary of the quality criteria for electrons [39] is listed in the following:

- 'Loose': Electrons need to have $|\eta| < 2.47$ and the energy leakage into the hadronic calorimeter must not be too high. Requirements are placed on the shower shape variables using the second layer of the electromagnetic calorimeter. The electrons are identified with high efficiency but the background is hardly suppressed.

- 'Medium': Additional cuts are placed on the energy deposits in the first layer of the electromagnetic calorimeter. At least one hit must be recorded in the PD and at least nine in the SCT. The transverse impact parameter d_0 must be shorter than 1 mm. The jet rejection factor is increased by a factor of 3-4 compared to only applying the 'loose' cuts.

- 'Tight': The electrons need to be isolated in addition. This means that they have to fulfil the requirement on the ratio of the transverse energy in a cone around the object with $\Delta R < 0.2$ to the total cluster transverse energy. An electron candidate must have at least one hit in the vertexing layer and the clusters and tracks need to be matching more precisely compared to 'medium' electrons. A certain number of hits is required in the TRT. In general all tools which are available to identify electrons are utilised to define the 'tight' quality criterion. Therefore the identification efficiency for isolated electrons is at minimum and jets are well rejected. The numbers for the identification efficiency are measured depending on the electron p_T and η in [60].

To select events for the physics analysis, the electrons are required to have a certain minimum p_T which is motivated by the trigger strategy and the corresponding turn-on curves of the electron triggers, see e.g. Section 6.7.1. The requirements on the longitudinal and transverse impact parameters are tightened. The electrons have to be isolated referring to their tracks in the ID ('ptcone'), referring to the sum of the calorimeter cells in a cone around the electron candidate in the η-ϕ-space ('etcone') or referring to the sum of the transverse energies of the topological clusters within a cone around the cluster barycentre ('topoEtcone').

A scale factor is applied to Monte-Carlo simulated events which contain an electron to account for the differences in the reconstruction efficiency in data and in Monte Carlo simulations. Furthermore the electron energy is smeared in Monte Carlo events to better reproduce the energy resolution in data.

PHOTONS As explained above, clusters which can be matched to a track are identified as electrons. If a cluster cannot be allocated to a track in the ID and cannot be associated to a conversion, the assigned cluster is considered as a photon candidate [39].

5.3.3. MUONS

Muons are identified and reconstructed using information from the ID and the MS.

STANDALONE For 'standalone' muons only information from the MS is used. The tracks are extrapolated to the beam line. The detector region until $|\eta| < 2.7$ is covered (with gaps at 0.0 and 1.2) by the MS while the ID only reaches until $|\eta| < 2.5$. Soft muons are not easily reconstructed since they do not always reach the outermost layers of the MS.

COMBINED The linked space points in the PD and the SCT are extended to the measurements from the outer layers of the ID. The ID muon tracks are then combined with the MS muon candidates to reconstruct 'combined' muons. Two algorithms are available: 'staco' and 'muid'. The decision if two tracks from the ID and the MS are combined is based on the χ^2 variable. It is a figure of merit for the quality of the match. The difference between 'staco' and 'muid' is that the first algorithm uses a statistical combination of the inner and outer track vectors while the 'muid' algorithm uses the inner track vector together with the covariance matrix and then the outer track to obtain the combined track vector.

SEGMENT-TAGGED For 'segment-tagged' muons, all tracks of the ID with a certain minimum momentum are extrapolated to the innermost stations of the MS. If sufficiently close segments with hits are found, the tracks in the ID are identified as muon candidates. Two examples for algorithms to reconstruct segment-tagged

muons are 'MuTag' and 'MuGirl' [39].

In analogy to the selection of electrons, muons are also required to be isolated, and cuts on the transverse and longitudinal impact parameters of the muon candidates are placed. For Monte Carlo events which contain muons, scale factors are applied in the same way as for electrons and the transverse momenta of the muons are smeared.

5.3.4. Taus

Tau leptons decay into the lighter leptons or into hadrons inside ATLAS. The products of the leptonically decaying taus are not distinguishable from prompt electrons and muons. The products of the hadronically decaying taus on the other hand can be identified.

Taus can decay into hadrons, i.e. pions, for example like $\tau^{\pm} \to \pi^{\pm}\nu_{\tau}$, $\pi^{\pm}\pi^{0}\nu_{\tau}$ and $\pi^{\pm}\pi^{0}\pi^{0}\nu_{\tau}$ with one charged hadron in the final state ('1 prong'), or $\tau^{\pm} \to \pi^{\pm}\pi^{\pm}\pi^{\mp}\nu_{\tau}$ and $\pi^{\pm}\pi^{\pm}\pi^{\mp}\pi^{0}\nu_{\tau}$ with three charged hadrons in the final state ('3-prong'). For their reconstruction, a jet which is identified with the anti-k_t jet clustering algorithm as described in Section 5.3.1 is used. For a 1-prong tau or a 3-prong tau, one or three tracks must be found in the ID in a cone of ΔR <0.2 around the axis of the seed jet. The tracks need to fulfil requirements on the p_T, on the number of hits in the PD and the SCT as well as on the transverse and longitudinal impact parameters. For a better distinction of the taus originating from pile-up vertices and of the taus originating from the primary vertex, a tau jet vertex fraction (TJVF) is used in analogy to the JVF. The algorithms which are implemented for the identification of taus are based on boosted decision trees (BDT algorithm) or on log-likelihood functions (LLH algorithm) [61].

5.3.5. Missing Transverse Energy

The SM neutrinos do not interact with detector material and are therefore invisible. The same holds for the supersymmetric neutralinos which can also not be reconstructed. The amount of energy which the invisible particles carry away can still be estimated due to the law of energy conservation in a closed system: the initial protons only carry momentum in the z-direction, therefore the momenta in the x- and in the y-direction of all the visible and invisible particles must add up to 0.

$$0 = \sum_i p_x^{i,visible} + \sum_i p_x^{i,invisible} = \sum_i p_y^{i,visible} + \sum_i p_y^{i,invisible} \tag{5.3}$$

The 'missing' energy can therefore be assigned to the invisible particles and must be equal to the negative sum of the energy of the visible particles:

$$E_{x(y)}^{miss} = -\sum_i E_{x(y)}^{i,visible}. \tag{5.4}$$

The missing transverse energy is defined as

$$E_T^{miss} = \sqrt{(E_x^{miss})^2 + (E_y^{miss})^2}. \tag{5.5}$$

E_T^{miss} is computed using the energies of the reconstructed and calibrated electrons, photons, muons, taus and jets. A so-called 'soft term' which contains the energy of topological clusters which are not associated to the reconstructed high-p_T physics objects is also added [62].

5.3.6. Overlap Removal Procedure

The following procedure is referred to as the 'overlap removal' (OR). It is performed for each event after the full reconstruction and selection of the physics objects since it is necessary to remove physical objects which are overlapping in the η-ϕ space, i.e. which have a too small $\Delta R = \sqrt{\Delta\eta^2 + \Delta\phi^2}$.

Electron, electron If two electrons are very close to each other (analysis of 2012 data: $\Delta R < 0.05$, 2011: $\Delta R < 0.1$) the one with lower transverse momentum is discarded since it is most likely originating from bremsstrahlung.

Electron, jet If a jet is close to an electron ($\Delta R < 0.2$), it is removed from the event. With high probability the very same cluster in the calorimeter is used for the reconstruction of the two objects.

Tau, electron/muon If a tau which is assumed to have decayed hadronically is close to an electron or a muon ($\Delta R < 0.2$), it is rejected because this tau is then more likely mis-identified.

Jet, electron/muon Electrons and muons which are found close to jets ($\Delta R < 0.4$) are removed. This is motivated by the fact that the leptons could be produced in semi leptonic decays of c- or b-hadrons inside the jet.

Electron, muon If an electron and a muon are found to be very close to each other (analysis of 2012 data: $\Delta R < 0.01$, 2011: $\Delta R < 0.1$), both are removed. The muon most likely emitted bremsstrahlung in the calorimeter and the electron is to be seen as a result of this process.

MUON, MUON If two muons are close to each other ($\Delta R < 0.05$), both are rejected from the object collection since it could be one single muon which is falsely reconstructed as two objects.

JET, TAU If a jet is found close to a hadronically decaying tau ($\Delta R < 0.2$), it is removed.

DILEPTON RESONANCES Low mass dilepton resonances like e.g. the J/ψ meson are removed by requiring that the invariant mass of any dilepton pair with same flavour and opposite signs has to be higher than 12 GeV. Otherwise the whole event is rejected.

5.4. EVENT CLEANING

In addition to a positive trigger decision, an event needs to pass the quality criteria which are listed in the following to be considered for the physics analysis :

- Only events from data runs for which all subdetectors were properly working are used.
- Data events are rejected when the physics objects are pointing to a calorimeter region which is suffering from noise bursts or which could not be read out properly.
- Only events with complete detector information are considered.
- Every event must have a chosen primary vertex. This is the vertex with the highest $\sum p_T^2$ of associated tracks, the other vertices are treated as pile-up. The primary vertex also must have at least five tracks.
- If the charge q and the momentum p of a muon fulfil the equation $\sigma(\frac{q}{p})/|\frac{q}{p}| > 0.2$, the muon is called 'badly' reconstructed and the event is rejected.
- Cosmic muons are identified by requiring $|z_0^{\mathrm{PV}}| > 1$ mm for the longitudinal impact parameter and $|d_0^{\mathrm{PV}}| > 0.2$ mm for the transverse impact parameter with respect to the event primary vertex. Events containing one or more cosmic muons are not considered for the physics analysis.

6. Direct Gaugino and Direct Slepton Production: Analysis and Trigger Studies with $\sqrt{s} = 7$ TeV Data

A search for final states with two leptons (electrons or muons) after the electroweak production of supersymmetric particles in the data recorded with ATLAS in 2011 at a centre-of-mass energy of $\sqrt{s} = 7$ TeV and with an integrated luminosity of 4.7 fb^{-1} is published in [63]. It is presented in this Chapter. The analysis is sensitive to the direct production of pairs of left handed sleptons and pairs of gauginos, while the direct production of right handed sleptons is not addressed because of the very low cross section. Particular attention is paid to the trigger strategy: the efficiency measurements in MC simulations are shown for an electron-muon trigger.

6.1. Addressed SUSY Signal Models

In this analysis the production of gauginos refers to the production of pairs of charginos and neutralinos like $\tilde{\chi}_1^{\pm}\tilde{\chi}_1^{\mp}$, $\tilde{\chi}_2^0\tilde{\chi}_2^0$ and $\tilde{\chi}_1^{\pm}\tilde{\chi}_2^0$. The neutralinos can then further decay into final states with e.g. two charged leptons, $\tilde{\chi}_2^0 \to (l^{\pm}\tilde{l}^{\pm})/(Z\tilde{\chi}_1^0) \to l^{\pm}l^{\mp}\tilde{\chi}_1^0$. The charginos at the same time decay like e.g. $\tilde{\chi}_1^{\pm} \to (W^{\pm}\tilde{\chi}_1^0)/(\tilde{l}^{\pm}\nu)/(l^{\pm}\tilde{\nu}) \to l^{\pm}\nu\tilde{\chi}_1^0$. A hadronic final state is possible via $\tilde{\chi}_1^{\pm} \to W^{\pm}\tilde{\chi}_1^0 \to q\bar{q}'\tilde{\chi}_1^0$.

For charginos as well as for neutralinos the decay through sleptons is possible. For this it is required that the sleptons are light enough to be produced on-shell, i.e. that the mass is sufficiently low and that the equations of motions are fulfilled when these particles are included in the system. The decay of e.g. $\tilde{\chi}_1^{\pm} \to \tilde{l}^{\pm}\nu(l^{\pm}\tilde{\nu}) \to l^{\pm}\nu\tilde{\chi}_1^0$ via an intermediate slepton yields different kinematics compared to the decay via W or Z bosons and the branching ratios for leptonic final states are maximised. This particular process is depicted in Figures 6.1 (a) and (c).

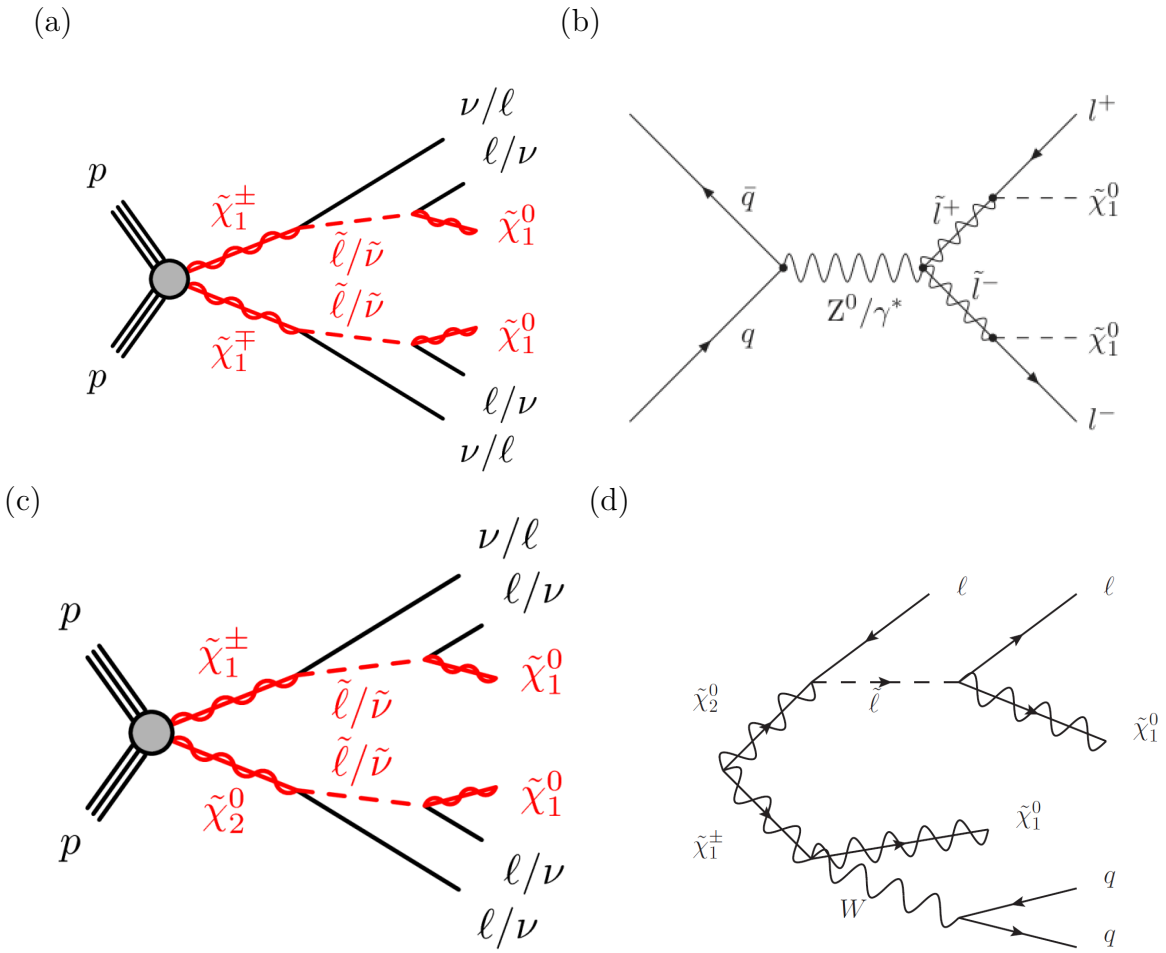

FIGURE 6.1.: *Graphs as examples for the decay chains of electroweakly produced sparticles, leading to two leptons (electrons or muons) in the final state.*
(a) $pp \to \tilde{\chi}_1^{\pm}\tilde{\chi}_1^{\mp} \to \tilde{l}^{\pm}\nu(l^{\pm}\tilde{\nu})\tilde{l}^{\mp}\nu(l^{\mp}\tilde{\nu}) \to (l^{\pm}\nu\tilde{\chi}_1^0)(l^{\mp}\nu\tilde{\chi}_1^0)$
(b) $q\bar{q} \to Z/\gamma^* \to \tilde{l}^{\pm}\tilde{l}^{\mp} \to l^{\pm}l^{\mp}\tilde{\chi}_1^0\tilde{\chi}_1^0$
(c) $pp \to \tilde{\chi}_2^0\tilde{\chi}_1^{\pm} \to \tilde{l}^{\pm}(\to l^{\pm}\tilde{\chi}_1^0)\tilde{l}^{\pm}(\to l^{\pm}\tilde{\chi}_1^0)l^{\mp}\nu$
(d) $pp \to \tilde{\chi}_2^0\tilde{\chi}_1^{\pm} \to (l^{\pm}l^{\mp}\tilde{\chi}_1^0)(qq\tilde{\chi}_1^0)$

All the diagrams shown in Figure 6.1 give examples for the possible decay chains after the direct production of sleptons or gauginos with two leptons in the final state. For the scenarios with a third lepton in the final state it is assumed that this lepton is not identified. In this way the analysis is orthogonal to the analysis that searches for SUSY in final states with three identified leptons. The direct production of two opposite sign sleptons is similar to the Drell-Yan production [64] and will lead to two same flavor (SF) leptons with opposite signs (OS) as well as two neutralinos in the final state, $\tilde{l}^{\pm}\tilde{l}^{\mp} \rightarrow l^{\pm}l^{\mp}\tilde{\chi}_1^0\tilde{\chi}_1^0$, and is depicted in Figure 6.1 (b).

One of the SUSY models considered for the search for direct slepton and for direct gaugino production is the pMSSM. For this model the results are interpreted by setting limits on the masses of the sleptons and neutralinos. The signal grid is Monte Carlo simulated with HERWIG [46]. The masses of the squarks, gluinos, staus and gauginos except for the $\tilde{\chi}_1^0$ are set to 2.5 TeV. The mass of the bino-like lightest neutralino $\tilde{\chi}_1^0$ is varied by scanning M_1 in 20-GeV-steps from 20 to 160 GeV. The mass of the selectron equals the mass of the smuon and is generated from 70 to 90 GeV in 20-GeV steps. The cross section decreases from 3.9 to 0.05 pb for $m_{\tilde{l}}$ rising from 70 to 190 GeV.

For the direct gaugino production, simplified models are used in which only the masses of the $\tilde{\chi}_1^0$, $\tilde{\nu}$, $\tilde{l}$, $\tilde{\chi}_1^{\pm}$ and $\tilde{\chi}_2^0$ are free parameters. Limits on the masses of the lightest neutralino and the chargino are deduced. The mass points of the grid are simulated with 'Herwig++' [65]. The $\tilde{\chi}_2^0$ is assumed to be wino-like, the $\tilde{\chi}_1^0$ is bino-like. The masses of the charged and the uncharged sleptons (i.e. the selectrons and the smuons) are degenerate and are set to $m_{\tilde{\nu}} = m_{\tilde{l}_L} = \frac{m_{\tilde{\chi}_1^0} + m_{\tilde{\chi}_1^{\pm}}}{2}$. The masses of the squarks, the gluinos and the staus are set to 2 TeV. The production cross section decreases from 3 pb for $m_{\tilde{\chi}_1^{\pm}} = 50$ GeV to 0.2 pb for $m_{\tilde{\chi}_1^{\pm}} > 200$ GeV.

6.2. SM Background

The SM background processes may have signatures which are very similar to the ones of the SUSY scenarios described above. For example the fully leptonic decay of a pair of top quarks also results in a final state with two OS leptons, $t\bar{t} \rightarrow (W^+b)(W^-\bar{b}) \rightarrow (l^+\bar{\nu}b)(l^-\nu\bar{b})$. This process is MC simulated with the POWHEG generator [66], using a top-quark mass of 172.5 GeV. $W \rightarrow l\nu$ or $Z \rightarrow l^+l^- + jets$ processes are generated with ALPGEN [52]. Diboson processes also contribute to the SM background: WW, WZ and ZZ are simulated with SHERPA [48] in the signal regions which require jets and with HERWIG [46] for all the other regions. The MC@NLO tool [49]- [51] is used for the simulation of the single top production.

6.3. Physics Object Definition

Events are selected as described in Section 5.4 and the physics objects are selected according to the algorithms presented in Section 5.3. They undergo the overlap removal from Section 5.3.6 except for the steps where tau objects are considered and the 'muon, muon' step.

Electrons Electrons are reconstructed with tight quality criteria and have $p_T >$ 10 GeV and $|\eta| < 2.47$. They are isolated; that means that the sum of the p_T of all tracks with $p_T >$10 GeV in a cone of $\Delta R = \sqrt{\Delta\eta^2 + \Delta\phi^2} = 0.2$ ('ptcone20') is smaller than 10% of the p_T of the electron.

Muons Muons must be reconstructed with the 'staco' algorithm for combined MS and ID measurements or with the 'segment-tagged' algorithm. They must fulfil a list of quality requirements, i.e. have a certain number of hits in the PD, the TRT and the SCT. The transverse momentum must be larger than 10 GeV and $|\eta| < 2.4$. They must be isolated, i.e. the sum of the p_T of all tracks in a cone with $\Delta R = 0.2$ ('ptcone20') is smaller than 1.8 GeV.

Jets Jets must have $p_T > 30$ GeV and $|\eta| < 2.5$ as well as a JVF of more than 0.75. b-jets are reconstructed with 80% efficiency for the b-tagging. The efficiency is determined in MC simulated $t\bar{t}$ samples. The misidentification rate for light-quark jets or gluon jets is less than 1%.

E_T^{miss} To calculate the missing transverse energy, all electrons, muons, jets and clusters of energy with $|\eta| < 4.9$ that are not associated to one of the other objects are taken into account. Instead of E_T^{miss}, $E_T^{miss,rel}$, the 'relative missing transverse energy', is used if the azimuthal angle, $\Delta\phi_{l,j}$, between the nearest lepton (l) or jet (j) and E_T^{miss} is smaller than $\frac{\pi}{2}$:

$$E_T^{miss,rel} = E_T^{miss} \cdot \sin\Delta\phi_{l,j} \tag{6.1}$$

This variable is introduced to suppress fake E_T^{miss} from $Z/\gamma^* \to ll + jets$ events and to reduce $Z/\gamma^* \to \tau\tau \to ee, e\mu, \mu\mu$ because in such events the missing transverse energy can be aligned with the direction of the mis-measured leptons.

6.4. Discriminating Variables

6.4.1. Stransverse Mass

Sensitivity to the SUSY signal is in this analysis mainly achieved by making use of a variable which is called 'stransverse mass' (m_{T2}). For events with pair-produced identical particles which decay into a final state with two visible and two (or more) invisible particles as in $\tilde{l}^{\pm}\tilde{l}^{\mp} \to l^{\pm}l^{\mp}\tilde{\chi}_1^0\tilde{\chi}_1^0$ or $\tilde{\chi}_1^{\pm}\tilde{\chi}_1^{\mp} \to (l^{\pm}\nu\tilde{\chi}_1^0)(l^{\mp}\nu\tilde{\chi}_1^0)$, the m_{T2} distribution has a characteristic kinematic endpoint which indicates the true mass of the $\tilde{l}^{\pm}$ or $\tilde{\chi}_1^{\pm}$.
The stransverse mass is based on the '(co-)transverse mass' m_T which is invariant under co-linear equal-magnitude Lorentz transformations in the z-direction; both decay products are boosted into the same frame. It is defined as $m_T = \sqrt{m^2 + p_x^2 + p_y^2}$ for a mother particle with the mass m and the momentum components p_x and p_y. For a two-body decay into a final state with one visible lepton and (at least) one invisible particle, the formula becomes

$$m_{\mathrm{T}} = \sqrt{2E_{\mathrm{T}}^{\mathrm{l}}E_{\mathrm{T}}^{\mathrm{miss}}(1-\cos\phi)} \tag{6.2}$$

where $E_{\mathrm{T}}^{\mathrm{l}}$ denotes the transverse energy of a lepton, $E_{\mathrm{T}}^{\mathrm{miss}}$ is the missing transverse energy of the event and ϕ is the angle between the lepton and the $E_{\mathrm{T}}^{\mathrm{miss}}$ component in the transverse plane. To obtain Equation 6.2, the masses of the daughter particles are assumed to be negligible with respect to the mass of the mother particle. The distribution of m_T has an endpoint at the mass of the mother particle in the two-body decay, $m_T \leq m$.

If the transverse momenta of the individual invisible decay products after the decay of $\tilde{l}^{\pm}\tilde{l}^{\mp}$ or $\tilde{\chi}_1^{\pm}\tilde{\chi}_1^{\mp}$ were known, the transverse masses of the sleptons or charginos could be individually computed. The maximum value of the transverse masses would allow to deduce a lower bound on the mass of the slepton or chargino. However, no information about how much missing transverse energy is contributed by which invisible final state particle exists, therefore the test values $\vec{q}_{\mathrm{T}}$ or $\vec{r}_{\mathrm{T}}$ for the momenta of the invisible final state particles in each leg of the sparticle-pair decay are used. The values of $\vec{q}_{\mathrm{T}}$ and $\vec{r}_{\mathrm{T}}$ are chosen in such way that they minimise the maximum of the transverse masses to not arbitrarily increase the lower bound on the slepton or chargino mass.

To obtain m_{T2} in an event, $\vec{p}_{\mathrm{T}}^{miss}$ is decomposed in $\vec{q}_{\mathrm{T}} + \vec{r}_{\mathrm{T}} = \vec{p}_{\mathrm{T}}^{miss}$ and the transverse masses are computed for the lepton with higher transverse momentum, $\vec{p}_{\mathrm{T}}^{l_1}$, and for the lepton with lower transverse momentum, $\vec{p}_{\mathrm{T}}^{l_2}$. The complete formula is

$$m_{\mathrm{T2}} = \min_{\vec{q}_{\mathrm{T}}+\vec{r}_{\mathrm{T}}=\vec{p}_{\mathrm{T}}^{\mathrm{miss}}} [\max(m_{\mathrm{T}}(\vec{p}_{\mathrm{T}}^{l_1}, \vec{q}_{\mathrm{T}}), m_{\mathrm{T}}(\vec{p}_{\mathrm{T}}^{l_2}, \vec{r}_{\mathrm{T}}))] \tag{6.3}$$

where the maximum is minimised by varying the decomposition of $\vec{p}_{\mathrm{T}}^{miss}$ [67].

6.4.2. Contransverse Mass

Another variable called 'contransverse mass' (m_{CT}) is used to remove events which are most likely from a $t\bar{t}$ process. The decay of two top quarks is an important background contribution to e.g. the signal process $\tilde{\chi}_2^0\tilde{\chi}_1 \rightarrow (l^{\pm}l^{\mp}\tilde{\chi}_1^0) + (q\bar{q}'\tilde{\chi}_1^0)$ since it can also lead to two OS leptons, jets and missing transverse energy in the final state via the fully leptonic decay $t\bar{t} \rightarrow (W^+b)(W^-\bar{b}) \rightarrow (l^+\bar{\nu}b)(l^-\nu\bar{b})$. The contransverse mass is defined as

$$m_{CT} = \sqrt{[E_T(v_1) + E_T(v_2)]^2 - [\vec{p}_T(v_1) - \vec{p}_T(v_2)]^2} \tag{6.4}$$

where v_1 and v_2 can be leptons or jets or lepton-jet combinations. The quantity is constructed from the momentum components measured in the laboratory plane transverse to the beam direction and is invariant under equal-magnitude Lorentz transformations in opposite directions, i.e. contra-linear boosts.
The contransverse mass is not representing the mass of a particle δ_i which decayed to produce v_i. The distribution of m_{CT} is nevertheless expected to show a characteristic endpoint as it is depending on $\vec{p}_T(v_1)$ and $\vec{p}_T(v_2)$ which in turn are bound by the mass of the mother particles δ_1 and δ_2. This is due to the fact that m_{δ_i} can be calculated from $\vec{p}_T(v_i)$:

$$\frac{m_{\delta_i}}{2} = |\vec{p}(v_i)| = \vec{p}_T(v_i) sin^{-1}(\theta_i) \tag{6.5}$$

with θ_i being the polar angle relative to the beam direction [68].

Since m_{CT} is bound by the masses of the top quarks or of the W bosons in a $t\bar{t}$ event, one can use this condition and veto those events which have values of the contransverse mass similar to the ones which are measured for $t\bar{t}$ events.

6.5. Signal Regions

To address the processes where sparticles are produced electroweakly and decay into final states with two leptons, four signal regions (SRs) are designed. They are summarised in Table 6.1.

TABLE 6.1.: *Summary of the four signal region definitions. 'OS' means oppositely charged leptons, 'SS' means that the two leptons carry the same charge. 'Z-veto' refers to $|m_{ll} - m_Z| > 10$ GeV with m_{ll} being the invariant mass of the two leptons.*

Requirements	*SR-m_{T2}*	*SR-OSjetveto*	*SR-SSjetveto*	*SR-2jets*
Charge	OS	OS	SS	OS
Flavour	any	any	any	SF
m_{ll}	Z-veto	Z-veto		Z-veto
Number of jets	0	0	0	≥ 2
Number of b-jets	-	-	-	0
$E_T^{miss,rel}$	> 40 GeV	> 100 GeV	> 100 GeV	> 50 GeV
Other	$m_{T2} > 90$ GeV	-	-	m_{CT}-veto

SR-m_{T2} *SR-m_{T2}* requires two OS leptons which may be of same or opposite flavour, a jet-veto and a relative missing transverse energy of more than 40 GeV. 'Jet veto' means that no events are considered which contain any reconstructed jet. Events where the invariant mass of the two leptons, m_{ll}, is inside a window of ± 10 GeV around the mass of the Z boson (91.2 GeV) are vetoed ('Z-veto'). The stransverse mass variable m_{T2} must be larger than 90 GeV. It therefore provides sensitivity to the processes $\tilde{\chi}_1^{\pm}\tilde{\chi}_1^{\mp} \rightarrow \tilde{l}^{\pm}\nu(l^{\pm}\tilde{\nu})\tilde{l}^{\mp}\nu(l^{\mp}\tilde{\nu}) \rightarrow (l^{\pm}\nu\tilde{\chi}_1^0)(l^{\mp}\nu\tilde{\chi}_1^0)$ and $\tilde{l}^{\pm}\tilde{l}^{\mp} \rightarrow l^{\pm}l^{\mp}\tilde{\chi}_1^0\tilde{\chi}_1^0$, illustrated in Figures 6.1 (a) and (b). Decay chains without intermediate sleptons are not considered since they hardly contribute compared to the scenarios with intermediate sleptons.

SR-OSjetveto The process without any jet in the final state but with two OS leptons, $\tilde{\chi}_2^0\tilde{\chi}_1^{\pm} \rightarrow \tilde{l}^{\pm}\tilde{l}^{\mp}l^{\pm}\nu \rightarrow (l_{unid}^{\pm}\tilde{\chi}_1^0)(l^{\mp}\tilde{\chi}_1^0)(l^{\pm}\nu)$, which is depicted in Figure 6.1 (c), (one of the same sign (SS) leptons is not identified, l_{unid}), and $\tilde{\chi}_1^{\pm}\tilde{\chi}_1^{\mp} \rightarrow \tilde{l}^{\pm}\nu(l^{\pm}\tilde{\nu})\tilde{l}^{\mp}\nu(l^{\mp}\tilde{\nu}) \rightarrow (l^{\pm}\nu\tilde{\chi}_1^0)(l^{\mp}\nu\tilde{\chi}_1^0)$ are addressed by a second SR, *SR-OSjetveto*. In addition to the jet-veto and to the Z-veto, in this SR it is required that $E_T^{miss} > 100$ GeV.

SR-SSjetveto From the process $\tilde{\chi}_2^0\tilde{\chi}_1^{\pm} \rightarrow \tilde{l}^{\pm}\nu(l^{\pm}\tilde{\nu}\tilde{l}^{\pm}l^{\mp}) \rightarrow (l^{\mp}l_{unid}^{\pm}\tilde{\chi}_j^0)(l^{\mp}\nu\tilde{\chi}_1^0)$ can also result a signature with two SS leptons and no jets when the third OS lepton is not identified. In addition to the two SS leptons and the jet-veto, $E_T^{miss,rel} > 100$ GeV is demanded for *SR-SSjetveto*.

SR-2jets A final state with two additional jets can arise e.g. from the process where a chargino decays hadronically in association to a neutralino: $\tilde{\chi}_2^0\tilde{\chi}_1^{\pm} \rightarrow (l^{\pm}l^{\mp}\tilde{\chi}_1^0)(q\bar{q}'\tilde{\chi}_1^0)$, the scenario is depicted in Figure 6.1 (d). *SR-2jets* therefore requires at least two jets,

no b-jets, two OS leptons, a Z-veto, $E_T^{miss,rel} > 50$ GeV and a veto on events where the value of m_{CT} is compatible to the one of a $t\bar{t}$ topology ('m_{CT}-veto').

6.6. Background Estimation

The event yields in the SRs due to SM background processes are estimated based on the event yields in control regions (CRs) which are enriched in a particular SM background process. The control regions are in general designed in such a way that they are kinematically very close to the corresponding signal region.

Top A physical process which provides the same signature as the SUSY signal process addressed by *SR-2jets* is the decay of a pair of top and anti-top quarks. The Monte Carlo simulation of $t\bar{t}$ and single top is compared to data in a control region. It is defined by requiring at least two jets, one must be b-tagged, the Z-veto and $E_T^{miss} > 40$, 50, 100 GeV (for the CRs corresponding to *SR-m_{T2}*, *SR-2jets*, *SR-OSjetveto*). Top events contribute more than 96% to the total yield in this CR. The number of top events in the SR, N_{SR}, follows from the number of data events in the CR, N_{CR}, after subtracting non-top backgrounds, multiplied by the transfer factor $\tau = \frac{N_{SR}^{MC}}{N_{CR}^{MC}}$. A scaling factor S_τ is applied to account for the different jet-veto efficiencies in data and MC:

$$N_{SR} = \frac{N_{SR}^{MC}}{N_{CR}^{MC}} \cdot N_{CR} \cdot S_\tau. \tag{6.6}$$

Z + X The $Z+X$ background consists of the $Z/\gamma^* + jets$, ZW and ZZ processes. It is estimated by normalising MC to data in a CR which requires the invariant mass of the two SFOS leptons in an event to be inside the window of ± 10 GeV around the mass of the Z boson. The Z-veto is therefore reverted. For *SR-m_{T2}*, the normalisation is performed before the cut on m_{T2}. Furthermore $E_T^{miss} > 40$, 50, 100 GeV is required, as well as ≥ 0, ≥ 2, $= 0$ jets and ≥ 0, $= 0$, ≥ 0 b-jets in the event (for the CRs corresponding to *SR-m_{T2}*, *SR-2jets*, *SR-OSjetveto*). For the CR corresponding to *SR-2jets*, the m_{CT}-veto is applied.

In data, the contamination by other processes inside this CR which is based on the Z-window is subtracted. It is measured to be less than 2%. For the subtraction, events with one electron and one muon in the final state which have an invariant mass close to the mass of the Z-boson are selected. A correction factor needs to be applied due to the different reconstruction efficiencies of the electrons and the muons. The subtraction also removes events from $Z/\gamma^* \to \tau\tau + jets$ processes. Because of the comparably small branching ratios for e.g. $Z \to \tau\tau \to l\nu\nu l\nu\nu$, the background contribution from $Z/\gamma^* \to \tau\tau + jets$ is estimated solely with MC simulation.

WW To estimate the WW background for *SR-m_{T2}*, the MC simulation is used. For the other SRs, a CR which requires $70 < E_T^{miss} < 100$ GeV is designed to be orthogonal to the SRs. A Z-veto and a jet-veto are applied. The contamination from top-quark events is 24% although an additional b-jet veto is applied. MC is then normalised to data in the CR.

The definitions of the three CRs are summarised in Table 6.2.

TABLE 6.2.: *Summary of the CR definitions for the estimation of the SM background processes for the decay of top quarks, $Z/\gamma^* \to ll$ and diboson processes. When the definition of a CR differs for the three OS SRs, the conditions are given as a comma-separated list (SR-m_{T2}, SR-2jets, SR-OSjetveto). 'Z-veto' refers to $|m_{ll} - m_Z| > 10$ GeV with m_{ll} being the invariant mass of the two leptons. 'Z-window' defines the reverse.*

Requirements	Top	$Z+X$	WW
m_{ll}	Z-veto	Z-window	Z-veto
Number of jets	≥ 2	$= 0, \geq 2, \geq 0$	$= 0$
Number of b-jets	≥ 1	$\geq 0, = 0, \geq 0$	$= 0$
$E_T^{miss,rel}$	> 40, 50, 100 GeV	> 40, 50, 100 GeV	70-100 GeV
Other	-	-, m_{CT}-veto, -	-

NON-PROMPT LEPTONS Jets can be mis-identified as leptons or leptons can originate from leptonic decays of hadrons. Conversions where a photon was emitted after the interaction of an electron with the detector material and where the photon then decays into e^+e^- are another possible source of non-prompt leptons. The detector signature based on these objects is called 'fake' background. In the presented analysis this background is estimated using the 'Matrix Method'. A formula relates the true composition of a sample in terms of real and fake leptons with its observable, i.e. measurable composition in terms of leptons reconstructed with more or less tight quality requirements. A detailed description for this method is given in Section 8.6.1.1.

CHARGE FLIP A trident event occurs when an electron emits a hard photon which again produces an electron-positron pair with a high-p_T positron, $e^{\pm} \to e^{\pm}\gamma_{hard} \to e^{\pm}(e^{\pm}_{hard}e^{\mp})$. This results in a SS event where the electron seems to flip its charge and the third lepton is not selected because it is too soft. The probability for this to happen is found to be negligible for muons. For electrons, it is measured in data with a likelihood method. To estimate the number of events with two OS leptons which appear as SS leptons, the probability is applied to MC events coming from $t\bar{t} \to e^{\pm}l^{\mp}$, $Z + jets$ and diboson processes.

6.7. Trigger Studies

The trigger configurations which can be useful for an analysis selecting events with two leptons in the final state and which were deployed during the 2011 data taking require one or two leptons with a certain minimum p_T and a certain reconstruction quality.

Single lepton triggers in general have a higher p_T threshold than dilepton triggers which require at least two leptons with a definite minimum p_T. The request of only one lepton is less strict and the data taking rate would be too high with a lower p_T threshold. Combining single and dilepton triggers optimises the coverage of the surface which is spanned by the p_T of the two leptons in an event.

6.7.1. Trigger Menu

Table 6.3.: *Lepton triggers used for the $\sqrt{s}=7$ TeV analysis. The corresponding offline p_T thresholds for the triggering objects and the data taking period in which the triggers are deployed are also given.*

Trigger configuration	Offline p_T threshold	Data taking period
e20_medium	25 GeV	A-J
e22_medium	25 GeV	K
e22vh_medium	25 GeV	L-M
2e12_medium	17 GeV	A-J
2e12T_medium	17 GeV	K
2e12Tvh_medium	17 GeV	L-M
mu18	20 GeV	A-I
mu18_medium	20 GeV	J-M
2mu10_loose	12 GeV	A-M
e10_medium_mu6	15 GeV, 8 GeV	A-M

The eligible triggers are listed in Table 6.3. The trigger configuration corresponds to the requirements on the Event Filter level of the ATLAS trigger system. A p_T threshold of e.g. 10 GeV for electrons on Event Filter level does not directly translate in a 10-GeV-p_T threshold for electrons after offline reconstruction; the algorithms which are run to reconstruct the electrons are not the same and therefore the p_T values may differ. For triggers, a figure of merit with high validity is the efficiency, defined as the number of events which passed a particular trigger, divided by the number of all events considered:

$$\epsilon = \frac{N_{triggered}}{N_{total}}. \tag{6.7}$$

The current convention is to choose the threshold where the 'turn-on curve' of the trigger, i.e. the p_T-dependent efficiency curve, reaches 90% of the plateau efficiency, as the offline p_T value. Events which contain leptons falling in the p_T range for which the efficiency is not stable should not be used in the analysis. An example is given in Section 6.7.3.

In comparison to electron triggers, muon triggers are less efficient due to the lower acceptance of muons. The MS cannot completely cover the whole solid angle. The logical OR of the single muon trigger and the dimuon trigger increases the muon trigger efficiency significantly and is therefore used for this analysis.

For individual areas of the p_T-surface for two muons ($\mu\mu$), two electrons ($e\mu$) or one muon and one electron ($e\mu$) in the final state, the most efficient trigger combination is chosen. The coverage is depicted in Figure 6.2.

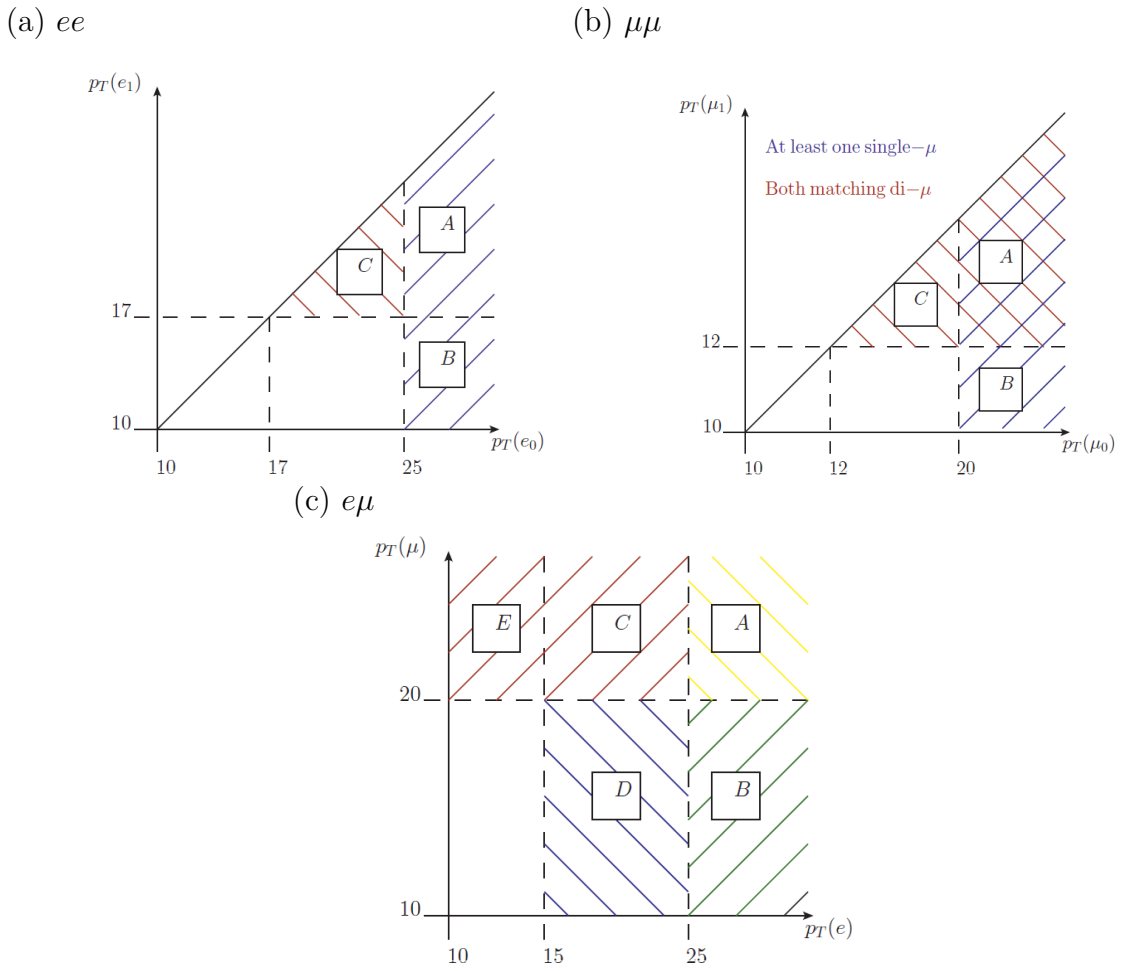

FIGURE 6.2.: *The diagrams show the surface spanned by the p_T of the two leptons in an event. The surfaces are covered by the single and dilepton triggers depending on the lepton flavours in the dilepton final state. The diagram in (a) shows the coverage for an electron with higher momentum ($p_T(e_0)$) and an electron with lower momentum ($p_T(e_1)$). For an event falling in regions A or B, the single lepton trigger must have a positive decision. For region C, the dielectron trigger is requested. For the final state with two muons, depicted in (b), single and dimuon triggers are combined with logical OR for region A, in region B the single muon trigger and in region C the dimuon trigger is used. For the $e\mu$ final state, single electron and single muon triggers are combined with logical OR in region A, region B is covered by the single electron trigger, C and E by the single muon trigger and D by the electron-muon trigger.*

A data event must have a positive trigger decision to be selected for analysis. In addition, one of the two offline leptons must be matched uniquely to the online object which caused the trigger. This is done in the η-ϕ space by requiring that $\Delta R = \sqrt{\Delta\eta^2 + \Delta\phi^2}$ between the offline and online object is smaller than 0.15. No other offline object may be closer to the online object and no other online object may be closer to the offline object.

6.7.2. Trigger Reweighting

Scale Factors The performance of the triggers is modelled in Monte Carlo simulated data, however the efficiencies in data and MC are not 100% comparable. Discrepancies are taken into account by applying a scale factor for each MC event which passed the simulated trigger. This reflects the actual detector performance. Such scale factor is defined as

$$SF = \frac{\epsilon_{data}}{\epsilon_{MC}}, \tag{6.8}$$

where ϵ_{data} is the trigger efficiency measured in data and ϵ_{MC} is the efficiency of the simulated trigger. The scale factor for a particular trigger is mapped in a meaningful parametrisation concerning the kinematics of the physics objects and is provided by the ATLAS trigger performance groups. However, not all possible combinations of various triggers with logical OR are covered. To determine the uncertainty on the event yield due to trigger efficiency measurements, the scale factors are treated as 100% correlated, which is not always true. Moreover only using MC events where the simulated trigger has as positive decision leads to a loss of MC statistics of (1 - ϵ) although the generation of those events is CPU-intensive.

Reweighting Method An alternative approach to using the trigger simulation is the 'Reweighting Method'. Each MC simulated event is weighted with the probability that this event has a positive trigger decision in the actual data taking. The probability is computed from the trigger efficiencies measured in ATLAS data. The uncertainties on the event yield due to the Reweighting Method can be deduced from the statistical uncertainties of the trigger efficiencies measured in data as well as from systematic errors.

The efficiencies and thus the weights can be strongly depending on the parametrisation concerning the kinematics of the trigger objects. The parametrisation and the binning of these kinematic variables needs to be chosen carefully [69].

To show the validity of the Reweighting Method, a closure test is performed. The outcome of the Reweighting Method is compared to the event yield when using the simulated triggers. A good agreement must be achieved between the estimated uncertainties.

PROBABILITIES The probability for an event to be triggered by a dilepton or a single lepton trigger is

$$P(2l \vee 1l) = P(1l) + P(2l|!1l) \cdot P(1 - P(1l)), \tag{6.9}$$

where $P(1l)$ is the probability for the single lepton trigger to have a positive decision. To compute $P(2l \vee 1l)$, the conditional probability $P(2l|!1l)$, the dilepton trigger having a positive decision while the single lepton trigger does not, also needs to be measured.

The probability for a single lepton trigger to have a positive decision in an event with n leptons, where the ith lepton has the kinematic-dependent efficiency ϵ_i, is

$$P(1l) = 1 - \prod_{i=1}^{n} (1 - \epsilon_i). \tag{6.10}$$

For an event with n leptons, the probability for a dilepton trigger to have a positive decision becomes

$$P(2l) = 1 - \prod_{j=1}^{n} (1 - \epsilon_j) - \sum_{j=1}^{n} \epsilon_j \prod_{i=1, i \neq j}^{n} (1 - \epsilon_i). \tag{6.11}$$

This is based on the assumption of the factorisability of the probability for a positive dilepton trigger decision,

$$P(A \wedge B) = P(A) \cdot P(B), \tag{6.12}$$

provided that $P(A)$ and $P(B)$ are stochastically independent.

6.7.3. TRIGGER EFFICIENCIES

As an example, in the following the measurement of the efficiencies for the electron-muon trigger as well as the closure test for the Reweighting Method will be discussed.

TAG & PROBE METHOD To study the performance of the triggers, to deduce the offline p_T values for the leptons and to compute the weights for Monte Carlo events, the single lepton trigger efficiencies are measured with the 'Tag & Probe Method'. Events in which a Z boson decays into two OS leptons are selected by requiring an invariant mass of the two SF leptons close to the mass of the Z boson, i.e. $|m_{ll} - m_Z| < 15$ GeV, $m_Z = 91.2$ GeV. The idea is to tag one of the two leptons and to then have a sample of probe leptons (the other daughter particle of the Z boson) which is used to measure the trigger efficiency. The tagging is done by requiring that the lowest p_T unprescaled trigger was released by that lepton, i.e. matching the offline probe lepton to the lepton on trigger level in the η-ϕ space.

The efficiency of the trigger of interest is measured by counting the number of probe leptons for which the trigger has a positive decision and for which the offline

probe lepton can be matched to the online lepton,

$$\epsilon = \frac{N_{probe\ leptons\ triggered\ and\ matched}}{N_{all\ probe\ leptons}}. \tag{6.13}$$

Each event is processed twice, investigating if also the second lepton can be tagged which means that the first lepton becomes the probe lepton.

SINGLE LEPTON TRIGGER EFFICIENCIES To study the electron-muon trigger, the efficiencies of the individual legs, i.e. e10_medium and mu6, need to be measured. $Z \to e^+e^-$ events are selected e.g. in ALPGENJIMMY MC samples [47], [52] and one of the two electrons is tagged if the lowest p_T unprescaled electron trigger, i.e. e20_medium, has a positive decision and if the offline electron with $p_T > 20$ GeV can be matched to the online electron on Event Filter level with $\Delta R < 0.15$. The efficiency e10_medium is then measured by counting the number of probe electrons which can be matched to an online electron which caused the e10_medium trigger.
The efficiency of the muon leg, mu6, is deduced from all MC events which have a positive trigger decision due to their muon signature. One of the offline muons in a $Z \to \mu^+\mu^-$ event in ALPGENJIMMY MC samples is tagged if it caused mu18, i.e. it can be matched by $\Delta R < 0.15$ to the online muon on Event Filter level which unleashed the lowest p_T unprescaled muon trigger and which has $p_T > 20$ GeV. The efficiency of mu6 is then given by the number of probe muons which can be matched to the online muon that released mu6, divided by the number of all probe muons.

What is meant by the expression 'turn-on curve' becomes clear looking at Figure 6.3 where the efficiencies of the single lepton triggers e10_medium and mu6 are shown. The efficiency of e10_medium is plotted with blue lines, depending on the offline p_T. The errors (shown as vertical lines in each bin) correspond to the statistical uncertainties. The trigger is not fully turned on, i.e. does not become fully efficient, as soon as the offline p_T threshold of 10 GeV is reached. Some events which have an offline p_T of less than 10 GeV already pass the trigger and not all events with $p_T \geq 10$ GeV are selected. An additional requirement on the offline p_T is placed to ensure that the efficiency is not strongly depending on the transverse momentum. In the case of the e10_medium trigger the threshold is 15 GeV. A horizontal line can be fit to the curve at an absolute 'plateau efficiency' of 98%.

The efficiency of the mu6 trigger is strongly depending on the pseudorapidity of the offline muon. Therefore it is shown once for the endcap region ($|\eta| > 1.05$) of the detector where the trigger becomes at maximum 88% efficient and once for the the barrel region ($|\eta| \leq 1.05$) where the trigger reaches the plateau at only 75% due to lower acceptance. The trigger is fully turned on at 8 GeV.

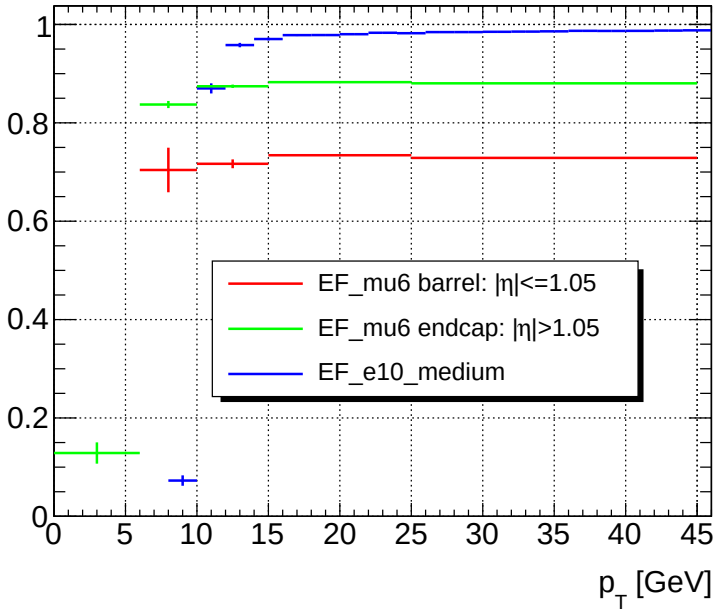

FIGURE 6.3.: *The efficiencies of the single lepton triggers e10_medium (blue) and mu6 for muons in the barrel ($|\eta| \leq 1.05$) (red) or endcap region ($|\eta| > 1.05$) (green) of ATLAS. The efficiencies are measured with the Tag & Probe Method in MC simulation and are shown depending on the p_T of the probe lepton. The errors show the statistical uncertainty due to the limited number of generated events.*

FACTORISABILITY OF DILEPTON TRIGGER EFFICIENCY The event and object selections as described in Section 6.3 are applied on a MC $t\bar{t}$ sample. The sample is generated with MC@NLO [49]- [51] JIMMY [47] with $\sigma \times BR_{dileptonic} = 98$ pb and 1 500 000 events. One electron and one muon are requested in the final state, the requirement on the lepton p_T is relaxed to 5 GeV.

The ratio of the number of events in which the electron-muon trigger has a positive decision over the number of all events is shown depending on the transverse momentum of the electron in Figure 6.4 (a) and depending on the transverse momentum of the muon in 6.4 (b). For muons detected in the barrel region of the detector the efficiency is shown in green colour, for muons in the endcap in red colour. The plateau values are reached at 70% and 85%, respectively.

(a) (b)

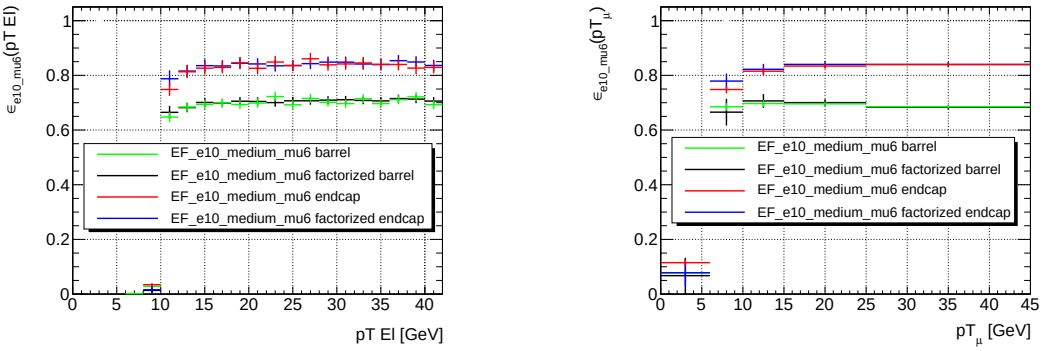

FIGURE 6.4.: *The factorised electron-muon trigger efficiency (black, blue) depending on the p_T of the electron (a) and muon (b) as well as the electron-muon trigger efficiency (green, red). All efficiencies are obtained from the MC trigger simulation. The efficiencies are shown for muons in the barrel ($|\eta| \leq 1.05$) (green, black) and endcap ($|\eta| > 1.05$) (red, blue) regions. The error is the statistical uncertainty due to the limited number of generated events.*

The efficiency of the electron-muon trigger as a function of the p_T of the electron is

$$\epsilon_{e10\_medium\_mu6}(p_T^{el}) = \int_0^\infty \epsilon_{e10\_mu6}(p_T^{el}, p_T^{\mu}) \cdot f(p_T^{el}; p_T^{\mu})\, dp_T^{\mu} \tag{6.14}$$

and as a function of the p_T of the muon

$$\epsilon_{e10\_medium\_mu6}(p_T^{\mu}) = \int_0^\infty \epsilon_{e10\_mu6}(p_T^{el}, p_T^{\mu}) \cdot f(p_T^{\mu}; p_T^{el})\, dp_T^{el}. \tag{6.15}$$

The probability function $f(p_T^{el}; p_T^{\mu})$ is derived from the distribution of the lepton transverse momenta.

To obtain the factorised efficiency of the dilepton trigger depending e.g. on p_T^{el}, the single lepton efficiencies are plugged in the following formula:

$$\epsilon_{e10\_medium\_mu6}(p_T^{el}) = \epsilon_{e10\_medium}(p_T^{el}) \int_0^{\infty} \epsilon_{mu6}(p_T^{\mu}) \cdot f(p_T^{el}; p_T^{\mu})\, dp_T^{\mu}. \tag{6.16}$$

The factorised efficiency is then plotted for electrons in Figure 6.4 (a) and for muons in 6.4 (b), split for barrel and endcap muons. The good agreement with the green and red curves, respectively, proves that the factorisability assumption holds and therefore that ϵ_{e10_medium} and ϵ_{mu6} are independent as expected.

6.7.4. Closure Test and Systematic Uncertainties

To perform the closure test which shows the validity of the Reweighting Method, the efficiencies are measured from $Z \to l^+l^-$ MC events with the Tag & Probe Method as described in the previous Section. They are parametrised in p_T, η and ϕ of the offline leptons. The binning is chosen according to the recommendations of the ATLAS trigger performance groups to optimally reflect the dependencies of the efficiencies. The last bin for the p_T dependency starts at 60 GeV for electrons and 45 GeV for muons to take into account the low statistics for $Z \to l^+l^-$ events with high p_T.

The efficiencies are projected on the η-ϕ-plane in Figure 6.5 (a) for e10_medium and in 6.5 (b) for the mu6 trigger. The region with zero efficiency in the plot for electrons is due to an outage in the LAr calorimeter. Therefore no electrons in $-0.1 \leq \eta \leq 1.5$, $-0.9 \leq \phi \leq -0.5$ are considered for the analysis.

(a) (b)

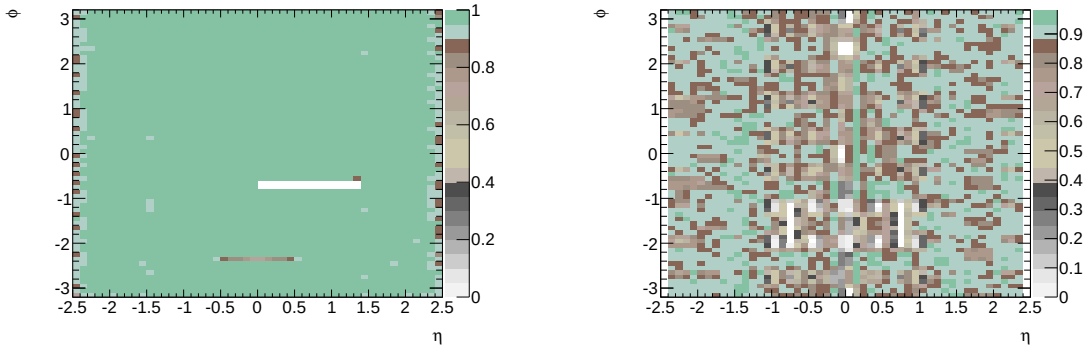

FIGURE 6.5.: *The efficiencies projected on the $\eta - \phi$ plane for the simulated single lepton triggers e10_medium (a) and mu6 (b).*

Closure Test for Reweighting Method

- For the closure test, first the efficiency of the dilepton trigger is obtained in the $t\bar{t}$ MC sample by requiring a positive trigger decision of the simulated e10_-medium_mu6 trigger. The efficiency is shown for the electron p_T in Figure 6.6 (a) and for the muon p_T in 6.6 (b) with red lines and reaches the plateau at an absolute efficiency of 75%. It is the same measurement the the one which was done for the green and red curves in the plots in Figure 6.4.

- In a second step, the efficiency of the dilepton trigger is obtained by dividing the number of weighted events by the number of unweighted events, $\epsilon_{weighted} = \frac{N_{weighted}}{N_{unweighted}}$. The weight is computed for each event according to the formula in Equation 6.11 with the single lepton efficiencies measured in the $Z \to l^+l^-$ MC samples: $w = \epsilon_{e10\_medium} \cdot \epsilon_{mu6}$. The efficiency $\epsilon_{weighted}$ is shown in Figure 6.6 in red lines.

(a) (b)

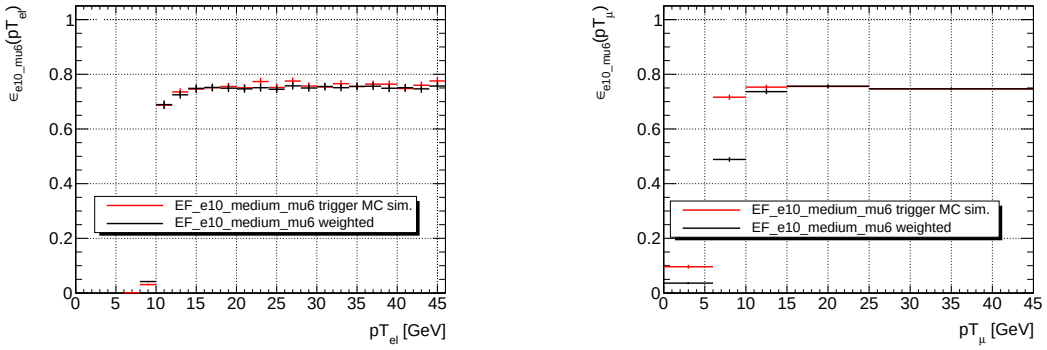

FIGURE 6.6.: *The efficiencies resulting from reweighting the $t\bar{t}$ MC events with the efficiencies measured in $Z \to ll$ MC events (black) and from requiring a positive simulated trigger decision in the $t\bar{t}$ sample (red) depending on the electron p_T (a) and the muon p_T (b).*

For the closure test the two methods, i.e. the black and red curves, are compared. The difference is on average less than 1% for leptons in the trigger plateau, showing that the Reweighting Method works well.

Systematic Uncertainties The observed difference of 1% is taken as a systematic uncertainty on the Reweighting Method concerning the validity of the factorisability assumption and the choice of the binning. Uncertainties which result from the Tag & Probe Method when varying the tagging trigger, the Z-mass window, the ΔR matching and from studying the dependencies on the pile-up and the run period for

the electron and muon triggers are also taken into account for the total systematic error. The results of these studies are summarised in Table 6.4. In addition to the statistical uncertainty on the trigger weight which is computed with Gaussian error propagation, a total systematic uncertainty of $\pm 1.5\%$ is applied on each event to obtain the error on the event yield due to trigger efficiency measurements and due to the Reweighting Method.

TABLE 6.4.: *The systematic uncertainties derived from the Tag & Probe Method and from the closure tests for the electron, muon and electron-muon triggers. 'X' refers to the momentum threshold and to the possible isolation criteria of the leptons on Event Filter level.*

Type of trigger	Tag & Probe Method	Reweighting Method
e2X_medium	1% ($\|\eta\|$ <1.5), 1.5% ($\|\eta\|$ >1.5)	1%
e1x_medium	1% ($\|\eta\|$ <1.5), 1.5% ($\|\eta\|$ >1.5)	1% (p_T >20 GeV), 2% (p_T <20 GeV)
2muX, 1muX	(included in closure test)	1.2%
e_mu	(see single lepton triggers)	1%

6.8. RESULTS AND INTERPRETATION

The comparison of the data event yields with the expected SM background favours the null hypothesis without SUSY signal since the numbers are in good agreement. The numbers are given in Table 6.5. For *SR-*m_{T2}, the SF channel is quoted separately since the $e\mu$ channel is not meaningful for the search for $\tilde{l}^{\pm}\tilde{l}^{\mp} \rightarrow l^{\pm}l^{\mp}\tilde{\chi}_1^0\tilde{\chi}_1^0$. Therefore the results are used to set limits on the masses of the sleptons and charginos in the pMSSM and in the simplified model.

The systematic uncertainties are dominated by the jet energy scale calibration, by the jet energy resolution, by the choice of the MC generator as well as by the lepton efficiencies and the lepton momentum measurements. They are taken into account together with the statistical uncertainties on the limited number of events in the SRs.

TABLE 6.5.: *The predicted contributions of the MC-simulated SM background processes and the observed number of data events for the SRs. The quoted errors are first the statistical error due to the limited number of MC events and second the total systematic uncertainty. $\sigma_{vis}^{obs(exp)}$ gives the observed (expected) 95% CL on the visible cross section for non-SM events [63].*

SR-m_{T2}					
	e^+e^-	$e^\pm\mu^\mp$	$\mu^+\mu^-$	all	SF
$Z+X$	3.2±1.1±1.7	0.3±0.1±0.2	3.6±1.3±1.7	7.1±1.7±2.1	6.8±1.7±2.1
WW	2.3±0.3±0.4	4.8±0.4±0.7	3.5±0.3±0.5	10.6±0.6±1.5	5.8±0.4±0.9
$t\bar{t}$, single top	2.6±1.2±1.3	6.2±1.6±2.9	4.1±1.3±1.6	12.9±2.4±4.6	6.8±1.8±2.3
Fake leptons	1.0±0.6±0.6	1.1±0.6±0.8	-0.02±0.01±0.05	2.2±0.9±1.4	1.0±0.6±0.6
Total	9.2±1.8±2.5	12.4±1.7±3.1	11.2±1.9±3.0	32.8±3.2±6.3	20.4±2.6±3.9
Data	7	9	8	24	15
$\sigma_{vis}^{obs(exp)}$ [fb]	1.5 (1.8)	1.6 (2.0)	1.6 (1.9)	2.5 (3.3)	1.9 (2.5)
SR-OSjetveto					
	e^+e^-	$e^\pm\mu^\mp$	$\mu^+\mu^-$	all	
$Z+X$	4.5±1.2±1.2	3.0±0.9±0.5	4.7±1.1±1.2	12.2±1.8±1.8	
WW	8.8±1.8±4.4	20.9±2.6±6.2	13.3±1.9±3.5	43.0±3.7±12.2	
$t\bar{t}$, single top	21.1±2.3±4.2	47.7±3.4±20.5	27.5±2.5±9.0	96.2±4.8±29.5	
Fake leptons	2.9±1.2±1.2	6.9±1.8±2.6	0.4±0.6±0.3	10.3±2.2±4.1	
Total	37.2±3.3±6.4	78.5±4.7±20.9	45.9±3.4±9.4	161.7±6.7±30.8	
Data	33	66	40	139	
$\sigma_{vis}^{obs(exp)}$ [fb]	3.3 (3.8)	6.8 (7.8)	4.0 (4.6)	9.8 (11.9)	
SR-SSjetveto					
	e^+e^-	$e^\pm\mu^\mp$	$\mu^+\mu^-$	all	
Charge Flip	0.49±0.03±0.17	0.34±0.02±0.11	–	0.83±0.04±0.18	
Diboson	0.62±0.13±0.18	1.93±0.23±0.36	0.94±0.16±0.26	3.50±0.31±0.54	
Fake leptons	3.2±0.9±1.7	2.9±0.9±1.9	0.6±0.6±0.3	6.6±1.4±3.8	
Total	4.3±0.9±1.7	5.1±1.0±1.9	1.5±0.6±0.4	11.0±1.5±3.9	
Data	1	5	3	9	
$\sigma_{vis}^{obs(exp)}$ [fb]	0.7 (1.1)	1.6 (1.6)	1.3 (0.9)	1.9 (2.1)	
SR-2jets					
	e^+e^-	$e^\pm\mu^\mp$	$\mu^+\mu^-$	all = SF	
$Z+X$	3.8±1.3±2.7	–	5.8±1.6±3.9	9.6±2.0±5.1	
WW	6.4±0.5±4.3	–	8.4±0.6±5.7	14.8±0.7±9.9	
$t\bar{t}$, single top	14.8±1.9±9.2	–	22.1±2.1±20.7	36.9±2.9±29.6	
Fake leptons	2.5±1.2±1.5	–	1.7±1.3±0.8	4.2±1.8±2.3	
Total	27.5±2.6±10.6	–	37.9±3.0±21.0	65.5±4.0±31.8	
Data	39	–	39	78	
$\sigma_{vis}^{obs(exp)}$ [fb]	6.9 (5.3)	–	7.7 (7.6)	13.6 (12.5)	

Figure 6.7 shows the 95% CL_s expected (dashed line) and observed (solid line) limits on the masses of the left-handed sleptons and the lightest neutralinos in the pMSSM direct $\tilde{l}^{\pm}\tilde{l}^{\mp}$-production. For these and for the solid yellow band around the expected limit which shows the $\pm 1\sigma$ result, all uncertainties are included in the fit except for the uncertainty on the theoretical signal cross section. The $\pm 1\sigma$ lines around the observed limit are created by moving the nominal signal cross section up or down by $\pm 1\sigma$ the theoretical uncertainty.

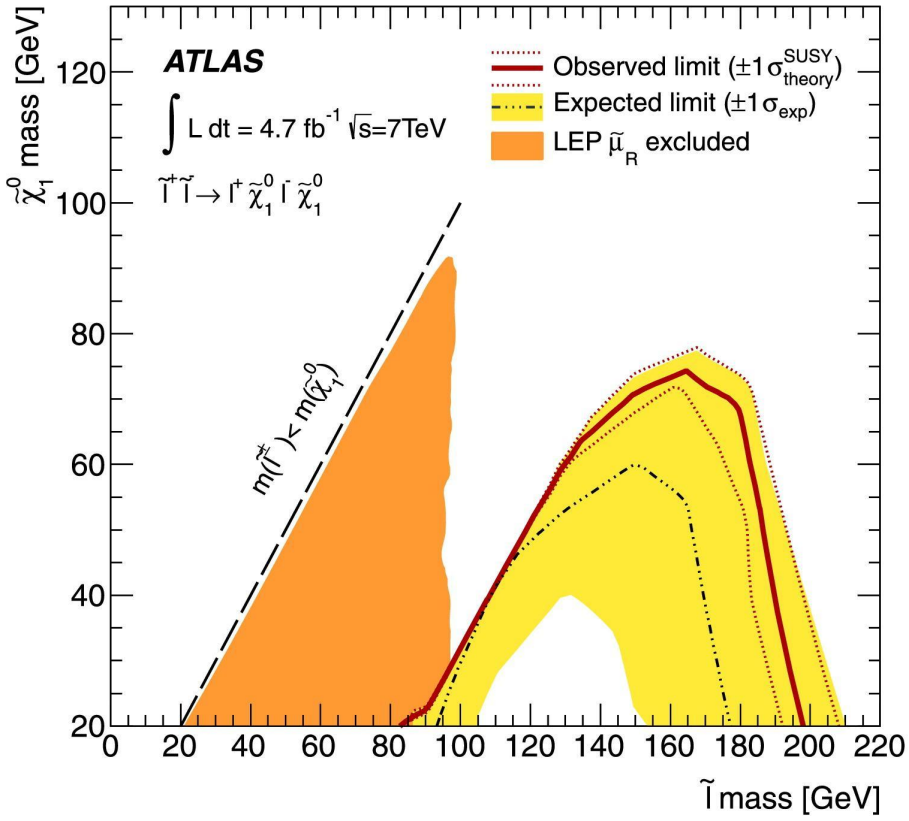

FIGURE 6.7.: *The 95% CL_s expected (dashed line) and observed (solid line) limits on the masses of the left-handed sleptons and the lightest neutralinos in the pMSSM direct $\tilde{l}^{\pm}\tilde{l}^{\mp}$-production. For these and the solid yellow band around the expected limit which shows the $\pm 1\sigma$ result all uncertainties are included in the fit except for the uncertainty on the theoretical signal cross section. The $\pm 1\sigma$ lines around the observed limit are created by moving the nominal signal cross section up or down by $\pm 1\sigma$ the theoretical uncertainty. Also shown are the exclusion limits from LEP in orange color [63].*

Also shown in Figure 6.7 are the exclusion limits from the data recorded with LEP which was in operation in the years 1989 - 2000. Limits are set on the mass of the right-handed $\tilde{\mu}_R$ and according to assumptions made for the analysis of LEP data, left-handed sleptons with the same mass are also automatically ruled out. For a $\tilde{\chi}_1^0$ mass of more than 20 GeV, left handed sleptons with masses from 85 to 195 GeV

can be excluded with the LHC data at $\sqrt{s}$ =7 TeV. For a higher neutralino mass of 60 GeV, the excluded range for $m_{\tilde{l}}$ is between 135 and 180 GeV.
The sensitivity decreases with smaller mass differences $m_{\tilde{l}} - m_{\tilde{\chi}_1^0}$ because for this exclusion plot, the results from the most sensitive SR, *SR-*m_{T2}, are used. For decreasing mass differences, the kinematic endpoint of the m_{T2} distribution is shifted to higher values, getting closer to the endpoint of the SM background distributions, as can be seen in Figure 6.8. From the same Figure it can also be deduced that the background estimation nicely describes the data.

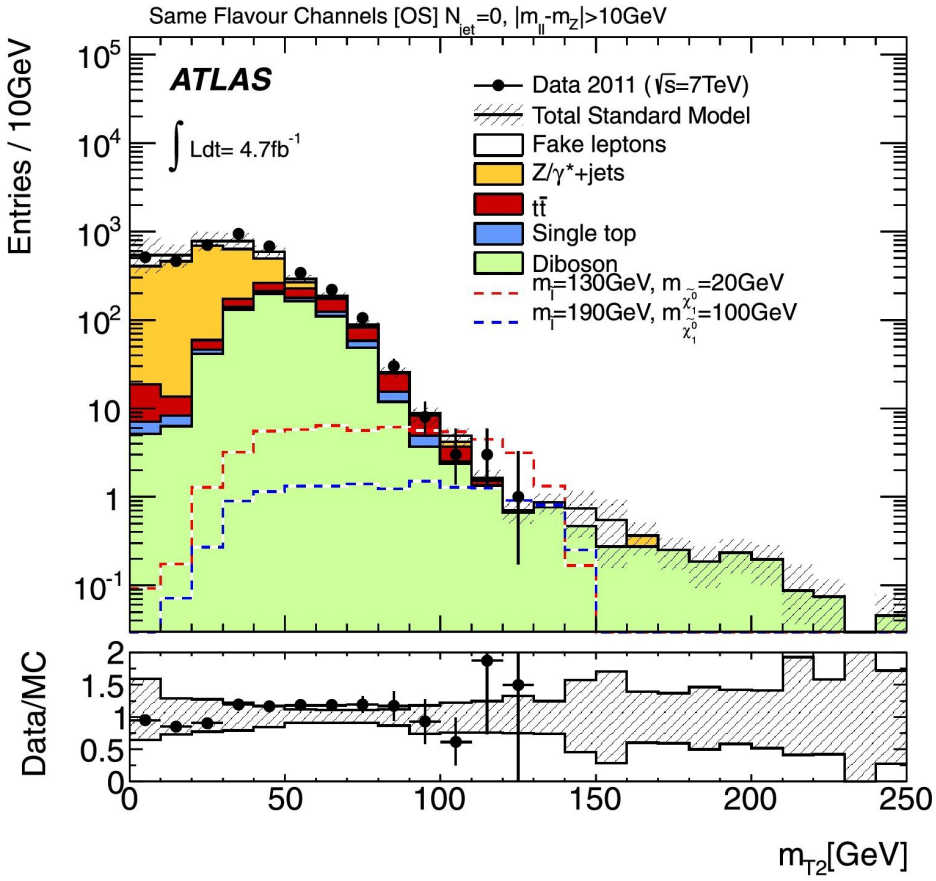

FIGURE 6.8.: *The distribution of m_{T2} in SR-m_{T2} before cutting on > 90 GeV in the same flavour lepton channels ee and $\mu\mu$. Since this SR addresses the direct slepton production SUSY signal, the corresponding mass points with $(m_{\tilde{l}}, m_{\tilde{\chi}_1^0})$ (130, 20) and (190, 100) GeV are superimposed (dashed lines). The coloured contributions show the MC background contributions which are the processes involving Z/γ^*+jets (yellow), $t\bar{t}$ quark pairs (red), single top quarks (blue) and two bosons (green). 'Fake leptons' (white colour) are estimated from data. The black dots represent ATLAS data. The hatched band illustrates the systematic and statistical uncertainties on the SM background. The lower ratio plot shows for each bin the number of data events over the number of MC events with the statistical error on data and again the error on the background as a band [63].*

From the interpretation of the results in the simplified model with direct $\tilde{\chi}_1^{\pm}\tilde{\chi}_1^{\mp}$ production, exclusion limits on the masses of the lightest neutralino and the $\tilde{\chi}_1^{\pm}$ can be deduced. For $m_{\tilde{\chi}_1^0} > 10$ GeV, $\tilde{\chi}_1^{\pm}$ with masses between 110 and 340 GeV are excluded at 95% CL_s. For each grid point, the SR with the best expected p-value is used to compute the limit. Figure 6.9 shows the expected and observed limit in the same way as for the pMSSM exclusion plot.

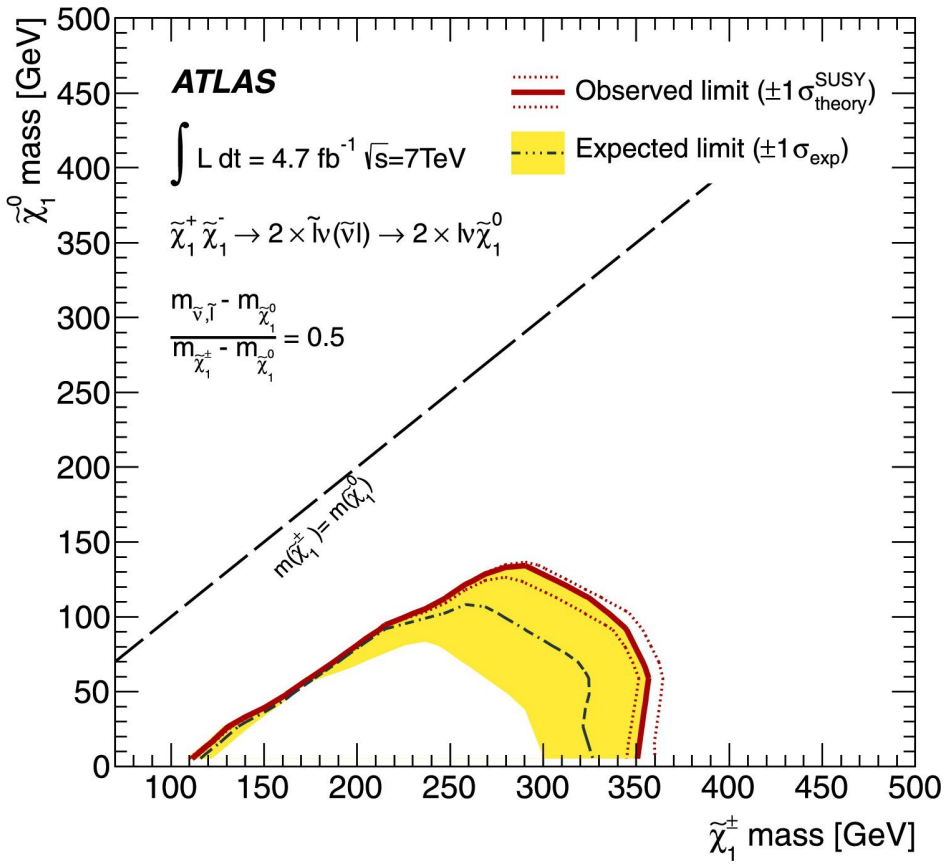

FIGURE 6.9.: *95% CL_s expected (dashed line) and observed (solid line) limits on the masses of the $\tilde{\chi}_1^0$ and the $\tilde{\chi}_1^{\pm}$ in the simplified model. For these and the solid yellow band around the expected limit which shows the $\pm 1\sigma$ result all uncertainties are included in the fit except for the uncertainty on the theoretical signal cross section. The $\pm 1\sigma$ lines around the observed limit are created by moving the nominal signal cross section up or down by $\pm 1\sigma$ the theoretical uncertainty [63].*

7. Direct Gaugino and Direct Slepton Production: Analysis and Trigger Studies with $\sqrt{s} = 8$ TeV Data

Another search for electroweakly produced supersymmetric particles is presented in this Chapter. It makes use of the full dataset of $\int dt\mathcal{L} = 20.3$ fb^{-1} which was recorded in 2012 with a centre-of-mass energy of $\sqrt{s} = 8$ TeV. SUSY scenarios which result in final states with two identified leptons with opposite signs (OS) are addressed. The trigger strategy is explained in great detail in Section 7.6. No significant data excess is observed and the results are interpreted in the pMSSM as well as in simplified models with a neutralino LSP. The analysis is published in [70].

7.1. SUSY Decay Scenarios

The SUSY scenarios to which this analysis is sensitive are shown in Figure 7.1.

Simplified Models To set limits on the masses of the $\tilde{\chi}_2^0$, the $\tilde{\chi}_1^0$ and the $\tilde{\chi}_1^\pm$, a simplified model with a $\tilde{\chi}_1^0$ as the LSP is assumed. The $\tilde{\chi}_1^\pm$ and the $\tilde{\chi}_2^0$ are pure wino and mass degenerate. The production via quark annihilation creates pairs of gauginos, $q\bar{q} \to (Z/\gamma)^* \to \tilde{\chi}_1^+\tilde{\chi}_1^-$ with cross sections of e.g. $\sigma = 6$ pb for $m_{\tilde{\chi}_1^\pm} = 100$ GeV or $\sigma = 10$ fb for $m_{\tilde{\chi}_1^\pm} = 450$ GeV. Another production mechanism is $q\bar{q} \to (W^\pm)^* \to \tilde{\chi}_1^\pm\tilde{\chi}_2^0$ with e.g. $\sigma = 11.5$ pb for $m_{\tilde{\chi}_1^\pm,\tilde{\chi}_2^0} = 100$ GeV or $\sigma = 40$ fb for $m_{\tilde{\chi}_1^\pm,\tilde{\chi}_2^0} = 400$ GeV.

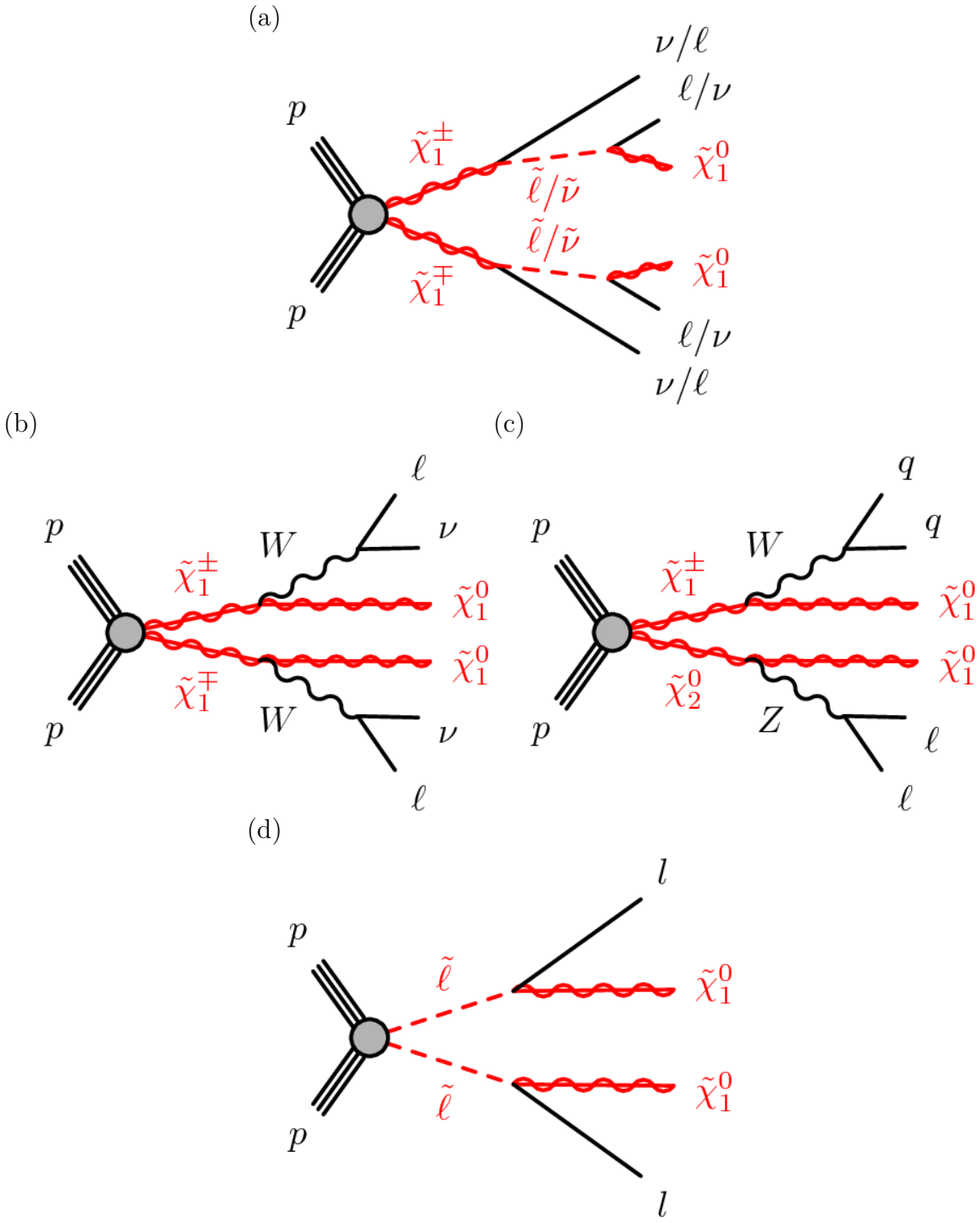

FIGURE 7.1.: *Graphs as examples for SUSY decay scenarios after electroweak production, leading to two OS leptons (electrons or muons) in the final state.*

The graph in Figure 7.1 (a) shows the decay of a pair of charginos via intermediate sleptons or sneutrinos. The values of the masses of the mass-degenerate sleptons and sneutrinos are set halfway between the values of the masses of the $\tilde{\chi}_1^\pm$ and the $\tilde{\chi}_1^0$. The branching ratio for the decay of the $\tilde{\chi}_1^\pm$ into $\tilde{l}^\pm\nu$ or $l^\pm\tilde{\nu}$ is set to $\frac{1}{6}$ each, according to the three lepton flavours. The masses of all six sleptons are degenerate.

In Figure 7.1 (b) the $\tilde{\chi}_1^\pm$ is assumed to be the next-to lightest supersymmetric particle (NLSP). The pair of charginos decays leptonically via W bosons.

For the graph shown in Figure 7.1 (c), the $\tilde{\chi}_2^0$ is made the co-NLSP. A pair of $\tilde{\chi}_1^\pm\tilde{\chi}_2^0$ decays hadronically via W bosons and leptonically via Z bosons, respectively. This leads to a final state with two OS leptons. The invariant masses of the two reconstructed jets and of the two reconstructed SFOS leptons are consistent with the masses of the W and Z bosons, respectively.

The direct slepton production is shown in Figure 7.1 (d). It leads to a final state with two OS leptons and two neutralinos. The production cross section for left-handed sleptons decreases from 127 fb to 0.5 fb and for right-handed sleptons from 49 fb to 0.2 fb for $m_{\tilde{l}}$ increasing from 100 GeV to 370 GeV.

pMSSM The motivation for the search for the particular SUSY scenarios is based on the assumption that in the framework of the pMSSM, the masses of the squarks, of the CP-odd Higgs and of the left-handed sleptons are set to high values. After the electroweak process which involves the constituents of the protons, $q\bar{q}'/q\bar{q} \to W^*/(Z/\gamma)^*$, then only the production of $\tilde{\chi}_1^\pm$ and $\tilde{\chi}_2^0$ is allowed. The gauginos can decay via right-handed sleptons, W, Z or the lightest Higgs bosons.

In a first model, the masses of the right-handed sleptons are set halfway between the masses of the neutralinos $\tilde{\chi}_1^0$ and $\tilde{\chi}_2^0$. The $\tilde{\chi}_2^0$ preferentially decays via intermediate sleptons, $\tilde{\chi}_2^0 \to \tilde{l}_R^\pm l^\mp \to \tilde{\chi}_1^0 l^\pm l^\mp$. The other free SUSY parameters are set to $\tan\beta = 6$ for the ratio of the expectation values of the SUSY Higgs fields and $M_1 = 100$, 140 or 250 GeV. Since M_1 is the bino mass parameter, it is varied to provide sensitivity to different $\tilde{\chi}_1^0$ compositions. $M_1 = 100$ GeV means a very bino-like neutralino, for higher values of M_1 the wino and higgsino rates are distinctly increased.

In a second model, also the right-handed sleptons are assumed to be very heavy. The parameter $\tan\beta$ is set to 10 and M_1 is set to 50 GeV. The charginos can therefore only decay via W, Z or H, and not via intermediate sleptons.

To interpret the results in the pMSSM, the exclusion in the $\mu - M_2$ grid for the Higgsino and the wino mass parameters is shown at the end of this Chapter.

7.2. SM Background

For the decay scenarios with intermediate sleptons or two W bosons, the expected SM background with a similar detector signature is due to the production of diboson states and top quarks such as $t\bar{t}$ and Wt. The latter is Monte Carlo simulated with

MC@NLO [49]- [51] and AcerMC [71] for the t-channel production of Wt. In the SF final states also the ZZ or WZ contributions are important. The MC samples for the diboson processes are generated by POWHEG-BOX [66].

For the SUSY signal with jets in the final state, shown in Figure 7.1 (c), $Z/\gamma^* + jets$ processes are the dominating SM background. Also the production of pairs of top quarks makes it difficult to filter the signal since one of the top quarks can decay hadronically and result in a final state with two jets. The $Z/\gamma^* + jets$ MC samples are simulated with a combination of SHERPA [48] and ALPGEN [52].

The SM background contribution due to non-prompt leptons, e.g. the leptonic decays of hadrons, is estimated with a data-driven technique.

7.3. Physics Object Definition

The collections of physics objects selected for this analysis are reconstructed using the algorithms described in Section 5.3. The overlap removal stated in Section 5.3.6 is performed. Events are selected according to the requirements listed in Section 5.4.

Electrons Electrons must be reconstructed with the 'tight++' reconstruction quality criteria. They have $|\eta| < 2.47$ and $p_T > 10$ GeV. They need to be isolated which means that the scalar sum of the p_T of the tracks which have $p_T > 0.4$ GeV within a cone of size $\Delta R = 0.3$ and which are associated to the primary vertex ('ptcone30') must be less than 16% of the electron p_T. The pile-up corrected sum of E_T of the surrounding calorimeter clusters in a cone of $\Delta R = 0.3$ ('Etcone30Corr') must be less than 18% of the electron p_T. The transverse impact parameter with respect to the event primary vertex, d_0^{PV}, must fulfil $|\frac{d_0^{PV}}{\sigma(d_0^{PV})}| < 5$ and the longitudinal impact parameter z_0 must fulfil $|z_0 \cdot sin(\theta)| < 0.4$ mm.

Muons Staco combined or segment-tagged muons must have $|\eta| < 2.4$ and $p_T > 10$ GeV. They must fulfil a list of quality requirements, i.e. have a certain number of hits in the PD, the TRT and the SCT. Muons also need to be isolated in the same way as electrons regarding the scalar sum of the p_T of tracks in $\Delta R = 0.3$. In addition, the distance of the closest approach of a muon to the primary vertex, d_0^{PV}, must be within 3σ and $|z_0 \sin\theta|$ must be smaller than 1 mm for the impact parameter along the beam direction.

Taus Tau-leptons which decay hadronically are not allowed in any event and are reconstructed by matching one or three tracks with $p_T > 1$ GeV to the calorimeter jets. A multivariate analysis technique is used to reconstruct taus: the Boosted Decision Tree (BDT) method. The algorithms of this method provide a possibility to distinguish between jets and taus and electrons and taus. The tau transverse momentum must exceed 20 GeV; $|\eta|$ must be smaller than 2.47.

JETS Jets are built using the anti-k_T clustering algorithm with distance parameter $\Delta R = 0.4$. They must fulfil $p_T > 20$ GeV and $|\eta| < 4.5$. The jets are further exclusively sorted in three categories: 'central b-jets' are identified with a b-jet identification algorithm with 80% identification efficiency and have $|\eta| < 2.4$. 'Central light-flavour jets' as well have $|\eta| < 2.4$ but must not be b-tagged. To select jets from the primary vertex and not from pile-up interactions, at least on of the tracks of such central jet with $p_T < 50$ GeV must originate from the primary vertex. 'Forward jets' have $2.4 < |\eta| < 4.5$ and $p_T > 30$ GeV.

E_T^{miss} The missing transverse energy is build from the electrons, muons and photons with $p_T > 10$ GeV as well as from jets with $p_T > 20$ GeV. Calorimeter clusters with $|\eta| < 4.9$ which are not allocated to any of the physics objects are also included in the computation of E_T^{miss}.

7.4. SIGNAL REGIONS

Seven SRs are designed to address the SUSY scenarios which are described in the beginning of this Chapter. The SRs are summarised in Table 7.1.

TABLE 7.1.: *Summary of the seven signal regions. 'SF' means that the two leptons have the same flavour. The requirements on $|m_{ll} - m_Z|$ are only placed on SF leptons. In SR-Zjets the central jets have $p_T > 45$ GeV.*

Requirements	*SR-WW^a*	*SR-WW^b*	*SR-WW^c*	*SR-m_{T2}^{90}*	*SR-m_{T2}^{120}*	*SR-m_{T2}^{150}*	*SR-Zjets*
Lepton flavour	any	any	any	any	any	any	SF
N central jets	0	0	0	0	0	0	≥ 2
N b-jets	0	0	0	0	0	0	0
N forward jets	0	0	0	0	0	0	0
$\|m_{ll} - m_Z\|$ [GeV]	> 10	> 10	> 10	> 10	> 10	> 10	< 10
m_{ll} [GeV]	< 120	< 170	–	–	–	–	–
$E_T^{miss,rel}$ [GeV]	> 80	–	–	–	–	–	> 80
p_T^{ll} [GeV]	> 80	–	–	–	–	–	> 80
m_{T2} [GeV]	–	> 90	> 100	> 90	> 120	> 150	–
ΔR_{ll}	–	–	–	–	–	–	[0.3, 1.5]
m_{jj} [GeV]	–	–	–	–	–	–	[50, 100]

SR-WW$^{a,\,b,\,c}$ The decay of a chargino pair via W bosons, $\tilde{\chi}_1^{\pm}\tilde{\chi}_1^{\mp} \rightarrow W^{\pm}\tilde{\chi}_1^0 W^{\mp}\tilde{\chi}_1^0 \rightarrow l\nu\tilde{\chi}_1^0 l\nu\tilde{\chi}_1^0$ is targeted by the three SRs which are called *SR-WW^a*, *SR-WW^b* and *SR-*

WW^c. The differences of the three SRs refer to the increasing mass difference of the gauginos $\tilde{\chi}_1^\pm$ and $\tilde{\chi}_1^0$, $m_{\tilde{\chi}_1^\pm} - m_{\tilde{\chi}_1^0}$. Two OS leptons and no jets are required as well as the Z-veto for SF leptons, $|m_{ll} - m_Z| > 10$ GeV. *SR-WW*^{b} and *SR-WW*^{c} further demand $m_{T2} > 90$ GeV and $m_{T2} > 100$ GeV, respectively, which copes with large values of $m_{\tilde{\chi}_1^\pm} - m_{\tilde{\chi}_1^0}$. The stransverse mass is expected to display a characteristic endpoint at the relatively high $m_{\tilde{\chi}_1^\pm}$. An additional requirement is put on the invariant mass of the two leptons, m_{ll}, in *SR-WW*^{b}: the variable has to be smaller than 170 GeV to enable a good distinction of the SUSY signal against the SM background.

SR-WW^a is designed for SUSY signal points with small mass splitting, i.e. $m_{\tilde{\chi}_1^\pm} - m_{\tilde{\chi}_1^0}$ close to the mass of the W boson. For that reason no requirement is placed on the stransverse mass since the mass of the $\tilde{\chi}_1^\pm$ is expected to be close to the mass of the W boson - m_{T2} then does not provide a good differentiation to the SM WW production. Cutting on this variable would most notably decrease the statistics. Albeit for the dilepton system the transverse momentum, p_T^{ll}, has to be higher than 80 GeV and the invariant mass has to be lower than 120 GeV. The motivation for the requirement on m_{ll} arises from the distributions of the SM background processes and of the SUSY signal. They are shown in Figure 7.2 (a) for SF final states and in Figure 7.2 (b) for DF final states. The background distributions show a peak for high m_{ll} values and thus background events can be rejected by placing an upper bound on this variable. The events with SUSY signal are expected to have a small opening angle between the two leptons which makes the $E_T^{miss,rel}$ distributions different for background and signal. It motivates the cut on $E_T^{miss,rel} >$80 GeV. The distributions of this variable are shown in Figures 7.2 (c) and (d) for SF and DF final states, respectively. The signal distribution is at maximum only for values of $E_T^{miss,rel}$ higher than 80 GeV and therefore the SM background can be nicely suppressed by this cut.

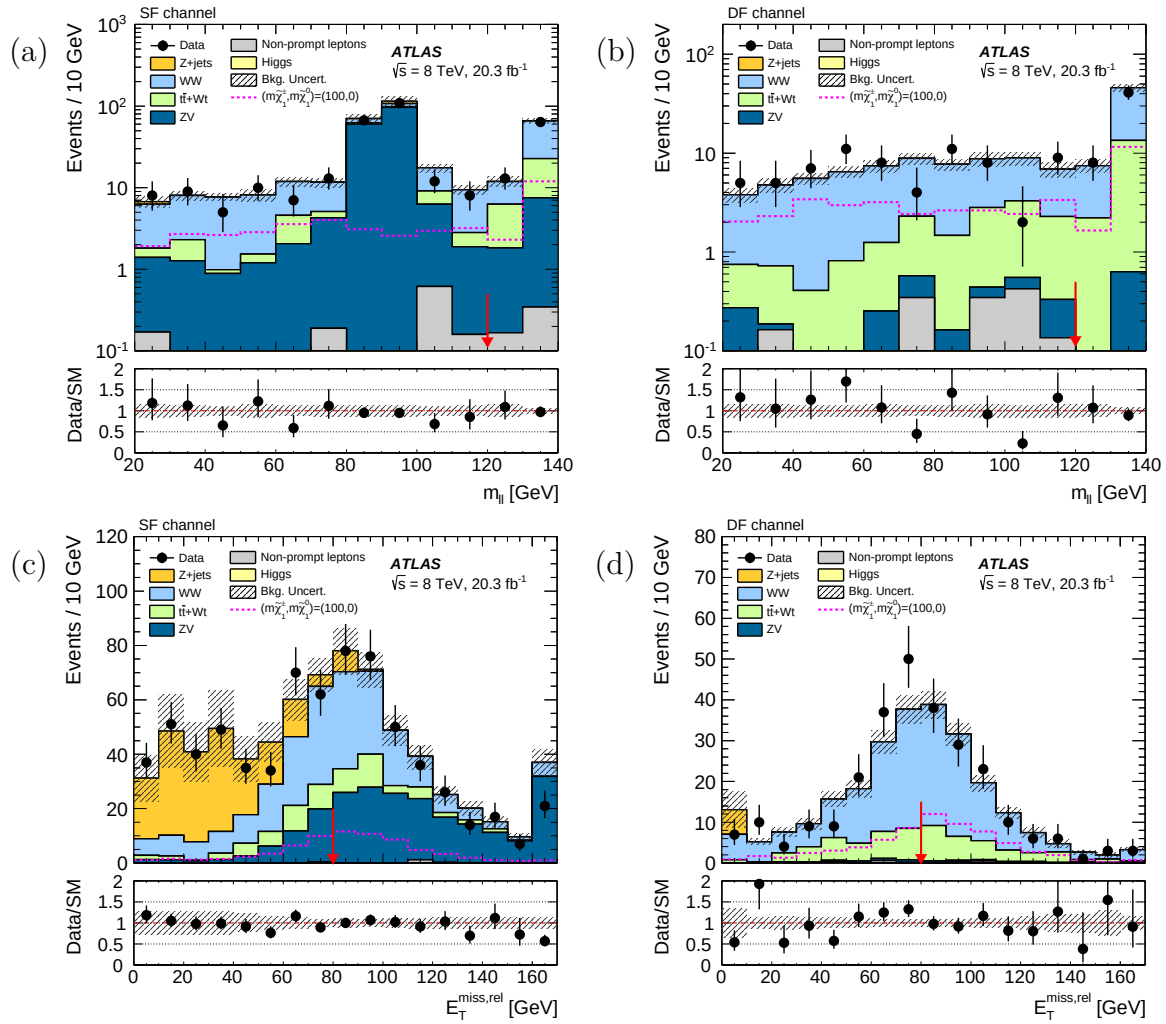

FIGURE 7.2.: *The distribution of the invariant mass of the two leptons, m_{ll}, in SR-WW[a]. The plot in (a) shows the SF final state, in (b) the DF final state. All cuts are applied except for the one on m_{ll}. The plots in (c) and (d) show the distributions of $E_T^{miss,rel}$ in the same SR for SF and DF final states, respectively. All SR-defining cuts are applied except for the ones on m_{ll} and $E_T^{miss,rel}$. The SM background contributions are represented in solid colours, the predicted SUSY signal in the simplified model with $m_{\tilde{\chi}_1^\pm} = 100$ GeV and $m_{\tilde{\chi}_1^0} = 0$ GeV is superimposed in a red dashed line. The hashed regions show the combined statistical and systematic errors. Red arrows indicate the cut on the variable for the final definition of SR-WW[a]. The bottom panel for each plot shows the ratio of data over the SM expectation together with the error on data as a hashed region. For the plot in (a), an additional Z-veto of $|m_{ll} - m_Z| > 10$ GeV is placed to reject the SM processes in this region, i.e. mainly diboson ZV [70].*

***SR-*$m_{T2}^{90,120,150}$** Three additional signal regions which are based on cuts on high values of the stransverse mass, namely $m_{T2} > 90$, 120 and 150 GeV, respectively, are designed. They aim to be sensitive to the $\tilde{\chi}_1^{\pm}$ decay via intermediate sleptons as depicted in Figure 7.1 (a), which leads to SF or DF final states with two OS leptons and no jets. These SRs are also sensitive to the scenario of the direct slepton pair production with a SF final state, see Figure 7.1 (d). The distribution of m_{T2} in *SR-*$m_{T2}^{90,120,150}$ before cutting on this variable is shown in Figure 7.3 (a) for SF and in (b) for DF final states, respectively. For high values of m_{T2} the distributions of the SM background processes decrease while the superimposed predicted SUSY signal stays rather constant. In the SF channels, a Z-veto is applied to suppress SM background originating from a $Z \to l^+l^-$ decay. In the same way as for *SR-WW*^{b} and *SR-WW*^{c}, the SRs with rather low requirements on the stransverse mass address the signal mass points with low mass splitting for slepton and neutralino $m_{\tilde{l}} - m_{\tilde{\chi}_1^0}$ or chargino and neutralino $m_{\tilde{\chi}_1^{\pm}} - m_{\tilde{\chi}_1^0}$, while a high threshold as in *SR-*m_{T2}^{150} addresses large mass differences.

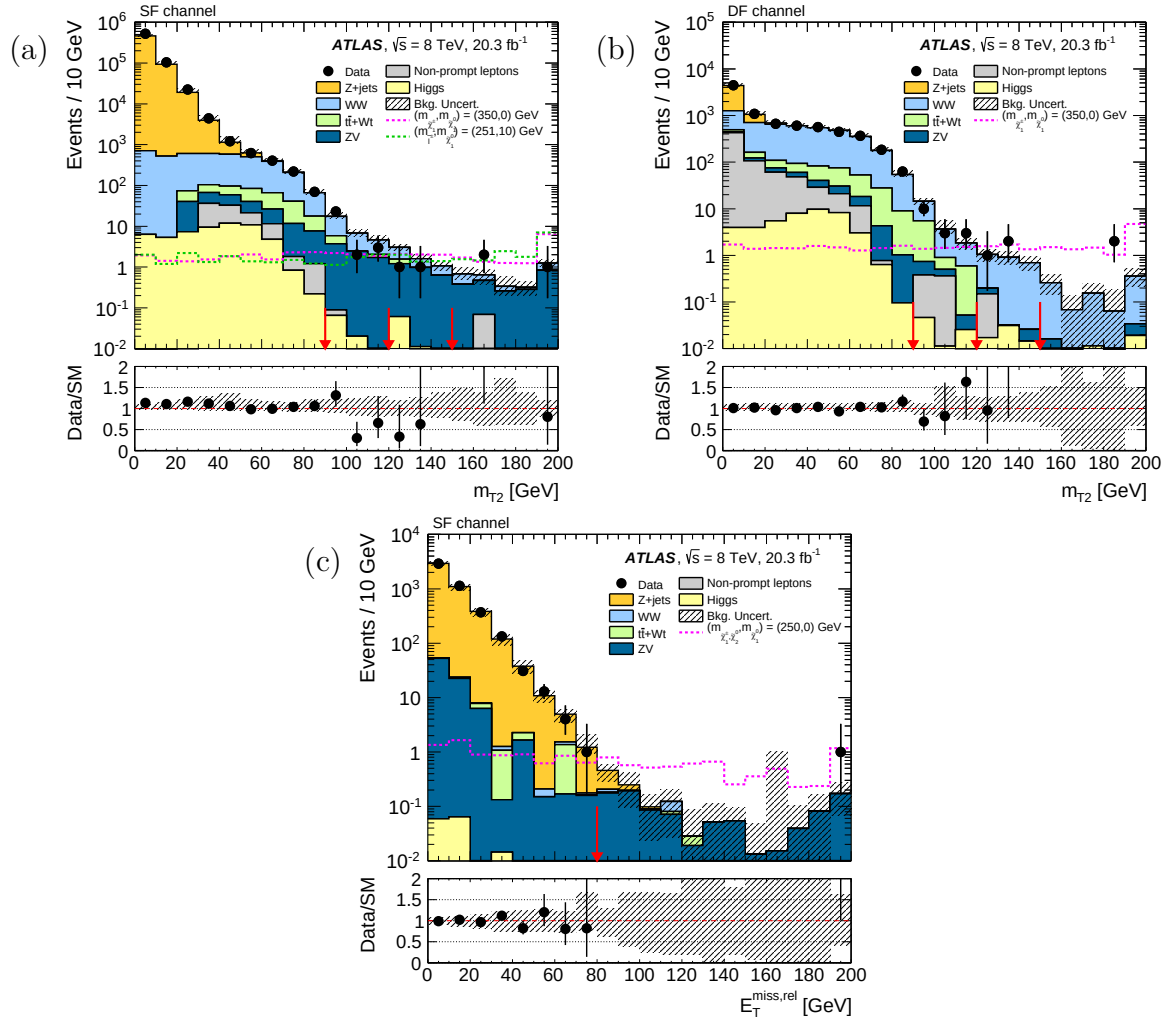

FIGURE 7.3.: *The distribution of the stransverse mass in SR-$m_{T2}^{90,120,150}$. All cuts are applied except for the one on m_{T2}. The plot in (a) shows the SF final state, in (b) the DF final state. Red arrows indicate the cuts on m_{T2} for the final definitions of SR-$m_{T2}^{90,120,150}$. The plot in (c) shows the distribution of $E_T^{miss,rel}$ in SR-Zjets. All SR-defining cuts are applied except for the one on $E_T^{miss,rel}$. The red arrow indicates the cut for the final definition of SR-Zjets. The SM background contributions are represented in solid colours, the predicted SUSY signal in the simplified model with $m_{\tilde{\chi}_1^0} = 0$ GeV and $m_{\tilde{\chi}_1^\pm} = 350$ GeV ((a), (b)) or 250 GeV (c) is superimposed in a red dashed line. The signal for $m_{\tilde{l}} = 251$ GeV and $m_{\tilde{\chi}_1^0} = 10$ GeV is superimposed in (a) in a blue dashed line. The hashed regions show the combined statistical and systematic errors. The bottom panel for each plot shows the ratio of data over the SM expectation together with the error on data as a hashed region [70].*

SR-Zjets *SR-Zjets* achieves sensitivity to the process where a pair of $\tilde{\chi}_2^0$ and $\tilde{\chi}_1^\pm$ decays via Z and W in a final state with two SFOS leptons, two hadrons and two neutralinos. The process is depicted in Figure 7.1 (c). The SR is defined by requiring at least two central light-flavour jets with $p_T > 45$ GeV and an invariant mass of the dijet system between 50 and 100 GeV to be close to the mass of the W boson which is 80.4 GeV. No other jet of any other classification is allowed. Furthermore, the two leptons must have the same flavour and a total invariant mass inside the Z-mass window of $m_Z \pm 10$ GeV. The transverse momentum of the dilepton system hast to be smaller than 80 GeV to ensure that the Z-boson which decays into the two leptons is recoiling against the other objects. For the distance in the η-ϕ plane, $0.3 < \Delta R_{ll} < 1.5$ must be fulfilled for the two leptons. High $E_T^{miss,rel}$ of at least 80 GeV is required in order to suppress SM $Z + jets$ processes where a mis-measured jet can significantly contribute to the relative missing transverse energy. The choice of the cut value is motivated by the distributions of the expected SM background processes and the predicted SUSY signal for $E_T^{miss,rel}$, shown in Figure 7.3 (c).

CORRELATIONS The SF channels of the various SRs are overlapping and are not statistically independent except for *SR-Zjets*. Therefore the SF and DF channels for every SR are treated separately. When computing the exclusion limits, the SRs are combined in such a way that the scenarios which can lead to a SF as well as to a DF final state are treated specially.

7.5. BACKGROUND ESTIMATION

The dominating SM background arises from processes involving the decays of two gauge bosons or of a top quark pair which also lead to final states with two leptons. To estimate the event yield due to SM background processes in the SRs, CRs are defined which are kinematically very close to the SRs but orthogonal to those. They are enriched in a particular background process and hardly suffer from signal contamination. From the CRs, normalisation factors are deduced by performing simultaneous likelihood fits. The fits take as input the number of observed events in the CRs and the number of events expected from studying MC simulations or from data-driven background estimates. The gained information about the SM background is migrated to the SRs. Correlations between the SRs, CRs and background processes are taken into account in the fits with nuisance parameters. The definitions of the CRs are summarised in Table 7.2.

FOR SIGNAL WITH HIGH GAUGINO MASS SPLITTING The SRs which place requirements on the stransverse mass, i.e. *SR-*$m_{T2}^{90,\,120,\,150}$ and *SR-WW*$^{b,\,c}$ have the same CR definitions:

- Enrichment in WW processes is achieved by demanding $50 < m_{T2} < 90$ GeV, i.e. a stransverse mass close to the mass of the W boson, and only DF leptons,

since the SF signature yields a too high contamination due to $Z/\gamma^* + jets$ processes. The events must not contain any jets. This is the definition of *WW-CR*.

- *Top-CR* is defined by requesting only DF leptons, at least one b-jet and no jets from any other category as well as $m_{T2} > 70$ GeV.

- Diboson processes involving ZV, $V = W$ or Z, are estimated after applying the same selection criteria as the ones of *SR*-m_{T2}^{90} but requiring two SFOS leptons with an invariant mass $m_{ll} - m_Z < 10$ GeV, which corresponds to a 'reversed' Z-veto. The dominating contamination for this *ZV-CR* are WW processes which only contribute 4.5%.

For *SR-WW^a* Since it has no requirement on the stransverse mass, for *SR-WW^a* a set of CRs is individually defined:

- To enrich a region in WW processes for *WW-CR*, the $E_T^{miss,rel}$ and the p_T^{ll} cuts are loosened: the variables are required to fulfil $60 < E_T^{miss,rel} < 80$ GeV and $p_{T,ll} > 40$ GeV. The other cuts are the same ones as for *SR-WW^a*, i.e. no jets are allowed and m_{ll} is smaller than 120 GeV. Only DF leptons are considered. The signal contamination is observed to be less than 10% for the simulation of $\tilde{\chi}_1^{\pm}\tilde{\chi}_1^{\mp} \to W^{\pm}W^{\mp}\tilde{\chi}_1^0\tilde{\chi}_1^0 \to l^{\pm}\nu\tilde{\chi}_1^0 l^{\mp}\bar{\nu}\tilde{\chi}_1^0$ with $m_{\tilde{\chi}_1^{\pm}} > 100$ GeV.

- In the *Top-CR* the signal contamination is negligible for the considered models. This CR only uses DF leptons and is defined in the same way as *SR-WW^a* but in addition requests at least one b-jet.

- The ZV background is estimated by requiring only SF leptons and reversing the Z-veto. The signal contamination in *ZV-CR* is less than 5%.

For *SR-Zjets* Due to the jets in the final state a different approach is chosen to estimate the background in *SR-Zjets*:

- A *Top-CR* is defined using the same requirements as for *SR-Zjets*. It is enriched in $t\bar{t}$ and $W + top$ processes by reversing the Z window requirement and by requesting at least one b-jet. The transverse momentum of the jets has to be higher than 20 GeV and the cut on m_{jj} is no longer applied to increase the statistics. The contamination from the predicted SUSY signal is negligible in *Top-CR*.

- A different method compared to the definition of CRs is used to estimate the ZV background contribution for *SR-Zjets*. Since $ZV \to l^+l^-q\bar{q}$ is already strongly suppressed by the cut on $E_T^{miss,rel} > 80$ GeV, only the $W^{\pm}Zqq \to l_{unid}\nu l^+l^-qq$ (with one unidentified lepton l_{unid}) and $ZZqq \to l^+l^-\nu\nu qq$ processes need to be

estimated. The event yield in the SRs results directly from MC simulated samples.

The WZ and ZZ background contributions are then validated in control samples: The simulation of the process $W^{\pm}Zqq \rightarrow l^{\pm}\nu l^{+}l^{-}qq$ is used, requiring at least one SFOS pair among the three reconstructed leptons which is a 'Z-candidate' with $|m_{ll} - m_Z| < 10$ GeV. Furthermore, $E_T^{miss} > 30$ GeV and $m_T > 40$ GeV are demanded, where for the computation of the transverse mass the one lepton which is not contributing to the Z-candidate is used. The SUSY signal contamination is found to be less than 10%.

The estimation of the $ZZqq$ process is validated in a second control sample, requiring 4 charged leptons and two jets in the final state for the process $ZZqq \rightarrow l^{+}l^{-}l^{+'}l^{-'}qq$. Among the leptons two SFOS lepton pairs which are Z-candidates must be found, E_T^{miss} must be smaller than 50 GeV and the event must contain at least two central light-flavour jets but no b-jets.

- The background of $Z/\gamma^{*} + jets$ is rather important for ***SR-Zjets*** due to the very similar detector signature in comparison to the SUSY signal. High E_T^{miss} can arise due to mis-measured jet p_T in the $Z/\gamma^{*} + jets$ SM process and is not well modelled in the MC simulation. This background contribution is estimated with a data-driven technique, using the so-called 'Jet Smearing Method':

  Seed events are taken from an ATLAS data sample. It is enriched in $Z/\gamma^{*} + jets$ events by using the definition of ***SR-Zjets*** but reversing the requirement on the relative missing transverse energy to $E_T^{miss,rel} < 80$ GeV. A high quality of the jet reconstruction is ensured by additionally requiring $E_T^{miss}/\sqrt{E_T^{miss}} < 1.5$ GeV$^{\frac{1}{2}}$. The events are then smeared by multiplying the jet four-momentum with a random number. The number is deduced from the jet response function $\frac{p_T^{reco}}{p_T^{true}}$. The function is measured in simulated data and corrected according to the comparison with measurements in data. The soft-term contribution to the missing transverse energy is also modified by using random numbers which are deduced from a $Z \rightarrow l^{+}l^{-}$ sample with zero jets. For every seed event, the smearing procedure is repeated 10 000 times.

  In the resulting pseudo-data the distribution for $E_T^{miss,rel}$ is normalised to data for $E_T^{miss,rel} < 40$ GeV and the resulting information is then used to estimate the $Z/\gamma^{*} + jets$ contribution in ***SR-Zjets***.

  For the validation of the Jet Smearing Method a control sample is selected according to the definitions of ***SR-Zjets***. But the p_T^{ll} cut is reversed and the ΔR_{ll} and m_{jj} cuts are removed to benefit high statistics. The seed events in addition need to fulfil $E_T^{miss,rel} < 40$ GeV and $E_T^{miss}/\sqrt{E_T^{miss}} < 1.5$ GeV$^{\frac{1}{2}}$. The validation takes place in a region which is defined by 40 GeV $< E_T^{miss,rel} < 80$ GeV.

NON-PROMPT The fake background which arises from non-prompt leptons in the final state contributes less than 5% to the total background in all SRs and is estimated by the Matrix Method. The method is explained in detail in Section 8.6.1.1.

TABLE 7.2.: *The summary of the control regions. 'SF' means that the two leptons have the same flavour, 'DF' means different flavour. In SR-Zjets the central jets must have $p_T > 20$ GeV, and at least one b-jet is required.*

	SR-$m_{T2}^{90,120,150}$, *SR-WW*^{b,c}			*SR-WW*^{a}			*SR-Zjets*
Requirements	*WW-CR*	*Top-CR*	*ZV-CR*	*WW-CR*	*Top-CR*	*ZV-CR*	*Top-CR*
Lepton flavour	DF	DF	SF	DF	DF	SF	SF
N of central jets	0	0	0	0	0	0	≥ 2
N of b-jets	0	≥ 1	0	0	≥ 1	0	≥ 1
N of forward jets	0	0	0	0	0	0	0
$\lvert m_{ll} - - m_Z \rvert$ [GeV]	–	–	< 10	–	–	< 10	> 10
m_{ll} [GeV]	–	–	–	< 120	< 120	–	–
$E_T^{miss,rel}$ [GeV]	–	–	–	[60, 80]	> 80	> 80	> 80
p_T^{ll} [GeV]	–	–	–	> 40	> 80	> 80	> 80
m_{T2} [GeV]	[50, 90]	> 70	> 90	–	–	–	–
ΔR_{ll}	–	–	–	–	–	–	[0.3, 1.5]

7.6. TRIGGER STRATEGY

When a data event fulfils the requirements listed in Section 5.4 it is only used for the analysis if in addition one of the designated triggers has a positive decision on Event Filter level and if the offline leptons can be matched to the trigger objects in the η-ϕ-space. A Monte Carlo event does not need to have a positive decision of the simulated triggers but is reweighted according to what is described for the Reweighting Method in Section 6.7.2.

Although various single lepton triggers are implemented for the data taking in 2012, the analysis is not incorporating those in any way. It turned out that the overall gain in the signal event yield would still never be more than 5% when the dilepton and single lepton triggers are combined with logical OR. In the larger part of the surface which is spanned by the p_T of the two leptons, the relative trigger efficiency could only be increased by 1-2%.

Due to the increased instantaneous luminosity and the therefore higher data taking rate in the year 2012 compared to 2011, the trigger thresholds for single lepton triggers needed to be tightened. Therefore some single lepton triggers require that

the triggering lepton is isolated. The data-driven Matrix Method which is used to estimate the background contribution due to non-prompt leptons uses the isolation requirement as a distinguishing feature. Therefore it was decided not to use the single lepton triggers in the trigger strategy.

The dilepton triggers are either symmetric, i.e. both leptons have to fulfil the same criteria to trigger the event on Event Filter level, or asymmetric, i.e. the second lepton has to fulfil only less tight p_T criteria to trigger the event compared to the leading lepton with higher p_T. The symmetric and asymmetric triggers can be combined with logical OR. This is particularly useful for the final states with two muons where the combination of two dimuon triggers significantly improves the coverage of the p_T surface.

7.6.1. Trigger Menu

The lowest p_T unprescaled dilepton triggers are listed in Table 7.3 together with the Level 1 trigger configuration which seeds the Level 2 and therefore also indirectly the Event Filter. Also given are the offline p_T thresholds which are in some cases slightly higher than the online p_T thresholds. They correspond to the values for which the absolute efficiency of the individual trigger legs reached 90%. The plots with the turn-on curves for e.g. the muon triggers can be found in Section 7.6.4.

Table 7.3.: *The list of the lowest p_T unprescaled dilepton triggers.*

Trigger	L1	Offline p_{T} threshold
2e12Tvh_loose1	2EM10VH	$p_{\mathrm{T}}(e_1) > 14$ GeV, $p_{\mathrm{T}}(e_2) > 14$ GeV
e24vh_medium1_e7_medium1	EM18VH	$p_{\mathrm{T}}(e_1) > 25$ GeV, $p_{\mathrm{T}}(e_2) > 8$ GeV
2mu13	2MU10	$p_{\mathrm{T}}(\mu_1) > 14$ GeV, $p_{\mathrm{T}}(\mu_2) > 14$ GeV
mu18_tight_mu8_EFFS	MU15	$p_{\mathrm{T}}(\mu_1) > 18$ GeV, $p_{\mathrm{T}}(\mu_2) > 8$ GeV
e12Tvh_medium1_mu8	EM10VH_MU6	$p_{\mathrm{T}}(e) > 14$ GeV, $p_{\mathrm{T}}(\mu) > 8$ GeV
mu18_tight_e7_medium1	MU15	$p_{\mathrm{T}}(e) > 8$ GeV, $p_{\mathrm{T}}(\mu) > 18$ GeV

A combination of two dilepton triggers with logical OR is only considered if the combined trigger efficiencies can be significantly increased for a particular area of the surface which is spanned by the p_T of the two leptons. This can be deduced from the p_T-dependent efficiency measurements.

7.6.2. Coverage of p_T surface

The decision on which combination of triggers to use for which region of the p_T surface is based on the possible increase of the overall efficiency on the studied

SUSY signal models for a particular region of the p_T surface. The coverage of the p_T surfaces for the final states with two electrons, the ee channel, with two muons, the $\mu\mu$ channel, or with one electron and one muon, the $e\mu$ channel, is summarised in Table 7.4.

TABLE 7.4.: *The dilepton triggers which are used in the different regions of the lepton p_T surface.*

Region	Trigger	x-axis	y-axis
ee channel:			
region A	2e12Tvh_loose1	$p_T^{el1} > 14$ GeV	$p_T^{el2} > 14$ GeV
region B	e24vh_medium1-		
	_e7_medium1	$p_T^{el1} > 25$ GeV	$10 < p_T^{el2} < 14$ GeV
$\mu\mu$ channel:			
region A	mu18_tight_mu8_EFFS	$p_T^{\mu 1} > 18$ GeV	$p_T^{\mu 2} > 18$ GeV
region B	mu18_tight_mu8_EFFS		
	or 2mu13	$p_T^{\mu 1} > 18$ GeV	$14 < p_T^{\mu 2} < 18$ GeV
region C	mu18_tight_mu8_EFFS	$p_T^{\mu 1} > 18$ GeV	$8 < p_T^{\mu 2} < 14$ GeV
region D	2mu13	$14 < p_T^{\mu 1} < 18$ GeV	$14 < p_T^{\mu 2} < 18$ GeV
$e\mu$ channel:			
region A	e12Tvh_medium1_mu8	$p_T^{el} > 14$ GeV	$p_T^{\mu} > 8$ GeV
region B	mu18_tight_e7_medium1	$10 < p_T^{el} < 14$ GeV	$p_T^{\mu} > 18$ GeV

ELECTRON-ELECTRON The electron trigger leg which only requires online electrons with 'loose1' reconstruction quality and which is used for the symmetric dielectron trigger is in general more efficient than the 'medium1' legs of the asymmetric dielectron trigger. Therefore it is very likely that an event which has a positive decision for the asymmetric dielectron trigger also causes the symmetric dielectron trigger. Using only the symmetric dielectron trigger for electrons with $p_T^{el1}, p_T^{el2} > 14$ GeV instead of both dielectron triggers means an efficiency loss of only 1%. These p_T requirements correspond to the ones for region A in Figure 7.4 (a). The asymmetric dielectron trigger has a lower p_T threshold and therefore covers region B for $p_T^{el1} > 25$ GeV and $10 < p_T^{el2} < 14$ GeV.

(a) ee

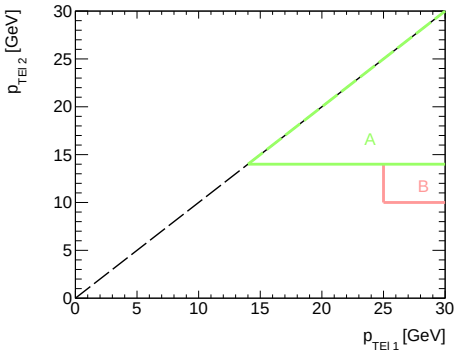

(b) $\mu\mu$

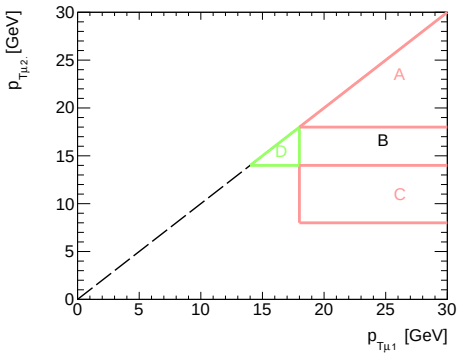

(c) $e\mu$

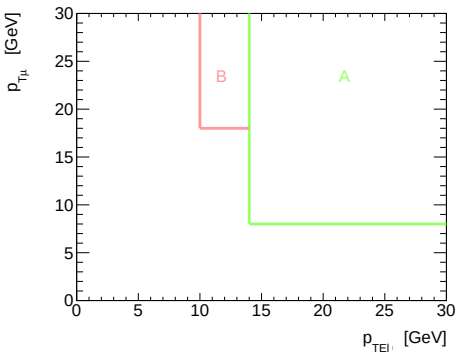

FIGURE 7.4.: *The coverage of the p_T surfaces for the final states with two electrons (a), two muons (b) or one electron and one muon (c).*

MUON-MUON For the muon triggers, it cannot clearly be stated if one dimuon trigger is more efficient than the other. In contrast to the symmetric dimuon trigger which requires a Level 1 seed ('2MU10') for both legs, the asymmetric dimuon trigger only requests a Level 1 seed for the 'mu18_tight' leg, 'MU15'. The situation becomes even less obvious regarding the 'Event Filter Full Scan' feature of the 'mu8_EFFS' leg of the asymmetric trigger (explanation in Section 7.6.4). Studies of the gain in efficiency for the possible combinations lead to the recommendations explained in the following paragraph.

For region A of the p_T surface in Figure 7.4 (b) for the $\mu\mu$ final state where $p_T^{\mu 1}, p_T^{\mu 2} > 18$ GeV, the asymmetric dimuon trigger is used. Here the muons have a p_T that is high enough to match both muons to the 'mu18_tight' leg of the trigger, which is the leg which is seeded by Level 1.

Region B is defined by $p_T^{\mu 1} > 18$ GeV and $14 < p_T^{\mu 2} < 18$ GeV, which means that only the leading muon can trigger the 'mu18_tight' leg. Studies showed that a logical OR of the asymmetric and the symmetric dimuon triggers actually improves the total efficiency in region B by 4-5%.

In region C, the logical OR does not significantly increase the overall efficiency and therefore only the asymmetric trigger is used for $p_T^{\mu 1} > 18$ GeV and $8 < p_T^{\mu 2} < 14$ GeV.

In region D with $14 < p_T^{\mu 1}, p_T^{\mu 2} < 18$ GeV, the pT for both muons is too low to trigger the 'mu18_tight' leg of the asymmetric dimuon trigger. Therefore this region is only covered by the symmetric dimuon trigger.

ELECTRON, MUON AND MUON, ELECTRON The surface which is spanned by the transverse momenta of a final state electron and a final state muon is depicted in Figure 7.4 (c). Region 'A' is defined by $p_T^{el} > 14$ GeV and $p_T^{\mu} > 8$ GeV and is covered by the electron-muon trigger e12Tvh_medium1_mu8. This trigger has looser muon requirements than the muon-electron trigger mu18_tight_e7_medium1.

The latter is used in region B with $10 < p_T^{el} < 14$ GeV and $p_T^{\mu} > 18$ GeV since this region is not accessible for the electron-muon trigger with the higher p_T threshold for online electrons.

7.6.3. REWEIGHTING PROCEDURE

To each MC simulated event used in the analysis described in this Chapter, a weight is assigned which corresponds to the probability that this event has a positive trigger decision in ATLAS data. The weight is computed from the efficiencies which are measured in data as described in Section 7.6.4.

7.6.3.1. Weight Computation

Symmetric Dilepton Trigger The symmetric dilepton trigger has a Level 1 seed for both legs. The probability for a dilepton trigger to have a positive decision in an event with n leptons is given in Equation 6.11. For $n = 2$ leptons, the formula reduces to

$$P(2l) = \epsilon_1 \cdot \epsilon_2 \tag{7.1}$$

with ϵ_1 being the efficiency of the leading lepton and ϵ_2 being the efficiency of the subleading lepton. With this formula, the weights for the p_T-surface regions for symmetric dilepton triggers like e.g. region D for the $\mu\mu$ channel can be computed.

Asymmetric Dilepton Trigger The asymmetric dilepton trigger only has a Level 1 seed for the first leg of the trigger but not for the second leg. Not both leptons need to fire both legs of the trigger, but this case also needs to be considered. It is reflected in the first line of the following equation.

$$P(2l) = P(^{lepton1}_{leg1}) \cdot P(^{lepton2}_{leg1}) \cdot P(^{lepton1}_{leg2|leg1}) \cdot P(^{lepton2}_{leg2|leg1}) \tag{7.2}$$

$$+P(^{lepton1}_{leg1}) \cdot (1 - P(^{lepton}_{leg1})) \cdot P(^{lepton1}_{leg2|leg1}) \cdot P(^{lepton2}_{leg2|!leg1}) \tag{7.3}$$

$$+(1 - P(^{lepton1}_{leg1})) \cdot P(^{lepton}_{leg1}) \cdot P(^{lepton1}_{leg2|!leg1}) \cdot P(^{lepton2}_{leg2|leg1}) \tag{7.4}$$

In the other two lines only one of the two leptons triggers the leg with the Level 1 requirement. $P(^{lepton1}_{leg2|leg1})$ is the probability for lepton 1 to cause leg2 of the asymmetric trigger when leg1 also was triggered by the same lepton. $P(^{lepton2}_{leg2|!leg1})$ is the probability for lepton 2 to cause leg2 of the asymmetric trigger under the condition that leg1 has a negative decision.

This formula is used to calculate the weight for e.g. p_T-surface region A of the $\mu\mu$ channel. Therefore it is necessary to measure the conditional efficiencies for the muon triggers 'mu8_EFFS|mu18_tight' (the efficiency of 'mu8_EFFS' if also 'mu18_tight' is caused) and 'mu8_EFFS|!mu18_tight' (the efficiency of 'mu8_EFFS' if 'mu18_tight' is not caused).

In a p_T-surface region where only the leading lepton has a p_T which is high enough to trigger the leg1 of the asymmetric dilepton trigger, the formula to compute the weight is given by the following equation:

$$P(2l) = P(^{lepton1}_{leg1}) \cdot P(^{lepton2}_{leg2}) \cdot P(^{lepton1}_{leg2|leg1}) = P(^{lepton1}_{leg1}) \cdot P(^{lepton2}_{leg2}) \tag{7.5}$$

With the assumption that $P(^{lepton1}_{leg2|leg1}) = 1$ because the requirements of leg1 are always tighter than the ones of leg2. This formula is used in e.g. region C of the $\mu\mu$ channel.

SYMMETRIC DILEPTON TRIGGER OR ASYMMETRIC DILEPTON TRIGGER For region B of the $\mu\mu$ channel, the probability for the symmetric dilepton trigger (S) OR the asymmetric dilepton trigger (A) having a positive decision needs to be computed. One starts with the general formula of

$$P(A \vee S) = P(S) + P(A|!S) \cdot P(!S). \tag{7.6}$$

The first term, $P(S)$, is given by Equation 7.1. One has to keep in mind that

- the symmetric trigger requires a Level 1 seed for both legs,
- the asymmetric trigger only requires a Level 1 seed for leg1 and
- the requirements of leg1 of the asymmetric trigger are always tighter than the ones of the legs of the symmetric trigger.

This means that the asymmetric trigger can only recover the Level 1 inefficiencies of the symmetric trigger. The probability for the asymmetric dilepton trigger to have a positive decision, $P(A)$, can be decomposed like the following:

$$P(A) = P(A_{leg1}^{lepton1} \vee A_{leg1}^{lepton2}) \tag{7.7}$$

$$= P(A_{leg1}^{lepton1}) + P(A_{leg1}^{lepton2}|A_{!leg1}^{lepton1}) \cdot P(A_{!leg1}^{lepton1}) \tag{7.8}$$

where it is indirectly assumed that each time the other lepton triggered leg2 of the asymmetric trigger. It is then also valid that

$$P(A|!S) = P((A_{leg1}^{lepton1} \vee A_{leg1}^{lepton2})|(S^{!lepton1} \vee S^{!lepton2})) \tag{7.9}$$

where $S^{!lepton\,i}$ means that lepton i does not cause the symmetric dilepton trigger.

The second term of Equation 7.6 can then be calculated with the following formula.

$$P(A|!S) \cdot P(!S) = P(A_{leg1}^{lepton1}|S^{lepton1} \wedge S^{!lepton2}) \cdot P(S^{lepton1} \wedge S^{!lepton2}) \tag{7.10}$$

$$+P(A_{leg1}^{lepton2}|S^{!lepton1} \wedge S^{lepton2}) \cdot P(S^{!lepton1} \wedge S^{lepton2}) \tag{7.11}$$

It is assumed that $P(A_{leg1}^{lepton1}|S^{!lepton1}) = P(A_{leg1}^{lepton2}|S^{!lepton2}) = 0$ because the Level 1 requirement of A is always tighter than the Level 1 requirement of S. The whole formula then becomes

$$P(2l) = S^{lepton1} \cdot S^{lepton2} \tag{7.12}$$

$$+P(A_{leg1}^{lepton1}) \cdot P(A_{leg2}^{lepton2}|S^{!lepton2}) \cdot P(S^{!lepton2}) \tag{7.13}$$

$$+P(A_{leg2}^{lepton1}) \cdot P(A_{leg1}^{lepton2}|S^{!lepton1}) \cdot P(S^{!lepton1}). \tag{7.14}$$

7.6.3.2. Closure Tests

The validity of the factorisability assumption and the Reweighting Method is shown in a closure test for each of the three channels $\mu\mu$, $e\mu$ and ee. Instead of measuring the efficiencies in ATLAS data to compute the weights for the MC events, the efficiencies of the simulated triggers are measured in appropriate MC samples. The weights which are based on those MC efficiencies are then applied on a $t\bar{t}$ MC sample generated with MC@NLO [49]- [51] and JIMMY [47] and compared to the efficiencies when asking for a positive decision of the simulated triggers in this $t\bar{t}$ sample.

Muon, Muon Closure Test $Z \rightarrow \mu\mu + jets$ events generated with ALPGEN [52] and JIMMY [47] are selected to measure the efficiencies of the muon triggers with the Tag & Probe Method. Details about the completely analogues measurements in ATLAS data will be given in Section 7.6.4.

The $t\bar{t}$ sample is then processed twice. In a first step, a positive trigger decision of the dimuon triggers is requested according to the strategy for the $\mu\mu$ channel. In a second step, the events are reweighted with the probability that the dilepton triggers have a positive decision, using the efficiencies measured in the $Z \rightarrow \mu\mu + jets$ MC sample. The distributions for the transverse momenta of the leading and subleading muon in the $t\bar{t}$ events as well as for the pseudorapidities are shown in Figures 7.5 (a) and (b), respectively.

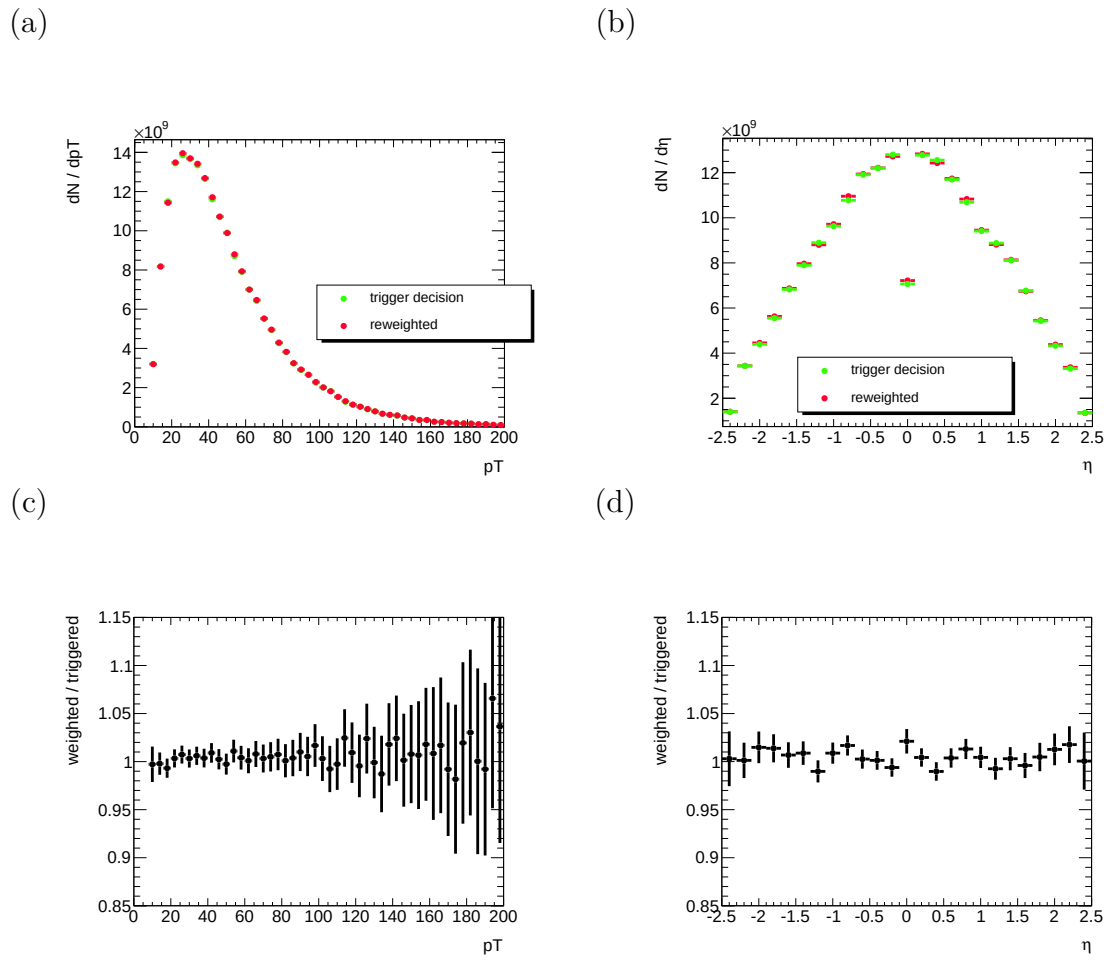

FIGURE 7.5.: *(a) and (b) show the distributions of p_T and η for the leading and subleading muons in $\mu\mu$ events of a $t\bar{t}$ MC sample. The green points show step one of the closure test, where a positive decision of the simulated triggers is requested. The red points show step two where a weight is applied on each event which is computed from the efficiencies measured in the $Z \to \mu\mu + jets$ MC samples. (c) and (d) show the ratios of the two curves in (a) and (b), respectively.*

The fact that the distributions agree within uncertainties proves that the factorisability assumption is correct and that the binning which is chosen for the parametrisation of the muon trigger efficiencies is reflecting the detector geometry of the MS very well. The efficiencies depend on η and ϕ, the binning is chosen according to recommendations of the ATLAS trigger group. The dependency on p_T is discarded not to introduce an additional statistical uncertainty due to fine binning. From the ratios shown in Figures 7.5 (c) and (d) which are defined by the number of weighted events divided by the number of events with a positive trigger decision for each bin, a deviation of 1% is deduced.

ELECTRON, MUON AND MUON, ELECTRON CLOSURE TESTS To perform the closure test in the final state with one electron and one muon, weights computed from efficiencies measured in $Z \to ee + jets$ and in $Z \to \mu\mu + jets$ MC samples which are generated with PYTHIA [45], and with ALPGEN [52] and JIMMY [47], respectively, are applied on $t\bar{t}$ MC events. For the $e\mu$ channel, i.e. the final state where the electron has a higher p_T than the muon, the distributions for the p_T and η of the electron are shown in Figures 7.6 (a) and (b). The distributions agree within errors. From the ratio plots in Figures 7.6 (c) and (d) a deviation of 1% is deduced.

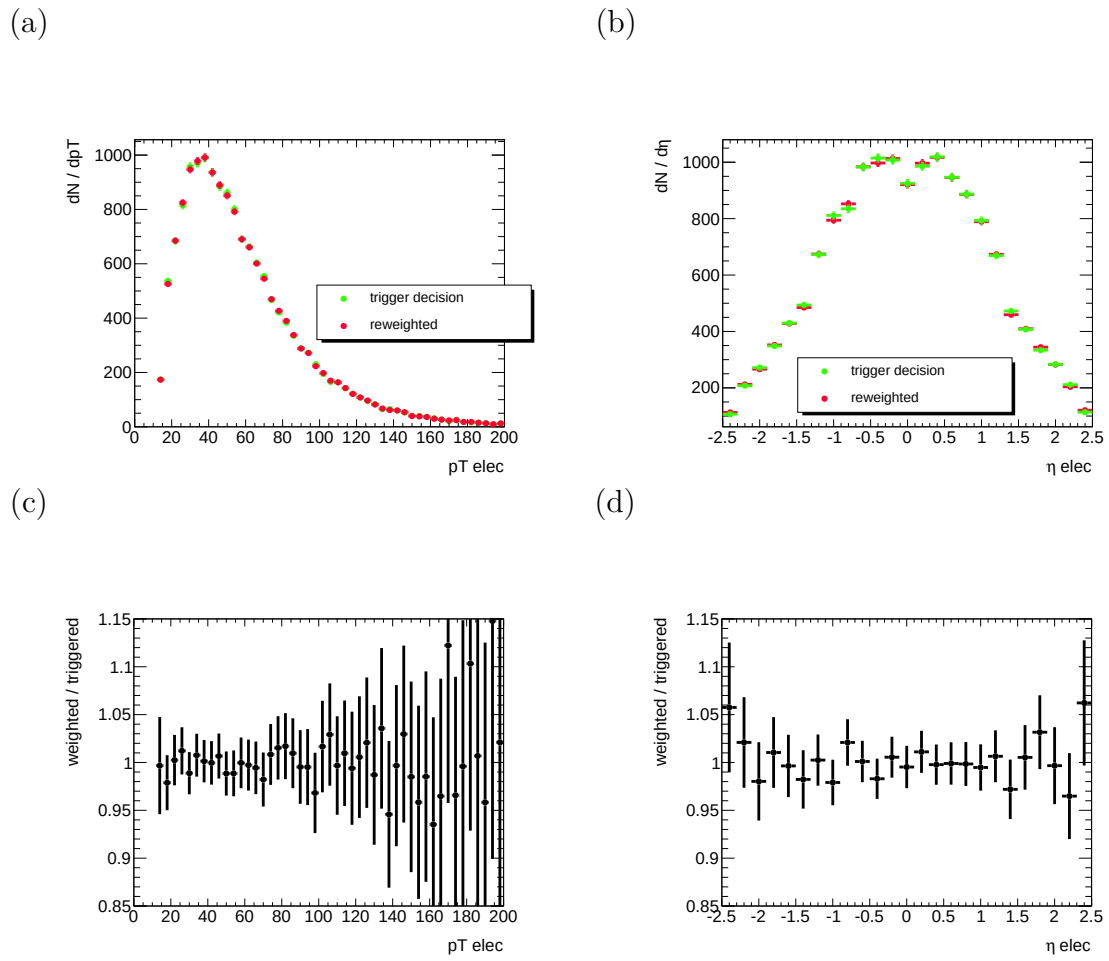

FIGURE 7.6.: *(a) and (b) show the distributions of p_T and η for the electron in $e\mu$ events of a $t\bar{t}$ MC sample. The green points show step one of the closure test, where a positive decision of the simulated triggers is requested. The red points show step two where a weight is applied on each event which is computed from the efficiencies measured in the $Z \to \mu\mu + jets$ and $Z \to ee + jets$ MC samples. (c) and (d) show the ratios of the two curves in (a) and (b), respectively.*

For the kinematics of the muon in μe events, the distributions are shown in Figures 7.7 (a) and (b). In almost every bin, the distributions of the events with the positive trigger decision lie above the distributions for the weighted events. This means that the Reweighting Method is underestimating the total event yield. From the ratio plots in Figures 7.7 (c) and (d), a deviation of 10% for $|\eta| > 1.37$ and a deviation of 30% for electrons with $|\eta| \leq 1.37$ is read off. The comparably large deviations are due to the usage of the efficiency of the 'e7T_medium1' trigger for factorising the muon-electron trigger mu18_tight_e7_medium1. More details are given in the next paragraph where the closure test for ee final states is explained.

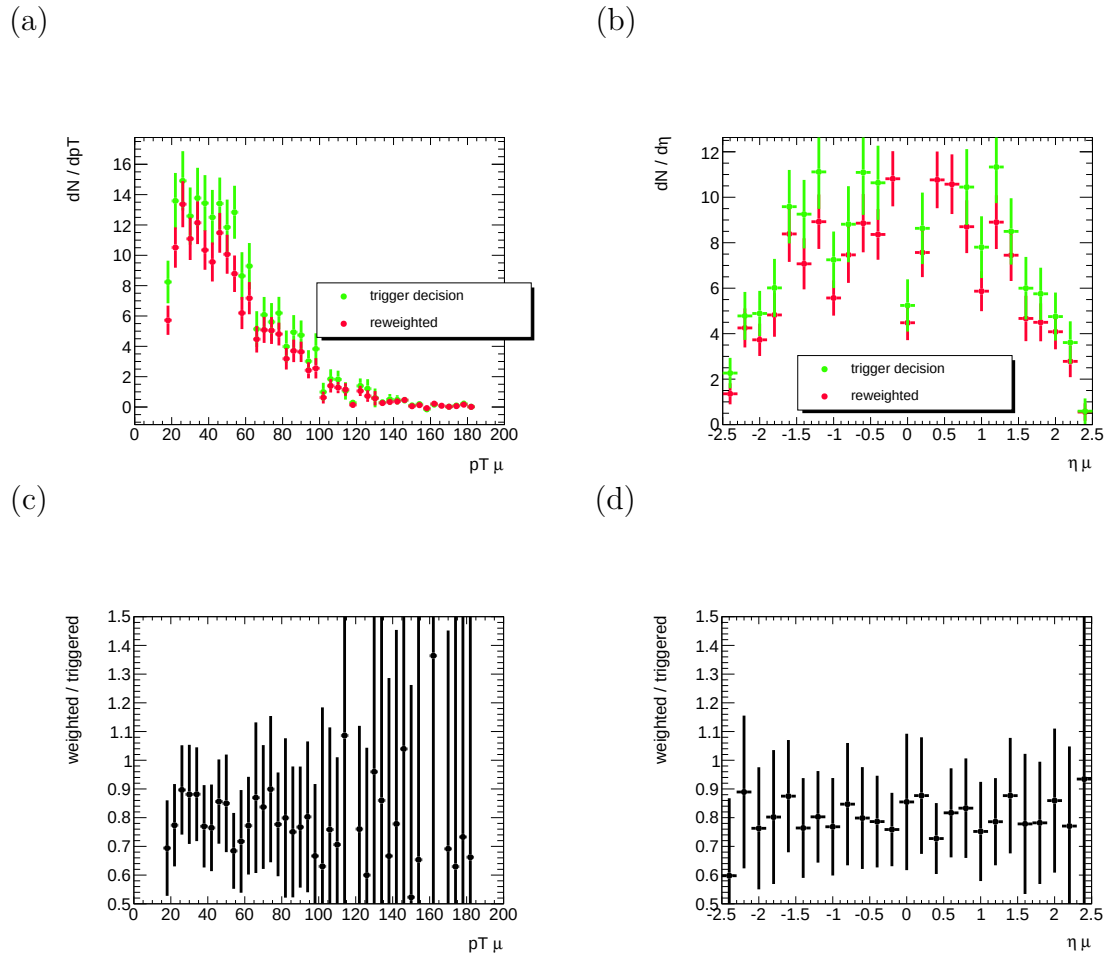

FIGURE 7.7.: *(a) and (b) show the distributions of p_T and η for the muon in μe events of a $t\bar{t}$ MC sample. The green points show step one of the closure test, where a positive decision of the simulated triggers is requested. The red points show step two where a weight is applied on each event which is computed from the efficiencies measured in the $Z \to \mu\mu + jets$ and $Z \to ee + jets$ MC samples. (c) and (d) show the ratios of the two curves in (a) and (b), respectively.*

ELECTRON, ELECTRON CLOSURE TEST For the closure test with events with two electrons in the final state, weights are computed based on the efficiencies measured for simulated triggers in $Z \to ee + jets$ events in a MC sample generated with PYTHIA [45]. For the part of the p_T-surface where the symmetric dielectron trigger is used, 2e12Tvh_loose1 in region A, a deviation of maximum 0.5% can be quoted. This is deduced from the comparison of the distribution for the $t\bar{t}$ MC events which have a positive trigger decision with the distribution for the events which are reweighted. It means that the factorisability assumption is correct and that the chosen parametrisation of the efficiencies, namely the dependencies on p_T and η in a binning which follows the recommendations of the ATLAS trigger group, is meaningful. The efficiencies found in $30 < p_T < 60$ GeV are extrapolated to high-p_T regions with low statistics.

In region B, however, where the asymmetric dielectron trigger e24vh_medium1_e7_medium1 is used, a deviation of 10% for electrons which are detected in the endcap region of ATLAS and a deviation of 40% for the electrons in the barrel region is found.

A problem occurred with the measurement of the efficiency of the 'e7_medium1' leg. This trigger was not implemented in the trigger menu for the 2012 data taking until the run period B14. It therefore needs to be rebuild with offline selection cuts in ATLAS data. It is also not simulated in Monte Carlo. For this reason for the closure test, the simulated 'e7T_medium1' trigger is used. Instead of 'EM3' for 'e7_medium1', it has a different seed at Level 1, namely 'EM6'. This fact as well as the poor quality of the electrons in the 10-14 GeV p_T range leads to the comparably large deviation in the closure tests for the asymmetric dielectron trigger as well as for the muon-electron trigger.

7.6.4. TRIGGER EFFICIENCIES IN DATA

To study the performance of the dilepton triggers listed in Table 7.3 in ATLAS data, the efficiencies of the individual legs, i.e. the single lepton triggers, are measured with the Tag & Probe Method which was introduced in Section 6.7.3. The efficiencies of the dilepton triggers can then be estimated by factorising them with the single lepton trigger efficiencies.

7.6.4.1. MUON TRIGGER EFFICIENCIES

If a muon in a $Z \to \mu^+\mu^-$ event can be tagged by matching it in the η-ϕ space with $\Delta R < 0.15$ to the muon on Event Filter level that released the lowest unprescaled single muon trigger, then the other muon becomes the probe muon. Each event is processed twice, and in the second attempt it is checked if the other muon can be tagged so that the first muon becomes the probe muon.

'MU13' To measure the efficiency of the 'mu13' trigger, all probe muons are checked if they can be matched to the online muons which unleashed the trigger. The efficiency depending on the p_T of the offline probe muons is shown in Figure 7.8 (a). Muons in the endcap region, $|\eta| > 1.05$, have in general a better acceptance already on Level 1 of the ATLAS trigger system and also a higher efficiency compared to the muons which are detected in the barrel region of the detector, $|\eta| \leq 1.05$. The efficiencies are therefore always shown separately for those two categories. The curve for endcap muons in Figure 7.8 (a) reaches 90% of the absolute efficiency at 14 GeV which is the value chosen for the offline p_T cut. The plateau efficiency, i.e. a rather stable value for high p_T, is reached at 88%. From the curve for the barrel muons the same offline p_T value is deduced as from the curve for the endcap muons, as was expected. The plateau efficiency for the barrel muons, however, reaches only 72%.

'MU18_TIGHT' FOR DIMUON TRIGGER Analogously, the plateau efficiencies for the trigger 'mu18_tight' are measured to be 86% for endcap muons and 66% for barrel muons. From the turn-on curves in Figure 7.8 (b) it can be read off that a cut on the offline p_T at 18 GeV ensures a stable efficiency as a function of the muon transverse momentum. When matching the probe muons to the online muons which triggered 'mu18_tight', it is in addition required that the so-called 'TrigMuonEF' algorithm was used to reconstruct the online muon. This particular algorithm is used for the asymmetric dimuon trigger.

'MU8' FOR DIMUON TRIGGER The token 'EFFS' in the name of the asymmetric dimuon trigger stands for 'Event Filter Full Scan' - on Event Filter level, the algorithms do exceptionally not only work with the Regions of Interest from Level 1 and Level 2, but enough time is admitted to perform a full scan of the muon information to recover the inefficiencies of the Level 1 trigger. The measurement of the 'mu8' leg of this trigger is not straight-forward because the requirement on the second muon only needs to be fulfilled on Event Filter level, not on Level 1: only the information about the decision of the complete asymmetric dimuon trigger is available.

The decision of the dimuon trigger is positive if two muons are found at Event Filter level, one of which had a p_T of more than 15 GeV on Level 1. On Event Filter level, one of the two muons fulfils the 'mu18_tight' condition and one muon the 'mu8' requirement. The information about the 'mu8' decision is not available independently of the 'mu18_tight' decision.

To measure the efficiency of the 'mu8' leg of this dimuon trigger, each tag muon is therefore not only matched to the muon which triggered the lowest p_T unprescaled single muon trigger. It must also be matched to one of the online muons which caused the asymmetric dimuon trigger and which has an online p_T of more than 18 GeV. The information about whether an online muon caused one leg of the mu18_tight_mu8_EFFS trigger is available, but not about which leg it was. For the efficiency measurement of the 'mu8' leg, one counts the number of probe muons

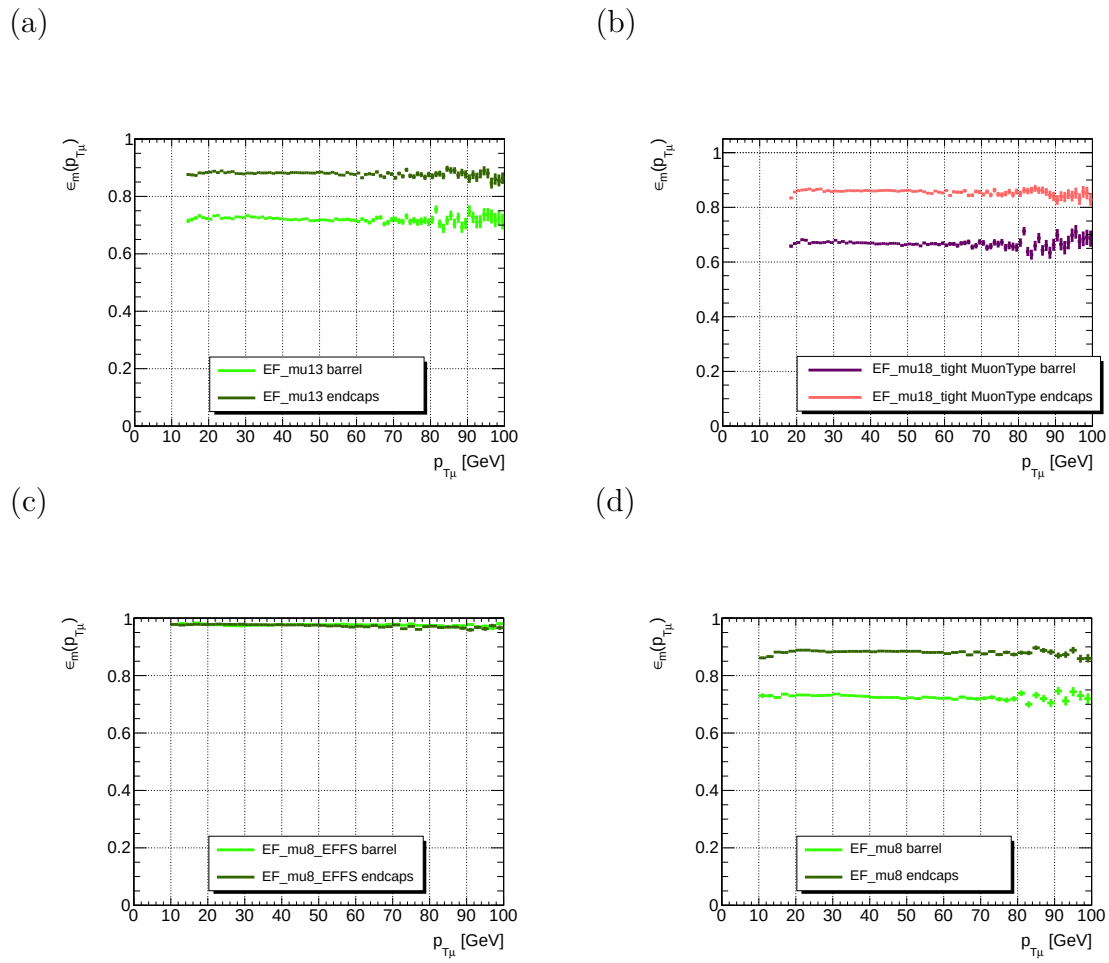

FIGURE 7.8.: *The efficiencies of the single muon triggers in ATLAS data of the 2012 run periods A and B, depending on the offline p_T of the probe muon. The efficiency of muons detected in the barrel region ($|\eta| \leq 1.05$) is represented by light green or purple lines, the efficiency of muons detected in the endcap region ($|\eta| > 1.05$) are represented by dark green or pink lines. The errors are statistical errors. The plot in (a) shows the efficiency for 'mu13', (b) for 'mu18_tight' for the asymmetric dimuon trigger, (c) for 'mu8_EFFS' and (d) for 'mu8'.*

which can be matched to another online muon that also caused the asymmetric dimuon trigger and that has an online p_T of more than 8 GeV.

Muons which are detected in the barrel region of the detector and muons in the endcap region have the same turn-on curves as can be seen in Figure 7.8 (c). The trigger is fully turned on for $p_T > 8$ GeV and the plateau efficiency is at 98%. Obviously the decreased acceptance for muons at Level 1 is recovered for this trigger.

'MU8' FOR ELECTRON-MUON TRIGGER The efficiency of 'mu8' also needs to be measured for the electron-muon trigger e12Tvh_medium1_mu8. The probe muons are matched to the online muons which triggered 'mu8' since in this case the information about the trigger decision is available independently of the 'e12Tvh_medium1' leg. The efficiency depending on the p_T of the probe muons is shown in Figure 7.8 (d). It reaches a plateau at 88% for muons in the endcap region and 73% for muons in the barrel region. The offline p_T cut value is at 8 GeV.

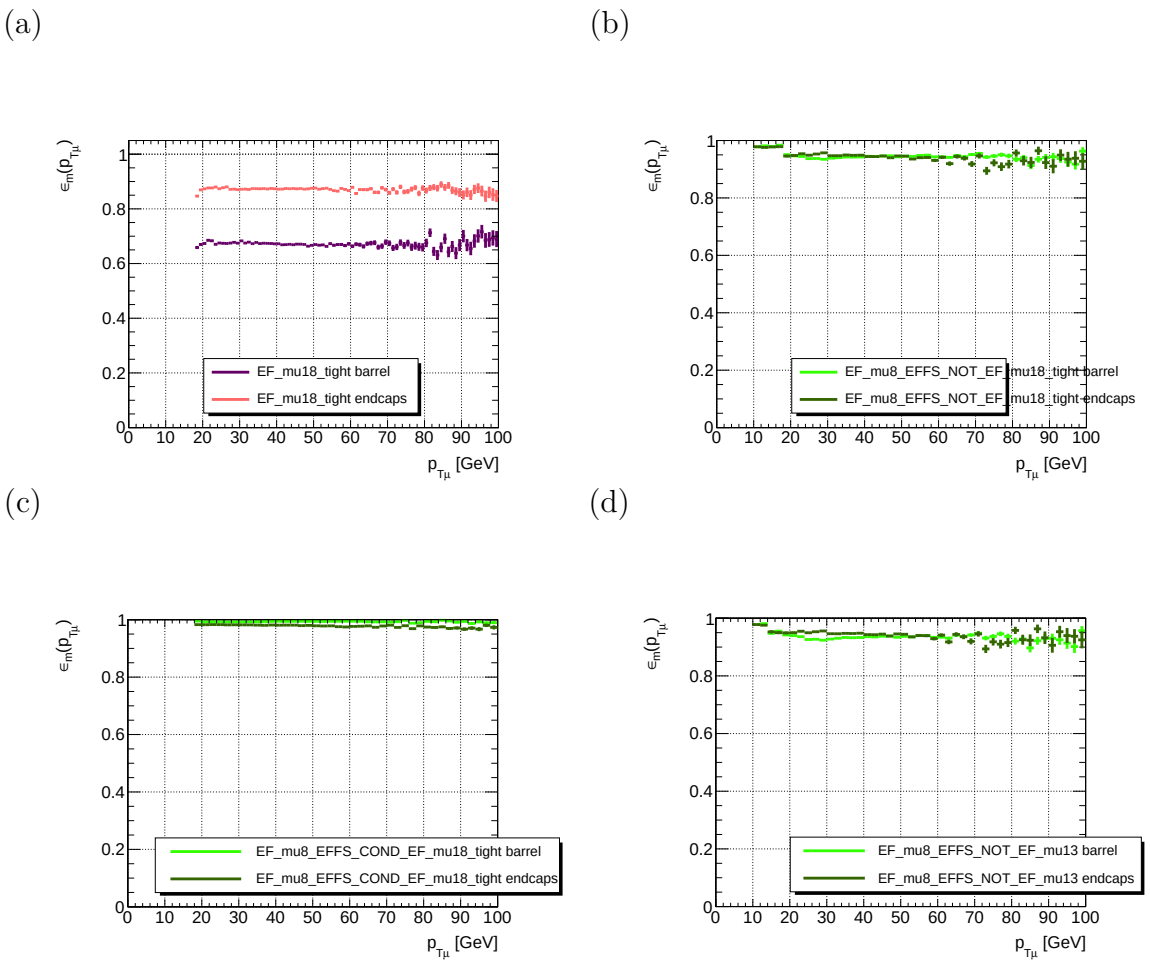

FIGURE 7.9.: *The (conditional) efficiencies of the single muon triggers in ATLAS data of the 2012 run periods A and B, depending on the p_T of the probe muon. The efficiency of muons detected in the barrel region ($|\eta| \leq 1.05$) is represented by light green or purple lines, the efficiency of muons detected in the endcap region ($|\eta| > 1.05$) are represented by dark green or pink lines. The errors are statistical errors. The plot in (a) shows the efficiency for mu18_tight for the muon-electron trigger, (b) the conditional efficiency mu8_EFFS|!mu18_tight for the symmetric dimuon trigger, (c) the conditional efficiency mu8_EFFS|mu18_tight for the symmetric dimuon trigger and (d) the conditional efficiency for mu8_EFFS|!mu13.*

'MU18_TIGHT' FOR MUON-ELECTRON TRIGGER For the muon-electron trigger mu18_tight_e7_medium1 the efficiency of 'mu18_tight' needs to be measured not only for the muons found by the TrigMuonEF algorithm. Another reconstruction algorithm is called 'MuGirl'. The resulting efficiency is shown for barrel muons and for endcap muons in Figure 7.9 (a) and is lower for barrel muons due to the inefficiency of Level 1 muon triggers. The plateau is reached at 87% for the endcap region and at 67% for the barrel region, the offline p_T cut is chosen to be 18 GeV.

CONDITIONAL 'MU8_EFFS|!MU18_TIGHT' For the combination with logical OR measurements of conditional efficiencies are needed. The efficiency for the 'mu8' leg of the asymmetric dimuon trigger under the condition that 'mu18_tight' has a negative decision is computed in this way: if a probe muon cannot be matched to the online muon which caused 'mu18_tight', the same checks for the tag and for the probe muons are done as for measuring the efficiency of 'mu8_EFFS'. The turn-on curves are shown in Figure 7.9 (b). The efficiencies for the barrel and endcap muons are again very similar and start at 98% for a p_T of the probe muons of more than 10 GeV. For $p_T >$ 18 GeV, the efficiency drops to a plateau value of 94% which is expected since the 'mu18_tight' trigger only becomes fully efficient only for $p_T >$ 18 GeV.

CONDITIONAL 'MU8_EFFS|MU18_TIGHT' The efficiency of 'mu8_EFFS' is measured once more in the same way if the probe muon can be matched to 'mu18_tight' to plot the turn-on curves for the positive conditional efficiency of 'mu8_EFFS|mu18_tight'. It is shown in Figure 7.9 (c). The curves for the endcap and for the barrel muons are very similar, the plateau efficiencies are reached at 99% and 98%, respectively, and the offline p_T threshold is chosen to be larger than 8 GeV.

CONDITIONAL 'MU8_EFFS|!MU13' One more conditional efficiency which needs to be measured is 'mu8_EFFS|!mu13'. If a probe muon cannot be matched to an online muon which caused 'mu13', the efficiency of 'mu8_EFFS' is computed with the matching procedure as described above. The turn-on curves lie on top of each other for endcap and for barrel muons as can be seen in Figure 7.9 (d). A plateau efficiency of 98% is reached for probe muons with $p_T >$ 8 GeV and it falls to 94% for $p_T >$ 14 GeV. That was expected since the 'mu13' trigger only becomes fully efficient for $p_T >$ 14 GeV.

7.6.4.2. ELECTRON TRIGGER EFFICIENCIES

For measuring the efficiencies of the single electron triggers which make up the legs of the dielectron triggers and the electron-muon triggers, the Tag & Probe Method is used. The tag electron is matched to the online electron which caused the lowest

unprescaled single electron trigger. The probe electron is then matched to the online electron which caused the trigger of interest.

The efficiencies of the single electron triggers as well as a summary of the muon trigger efficiencies are listed in Table 7.5.

TABLE 7.5.: *The summary of the single lepton trigger efficiencies, measured in period A of the 2012 ATLAS data. The barrel region spans up to $|\eta| = 1.05$ for muons and to $0.1 < |\eta| < 1.37$ for electrons. The endcap region for electrons is $1.52 \geq |\eta| < 2.01$. For the measurements of the quoted efficiencies, a transition region and a region at $|\eta| \geq 2.01$ is excluded. Also listed are the recommended offline p_T thresholds to ensure a stable efficiency regarding the p_T-dependency.*

Trigger	Offline p_T threshold [GeV]	$\epsilon_{\text{endcaps}}$	ϵ_{barrel}
e12Tvh_loose1	14	0.99	0.97
e24vh_medium1	25	0.96	0.91
e7_medium1	10	0.97	0.93
mu13	14	0.72	0.88
mu18_tight (dimuon trigger)	18	0.66	0.86
mu8_EFFS	8	0.98	0.98
mu8	8	0.73	0.88
mu18_tight (muon-electron trigger)	18	0.67	0.87

7.6.5. TRIGGER SYSTEMATICS

The deviations observed in the closure tests are used to assign a systematic uncertainty to the Reweighting Method. They take into account the accuracy of the factorisability assumption and the parametrisation and binning of the efficiencies measured in ATLAS data. These uncertainties are combined with the errors assigned to the Tag & Probe Method. In the following the latter are deduced for muon triggers.

7.6.5.1. TAG & PROBE METHOD - ERRORS FOR MUON TRIGGERS

DEPENDENCY ON RUN PERIODS A possible dependency on the run periods of the 2012 ATLAS data taking is taken into account by measuring the efficiencies of the muon triggers individually for the run periods A, B, C, D, E, G, H, I, J, L. That there is indeed a difference for e.g. the comparably short run period A and the run period B, but that the efficiency of a trigger stays rather constant during the subdivisions of run period B, becomes obvious in the plot in Figure 7.10 (a). It shows the efficiency of

mu13 depending on the pseudorapidity of the probe muons for the measurement in data of run period A in pink dots and the measurement in run period B in the other colours. The efficiency is in some bins lower for run period A, but the efficiencies in the subdivisions of run period B are very similar and no obvious tendency is observed.

(a) (b)

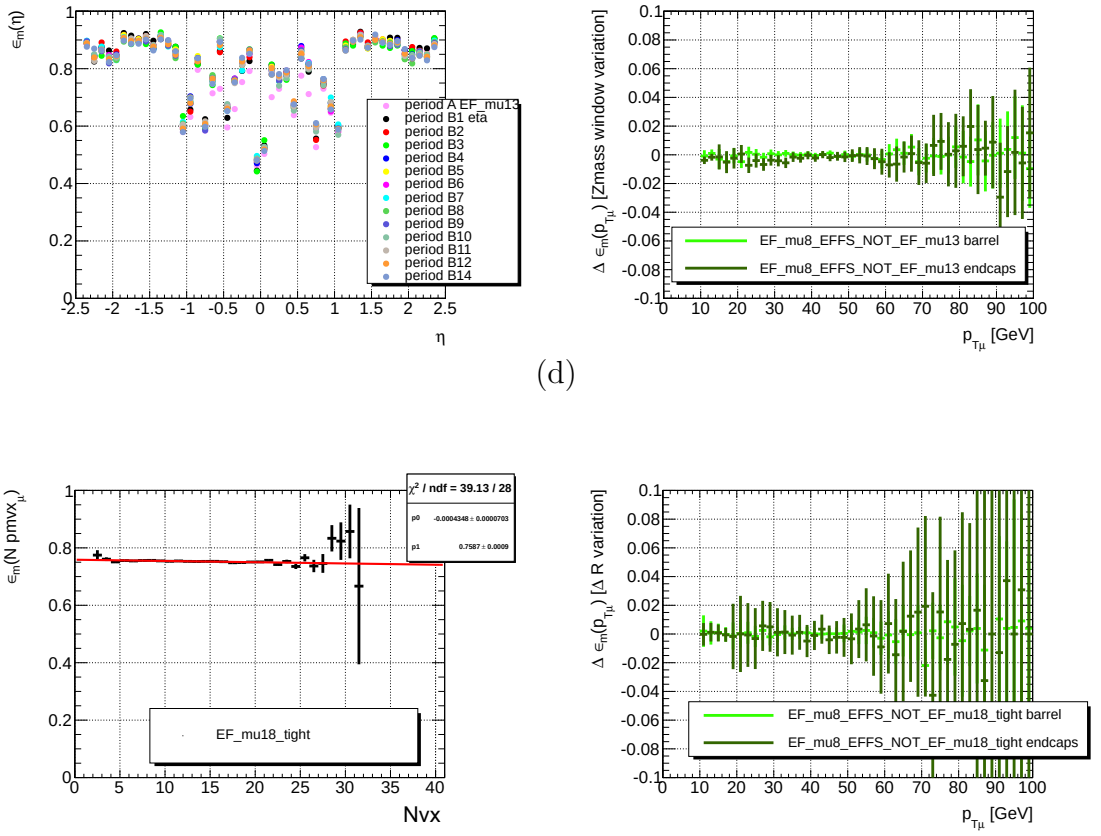

(c) (d)

FIGURE 7.10.: *(a) shows the efficiency measurements of the mu13 trigger for run period A and the subdivisions of run period B depending on η of the probe muons. (b) shows the conditional efficiency of mu8_EFFS!!mu18_tight for a Z-mass window of size 8 GeV, subtracted from the efficiency for a Z-mass window of size 25 GeV (run period B). (c) shows the efficiency of the mu18_tight trigger for the muon-electron trigger depending on the number of vertices for data recorded in the 2012 ATLAS run period B. It is fitted with a linear function (red line). (d) shows the conditional efficiency of mu8_EFFS!!mu13 for $\Delta R < 0.1$ for the matching of the probe muon to the online muon minus $\Delta R < 0.2$ in ATLAS run period A. The distributions in light green colour show the difference for muons in the barrel region ($|\eta| \leq 1.05$) and the distributions in dark green colour for muons in the endcap region ($|\eta| > 1.05$).*

The dependency on run periods is taken into account for the study of the systematic errors of the Tag & Probe Method by comparing the variations of e.g. ΔR for the matching of the offline and online leptons for the two datasets of run period A and B.

Variation of Z-mass Window For muon triggers, the 'Z mass window' to select SFOS leptons which have a total invariant mass inside the window and which most likely result from a Z boson decay is nominally set to $m_Z \pm$ 10 GeV. It is varied to $\pm$ 25 and $\pm$ 8 GeV to study the influence on the efficiency measurements. This results in an error of 1% for the bins with reasonably high statistics. In Figure 7.10 (b), the difference for the conditional efficiencies of e.g. mu8_EFFS|!mu13 is shown for ϵ(Z-mass window $\pm$ 25 GeV) $-\epsilon$(Z-mass window $\pm$ 8 GeV) for muons detected in the barrel and in the endcap region of ATLAS, respectively. For this plot the efficiency is measured in ATLAS data of the run period B.

Dependency on Pile-up The dependency of the efficiency measurements on pile-up, i.e. the number of vertices N_{vx}, is evaluated. Figure 7.10 (c) shows the efficiency of mu18_tight for the muon-electron trigger depending on N_{vx}. The efficiency values vary significantly in the bins with low statistics ($N_{vx} \geq 23$) compared to the plateau values. But since the statistical error in those bins is relatively high, it was decided to fit a linear function to the efficiency curve, depicted by a red line in Figure 7.10 (c). The slope of the function is chosen to be the systematic uncertainty on the number of vertices. With this method, a maximum uncertainty of 0.5% is assigned to the variation of N_{vx} for $N_{vx} < 23$ and 5% for $N_{vx} \geq 23$.

Variation of ΔR Cut To match the offline muons to the online muon which caused the triggers on Event Filter level, $\Delta R = \sqrt{\Delta\eta^2 + \Delta\phi^2}$ must be smaller than 0.15. This threshold is varied to 0.1 and to 0.2 to study the influence on the efficiency measurements. Figure 7.10 (d) shows the difference for the conditional efficiency measurement in data of the run period A of mu8_EFFS|!mu18_tight for $\Delta R < 0.1$ and $\Delta R < 0.2$. In this plot, the difference is at maximum 0.9%. For the measurements in data of the run period B, in most cases a difference of 0.2% is found.

Dependency on p_T For the Reweighting Method, the dependency of the efficiencies of the muon triggers on the transverse momentum is not included. To take into account possible deviations from the quoted plateau efficiency values, an uncertainty of 1% is concluded.

7.6.5.2. Tag & Probe Method - Errors for Electron Triggers

To assign an error to the efficiency measurements for the electron triggers, the same variations and dependencies are studied as for the muon triggers. The electron trig-

ger efficiencies are measured individually for the run period subdivisions of A, B1 - B3, B4 - B8, B9 - B14, C - D3, D4 - D7, D8 - E and I - L.

The nominal value for the Z-mass window is $\pm$ 10 GeV. It is varied to $\pm$ 15 and $\pm$ 25 GeV. The difference between the efficiencies is found to be smaller than 0.4%.

The largest uncertainty is found for the dependency of the efficiency measurements on pile-up, i.e. the number of the vertices. It can be up to 0.5% when comparing the efficiencies for $N_{vx} \geq 14$ and $N_{vx} < 14$.

When the ΔR threshold for matching the offline electrons to the Event Filter electrons is varied from nominal 0.15 to 0.1 or 0.2, the difference is 0.1%.

In contrast to the muon efficiencies, the electron efficiencies depend on the p_T of the electrons. An additional check was performed for the electron trigger efficiencies: the dependency on the quality of the tag electron, i.e. whether it is 'tight++' (nominal requirement) or 'medium++' (loosened requirement). The tag quality does not have much influence on the efficiency measurements since a difference of maximum 0.2% is found.

The uncertainties are in general higher for electron triggers with a 'medium1' quality requirement for the online electron and $|\eta| > 2.37$, $p_T < 50$ GeV for the offline electrons.

7.6.5.3. Summary of Trigger Uncertainties

Table 7.6 summarises the errors for the muon trigger efficiencies and Table 7.7 for the electron trigger efficiencies. The errors from the Tag & Probe Method need to be applied to each muon or electron in an event.

Table 7.6.: *The summary of the systematic uncertainties for the muon triggers, coming from the Tag & Probe Method or the closure test. The errors from the Tag & Probe Method need to be applied to each electron in an event. The error from the closure test is for a $\mu\mu$ event.*

Trigger	Uncertainty Tag & Probe Method	Uncertainty Closure Test
period A		
$N_{vx} < 23$	1.2%	1.0%
$N_{vx} \geq 23$	5.2%	1.0%
period B		
$N_{vx} < 23$	1.2%	1.0%
$N_{vx} \geq 23$	5.2%	1.0%

The errors from the Tag & Probe Method are added linearly for the two leptons in an event, i.e. they are correlated. They are uncorrelated with the errors from the closure tests. Both types of errors are combined to the total systematic errors.

TABLE 7.7.: *The summary of the systematic uncertainties for the electron triggers, coming from the Tag & Probe Method or the closure test. The errors from the Tag & Probe Method need to be applied to each electron in an event. The error from the closure test is for a ee event.*

Trigger	Kinematics	Uncertainty Tag & Probe Method	Uncertainty Closure Test
e12Tvh_medium1, e24vh_medium1	$\|\eta\| < 2.37$ or $p_T > 50$ GeV	0.5%	0.5%
	$\|\eta\| > 2.37$ and $p_T < 50$ GeV	2.5%	0.5%
e7_medium	$\|\eta\| < 1.5$	0.5%	40%
	$1.5 < \|\eta\| < 2.37$ or $p_T > 50$ GeV	0.5%	10%
	$\|\eta\| > 2.37$, $p_T < 50$ GeV	2.5%	10%

For events with one electron and one muon in the final state, the same errors as quoted in Tables 7.6 and 7.7 are used for the Tag & Probe Method. For the closure test, the errors are summarised in Table 7.8.

TABLE 7.8.: *The summary of the systematic uncertainties for the electron-muon triggers, coming from the closure test for an $e\mu$ or μe event.*

Trigger	Kinematics	Uncertainty Closure Test
e12Tvh_medium1_mu8 (region A)		1%
mu18_tight_e7_medium1 (region B)	$\|\eta^{el}\| > 1.37$	10%
	$\|\eta^{el}\| \leq 1.37$	30%

The total systematic uncertainty is added in quadrature to the statistical error which is propagated with the Gaussian error propagation when varying the weights from the Reweighting Method to estimate the change in the event yield. The same systematic errors are used for all periods of ATLAS 2012 data.

7.7. SYSTEMATIC UNCERTAINTIES ON EVENT YIELDS

The estimated numbers of events in the SRs and CRs are affected by systematic effects. The errors on the event yields are obtained by lowering or increasing the in-

dividual input parameters within their uncertainties. They are listed in detail in 8.7. For their combinations, possible correlations are taken into account.

The dominant systematic uncertainties in this analysis are due to the propagation of JES calibration and JER uncertainties. Other jet-related systematic uncertainties such as the differences between quark and gluon jets as well as between heavy flavour (HF) and light flavour (LF) jets and the effect of pile-up interactions are considered. Lepton-related uncertainties and systematic shifts affecting the E_T^{miss} soft term and b-tagging uncertainties are computed.

The uncertainties on the methods used for the background estimate are taken into account by e.g. comparing the control sample data for the ZV background estimation in *SR-Zjets* with the Monte Carlo simulated $WZjj \to l_{unid}\nu lljj$ and $ZZjj \to ll\nu\nu jj$ samples. Errors are associated to the Jet Smearing Method due to the uncertainty on the $E_T^{miss}/\sqrt{E_T^{miss}}$ cut and the fluctuations in the non-Gaussian tails of the jet response function. For the estimate of MC generator uncertainties, various generators are compared.

7.8. Results

The expected numbers of events in *SR*-$m_{T2}^{90,120,150}$ are given for each background contribution and for the total expected SM background in Table 7.9, together with the event yield measured in ATLAS data. The predicted SUSY signal yields for the simplified model mass points with $m_{\tilde{\chi}_1^\pm} = 350$ GeV and $m_{\tilde{\chi}_1^0} = 0$ GeV for the $\tilde{\chi}_1^+\tilde{\chi}_1^- \to \tilde{l}\nu(l\tilde{\nu})\tilde{l}\nu(l\tilde{\nu}) \to l^+\nu\tilde{\chi}_1^0 l^-\bar{\nu}\tilde{\chi}_1^0$ process as well as with $m_{\tilde{l}} = 251$ GeV and $m_{\tilde{\chi}_1^0} = 10$ GeV for the $\tilde{l}^+\tilde{l}^- \to l^+\tilde{\chi}_1^0 l^-\tilde{\chi}_1^0$ process are also given.

TABLE 7.9.: *The expected SM background contributions and the observed numbers of events in SR-$m_{T2}^{90,120,150}$. The 'others' background category summarises contributions from non-prompt leptons, $Z/\gamma^* + jets$ and SM Higgs. Signal predictions for a mass point of the simplified model process $\tilde{\chi}_1^+\tilde{\chi}_1^- \to W^+\tilde{\chi}_1^0 W^-\tilde{\chi}_1^0 \to l^+\nu\tilde{\chi}_1^0 l^-\bar{\nu}\tilde{\chi}_1^0$ and for a mass point of the process $\tilde{l}^+\tilde{l}^- \to l^+\tilde{\chi}_1^0 l^-\tilde{\chi}_1^0$ are given. The one-sided p-value p_0 is shown together with the observed and expected 95% CL upper limits on the visible cross section σ_{vis}^{95} [70].*

	SR-m_{T2}^{90}		SR-m_{T2}^{120}		SR-m_{T2}^{150}	
	SF	DF	SF	DF	SF	DF
Expected Background						
WW	22.1±4.3	16.2±3.2	3.5±1.3	3.3±1.2	1.0±0.5	0.9±0.5
ZV	12.9±2.2	0.8±0.2	4.9±1.6	0.2±0.1	2.2±0.5	< 0.1
Top	3.0±1.8	5.5±1.9	$0.3\ ^{+0.4}_{-0.3}$	< 0.1	< 0.1	< 0.1
Others	0.3±0.3	0.8±0.6	$0.1\ ^{+0.4}_{-0.1}$	0.1±0.1	$0.1\ ^{+0.4}_{-0.1}$	$0.0\ ^{+0.4}_{-0.0}$
Total	38.2±5.1	23.3±3.7	8.9±2.1	3.6±1.2	3.2±0.7	1.0±0.5
Observed Events	33	21	5	5	3	2
Predicted signal						
($m_{\tilde{\chi}_1^\pm}$, $m_{\tilde{\chi}_1^0}$) = (350, 0)	24.2±2.5	19.1±2.1	18.1±1.8	14.7±1.7	12.0±1.3	10.1±1.3
($m_{\tilde{l}}$, $m_{\tilde{\chi}_1^0}$) = (251, 10)	24.0±2.7	–	19.1±2.5	–	14.3±1.7	-
p_0	0.50	0.50	0.50	0.27	0.50	0.21
Observed σ_{vis}^{95} [fb]	0.63	0.55	0.26	0.36	0.24	0.26
Expected σ_{vis}^{95} [fb]	$0.78\ ^{+0.32}_{-0.23}$	$0.62\ ^{+0.26}_{-0.18}$	$0.37\ ^{+0.17}_{-0.11}$	$0.30\ ^{+0.13}_{-0.09}$	$0.24\ ^{+0.13}_{-0.08}$	$0.19\ ^{+0.10}_{-0.06}$

For example for SR-m_{T2}^{120}, the total expected event yield from SM processes for SF final states is 8.9 ± 2.1, but only 5 events are observed in data, including potential SUSY signal. The quoted errors combine the statistical and systematic uncertainties. This leads to a one-sided p-value p_0 of 0.50 and to a 0.26 fb observed 95% CL upper limit on the visible cross section for non-SM events, σ_{vis}^{95}, as well as to $0.37^{+0.17}_{-0.11}$ fb for the expected limit on σ_{vis}^{95}. Actually, when the value for p_0 exceeds 0.50, it is by default set to 0.50.

The p-value gives the probability of the background alone to fluctuate to the observed number of events or higher. To obtain this value, a simultaneous likelihood fit is performed which also takes as input the number of observed events in the SR.

The visible cross section is the cross section multiplied with the acceptance A and the selection efficiency ϵ, $\sigma_{vis} = \sigma \cdot A \cdot \epsilon$. The acceptance is the ratio of the number of events in the SR using cuts on truth information over the number of MC generated events. The truth information of an event uses the parameters of the physics objects with which the event was generated. The efficiency is the number of reconstructed events in the SR divided by the number of events in the SR using cuts on truth

information. σ_{vis}^{95} is the result of a fit which also takes into account the observed number of events in the SRs. The systematic uncertainties and possible correlations are taken into account as nuisance parameters.

For DF final states, in total 2.6 $\pm$ 1.2 events are expected and 5 events are observed in data. The underprediction leads to a lower p-value of 0.27 and to the observed limit on σ_{vis}^{95} exceeding the expected limit on σ_{vis}^{95}, 0.36 fb vs. 0.30 $^{+0.13}_{-0.09}$ fb.

Analogously, the numbers are given for *SR-WW*$^{a,\,b,\,c}$ in Table 7.10 and for *SR-Zjets* in Table 7.11. Only for *SR-WW*^{c} in the DF channel are more events measured than predicted, 11 vs. 9.0 $\pm$ 2.2, what leads to a p-value of 0.31. In general, good agreement between the prediction and measurement is observed.

TABLE 7.10.: *The expected SM background contributions and the observed numbers of events in SR-WW*$^{a,\,b,\,c}$*. The 'others' background category summarises contributions from non-prompt leptons,* $Z/\gamma^{*}+jets$ *and SM Higgs. Signal predictions for mass points of the simplified model* $\tilde{\chi}_1^+\tilde{\chi}_1^- \rightarrow W^+\tilde{\chi}_1^0 W^-\tilde{\chi}_1^0 \rightarrow l^+\nu\tilde{\chi}_1^0 l^-\bar{\nu}\tilde{\chi}_1^0$ *process are given. The one-sided* p*-value* p_0 *is shown together with the observed and expected 95% CL upper limits on the visible cross section* σ_{vis}^{95} *[70].*

	SR-WW^{a}		*SR-WW*^{b}		*SR-WW*^{c}	
	SF	DF	SF	DF	SF	DF
Expected background						
WW	57.8±5.5	58.2±6.0	16.4±2.5	12.3±2.0	10.4±2.7	7.3±1.9
ZV	16.3±3.5	1.8±0.5	10.9±1.9	0.6±0.2	9.2±2.1	0.4±.02
Top	9.2±3.5	11.6±4.3	2.4±2.7	4.3±1.6	0.6 $^{+1.2}_{-0.6}$	0.9±0.8
Others	3.3±1.5	2.0±1.1	0.5±0.4	0.9±0.6	0.1 $^{+0.5}_{-0.1}$	0.4±0.3
Total	86.5±7.4	73.6±7.9	30.2±3.5	18.1±2.6	20.3±3.5	9.0±2.2
Observed events	73	70	26	17	10	11
Predicted signal						
($m_{\tilde{\chi}_1^\pm}$, $m_{\tilde{\chi}_1^0}$) = (100, 0)	25.6±3.3	24.4±2.2				
($m_{\tilde{\chi}_1^\pm}$, $m_{\tilde{\chi}_1^0}$) = (140, 20)			8.3±0.8	7.2±0.8		
($m_{\tilde{\chi}_1^\pm}$, $m_{\tilde{\chi}_1^0}$) = (200, 0)					5.2±0.5	4.6±0.4
p_0	0.50	0.50	0.50	0.50	0.50	0.31
Observed σ_{vis}^{95} [fb]	0.78	1.00	0.54	0.49	0.29	0.50
Expected σ_{vis}^{95} [fb]	1.13 $^{+0.46}_{-0.32}$	1.11 $^{+0.44}_{-0.31}$	0.66 $^{+0.28}_{-0.20}$	0.53 $^{+0.23}_{-0.16}$	0.52 $^{+0.23}_{-0.16}$	0.41 $^{+0.19}_{-0.12}$

TABLE 7.11.: *The expected SM background contributions and the observed number of events in SR-Zjets. The 'others' background category summarises contributions from non-prompt leptons, $Z/\gamma^* + jets$ and SM Higgs. Signal predictions for mass points of the simplified model $\tilde{\chi}_1^\pm \tilde{\chi}_2^0 \to W^\pm \tilde{\chi}_1^0 Z \tilde{\chi}_1^0 \to qq\tilde{\chi}_1^0 l^+ l^- \tilde{\chi}_1^0$ process are given. The one-sided p-value p_0 is shown together with the observed and expected 95% CL upper limits on the visible cross section σ_{vis}^{95} [70].*

	SR-Zjets
Expected background	
WW	0.1±0.1
ZV	1.0±0.6
Top	< 0.1
Others	0.3±0.2
Total	1.4±0.6
Observed events	1
Predicted signal	
$(m_{\tilde{\chi}_2^0,\tilde{\chi}_1^\pm}, m_{\tilde{\chi}_1^0})$ = (250, 0)	6.4±0.8
$(m_{\tilde{\chi}_2^0,\tilde{\chi}_1^\pm}, m_{\tilde{\chi}_1^0})$ = (350, 50)	3.7±0.2
p_0	0.50
Observed σ_{vis}^{95} [fb]	0.17
Expected σ_{vis}^{95} [fb]	$0.19\ ^{+0.11}_{-0.06}$

7.9. INTERPRETATION OF RESULTS

Since no significant excess is observed in data for the SRs described in this Chapter, limits are set on the sparticle masses in simplified models and on SUSY parameters in the pMSSM.

SIMPLIFIED MODELS The results obtained when selecting events with the definitions of *SR*-$m_{T2}^{90,120,150}$ are interpreted in the simplified model for the $\tilde{\chi}_1^+\tilde{\chi}_1^- \to \tilde{l}\nu(l\tilde{\nu})\tilde{l}\nu(l\tilde{\nu}) \to l^+\nu\tilde{\chi}_1^0 l^-\bar{\nu}\tilde{\chi}_1^0$ process which is depicted in Figure 7.1 (a). The 95% CL exclusion limit is shown in Figure 7.11 (a). The continuous red line shows the observed limit together with the $\pm$ 1 σ_{theory}^{SUSY} band indicated by red dashed lines. The latter is computed by moving the nominal signal cross section up or down by $\pm$ 1 σ the theoretical uncertainty. The expected 95% CL exclusion region is given by the black dashed line, the solid yellow band shows the $\pm$ 1 σ_{exp} variation. All statistical and systematic uncertainties on the expected SM background and SUSY signal yields are taken into account except for the the error on the cross section of the signal process. For a neutralino mass of $m_{\tilde{\chi}_1^0} = 0$ GeV, $\tilde{\chi}_1^\pm$ with masses between 140 and 465 GeV are

excluded at 95% CL.

The results of *SR-WW*^{a,b,c} and of *SR-Zjets* are also interpreted in simplified models. The exclusion plots can be found in [70]. For *SR-WW*^{a,b,c} the simplified model process of $\tilde{\chi}_1^+\tilde{\chi}_1^- \to W^+\tilde{\chi}_1^0 W^-\tilde{\chi}_1^0 \to l^+\nu\tilde{\chi}_1^0 l^-\bar{\nu}\tilde{\chi}_1^0$, depicted in Figure 7.1 (b), is used to exclude $\tilde{\chi}_1^\pm$ masses between 100 and 105 GeV, 120 and 135 GeV and 145 and 160 GeV at 95% confidence level for $m_{\tilde{\chi}_1^0} = 0$ GeV.

To interpret the results of *SR-Zjets*, the simplified model for $\tilde{\chi}_1^\pm\tilde{\chi}_2^0 \to W^\pm\tilde{\chi}_1^0 Z\tilde{\chi}_1^0 \to qq\tilde{\chi}_1^0 l^+l^-\tilde{\chi}_1^0$ is used. The process is illustrated in Figure 7.1 (c). Degenerate $\tilde{\chi}_1^\pm$ and $\tilde{\chi}_2^0$ masses between 180 and 355 GeV are excluded for a massless $\tilde{\chi}_1^0$.

The masses of the same particles can be excluded between 100 and 415 GeV due to the increased sensitivity when combining the results from the analysis presented in this Chapter with the analysis in [72] which looks for electroweakly produced SUSY with three leptons in the final state. For the combination, the fit is performed on the combined likelihood function when using all relevant SRs, possible correlations between channels and processes are taken into account.

Using the results from *SR-*$m_{T2}^{90,120,150}$ in the simplified model process of $\tilde{l}^+\tilde{l}^- \to l^+\tilde{\chi}_1^0 l^-\tilde{\chi}_1^0$ makes the exclusion of slepton masses between 90 and 325 GeV possible at 95% CL. The $\tilde{\chi}_1^0$ is assumed to be massless and the right and left handed sleptons are mass degenerate. The exclusion plot is shown in Figure 7.11 (b).

pMSSM The 95% CL exclusion limits on the pMSSM with the ratio of the expectation values of the Higgs fields $\tan\beta$ set to 6 and the gaugino mass parameter M_1 set to 100 GeV is shown in the exclusion plot in Figure 7.11 (c). The plot shows the regions which are excluded in the $\mu - M_2$ plane at 95% CL. For each model point the SR with the best expected sensitivity is used. The continuous red line shows the observed limit, the red dashed lines indicate the region including the theoretical uncertainty. The expected limit at 95% CL is shown by the dashed black line and the $\pm$ 1 σ_{exp} by the solid yellow band. The green colour shows the area which is excluded by the -1σ expected limit. The continuous blue line indicates the regions which are excluded by previous ATLAS analyses [73] and the solid orange colour shows the LEP limits [74], [75].

The exclusion plots where $tan(\beta) = 6$ and $M_1 = 140$ or 250 GeV as well as the combination with the ATLAS three lepton analysis from [72] are to be found in [70].

The interpretation with the pMSSM model with very large slepton masses, $\tan\beta = 10$ and $M_1 = 50$ GeV is shown in Figure 7.11 (d), i.e. the exclusion limits at 95% CL. For this plot the results of *SR-Zjets* are combined with the results of the three-lepton analysis presented in [72].

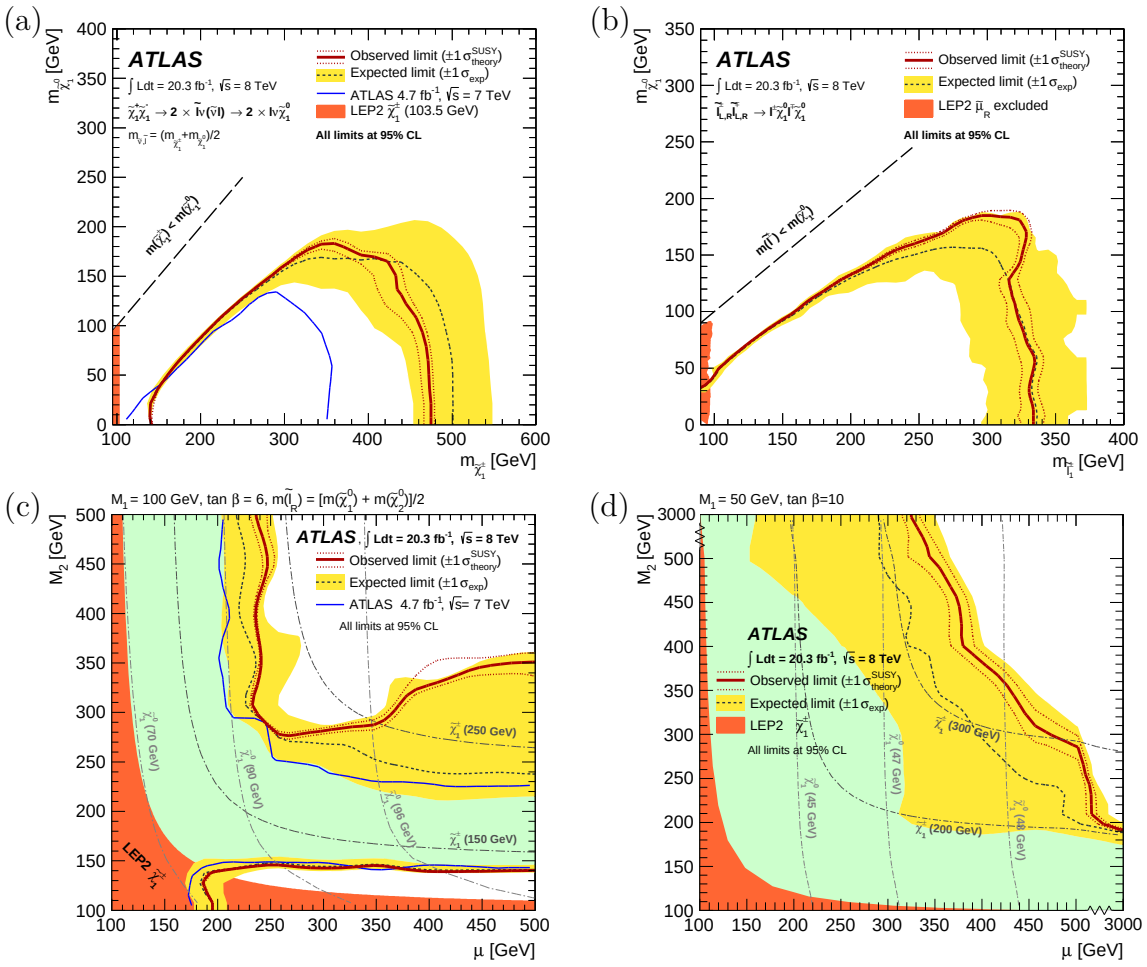

FIGURE 7.11.: *The observed and the expected 95% CL limits. The continuous red line shows the observed limit, the dashed red lines the* $\pm$ *1* σ^{SUSY}_{theory} *region which is computed by moving the nominal signal cross section up or down by* $\pm$ *1* σ *the theoretical uncertainty. The expected limit at 95% CL is indicated by the black dashed line, the solid yellow band shows the* $\pm$ *1* σ_{exp} *region. All statistical and systematic uncertainties on the expected yields are taken into account except for the the error on the cross section of the signal process. The blue line indicates exclusion limits obtained by previous ATLAS analyses, [63] for (a) and [73] for (c). The green colour in (c) and (d) indicates the area which is excluded by the* -1σ *expected limit. (a) shows the exclusion limits in the simplified model for* $\tilde{\chi}_1^+\tilde{\chi}_1^- \rightarrow \tilde{l}\nu(l\tilde{\nu})\tilde{l}\nu(l\tilde{\nu}) \rightarrow l^+\nu\tilde{\chi}_1^0 l^-\bar{\nu}\tilde{\chi}_1^0$ *using the results of SR-*$m_{T2}^{90,120,150}$*. (b) uses the same results but interprets them in the simplified model process of* $\tilde{l}^+\tilde{l}^- \rightarrow l^+\tilde{\chi}_1^0 l^-\tilde{\chi}_1^0$*. (c) shows the exclusion limits for the pMSSM model with* $\tan\beta = 6$ *and* $M_1 = 100$ *GeV, using the SR with the best expected sensitivity for each model point. (d) uses the results of SR-Zjets in combination with the one of [72] to set limits on pMSSM models with very large slepton masses,* $\tan\beta = 10$ *and* $M_1 = 50$ *GeV [70].*

8. Chargino-Neutralino Production Followed by a Decay with Intermediate Higgs Boson

The two analyses which were presented in this thesis so far, do not explicitly address the decay modes of electroweakly produced SUSY into a Higgs boson. The discovery of a Higgs-like particle in the year 2012 [7], [8] and the subsequent confirmation of this particle being the SM Higgs boson is the motivation to especially search for the SUSY decay scenarios which involve a Higgs boson. The analysis which is presented in this Chapter looks for SUSY after the electroweak production of $\tilde{\chi}_1^{\pm}\tilde{\chi}_2^0$ with two same sign leptons in the final state. It is assumed that the $\tilde{\chi}_1^{\pm}$ decays into a $W^{\pm}$ boson and a $\tilde{\chi}_1^0$, and that the $\tilde{\chi}_2^0$ decays into a H and a $\tilde{\chi}_1^0$. The data which was recorded in 2012 at $\sqrt{s} = 8$ TeV, corresponding to an integrated luminosity of 20.3 fb^{-1}, is analysed. The background estimation and the signal region optimisation are discussed in the following Sections. The expected results are shown at the end of this Chapter. The publication of this analysis is in preparation.

8.1. SUSY Decay Scenario

It is assumed that a pair of $\tilde{\chi}_1^{\pm}\tilde{\chi}_2^0$ is produced electroweakly and that it decays into a SM Higgs boson in association with a W boson. For a final state with two leptons the following decay chains are possible:

- $H(\rightarrow ZZ)\tilde{\chi}_1^0 W^{\pm}\tilde{\chi}_1^0 \rightarrow l^+l^-\nu\bar{\nu}\tilde{\chi}_1^0 q\bar{q}'\tilde{\chi}_1^0$,
- $H(\rightarrow ZZ)\tilde{\chi}_1^0 W^{\pm}\tilde{\chi}_1^0 \rightarrow l^+l^-q\bar{q}\tilde{\chi}_1^0 q\bar{q}'\tilde{\chi}_1^0$,
- $H(\rightarrow W^+W^-)\tilde{\chi}_1^0 W^{\pm}\tilde{\chi}_1^0 \rightarrow l^+\nu l^-\bar{\nu}\tilde{\chi}_1^0 q\bar{q}'\tilde{\chi}_1^0$ and
- $H(\rightarrow W^+W^-)\tilde{\chi}_1^0 W^{\pm}\tilde{\chi}_1^0 \rightarrow l^{\pm}\nu q\bar{q}'\tilde{\chi}_1^0 l^{\pm}\nu\tilde{\chi}_1^0$.

The first three decay chains lead to two OS leptons and to two or four quarks in the final state. They have a detector signature which is very similar to the SM processes of $Z + jets$ and $t\bar{t}$ production. The analysis in this Chapter focuses only on the final state with two SS leptons - the last decay chain in the list above leads to two OS or SS leptons. The process is depicted in Figure 8.1.

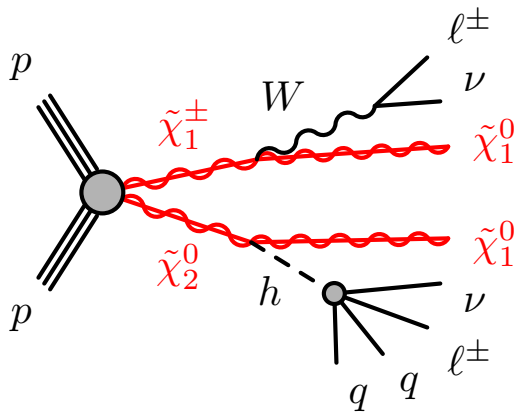

FIGURE 8.1.: *The graph for the SUSY decay scenario after the electroweak production of $\tilde{\chi}_1^{\pm}\tilde{\chi}_2^0$, leading to two OS or SS leptons (electrons, muons) in the final state.*

SIMPLIFIED MODEL 28 mass points are simulated in a simplified model, varying the masses of the $\tilde{\chi}_1^0$, $\tilde{\chi}_2^0$ and $\tilde{\chi}_1^{\pm}$. The $\tilde{\chi}_2^0$ and $\tilde{\chi}_1^{\pm}$ are wino-like and mass-degenerate, the $\tilde{\chi}_1^0$ is bino-like. The cross section for the production of $\tilde{\chi}_1^{\pm}\tilde{\chi}_2^0$ is 4.24 pb for $m\tilde{\chi}_1^{\pm},\tilde{\chi}_2^0 =$ 130 GeV and decreases to 220 fb for $m\tilde{\chi}_1^{\pm},\tilde{\chi}_2^0 =$ 275 GeV. The slepton and squark masses are set to high values ($\mathcal{O}$ (100 GeV)). The branching ratios for the decay of $\tilde{\chi}_1^{\pm} \to W^{\pm}\tilde{\chi}_1^0$ and $\tilde{\chi}_2^0 \to H\tilde{\chi}_1^0$ are both 100%. The mass of the Higgs boson is set to 125 GeV and the branching ratios are the same as in the SM. The signal samples are generated using Herwig++ [65].

PMSSM The pMSSM which will be used for interpreting the results is the same as the one for the analysis in Chapter 7 with $\tan\beta =$10. The masses of the squarks, the gluinos, the CP-odd Higgs and the sleptons are very high. $\tilde{\chi}_1^{\pm}\tilde{\chi}_2^0$ can thus only decay via W, Z or H bosons. M_1 is set to 50 GeV and the μ and M_2 parameters are varied. The branching ratios for the Higgs decays are similar to the ones in the SM but for $\mu =$ 200 GeV (100 GeV), the branching ratio for $H \to \tilde{\chi}_1^0\tilde{\chi}_1^0$ BR rises to 20% (70%).

8.2. SM BACKGROUND

The SM processes that can have a signature similar to the SUSY signal final state, i.e. two SS leptons, at least two jets and missing transverse energy from the undetected particles, are: non-prompt leptons, i.e. jets which fake leptons, and diboson processes like $W^{\pm}Z \to l^{\pm}\nu l^{+}l^{-}$ or $ZZ \to l^{+}l^{-}l^{+}l^{-}$ when not all leptons are identified. The contribution due to fake leptons is estimated with a data-driven method. The diboson processes are simulated with the Monte Carlo generator SHERPA [48]. Genuine SM background processes which lead to two SS leptons in the final state are

e.g. $t\bar{t}+V$ and WWW^* which are simulated with MADGRAPH [53] and POWHEG [66], respectively.

The contribution from OS events due to charge mis-identification is studied as well.

8.3. Physics Object Definition

The events and physics objects used in this analysis are selected according to the criteria stated in Sections 5.4 and 5.3. Except for the isolation criteria the physics objects have to fulfil the same requirements as for the analysis described in Chapter 7. They undergo the over overlap removal described in Section 5.3.6.

Electrons Electrons need to have $p_T >$ 10 GeV and the absolute value of the pseudorapidity of the utilised calorimeter clusters must be smaller than 2.47. They need to be reconstructed with the 'tight++' criteria and have to fulfil the following requirements on their impact parameters: $|\frac{d_0^{PV}}{\sigma(d_0^{PV})}| < 3$ for the transverse one and $|z_0 \cdot sin(\theta)| <$ 0.4 mm for the longitudinal one. They must be isolated, i.e. the scalar sum of the p_T of tracks with $p_T >$ 0.4 GeV, $|d_0^{PV}| < 1.5$ mm, a b-layer hit and $\geq$ 9 hits in the SCT within a cone of size $\Delta R =$ 0.3 ('ptcone30') around the electron must be less than 7% of the electron p_T, but at maximum 4.2 GeV. The b-layer is the innermost layer of the PD. Another isolation criterion is that the pile-up corrected sum of E_T of the calorimeter clusters which surround the electron in a cone of $\Delta R =$ 0.3 ('Etcone30Corr') must be less than 13% of the electron p_T, but at maximum 7.8 GeV.

Muons Combined muons which are reconstructed with the staco algorithm are used as well as segment-tagged muons. They must fulfil a list of quality requirements, i.e. have a certain number of hits in the PD, the TRT and the SCT. The p_T must be larger than 10 GeV and $|\eta|$ must be smaller than 2.5. Regarding the impact parameter, all reconstructed muons need to fulfil $|\frac{d_0^{PV}}{\sigma(d_0^{PV})}| < 3$ and $|z_0 \cdot sin(\theta)| <$ 1 mm. Only isolated muons are used, for this the pile-up corrected sum of E_T which is defined in a similar way as for electrons ('Etcone30Corr') must be smaller than 14% of the muon p_T in $\Delta R =$ 0.3, but at maximum 8.4 GeV. The ptcone30 variable must be smaller than 6% of the muon p_T, but at maximum 3.6 GeV.

Taus The tau identification is based on a multivariate analysis technique. The technique is used to discriminate the hadronically decaying taus from jets or electrons. Taus must have a p_T of more than 20 GeV, $|\eta| <$ 2.5 and one or three tracks. Events are vetoed if they contain any tau.

JETS Jets are reconstructed with the anti-k_T algorithm with the distance parameter $R = 0.4$ and topological clusters as input. Baseline jets are calibrated as described in Section 5.3.1 and need to have $p_T > 20$ GeV and $|\eta| < 4.9$ before they undergo the overlap removal procedure.

The jets are further defined according to the requirements listed in Table 8.1. The criteria concern the transverse momentum, the pseudorapidity and the JVF of the objects. The b-jets in addition must satisfy the ATLAS MV1 b-tagging algorithm working point for which the tagging efficiency is 80%.

TABLE 8.1.: *The definitions of the signal jets.*

	Central light jets	Central b-jets	Forward jets
p_{T} [GeV]	≥ 20	≥ 20	≥ 30
$\|\eta\|$	≤ 2.4	≤ 2.4	[2.4,4.5]
JVF	$\|\mathrm{JVF}\| > 0$ if $p_T < 50$ GeV	-	-

E_T^{miss} The missing transverse energy is computed using the transverse momenta of the electrons, muons and photons with $p_T > 10$ GeV and of the jets with $p_T > 20$ GeV. The soft terms, i.e. the calibrated calorimeter clusters which are not associated to a physics object, are also taken into account. For the calculation of E_T^{miss}, the calibrated and/or smeared transverse momenta are used.

8.4. DISCRIMINATING VARIABLES

To better distinguish the SUSY signal process from the SM background, among others the 'effective mass' and the reconstructed invariant mass of the Higgs boson are used.

EFFECTIVE MASS The effective mass m_{eff} is the sum of the transverse momenta of the two SS leptons, the N central light jets (see Table 8.1) and the missing transverse energy:

$$m_{eff} = p_T^{l1} + p_T^{l2} + \sum_i^N p_T^{jet,i} + E_T^{miss}. \tag{8.1}$$

m_{lj}, m_{ljj} The invariant mass of the Higgs boson which decays into W^+W^- and then into $l^{\pm}\nu q\bar{q}'$, m_{ljj}, is computed from the invariant mass of the lepton-dijet system. The system is formed by the two central light jets with the highest transverse momenta in the event and by the lepton which is closest in the η-ϕ-space. The distribution of m_{ljj} is expected to peak below the mass of the Higgs boson because the missing transverse energy due to the neutrino is not regarded in the computation. In

events where only one of the two expected jets is reconstructed, the m_{lj} variable is computed from the total invariant mass of the central jet and the closest lepton.

8.5. Event Selection

The goal of the analysis is to select events of the signal process $H(\rightarrow W^+W^-)\tilde{\chi}_1^0 W^{\pm}\tilde{\chi}_1^0 \rightarrow l^{\pm}\nu q\bar{q}'\tilde{\chi}_1^0 l^{\pm}\nu\tilde{\chi}_1^0$ and to suppress SM background processes which have a similar detector signature. The events need to have a positive decision of one of the dilepton triggers listed in Table 7.3 for the analysis of $\sqrt{s} = 8$ TeV 2012 data, according to the trigger strategy explained in 7.6.2. MC events are reweighted with the probability that the trigger has a positive decision.

Exactly two SS leptons and no hadronically decaying taus, b-jets or forward jets are required. Although in the addressed SUSY scenario two quarks are expected in the final state, also events with only one central light jet are considered because the second jet could be not reconstructed. Events with three central light jets can also increase the sensitivity to this simplified model because a third jet can be the result of initial state radiation.

8.5.1. Third Lepton Veto

For the final states with two muons or one electron and one muon in the final state, the diboson processes ZV, where V=W or Z, are a dominating background contribution along side the background due to non-prompt leptons. For ee events, the contribution from $Z + jets$ processes is relatively high. This is shown in the distributions in Figure 8.2 for the transverse momentum of the leading lepton in ee, $\mu\mu$ or $e\mu$ events when requiring two SS leptons and one, two or three central light jets.

(a) ee

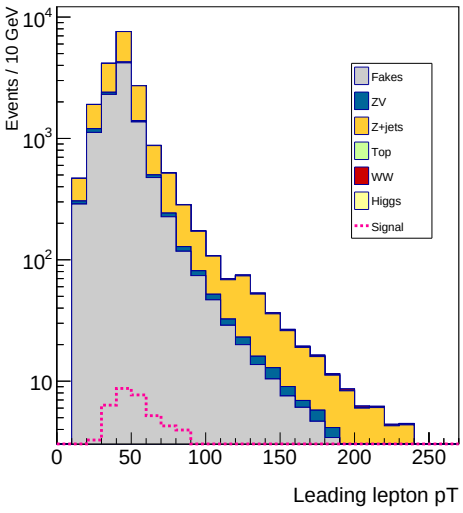

(b) $\mu\mu$

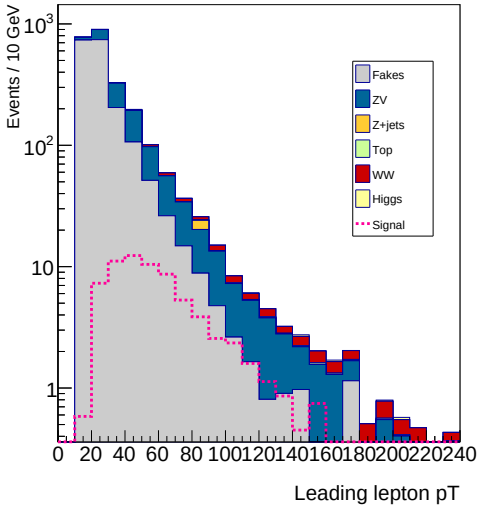

(c) $e\mu$

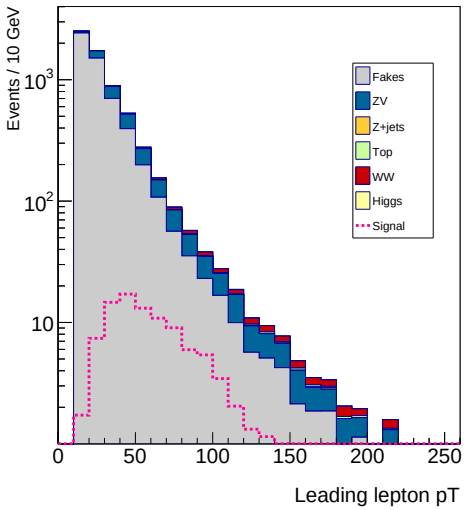

FIGURE 8.2.: *The histograms show the distribution of the p_T of the leading lepton in (a) ee events, (b) $\mu\mu$ events and (c) $e\mu$ events. The solid colours indicate the expected SM background, Higgs in yellow, non-prompt leptons ('Fake') in grey, ZV in light green, Top in red and WW in dark green colour. The signal prediction for the simplified model mass point $(m_{\tilde{\chi}_1^\pm,\tilde{\chi}_2^0}, m_{\tilde{\chi}_1^0}) = (130, 0)$ GeV is superimposed (dashed pink line).*

The $W^{\pm}Z \to l^{\pm}\nu l^{+}l^{-}$ process has the same detector signature as the SUSY signal process if the third lepton in the final state does not pass the selection criteria for electrons or muons. In order to further suppress this process, a loose third lepton is selected in addition to the two SS leptons and is combined with one of the two SS leptons to obtain a SFOS pair. If the invariant mass of the SFOS pair is close to the mass of the Z boson (inside the window of 91.2 $\pm$ 20 GeV), the event is rejected.

All leptons with a p_T larger than 6 GeV which fulfil the requirements on the impact parameters for electrons and muons as listed in 8.3 and which are reconstructed with 'medium++' criteria, are considered as candidates for the third leptons. These candidates must not overlap with any of the two SS leptons; the distance in the η-ϕ-space, ΔR, must be larger than 0.05.

A study shows why the lepton selection is not passed by the loose leptons defined above. The histograms in Figure 8.3 show in the first bin the total number of third leptons. Events with two SS leptons and one, two or three central light jets are selected. The second bin shows the number of third leptons which have a transverse momentum which is too low to be selected according to the trigger-dependent offline thresholds. Most third lepton candidates are not selected because they are too soft. In many ee or $e\mu$ events in which the third lepton is an electron, see Figures 8.3 (a) and (c), the third electrons do not pass the selection criteria because they are too close to another physics object, i.e. they do not pass the overlap removal procedure. They may also not be properly isolated or not reconstructed with the 'tight++' quality. Each of these criteria has a corresponding bin in the histograms which is labelled accordingly. Third muon candidates for $mu\mu$ or $e\mu$ events, see Figures 8.3 (b) and (d), may pass the overlap removal procedure, may not be well isolated or may not be prompt (using the truth information).

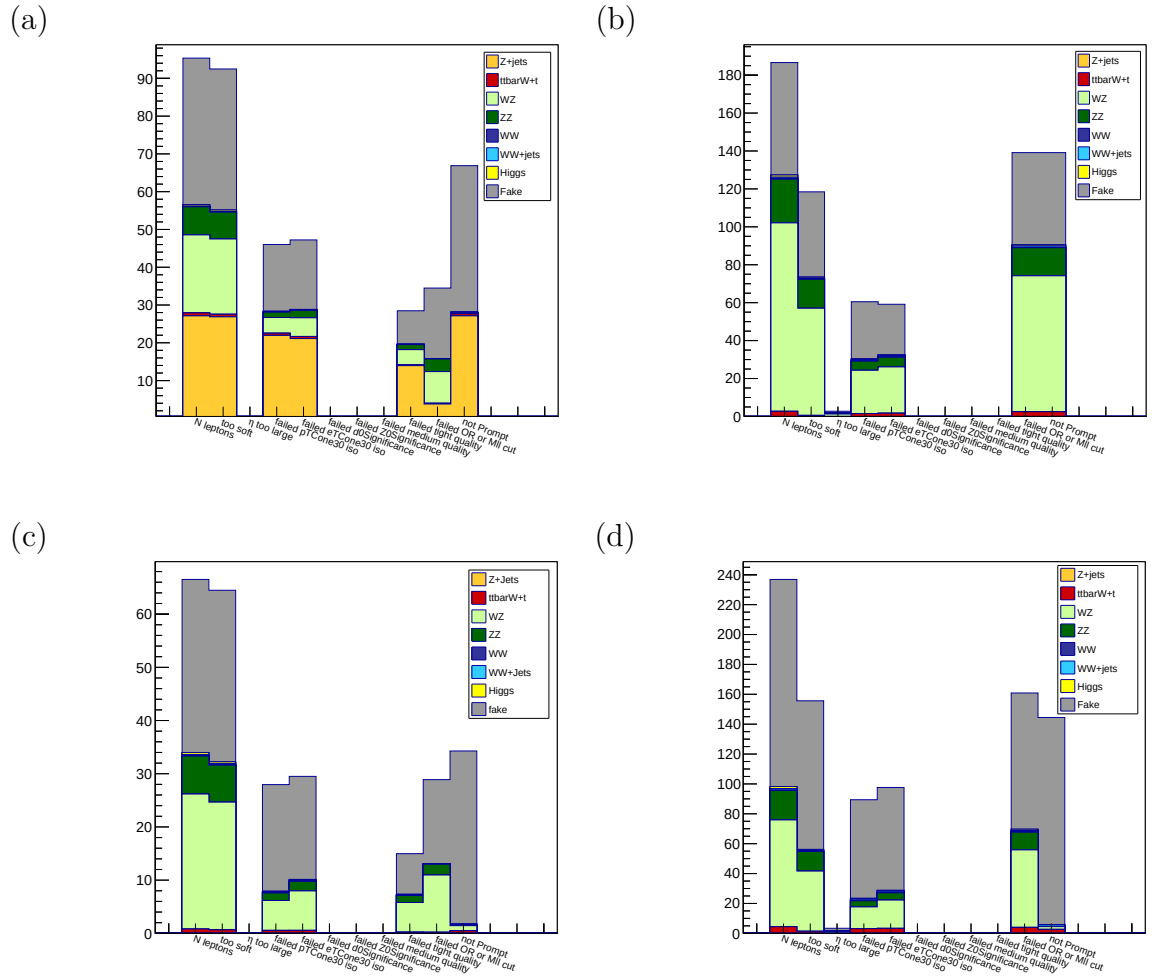

FIGURE 8.3.: *For events with two SS leptons and one, two or three central light jets, the first bin of the histograms shows the total number of third leptons which can be combined to a SFOS pair with one of the two SS leptons. The other bins show how many of the third leptons do not pass the selection because of p_T, η, isolation or impact parameter requirements, because of the reconstruction quality, the overlap removal or because they are not prompt. By definition the background contribution due to non-prompt leptons (grey colour) only has third leptons which are 'not prompt'. The MC simulated WZ processes are shown in light green colour. Figure (a) contains third leptons which are electrons in the ee channel, (b) muons in the $\mu\mu$ channel, (c) electrons in the $e\mu$ channel and (d) muons in the $e\mu$ channel.*

Only leptons which are not originating from a semileptonic b- or c-decay inside a jet or from bremsstrahlung, i.e. which are prompt, should be considered as third lepton candidates. The third lepton which can be used to form a SFOS pair with one of the two SS leptons and for which the pair has an invariant mass close to m_Z is often close to a jet in the η-ϕ-space. The two-dimensional histograms in Figure 8.4 show on the y-axis the invariant mass of the SFOS pair in an event whose invariant mass is closest to the mass of the Z boson. The ΔR of the third lepton to any baseline jet in the event is shown on the x-axis. The Z-mass window is indicated by two horizontal orange lines. From the distribution in Figures 8.4 (a) and (c) for third electrons in ee or $e\mu$ events it can be concluded that the third electrons and jets are well separated. The third muons in $\mu\mu$ and $e\mu$ events on the other hand are close to jets in most cases, see Figures 8.4 (b) and (d). These muons would be removed in the overlap removal procedure.

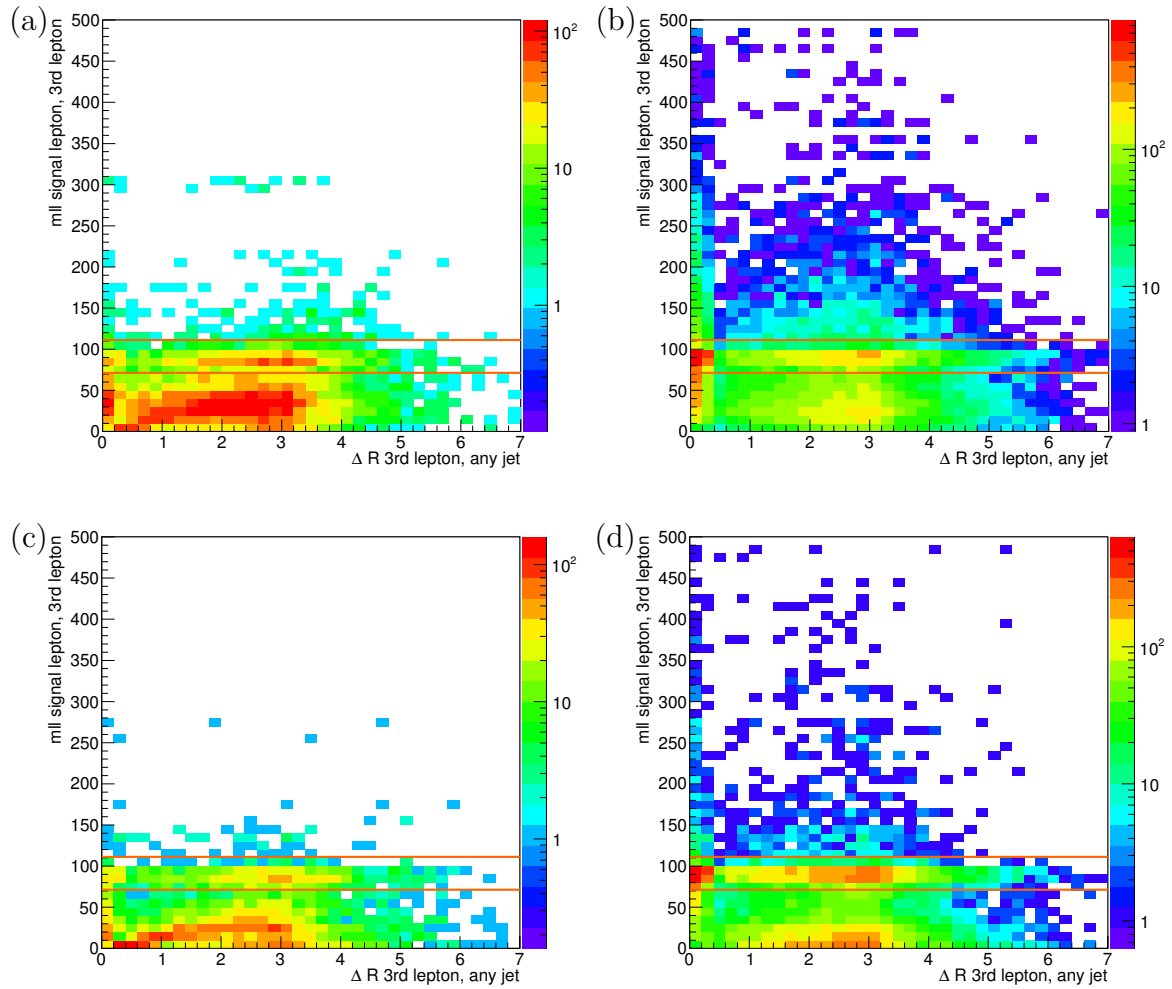

FIGURE 8.4.: *The invariant mass of the SFOS pair (one third lepton and one of the two SS leptons) in the event whose mass is closest to the mass of the Z boson vs. ΔR between the third lepton and any baseline jet in the event. The horizontal orange lines indicate the 91.2 $\pm$ 20 GeV window. Figure (a) contains third leptons which are electrons in the ee channel, (b) muons in the $\mu\mu$ channel, (c) electrons in the $e\mu$ channel, (d) muons in the $e\mu$ channel.*

The origin of the third leptons which are closer to a jet than $\Delta R = 0.4$ and which are part of a SFOS pair with in an invariant mass inside the Z-window is studied and listed in Table 8.2. In most of the WZ events (92 - 99%) in which a Z-candidate is found, the third lepton is prompt, i.e. originating from the decays of Z/γ^* bosons, W bosons or τ leptons. Thus most third lepton candidates are not the result from a semi-leptonic c- or b-decay inside a jet. Only in very few events ($< 6\%$) the third lepton is originating from a 'heavy flavour' (HF) or 'light flavour' (LF) jet as indicated in the truth information. 'Heavy flavour' refers to b- and c-hadrons, 'light flavour' to the lighter quarks. Thus, events in which the third lepton candidate is close to a jet, but the SFOS pair has a mass inside the Z-window, can be safely rejected.

To visualise the effect of the veto, Table 8.3 shows the event yield in the six SRs which will be defined in Section 8.5.2 without applying the 'third lepton veto' to suppress the WZ background ('before') and when additionally applying the third lepton veto ('after'). The largest reduction is observed for $\mathrm{SR}^{e\mu}_{1\,\mathrm{jet}}$ in which the event yield for simulated WZ processes is decreased by 28%. In $\mathrm{SR}^{\mu\mu}_{1\,\mathrm{jet}}$ a cutback of 22% is achieved. For the other background contributions no events are rejected or the event yield is minimally decreased within the statistical uncertainty. For the predicted SUSY signal a maximum reduction of 3.68% in $\mathrm{SR}^{\mu\mu}_{1\,\mathrm{jet}}$ is obtained, using the mass point with $(m_{\tilde{\chi}_1^\pm,\tilde{\chi}_2^0}, m_{\tilde{\chi}_1^0}) = (130, 0)$ GeV.

TABLE 8.2.: *For the WZ MC sample, the number of all events with a Z-candidate formed by one of the SS leptons and a third lepton is given. The percentage of events in which a jet is found close to the third lepton, i.e. $\Delta R < 0.4$, and for which the third lepton truly is prompt, a HF jet or a LF jet, is also listed.*

	ee	$\mu\mu$	eμ	
			electrons	muons
Number of events with Z-candidate	405	3987	413	2554
Third lepton is prompt	91.6%	94.4%	97.8%	98.8%
Third lepton is HF jet	2.2%	3.5%	0.5%	0.7%
and in addition $\Delta R < 0.4$	2.0%	3.0%	0.5%	0.6%
Third lepton is LF jet	5.7%	2.1%	1.2%	0.5%
and in addition $\Delta R < 0.4$	4.2%	2.0%	1.2%	0.5%

TABLE 8.3.: *The event yield for the different background contributions with the full SR definition applied except for the third lepton veto ('before') and after the additional third lepton veto ('after'). The statistical errors are quoted. The reduction in percent when applying the third lepton veto is given in brackets. The 'signal' is the prediction for the simplified model mass point for* $(m_{\tilde{\chi}_1^\pm, \tilde{\chi}_2^0}, m_{\tilde{\chi}_1^0}) = (130, 0)$ *GeV. The events are normalised to an integrated luminosity of 20.3 fb*$^{-1}$.

	$SR^{ee}_{1\,jet}$		$SR^{\mu\mu}_{1\,jet}$		$SR^{e\mu}_{1\,jet}$	
	before	after	before	after	before	after
Fake	3.2±0.6	3.2±0.6(0%)	0.15±0.23	0.00±0.12(100%)	3.0±0.6	3.0±0.6(0%)
WZ	2.4±0.4	2.2±0.4(6.8%)	5.0±0.6	3.9±0.5(21.6%)	4.6±0.6	3.3±0.5(27.6%)
WW	0.39±0.04	0.39±0.04(0%)	0.27±0.04	0.27±0.04(0.99%)	0.46±0.04	0.46±0.04(0%)
$t\bar{t}+Wt$	0.12±0.01	0.12±0.01(0%)	0.01±0.01	0.01±0.01(0%)	0.14±0.01	0.14±0.01(0.76%)
$Z+jets$	0.06±0.02	0.06±0.02(0%)	0±0	0±0(0%)	0±0	0±0(0%)
Higgs	0±0	0±0(0%)	0.13±0.05	0.13±0.05(1.83%)	0.09±0.04	0.08±0.03(6.74%)
Total	6.1±0.7	6.0±0.7(1.9%)	5.5±0.7	4.3±0.6(0.8%)	8.3±0.8	7.1±0.7(0.9%)
Signal	2.4±0.4	2.4±0.4(0%)	4.6±0.5	4.5±0.5(3.7%)	5.6±0.6	5.6±0.55(0%)

	$SR^{ee}_{2,3\,jet}$		$SR^{\mu\mu}_{2,3\,jet}$		$SR^{e\mu}_{2,3\,jet}$	
	before	after	before	after	before	after
Fake	2.1±0.5	2.1±0.5 (0%)	0.14±0.06	0.11±0.05 (19.11%)	0.7±0.3	0.6±0.3 (9.0%)
WZ	0.89±0.25	0.73±0.22 (18.16%)	2.0±0.4	1.6±0.4 (17.8%)	1.17±0.26	1.11±0.26 (5.71%)
WW	0.34±0.05	0.34±0.05 (0%)	0.41±0.06	0.40±0.06(1.28%)	0.24±0.04	0.24±0.04 (0%)
$t\bar{t}+Wt$	0.08±0.01	0.08±0.01 (0.48%)	0.02±0.01	0.02±0.01 (0%)	0.07±0.01	0.07±0.01 (0%)
$Z+jets$	0.58±0.14	0.58±0.14 (0%)	0±0	0±0 (0%)	0±0	0.00±0 (0%)
Higgs	0.04±0.03	0.04±0.03 (0%)	0.04±0.02	0.04±0.02 (0%)	0.03±0.02	0.03±0.02 (0%)
Total	4.1±0.6	3.9±0.6 (4.0%)	2.3±0.4	2.0±0.4 (0.9%)	2.2±0.4	2.1±0.4 (0.9%)
Signal	2.4±0.4	2.4±0.4 (0%)	3.5±0.5	3.4±0.5 (1.6%)	3.4±0.4	3.4±0.4 (0%)

8.5.2. Definition of the SRs

The optimisation of the six SRs split depending on the lepton flavours (ee, $\mu\mu$ and $e\mu$) and the number of central light jets (one jet or two and three jets), is based on the significance variable Z_N as defined in Chapter 3. The distributions of geometrical and kinematic event and object variables are studied to deduce the cut values which maximise the significance.

8.5.2.1. $SR^{ee}_{1\,\mathrm{jet}}$, $SR^{ee}_{2,3\,\mathrm{jet}}$

For the final state with two SS electrons, the SM background processes due to the $Z+jets$ production dominate over the predicted signal for the invariant masses of the dilepton system being close to the mass of the Z boson. The distribution is shown in Figure 8.5 (a) for final states with exactly one central light jet and in Figure 8.5 (b) for two and three central light jets. Only events with $|m_{ee}-$ 92.1 GeV$| >$ 10 GeV are selected.

The cut efficiency for increasing cut values (decreasing cut values for m_{lj}, m_{ljj}) for the SM background expectation and for the predicted SUSY signal, and the significance Z_N are shown for each bin .

The transverse momentum of the leading electron must be larger than 30 GeV and the transverse momentum of the subleading electron must be larger than 20 GeV. For $SR^{ee}_{1\,\mathrm{jet}}$, m_{lj} must be smaller than 90 GeV and the effective mass must be larger than 200 GeV. The maximum of the transverse masses of the leading lepton and the missing transverse energy, $m_T(l^1, E_T^{miss})$, and the subleading lepton and the missing transverse energy, $m_T(l^2, E_T^{miss})$ is abbreviated by '$max(m_T)$' and must be larger than 110 GeV for $SR^{ee}_{2,3\,\mathrm{jet}}$. For the SR with two or three jets, m_{ljj} must be smaller than 120 GeV.

Due to the neutrinos and neutralinos in the final state of the SUSY signal process it is meaningful to require a minimum value for the relative missing transverse energy. The $E_T^{miss,rel}$ distributions for $SR^{ee}_{1\,\mathrm{jet}}$ and $SR^{ee}_{2,3\,\mathrm{jet}}$ are shown in Figures 8.5 (c) and (d), respectively. The predicted SUSY signal for the mass point with $(m_{\tilde{\chi}_1^\pm,\tilde{\chi}_2^0}, m_{\tilde{\chi}_1^0}) = (130,\ 0)$ GeV is almost flat while the distribution for the SM background processes peaks at low values. The SM background is suppressed when cutting on $E_T^{miss,rel}$ larger than 55 GeV (30 GeV) for $SR^{ee}_{1\,\mathrm{jet}}$ ($SR^{ee}_{2,3\,\mathrm{jet}}$).

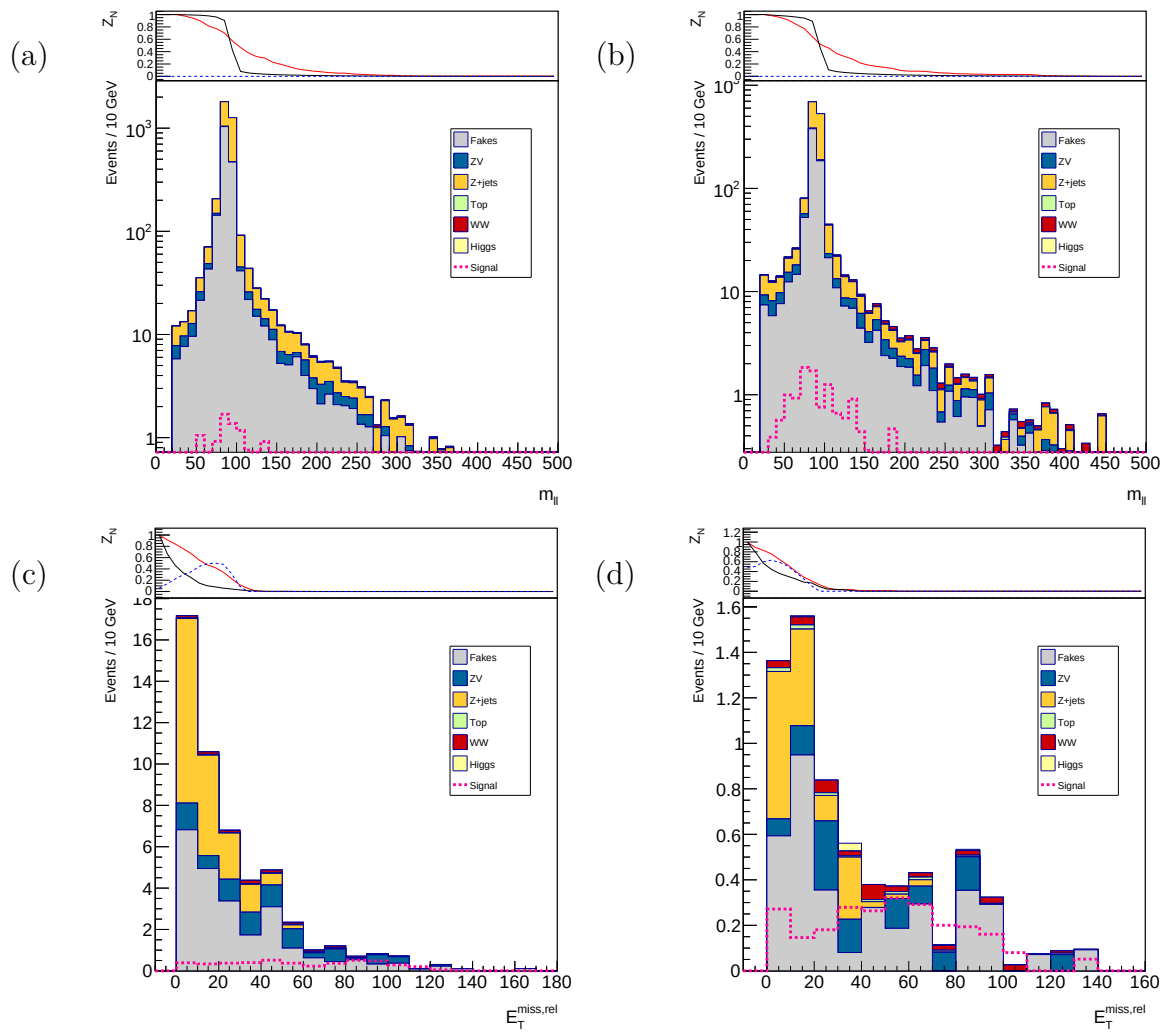

FIGURE 8.5.: *The lower plots show the distributions for the variables which motivate the cuts for the SR definition. The events are not selected due to the full SR definition but the cuts are applied in the order which is given in the Table 8.4. 'Fake' is the expected bg contribution due to non-prompt leptons which is estimated data-driven with the Matrix Method (grey colour). The other SM background processes ZV (blue), $Z+jets$ (orange), Top (light green), WW (red) and Higgs (yellow) are simulated with MC. The predicted SUSY signal for the mass point with $(m_{\tilde{\chi}_1^\pm,\tilde{\chi}_2^0}, m_{\tilde{\chi}_1^0}) = (130, 0)$ GeV is superimposed (pink dashed line). The upper plots show the cut efficiency for increasing cut values for the SM background expectation (black line) and for the predicted SUSY signal (red line). The blue stacked line shows the significance Z_N. (a) shows the distribution for the total invariant mass of the two electrons in $SR^{ee}_{1\,\mathrm{jet}}$, (b) shows it for $SR^{ee}_{2,3\,\mathrm{jet}}$. (c) shows the distribution of $E_T^{miss,rel}$ in $SR^{ee}_{1\,\mathrm{jet}}$ and (d) shows it for $SR^{ee}_{2,3\,\mathrm{jet}}$.*

The distributions of the mentioned variables are shown in Figures A.1, A.2 and A.3 in Appendix A.1. The SR-defining cuts are applied in the order given in Table 8.4 and the distribution of each variable is shown before the cut on the particular parameter. For example is the distribution for m_{lj} in $\mathrm{SR}^{ee}_{1\,\mathrm{jet}}$ shown after the requirement on m_{ll}, on the transverse momenta of the leptons and on $max(m_T)$, but before cutting on m_{lj}, m_{eff} or $E_T^{miss,rel}$.

When the full SR definitions are applied, event yields from the SM background and the predicted SUSY signal are used to estimate the expected sensitivity. The significance Z_N is computed for each mass point. A flat uncertainty of 30% is applied on the background in each SR to be conservative. Z_N is shown for the different values of the degenerate masses of the $\tilde{\chi}_1^\pm$ and the $\tilde{\chi}_2^0$ and the mass of the $\tilde{\chi}_1^0$ for the event yield in $\mathrm{SR}^{ee}_{1\,\mathrm{jet}}$ in Figure 8.6 (a) and for $\mathrm{SR}^{ee}_{2,3\,\mathrm{jet}}$ in Figure 8.6 (b). The point with $(m_{\tilde{\chi}_1^\pm,\tilde{\chi}_2^0}, m_{\tilde{\chi}_1^0}) = (130,\ 0)$ GeV has the maximum value of Z_N of 0.50 for $\mathrm{SR}^{ee}_{1\,\mathrm{jet}}$ and of 0.68 for $\mathrm{SR}^{ee}_{2,3\,\mathrm{jet}}$. The ee channels are therefore most sensitive to this mass point.

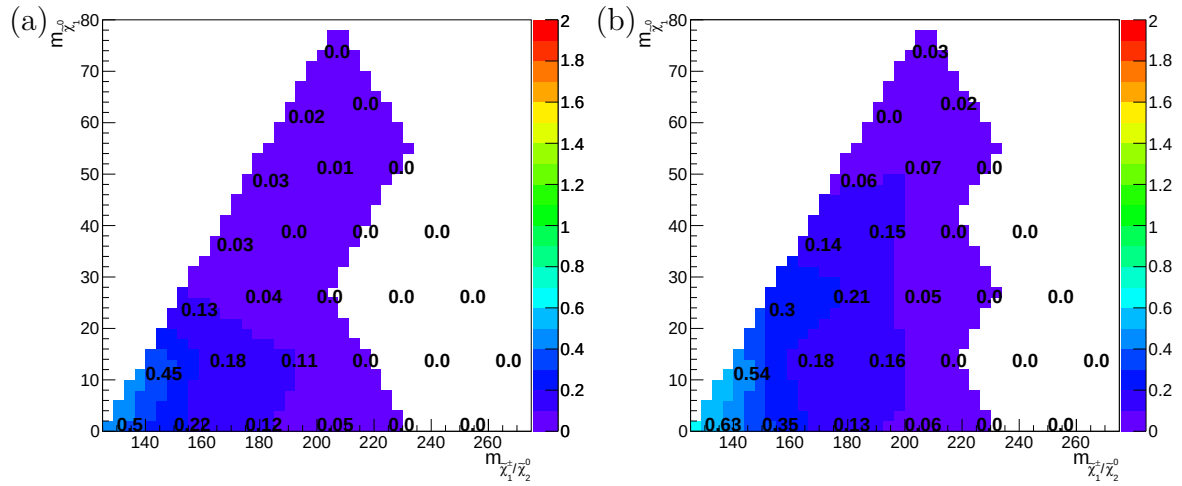

FIGURE 8.6.: *When applying all the cuts of the definition for $SR^{ee}_{1\,\mathrm{jet}}$ (a) and $SR^{ee}_{2,3\,\mathrm{jet}}$ (b), the expected Z_N can be computed from the resulting event yield for all mass points of the simplified model grid. Various values of the masses of $\tilde{\chi}_1^\pm$, $\tilde{\chi}_2^0$ and $\tilde{\chi}_1^0$ are scanned. The colour index and the printed numbers show the results for Z_N for each mass point. The events are normalised to an integrated luminosity of 20.3 fb^{-1}.*

8.5.2.2. $\mathrm{SR}^{\mu\mu}_{1\,\mathrm{jet}}$, $\mathrm{SR}^{\mu\mu}_{2,3\,\mathrm{jet}}$

The SRs with two muons in the final state are designed as explained in the following.

For the SR with exactly one central light jet, the leading muon has $p_T > 30$ GeV and the subleading muon has $p_T > 20$ GeV. The pseudorapidity between the two muons, $\Delta\eta_{ll}$, must be smaller than 1.5. This requirement is motivated by the distribution of $\Delta\eta_{ll}$ in Figure 8.7 (a) where both the distributions for the background

processes and for the predicted SUSY signal peak at low values, but the signal distribution decreases quicker for higher values of $\Delta\eta_{ll}$.

In $\mathrm{SR}^{\mu\mu}_{1\,\mathrm{jet}}$, $max(m_T)$ must be larger than 110 GeV. The distribution for m_{lj} after applying the cuts on the p_T of the leptons, $\Delta\eta_{ll}$ and $max(m_T)$, but before the cut on m_{eff} (the order of cuts is given in Table 8.4) is shown in Figure 8.7 (c). Only using events for which m_{lj} is lower than 90 GeV cuts away the tail of background events. The difference between the cut efficiencies for signal and background is maximum at $\sim$ 90 GeV and Z_N, the blue stacked line, is very high.

The effective mass must be larger than 200 GeV in $\mathrm{SR}^{\mu\mu}_{1\,\mathrm{jet}}$. The plots for the distributions of the other variables can be found in Appendix A.2 in Figures A.4 and A.5.

The definition of $\mathrm{SR}^{\mu\mu}_{2,3\,\mathrm{jet}}$ requires that both muons have a p_T of more than 30 GeV. The variable $\Delta\eta_{ll}$ must be smaller than 1.5. The corresponding plots can be found in Figures A.4 and A.5 in Appendix A.2. In Figure 8.7 (b), the distribution for m_{ljj}, the variable that reconstructs the mass of the Higgs boson under the assumption that $H \to W^+W^- \to l\nu q\bar{q}'$, is shown. The SUSY signal distribution for this variable should have its maximum for values lower than $m_H = 125$ GeV. For m_{ljj} higher than 120 GeV, the distribution of the predicted SUSY signal indeed decreases steeply while it has a peak for values of 120 GeV. Therefore the requirement of $m_{ljj} < 120$ GeV mainly suppresses SM background processes.

Requiring that the effective mass must be larger than 200 GeV selects mainly signal events since the SM background distribution peaks at values for $m_{eff} < 200$ GeV, as shown in Figure 8.7 (d).

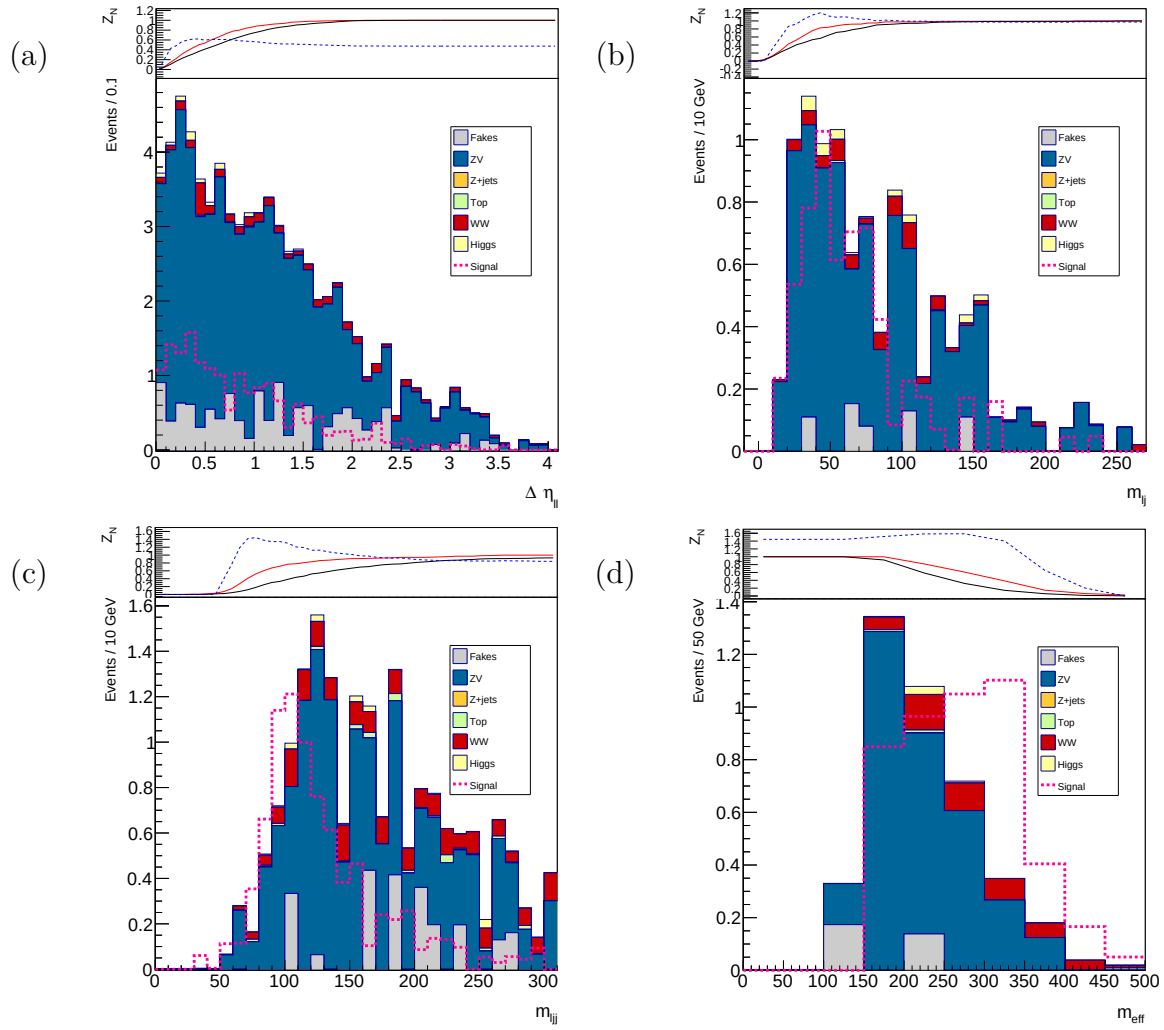

FIGURE 8.7.: *The lower plots show the distributions for the variables which motivate the cuts for the SR definition. The events are not selected due to the full SR definition but the cuts are applied in the order which is given in the Table 8.4. The expected SM background consists of 'Fakes' (grey colour), ZV (blue), $Z+jets$ (orange), Top (light green), WW (red) and Higgs (yellow).. The predicted SUSY signal for the mass point with $(m_{\tilde{\chi}_1^\pm,\tilde{\chi}_2^0}, m_{\tilde{\chi}_1^0}) = (130, 0)$ GeV is superimposed (pink dashed line). The upper plots show the cut efficiency for increasing cut values (decreasing cut values for m_{lj}, m_{ljj}) for the SM background expectation (black line) and for the predicted SUSY signal (red line). The blue stacked line shows the significance Z_N. (a) shows the distribution of $\Delta\eta_{ll}$ in $SR^{\mu\mu}_{1\,\mathrm{jet}}$, (b) shows m_{lj} for $SR^{\mu\mu}_{1\,\mathrm{jet}}$. (c) shows the distribution of m_{ljj} in $SR^{\mu\mu}_{2,3\,\mathrm{jet}}$ and (d) shows the effective mass for $SR^{\mu\mu}_{2,3\,\mathrm{jet}}$.*

The significance Z_N is computed for each mass point of the simplified model grid, using the event yield of the expected SM background and of the predicted SUSY signal in $\mathrm{SR}^{\mu\mu}_{1\,\mathrm{jet}}$ and $\mathrm{SR}^{\mu\mu}_{2,3\,\mathrm{jet}}$. The plots are shown in Figure 8.8 (a) and (b). Again the SRs are most sensitive to the point with $(m_{\tilde{\chi}_1^\pm,\tilde{\chi}_2^0}, m_{\tilde{\chi}_1^0}) = (130,\ 0)$ GeV. In $\mathrm{SR}^{\mu\mu}_{2,3\,\mathrm{jet}}$, the significance of this point is equal to 1.58.

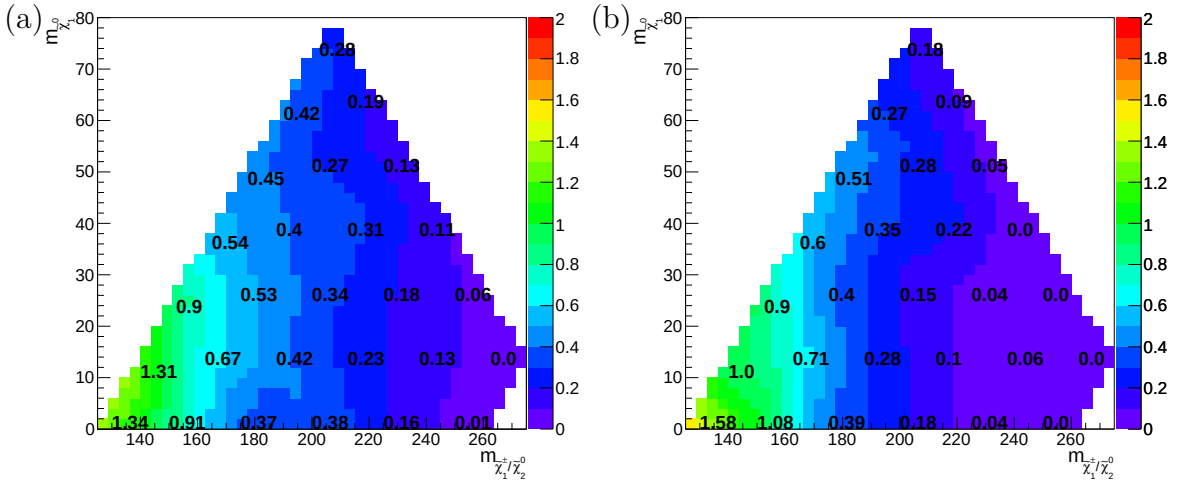

FIGURE 8.8.: *When applying all the cuts of the definition for $\mathrm{SR}^{\mu\mu}_{1\,\mathrm{jet}}$ (a) and $\mathrm{SR}^{\mu\mu}_{2,3\,\mathrm{jet}}$ (b), the expected Z_N can be computed from the resulting event yield for all mass points of the simplified model grid. Various values of the masses of $\tilde{\chi}_1^\pm$, $\tilde{\chi}_2^0$ and $\tilde{\chi}_1^0$ are scanned. The colour index and the printed numbers show the results for Z_N for each mass point. The events are normalised to an integrated luminosity of 20.3 fb^{-1}.*

8.5.2.3. $\mathrm{SR}^{e\mu}_{1\,\mathrm{jet}}$, $\mathrm{SR}^{e\mu}_{2,3\,\mathrm{jet}}$

The SRs with one electron and one muon with same electrical charge in the final state require $p_T > 30$ GeV both for the leading and the subleading lepton. In addition, $\Delta\eta_{ll}$ has to be smaller than 1.5. Figures 8.9 (a) and (b) show the distribution of the maximum of the transverse masses of the leading lepton and E_T^{miss} and the subleading lepton and E_T^{miss}. In both histograms, the distribution for the predicted SUSY signal is rather symmetric and peaks at $\sim$ 110 GeV. The distribution for the SM background on the other hand peaks at values lower than 110 GeV. For $\mathrm{SR}^{e\mu}_{1\,\mathrm{jet}}$ as well as for $\mathrm{SR}^{e\mu}_{2,3\,\mathrm{jet}}$ it is therefore required that this variable exceeds 110 GeV.

m_{lj} is shown in Figure 8.9 (c) for $\mathrm{SR}^{e\mu}_{1\,\mathrm{jet}}$ and in Figure 8.9 (d) for $\mathrm{SR}^{e\mu}_{2,3\,\mathrm{jet}}$. In both histograms, the distribution for the predicted SUSY signal peaks at low values; in this region the contribution of the SM background is rather low. Therefore $\mathrm{SR}^{e\mu}_{1\,\mathrm{jet}}$ requires $m_{lj} < 90$ GeV and $\mathrm{SR}^{e\mu}_{2,3\,\mathrm{jet}}$ requires $m_{ljj} < 120$ GeV. Furthermore the effective mass in both SRs must be larger than 200 GeV. The histograms of the other variables with cuts applied in the order as given in Table 8.4 are to be found in Appendix A.3 in Figures A.6 and A.7.

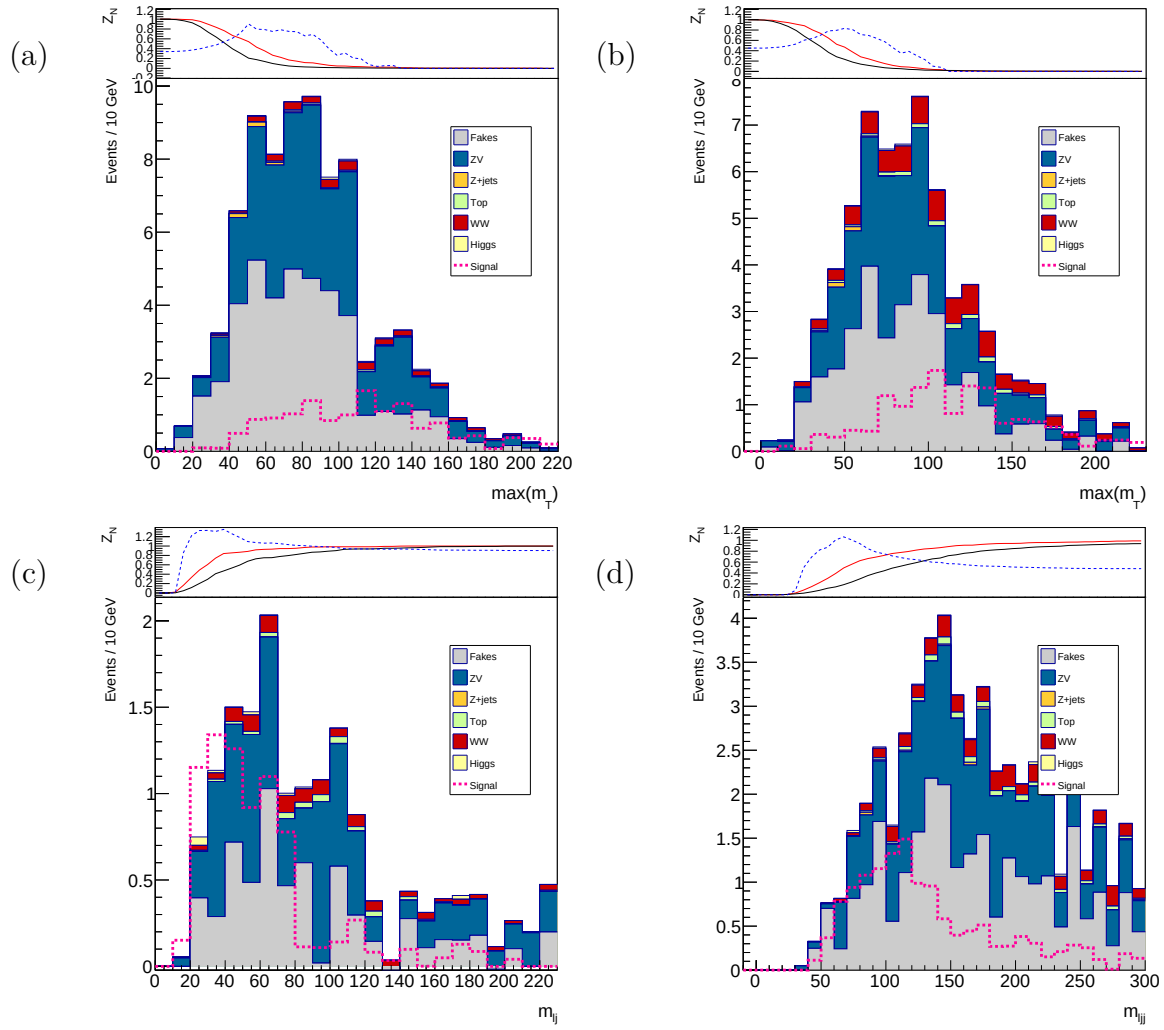

FIGURE 8.9.: *The lower plots show the distributions for the variables which motivate the cuts for the SR definition. The events are not selected due to the full SR definition but the cuts are applied in the order which is given in the Table 8.4. The expected SM background consists of 'Fakes' (grey colour), ZV (blue), $Z+jets$ (orange), Top (light green), WW (red) and Higgs (yellow). The predicted SUSY signal for the mass point with $(m_{\tilde{\chi}_1^\pm,\tilde{\chi}_2^0}, m_{\tilde{\chi}_1^0}) = (130, 0)$ GeV is superimposed (pink dashed line). The upper plots show the cut efficiency for increasing cut values (decreasing cut values for m_{lj}, m_{ljj}) for the SM background expectation (black line) and for the predicted SUSY signal (red line). The blue stacked line shows the significance Z_N. (a) shows the distribution of $max(m_T)$ before cutting on it in $SR^{e\mu}_{1\,\mathrm{jet}}$, (b) shows it for $SR^{e\mu}_{2,3\,\mathrm{jet}}$. (c) shows the distribution of m_{lj} in $SR^{e\mu}_{1\,\mathrm{jet}}$ and (d) shows m_{ljj} for $SR^{e\mu}_{2,3\,\mathrm{jet}}$.*

For each mass point of the simplified model grid, the significance is computed from the expected event yield in the SRs. For $SR^{e\mu}_{1\,\mathrm{jet}}$ the distribution is shown in Figure 8.10 (a); the most sensitive mass point reaches $Z_N = 1.22$. For $SR^{e\mu}_{2,3\,\mathrm{jet}}$, shown in Figure 8.10 (b), the significance reaches a maximum value of 1.51 for the same mass point with $(m_{\tilde{\chi}_1^\pm,\tilde{\chi}_2^0}, m_{\tilde{\chi}_1^0}) = (130, 0)$ GeV.

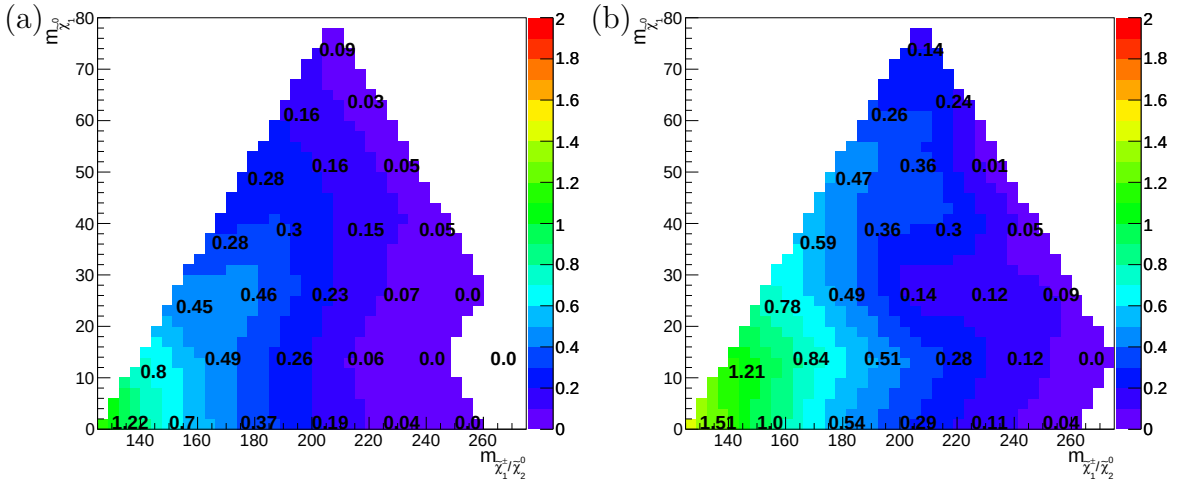

FIGURE 8.10.: *When applying all the cuts of the definition for $SR^{e\mu}_{1\,\mathrm{jet}}$ (a) and $SR^{e\mu}_{2,3\,\mathrm{jet}}$ (b), the expected Z_N can be computed from the resulting event yield for all mass points of the simplified model grid. Various values of the masses of $\tilde{\chi}_1^\pm$, $\tilde{\chi}_2^0$ and $\tilde{\chi}_1^0$ are scanned. The colour index and the printed numbers show the results for Z_N for each mass point. The events are normalised to an integrated luminosity of 20.3 fb^{-1}.*

TABLE 8.4.: *The signal region definitions.*

	$SR^{ee}_{1\,jet}$	$SR^{ee}_{2,3\,jet}$	$SR^{\mu\mu}_{1\,jet}$	$SR^{\mu\mu}_{2,3\,jet}$	$SR^{e\mu}_{1\,jet}$	$SR^{e\mu}_{2,3\,jet}$
Leptons	2	2	2	2	2	2
Hadronic taus	0	0	0	0	0	0
Lepton flavour	ee	ee	$\mu\mu$	$\mu\mu$	$e\mu$	$e\mu$
3rd lepton veto	yes	yes	yes	yes	yes	yes
Central light jets	1	2 or 3	1	2 or 3	1	2 or 3
Central b-jets	0	0	0	0	0	0
Forward jets	0	0	0	0	0	0
$\lvert m_{\ell\ell} - m_Z \rvert$ [GeV]	> 10	> 10	—	—	—	—
$p_T(\ell_0, \ell_1)$ [GeV]	30, 20	30, 20	30 ,20	30, 30	30, 30	30, 30
$\Delta\eta_{ll}$	—	—	< 1.5	< 1.5	< 1.5	< 1.5
$max(m_T)$[GeV]	—	> 110	> 110	—	> 110	> 110
m_{lj} or m_{ljj} [GeV]	< 90	< 120	< 90	< 120	< 90	< 120
m_{eff} [GeV]	> 200	—	> 200	> 200	> 200	> 200
$E_T^{miss,rel}$ [GeV]	> 55	> 30	—	—	—	—

8.6. BACKGROUND ESTIMATION

The dominating background contribution due to non-prompt leptons is estimated with a data-driven method; all other SM processes are simulated with MC.

8.6.1. NON-PROMPT LEPTONS

Non-prompt leptons can originate from leptonic decays inside jets or can truly be mis-identified jets. When a particle interacts with detector material, a photon can be emitted and produce a e^+e^- pair. The resulting electrons are non-prompt. The goal is to estimate the number of events in which a process leads to one or two non-prompt leptons which fulfil the selection criteria for electrons or muons.

8.6.1.1. MATRIX METHOD

The MC simulation of QCD multi-jet background is difficult because the modelling of the hadronisation processes is very CPU intensive due to the high cross sections. The probability for a lepton to be non-prompt is measured in all available Monte Carlo simulated samples for SM processes, for which the truth information, i.e. the information about the actual origin of a lepton, is accessible. The expected number of events which contains at least one signal lepton that is non-prompt is estimated

from ATLAS data:

The idea of the Matrix Method will first be explained for events with exactly one lepton in the final state. The number of leptons which fulfil 'loose' requirements, N^L, and the number of leptons which in addition fulfil 'tight' requirements, N^T, are measured. They are composed from leptons which are 'loose' and 'real' (N_R^L), loose and 'fake' (N_F^L), 'tight' and 'real' (N_R^T) or 'tight' and 'fake' (N_F^T):

$$N^L = N_R^L + N_F^L. \tag{8.2}$$

and

$$N^T = N_R^T + N_F^T = \frac{N_R^T}{N_R^L} \cdot N_R^L + \frac{N_F^T}{N_F^L} \cdot N_F^L =: r \cdot N_R^L + f \cdot N_F^L. \tag{8.3}$$

'Loose' electrons only need to have a p_T of more than 10 GeV, $|\eta| < 2.47$ and 'medium++' reconstruction quality. 'Loose' muons only need to have $p_T > 10$ GeV and $|\eta| < 2.5$. In contradiction to the 'tight' leptons, loose leptons may not fulfil the requirements on the impact parameters or isolation and may not pass the overlap removal procedure.

The probability for a lepton to be prompt, the real efficiency $r = \frac{N_R^T}{N_R^L}$, and the probability for a lepton to originate from a jet or from a conversion process, the fake rate $f = \frac{N_F^T}{N_F^L}$, are measured in MC samples with the help of the truth information. The system of the two linear equations can then be solved to obtain the number of events with a tight lepton which is fake, i.e. non-prompt.

The true composition of the sample, i.e. the origins of the leptons which are not measurable in ATLAS data, is related to the observable composition of the sample, i.e. how many leptons fulfil the tight requirements [76].

For a final state with exactly two leptons, estimating the SM background due to non-prompt leptons means estimating the number of events where one or two leptons are non-prompt. Measurable are the number of events in which the leading lepton is tight and the subleading lepton is only loose, N^{TL}, the number of events in which the leading lepton is only loose and the subleading lepton is tight, N^{LT}, and the number of events in which both leptons are tight, N^{TT}, or in which no lepton is tight, N^{LL}.

These numbers can be related to the number of events with one or two loose and fake leptons, N_{FR}^{LL}, N_{RF}^{LL} and N_{FF}^{LL}, or with two loose and real leptons, N_{RR}^{LL}, by the following matrix formula:

$$\begin{pmatrix} N^{TT} \\ N^{TL} \\ N^{LT} \\ N^{LL} \end{pmatrix} = \begin{pmatrix} r_1 r_2 & r_1 f_2 & f_1 r_2 & f_1 f_2 \\ r_1 \bar{r}_2 & r_1 \bar{f}_2 & f_1 \bar{r}_2 & f_1 \bar{f}_2 \\ \bar{r}_1 r_2 & \bar{r}_1 f_2 & \bar{f}_1 r_2 & \bar{f}_1 f_2 \\ \bar{r}_1 \bar{r}_2 & \bar{r}_1 \bar{f}_2 & \bar{f}_1 \bar{r}_2 & \bar{f}_1 \bar{f}_2 \end{pmatrix} \begin{pmatrix} N_{RR}^{LL} \\ N_{RF}^{LL} \\ N_{FR}^{LL} \\ N_{FF}^{LL} \end{pmatrix}.$$

$\bar{f}_i = 1 - f_i$, $\bar{r}_i = 1 - r_i$, where r_i is the real efficiency for lepton i, and f_i is the fake rate for lepton i.

RATES The fake rates and real efficiencies are measured individually for electrons and muons. They depend on the origin of the lepton, i.e. the information if a lepton is truly due to a HF jet, a LF jet or if an electron is the result of a conversion process (conv). The rates are studied individually in $Z+jets$, $W+jets$, $t\bar{t}$, $b\bar{b}/c\bar{c}$ and diboson SM processes, all simulated with MC. PYTHIA [45] is used to generate the $b\bar{b}/c\bar{c}$ sample. The probability for a lepton of a certain origin to be tight (i.e. a signal lepton) under the condition that it is loose (i.e. a baseline lepton) is measured depending on η and p_T in so-called extraction regions. For the extraction regions exactly two baseline leptons with any sign, at least one central loose jet and no taus are required.

SCALE FACTORS Since the simulation of the detector response is not perfect, scale factors (SFs) need to be applied on the fake rates and real efficiencies. They take into account the differences between the event yield of the expected SM background and the event yield of data in CRs which are enriched in non-prompt HF, LF or conversion leptons. The SFs depend on the lepton p_T and for electrons also on the pseudorapidity; the values are measured in the central ($|\eta| < 1.37$) or forward region ($|\eta| > 1.37$).

- For real efficiencies, scale factors are deduced from a sample of real leptons. To define the sample, tag leptons are selected with the Tag & Probe method in $Z \to l^+l^-$ events. They must have $p_T > 25$ GeV and pass the single-lepton trigger. The SFs are found to be consistent with unity within 1%.

- A CR enriched in $b\bar{b}/c\bar{c}$ processes is defined to deduce the SF for HF non-prompt leptons. The Tag & Probe method is applied by tagging muons which are overlapping with b-jets in the η-ϕ-space and which have $p_T > 20$ GeV. The other probe lepton in the event can be a muon or an electron. The event must have a positive decision for the corresponding dilepton trigger. The missing transverse energy must not be larger than 40 GeV. The missing transverse energy and the probe lepton are used to compute the transverse mass, $m_T(l, E_T^{miss})$, which must not be higher than 40 GeV. The contamination from genuine $W+jets$ events is estimated in the region $40 < m_T(l, E_T^{miss}) < 100$ GeV and is subtracted from the CR.

  If the probe lepton is a muon, the dilepton invariant mass must be larger than 40 GeV and must be outside the Z-mass window.

  For central muons (electrons), the SF value is 1.02 ± 0.23 (0.81 ± 0.17) and for forward muons (electrons) 1.31 ± 0.38 (0.62 ± 0.15). The errors are statistical.

- To measure the SF for conversion electrons, events with exactly two OS signal muons and one baseline electron are selected. The three objects must have

a total invariant mass close to the mass of the Z boson. $E_T^{miss} < 50$ GeV and $m_T(e, E_T^{miss}) < 40$ GeV are required. For central electrons, the resulting SF is 1.08 ± 0.24 and for forward electrons, 0.88 ± 0.17.

- The contribution from LF non-prompt leptons is less than 20% and the SF is assumed to be equal to unity. No MC simulated samples for LF jets are available.

Lepton Composition The rates are averaged for the various kinds of SM processes and the types of lepton origins. It is therefore measured how many of all real, HF, LF and conversion leptons result from a process p, i.e. $Z+jets$, $W+jets$, $t\bar{t}$, $b\bar{b}/c\bar{c}$ or diboson processes. The fractions must then add up to 100% when summing over all processes:

$$\sum_p R_p^{HF} + R_p^{LF} + R_p^{conv} = \sum_p R_p^{real} = 1. \tag{8.4}$$

Measurements in MC simulated samples show that non-prompt electrons are mostly resulting from conversion processes in $W+jets$, $Z+jets$ or diboson processes. The main source for non-prompt muons are HF $b\bar{b}/c\bar{c}$ processes. As was expected, for real leptons, most electrons originate from $Z+jets$ processes and most muons from $W+jets$ processes.

Weighted Averaged Rates The fake rates and real efficiencies are then averaged and weighted according to the following formulae:

- The fake rate for electrons

$$f_e = \sum_p [f_p^{HF} \cdot SF^{HF} \cdot R_p^{HF} + f_p^{LF} \cdot SF^{LF} \cdot R_p^{LF} + f_p^{conv} \cdot SF^{conv} \cdot R_p^{conv}] \tag{8.5}$$

  for which the values range from 0.072 ± 0.013 to 0.090 ± 0.016,

- the fake rate for muons

$$f_\mu = \sum_p [f_p^{HF} \cdot SF^{HF} \cdot R_p^{HF} + f_p^{LF} \cdot SF^{LF} \cdot R_p^{LF}] \tag{8.6}$$

  for which the values range from 0.118 ± 0.027 to 0.215 ± 0.112 over the four η and p_T dependent bins for fake rates,

- the real efficiency for electrons

$$r_e = \sum_p [r_p \cdot SF^{real} \cdot R_p^{real}] \tag{8.7}$$

  for which the values range from 0.61 ± 0.03 to 0.84 ± 0.01 and

- and the real efficiency for muons

$$r_\mu = \sum_p [r_p \cdot SF^{real} \cdot R_p^{real}] \tag{8.8}$$

for which the values range from 0.80 ± 0.05 to 0.97 ± 0.04 over the six η and p_T dependent bins for real efficiencies.

8.6.1.2. Validation Region

The estimation of the background due to non-prompt leptons needs to be validated. Three validation regions (VRs) are defined for ee, $\mu\mu$ and $e\mu$ final states which are orthogonal to the SRs due to the reversed cut on m_{lj} or m_{ljj} for events with one jet or two or three jets. Events with two SS leptons are selected which must have a p_T of at least 20 or 30 GeV. The exact definitions are given in Table 8.5. Events with two electrons must have an invariant dilepton mass outside the Z-mass window and $E_T^{miss,rel} > 40$ GeV.

Table 8.5.: *The definition of the VRs which are enriched in non-prompt leptons and ZV processes for ee, $\mu\mu$ and $e\mu$ final states. The events have exactly one jet or two or three jets. Accordingly a cut is placed on either ml_{lj} or m_{ljj}.*

	ee ZV+fake	$\mu\mu$ ZV+fake	$e\mu$ ZV+fake
p_T^{l1} [GeV]	> 20	> 30	> 30
p_T^{l2} [GeV]	> 20	> 20	> 20
ml_{lj} ($N_j = 1$) [GeV]	> 90	> 90	> 90
ml_{ljj} ($N_j = 2,3$) [GeV]	> 120	> 120	> 120
$\lvert m_{ll} - m_Z \rvert$ [GeV]	> 10	-	-
$E_T^{miss,rel}$ [GeV]	> 40	-	-

Table 8.6 gives the yield for the various SM background contributions estimated from MC samples and with the Matrix Method for the non-prompt leptons. The first error is the statistical error due to the limited number of events in the samples, the second error is due to systematic variations. The contributions due to non-prompt leptons and ZV processes are dominating. The measured event yield in ATLAS data agrees within the errors with the total expected event yield due to SM processes. The last row gives the predicted event yield for the SUSY signal mass point with $(m_{\tilde{\chi}_1^\pm, \tilde{\chi}_2^0}, m_{\tilde{\chi}_1^0}) = (130, 0)$ GeV.

TABLE 8.6.: *The event yield in the VRs which are enriched in non-prompt leptons and ZV processes. 'Fake' gives the yield when using the data-driven Matrix Method. ZV, WW, $t\bar{t}+Wt$, $Z+jets$ and Higgs are estimated from MC samples. The yield for 'signal' corresponds to the simplified model mass point with $(m_{\tilde{\chi}_1^\pm,\tilde{\chi}_2^0}, m_{\tilde{\chi}_1^0}) = (130, 0)$ GeV. The first error is statistical, the second error is due to systematic variations. The events are normalised to an integrated luminosity of 20.3 fb^{-1}.*

	ee	$\mu\mu$	$e\mu$	Total
Fake	$28.3 \pm 1.8\ ^{+6.8}_{-6.0}$	$28.4 \pm 2.6\ ^{+10.7}_{-10.4}$	$131.95 \pm 4.26\ ^{+27.88}_{-24.18}$	$188.7 \pm 5.3\ ^{+30.6}_{-27.0}$
ZV	$9.6 \pm 0.8\ ^{+2.9}_{-2.9}$	$47.0 \pm 1.9\ ^{+14.2}_{-14.2}$	$87.1 \pm 2.4\ ^{+26.3}_{-26.2}$	$143.8 \pm 3.1\ ^{+30.0}_{-29.8}$
WW	$4.76 \pm 0.19\ ^{+5.04}_{-5.04}$	$15.83 \pm 0.35\ ^{+17.83}_{-17.82}$	$23.3 \pm 0.4\ ^{+25.3}_{-25.3}$	$43.9 \pm 0.6\ ^{+31.3}_{-31.3}$
$t\bar{t}+Wt$	$0.92 \pm 0.06\ ^{+1.04}_{-1}$	$1.07 \pm 0.08\ ^{+1.16}_{-1.13}$	$3.19 \pm 0.10\ ^{+3.58}_{-3.44}$	$5.18 \pm 0.14\ ^{+3.90}_{-3.76}$
$Z+jets$	$1.77 \pm 0.18\ ^{+2.13}_{-2.07}$	$0 \pm 0\ ^{+0}_{-0}$	$0.73 \pm 0.08\ ^{+0.85}_{-0.83}$	$2.50 \pm 0.20\ ^{+2.29}_{-2.23}$
Higgs	$0.14 \pm 0.04\ ^{+0.14}_{-0.14}$	$0.56 \pm 0.09\ ^{+0.59}_{-0.59}$	$0.92 \pm 0.10\ ^{+0.96}_{-0.96}$	$1.62 \pm 0.14\ ^{+1.14}_{-1.14}$
Total	$45.51 \pm 2.00\ ^{+9.43}_{-8.74}$	$92.89 \pm 3.23\ ^{+25.26}_{-25.06}$	$247.3 \pm 4.9\ ^{+46.2}_{-43.8}$	$385.7 \pm 6.2\ ^{+53.5}_{-51.3}$
Data	49	76	279	404
Signal	$3.1 \pm 0.4\ ^{+0.8}_{-0.3}$	$12.3 \pm 0.8\ ^{+1.8}_{-1.0}$	$18.4 \pm 1.0\ ^{+2.1}_{-1.4}$	$33.8 \pm 1.34\ ^{+2.82}_{-1.74}$

8.6.2. TRIDENT EVENTS AND CHARGE FLIP

When selecting events with two SS leptons in the final state, it should be taken into account how likely it is that the sign of the electromagnetic charge is not changed in an intermediate process. For example, in a so-called 'trident event' an electron emits a photon and gives the major part of its energy to the γ. The high-p_T photon then produces an electron-positron pair where the positron carries most of the energy: $e^\pm \to e^\pm_{soft}\gamma_{hard} \to e^\pm_{soft}e^+_{hard}e^-_{soft}$. It looks like the initial electron flips its sign and becomes a positron. This is especially the case when the accompanying electrons in the event are very soft.

CHARGE FLIP RATE The probability for such 'charge flip' to happen is observed to be lower in data than in MC simulation. It is measured in data, depending on the transverse momentum and the pseudorapidity of the electrons. The events with two electrons of any sign and the events with two SS electrons are counted. For this procedure events for which the invariant mass of the two electrons is inside the Z-mass window are selected and the background due to non-prompt leptons is subtracted. A likelihood minimisation procedure uses these numbers as input to map the charge flip rate r^{cf} depending on $|\eta|$ and p_T.

From the charge flip rate for the leading (r_1^{cf}) and subleading electron (r_2^{cf}) in an OS event, a weight is computed,

$$w = \frac{r_1^{cf} + r_2^{cf}}{(1 - r_1^{cf}) \cdot (1 - r_2^{cf})}, \tag{8.9}$$

and applied to the event to estimate the number of background OS events which appear as SS events. The values for r^{cf} are e.g. 0.0001 $\pm$ 0.0000 for central electrons with $p_T = 30$ GeV or 0.0292 $\pm$ 0.0023 for electrons with a transverse momentum of more than 70 GeV which are detected in $2.25 < |\eta| < 2.47$.

The probability for a muon to be part of such trident event is found to be negligible.

CORRECTION FACTOR For the estimation of the background contribution due to non-prompt electrons, conversion processes are taken into account. In other words, for each event with an electron, the probability that the electron is the result of a particle reaction with detector material and the subsequent process of $\gamma \to e^+e^-$ is considered. This process is also taken into account in the charge flip measurement. Therefore the two methods of background estimation have an overlap. A correction factor is deduced from the comparison of data with SM prediction in events with two SS electrons which have a total invariant mass close to the mass of the Z boson. The value of the correction factor is found to be 0.37 $\pm$ 0.19.

8.7. SYSTEMATIC UNCERTAINTIES

The statistical and the systematic uncertainties vary the event yields in the CRs and SRs. The statistical error is due to the limited number of events in a sample. The following individual sources are taken into account for systematic uncertainties :

- Jet-related systematic uncertainties:
  - Jet energy scale (JES).
  - Jet energy resolution (JER).
  - b-tagging.
- Lepton-related systematic uncertainties:
  - Scale factors (data - MC agreement for reconstruction efficiencies) and trigger weights for electrons and muons.
  - Momentum resolution (ID and MS measurements) of muons.
  - Calibration of the energy scale for electrons.
  - Calorimeter resolution of electron p_T.

- E_T^{miss} soft-term-related systematic uncertainties: Energy scale calibration and resolution.
- Systematic uncertainties related to non-prompt leptons:
  - Dependency on the binning and the choice of the extraction region for fake rates.
  - Uncertainty due to potential differences in the non-prompt lepton compositions in the extraction regions and SRs for the measurement of fake rates.
  - Dependency on the binning and choice of extraction regions for real efficiencies.
  - Statistical uncertainties.
- Luminosity-related systematic uncertainty: flat 2.8%.
- Systematic uncertainties due to SM background modelling:
  - Uncertainty on cross sections for the production of SM background processes.
  - Uncertainty on the choice of the MC generators: 100% for the production of $t\bar{t}$, $t\bar{t}V$, $Z/\gamma + jets$, triboson and Higgs (these processes contribute less than 10 % to the total SM background).
  - Uncertainty due to diboson MC generator: Events with three leptons are selected to address the process $W^{\pm}Z \to l^{\pm}l^{+}l^{-}$. One SFOS lepton pair must have an invariant mass close to m_Z. The distributions of the variables which are used to define the SRs are compared to ATLAS data for the SS lepton pair in the three-lepton event, ignoring the third lepton. 36.8% is found to be a conservative estimate for the deviations. This difference is used as systematic uncertainty.
- Uncertainty on pile-up reweighting.
- Uncertainties on the charge flip probability of electrons and on the correction factor on the overlap with the estimation of the non-prompt leptons background.

The individual systematic variations are combined to a total systematic uncertainty, regarding potential correlations between the SM production processes or SRs and CRs: correlated errors are added linearly. The dominant systematic uncertainties on the individual SR event yields are due to background modelling (7 - 29%), the estimate of the non-prompt leptons background (1 - 19%) and the jet-related systematic variations (2 - 15%).

8.8. Preliminary Results and Interpretation

The full event selection of the SRs summarised in Table 8.4 are applied on the expected SM background. Data is 'blinded', i.e. not shown in the region of the plots which are inside the SR for the particular variables and the data yield is not given in the tables. The reason is that the analysis is not yet published.

The histograms in Figure 8.11 show the distribution of m_{lj} which has high sensitivity to the SUSY signal process for some SRs. The data distribution is given by black dots with the statistical error as vertical lines. The dashed region includes the combined statistical and systematic error on the expected SM background. The red arrow indicates the cut value according to the SR definition. The lower plots show the ratio between ATLAS data and the SM prediction, the vertical lines indicate the statistical error on data. The dashed region in the lower plots includes the combined statistical and systematic error for the expected SM background.

An example is the histogram for $\mathrm{SR}^{e\mu}_{2,3\,\mathrm{jet}}$ in Figure 8.9 (d) since the distributions for the predicted SUSY signal and the expected SM background have different shapes. The data yield is only shown for $m_{lj} > 90$ GeV in Figure 8.11 (a) for the ee final state, in (b) for $\mu\mu$ and in (c) for $e\mu$. The lower plot shows the ratio of ATLAS data over the SM expectation in the non-blinded regions.

Figure 8.12 (a) shows the distribution for m_{ljj} in $\mathrm{SR}^{ee}_{2,3\,\mathrm{jet}}$, (b) in $\mathrm{SR}^{\mu\mu}_{2,3\,\mathrm{jet}}$ and (c) in $\mathrm{SR}^{e\mu}_{2,3\,\mathrm{jet}}$. Data is blinded for $m_{ljj} < 120$ GeV.

The histograms in Figures 8.11 and 8.12 have low statistics due to the tight cuts of the SR definitions. The agreement of the SM expectation with the ATLAS data is better visible in the combination of $\mathrm{SR}^{ee}_{1\,\mathrm{jet}}$ with $\mathrm{SR}^{\mu\mu}_{1\,\mathrm{jet}}$ and $\mathrm{SR}^{e\mu}_{1\,\mathrm{jet}}$ in Figure 8.13 (a) for m_{lj} and in Figure 8.13 (b) for m_{ljj} in the combination of $\mathrm{SR}^{ee}_{2,3\,\mathrm{jet}}$ with $\mathrm{SR}^{\mu\mu}_{2,3\,\mathrm{jet}}$ and $\mathrm{SR}^{e\mu}_{2,3\,\mathrm{jet}}$. The prediction and data agree within the combined statistical and systematic errors (hatched band for MC).

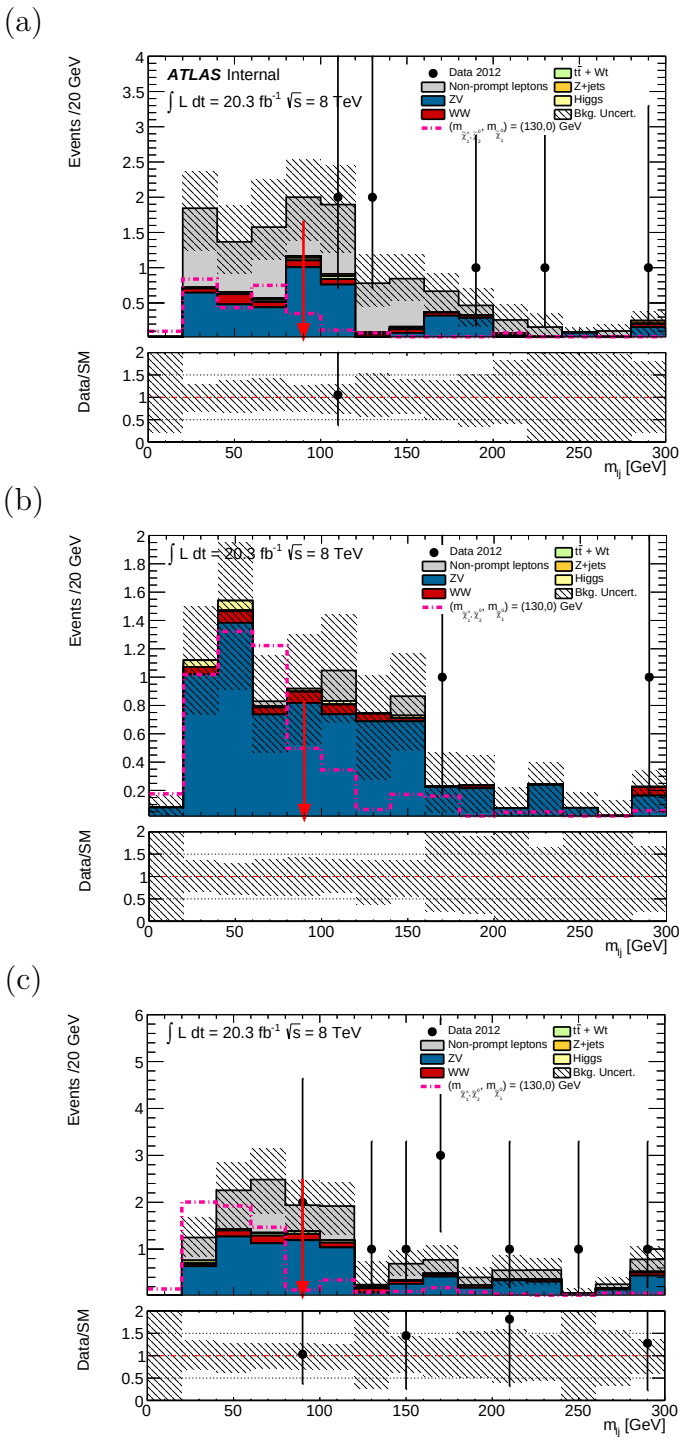

FIGURE 8.11.: *The upper plots show the distributions of the variable m_{lj}. The events are selected due to the full SR definition except for the cut on the shown variable. The expected background processes are non-prompt leptons (grey), ZV (blue), $Z+jets$ (orange), $t\bar{t}+Wt$ (green), WW (red) and Higgs (yellow). The SR is blinded for data. The predicted SUSY signal for the mass point with $(m_{\tilde{\chi}_1^\pm,\tilde{\chi}_2^0}, m_{\tilde{\chi}_1^0}) = (130, 0)$ GeV is superimposed (pink dashed line). (a) shows the distribution for m_{lj} in $SR^{ee}_{1\,\mathrm{jet}}$, (b) shows it for $SR^{\mu\mu}_{1\,\mathrm{jet}}$ and (c) shows it for $SR^{e\mu}_{1\,\mathrm{jet}}$.*

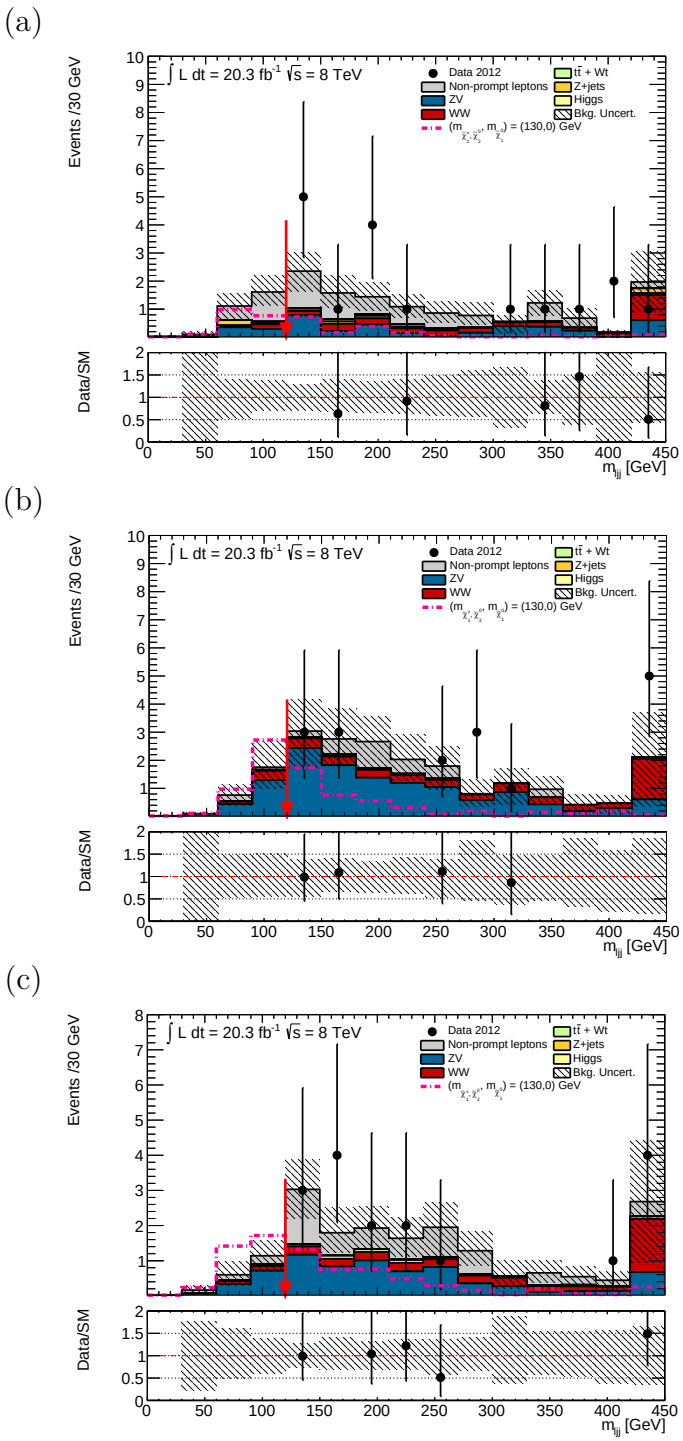

FIGURE 8.12.: *The upper plots show the distributions of the variable m_{ljj}. The events are selected due to the full SR definition except for the cut on the shown variable. The expected background processes are non-prompt leptons (grey), ZV (blue), $Z+jets$ (orange), $t\bar{t}+Wt$ (green), WW (red) and Higgs (yellow). The SR is blinded for data. The predicted SUSY signal for the mass point with $(m_{\tilde{\chi}_1^\pm,\tilde{\chi}_2^0}, m_{\tilde{\chi}_1^0}) = (130, 0)$ GeV is superimposed (pink dashed line). (a) shows the distribution for m_{ljj} in $SR^{ee}_{2,3\text{jet}}$, (b) shows it for $SR^{\mu\mu}_{2,3\text{jet}}$ and (c) shows it for $SR^{e\mu}_{2,3\text{jet}}$.*

(a)

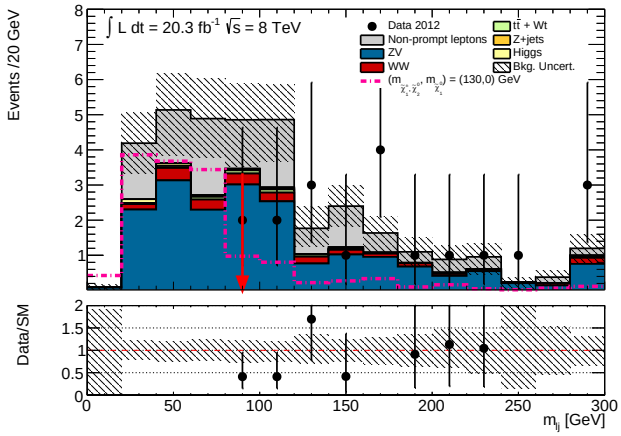

(b)

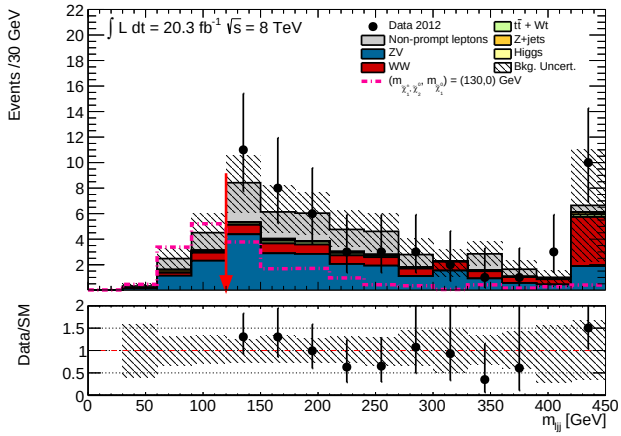

FIGURE 8.13.: *The upper plots show the distributions of the variable which is supposed to reconstruct the mass of the Higgs boson. The events are selected due to the full SR definition except for the cut on the shown variable. The expected background processes are non-prompt leptons (grey), ZV (blue), $Z+jets$ (orange), $t\bar{t}+Wt$ (green), WW (red) and Higgs (yellow). The SR is blinded for data. The predicted SUSY signal for the mass point with $(m_{\tilde{\chi}_1^\pm,\tilde{\chi}_2^0}, m_{\tilde{\chi}_1^0}) = (130, 0)$ GeV is superimposed (pink dashed line). (a) shows the distribution for m_{lj} in the combination of $SR^{ee}_{1\,\mathrm{jet}}$, $SR^{\mu\mu}_{1\,\mathrm{jet}}$ and $SR^{e\mu}_{1\,\mathrm{jet}}$ before cutting on it and (b) shows m_{ljj} for the combination of $SR^{ee}_{2,3\,\mathrm{jet}}$, $SR^{\mu\mu}_{2,3\,\mathrm{jet}}$ and $SR^{e\mu}_{2,3\,\mathrm{jet}}$.*

BLINDED RESULTS The event yield in the six SRs is given in Table 8.7. The assumption of a flat uncertainty of 30% on the background yield during the optimisation process is proven to be too conservative. The predicted SUSY signal for the most sensitive mass point of the simplified model, $(m_{\tilde{\chi}_1^\pm,\tilde{\chi}_2^0}, m_{\tilde{\chi}_1^0}) = (130, 0)$ GeV is given.

TABLE 8.7.: *The expected numbers of SM background events in the SRs with exactly one central light jet or two and three jets, scaled to an integrated luminosity of 20.3 fb^{-1}. The first error is the statistical uncertainty and the second the systematic one.*

	$SR^{ee}_{1\,jet}$	$SR^{\mu\mu}_{1\,jet}$	$SR^{e\mu}_{1\,jet}$	Total
Fake	$3.4 \pm 0.6^{+0.8}_{-0.7}$	$0.01 \pm 0.15\ ^{+0.11}_{-0.15}$	$3.0 \pm 0.6\ ^{+0.8}_{-0.7}$	$6.4 \pm 0.8\ ^{+1.2}_{-1.0}$
ZV	$2.2 \pm 0.4\ ^{+0.5}_{-0.5}$	$3.4 \pm 0.50\ ^{+0.7}_{-0.64}$	$3.3 \pm 0.5\ ^{+0.7}_{-0.7}$	$8.96 \pm 0.80\ ^{+1.06}_{-1.07}$
WW	$0.33 \pm 0.04\ ^{+0.3}_{-0.31}$	$0.24 \pm 0.04\ ^{+0.29}_{-0.29}$	$0.4 \pm 0.04\ ^{+0.38}_{-0.38}$	$0.97 \pm 0.07\ ^{+0.56}_{-0.57}$
$t\bar{t}+Wt$	$0.09 \pm 0.01\ ^{+0.11}_{-0.1}$	$0.01 \pm 0.01\ ^{+0.01}_{-0.01}$	$0.11 \pm 0.01\ ^{+0.14}_{-0.13}$	$0.21 \pm 0.02\ ^{+0.18}_{-0.16}$
$Z+jets$	$0.04 \pm 0.02\ ^{+0.09}_{-0.04}$	$0 \pm 0\ ^{+0}_{-0}$	$0 \pm 0\ ^{+0}_{-0}$	$0.04 \pm 0.02\ ^{+0.09}_{-0.04}$
Higgs	$0 \pm 0\ ^{+0}_{-0}$	$0.13 \pm 0.05\ ^{+0.13}_{-0.14}$	$0.08 \pm 0.03\ ^{+0.09}_{-0.09}$	$0.21 \pm 0.06\ ^{+0.16}_{-0.17}$
Total	$6.0 \pm 0.7\ ^{+1.0}_{-0.9}$	$3.8 \pm 0.5\ ^{+0.7}_{-0.7}$	$7.0 \pm 0.7\ ^{+1.1}_{-1.1}$	$16.81 \pm 1.16\ ^{+1.69}_{-1.6}$
Signal	$2.4 \pm 0.4\ ^{+0.2}_{-0.5}$	$4.2 \pm 0.5\ ^{+0.3}_{-0.5}$	$5.6 \pm 0.65\ ^{+0.5}_{-0.9}$	$12.1 \pm 0.8\ ^{+0.6}_{-1.1}$
	$SR^{ee}_{2,3\,jet}$	$SR^{\mu\mu}_{2,3\,jet}$	$SR^{e\mu}_{2,3\,jet}$	Total
Fake	$1.6 \pm 0.4\ ^{+0.4}_{-0.3}$	$0.28 \pm 0.34\ ^{+0.09}_{-0.13}$	$0.48 \pm 0.25\ ^{+0.15}_{-0.12}$	$2.4 \pm 0.6\ ^{+0.4}_{-0.4}$
ZV	$0.66 \pm 0.21\ ^{+0.36}_{-0.25}$	$1.8 \pm 0.4\ ^{+0.8}_{-0.7}$	$1.11 \pm 0.26\ ^{+0.44}_{-0.46}$	$3.6 \pm 0.5\ ^{+1.1}_{-0.9}$
WW	$0.22 \pm 0.04\ ^{+0.23}_{-0.23}$	$0.43 \pm 0.06\ ^{+0.49}_{-0.49}$	$0.23 \pm 0.04\ ^{+0.26}_{-0.25}$	$0.88 \pm 0.08\ ^{+0.6}_{-0.6}$
$t\bar{t}+Wt$	$0.05 \pm 0.01\ ^{+0.08}_{-0.06}$	$0.02 \pm 0.01\ ^{+0.03}_{-0.02}$	$0.06 \pm 0.01\ ^{+0.08}_{-0.07}$	$0.13 \pm 0.02\ ^{+0.12}_{-0.09}$
$Z+jets$	$0.22 \pm 0.11\ ^{+0.27}_{-0.27}$	$0 \pm 0\ ^{+0}_{-0}$	$0 \pm 0\ ^{+0}_{-0}$	$0.22 \pm 0.11\ ^{+0.27}_{-0.27}$
Higgs	$0.04 \pm 0.03\ ^{+0.05}_{-0.05}$	$0.04 \pm 0.02\ ^{+0.05}_{-0.04}$	$0.03 \pm 0.02\ ^{+0.03}_{-0.03}$	$0.11 \pm 0.04\ ^{+0.08}_{-0.07}$
Total	$2.8 \pm 0.5\ ^{+0.7}_{-0.6}$	$2.6 \pm 0.5\ ^{+1.0}_{-0.9}$	$1.9 \pm 0.4\ ^{+0.6}_{-0.6}$	$7.3 \pm 0.8\ ^{+1.4}_{-1.2}$
Signal	$1.9 \pm 0.4\ ^{+0.2}_{-0.2}$	$3.8 \pm 0.5\ ^{+0.6}_{-0.6}$	$3.4 \pm 0.4\ ^{+0.5}_{-0.3}$	$9.1 \pm 0.7\ ^{+0.8}_{-0.7}$

INTERPRETATION OF RESULTS In Figure 8.14 the mass points that are expected to be excluded at 95% CL are shown. The significance of each of the six SRs i is combined to a 'total' Z_N for each simplified model mass point with the formula given by

$$Z_N^{total} = \sqrt{\sum_{i=1}^{n} Z_{N,i}^2} \tag{8.10}$$

with $n = 6$. Since Z_N exceeds the value of 1.64 for the mass points with $(m_{\tilde{\chi}_1^\pm,\tilde{\chi}_2^0}, m_{\tilde{\chi}_1^0}) =$ (130, 0) GeV ($Z_N^{total} = 2.95$), $(m_{\tilde{\chi}_1^\pm,\tilde{\chi}_2^0}, m_{\tilde{\chi}_1^0}) =$ (140, 10) GeV ($Z_N^{total} = 1.91$) and $(m_{\tilde{\chi}_1^\pm,\tilde{\chi}_2^0}, m_{\tilde{\chi}_1^0}) =$ (150, 0) GeV ($Z_N^{total} = 2.31$), these points are expected to be excluded at 95% CL when data is 'unblinded'.

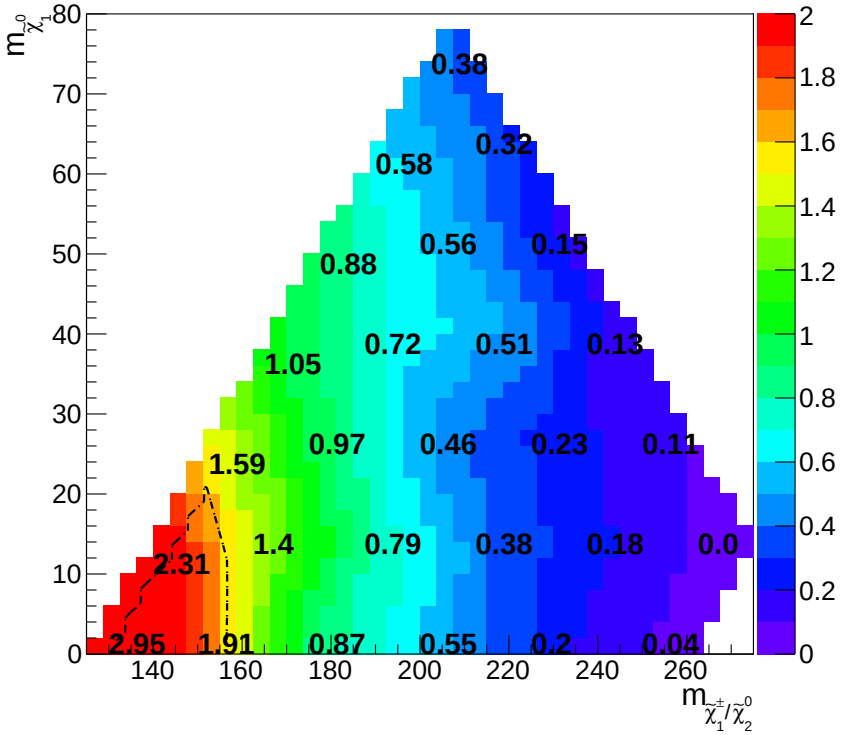

FIGURE 8.14.: *The expected significance Z_N of all six SRs is combined for each mass point of the simplified model grid with the formula given in Equation 8.10. The dashed black line indicates which region is expected to be excluded at 95% CL. The events are normalised to an integrated luminosity of 20.3 fb^{-1}.*

The expected significance to the mass points of the pMSSM with $\tan\beta$ =10 is shown in Figure 8.15. Only the point with $\mu =$ 150 GeV and $M_2 =$ 100 GeV is expected to be excluded at 95% CL with Z_N =2.48 according to formula 8.10.

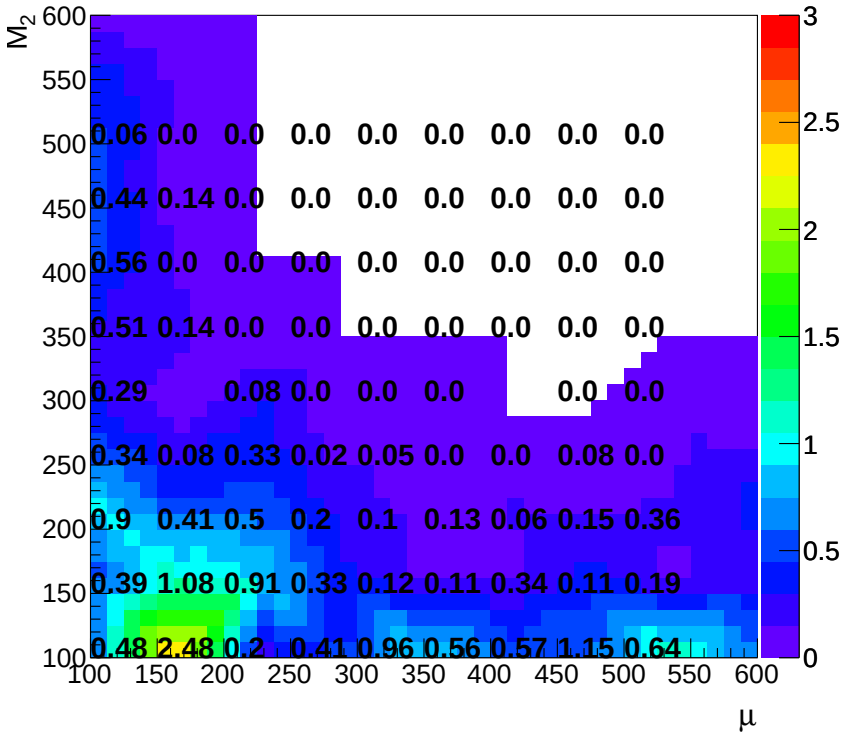

FIGURE 8.15.: *The expected significance Z_N of all six SRs is combined for each mass point of the pMSSM grid with the formula given in Equation 8.10. The events are normalised to an integrated luminosity of 20.3 fb^{-1}.*

9. Summary and Outlook

The Standard Model of elementary particle physics has limitations; it cannot explain why for example the mass of the Higgs boson is many orders of magnitudes smaller than the Planck mass or why extreme fine-tuning is needed for the correction terms of the Higgs mass. Supersymmetry is a possible extension to the Standard Model which can provide solutions to these problems and which in addition provides a candidate for Dark Matter - the neutralino.

Since strongly interacting particles like the gluinos have already been excluded in simplified models for masses up to 1.34 TeV [18], the search for electroweakly produced sparticles, which have a comparably low production cross section in LHC proton-proton collisions, becomes important. In this thesis, three analyses which address final states with exactly two leptons (electrons or muons), jets and missing transverse energy due to the non-detectable neutrinos and neutralinos were presented.

For the search for Supersymmetry in 4.7 fb^{-1} of ATLAS data recorded at $\sqrt{s} = 7$ TeV in the year 2011, four signal regions are designed for four different SUSY decay scenarios. $\tilde{\chi}_1^+\tilde{\chi}_1^-$- or $\tilde{\chi}_1^\pm\tilde{\chi}_2^0$ pairs decay via intermediate sleptons into final states with two identified leptons, jets and missing transverse energy. Another possibility is the direct production of a pair of sleptons, similar to the Standard Model Drell-Yan production mechanism.

The scenarios are generated with Monte Carlo in the context of the pMSSM with very heavy strongly-interacting sparticles, staus and gauginos. Only the mass of the $\tilde{\chi}_1^0$ is varied as well as the bino mass parameter M_1. Simplified models are simulated for the direct gaugino production scenarios with variable masses for the $\tilde{\chi}_1^0$, $\tilde{\nu}$, $\tilde{l}$, $\tilde{\chi}_1^\pm$ and $\tilde{\chi}_2^0$.

The signal regions make use of a Z-veto and put requirements on the relative missing transverse energy of at least 40, 50 or 100 GeV. The stransverse mass variable is used to suppress SM background processes. In the signal region which requires at least two jets, events in which the contransverse mass has values which are similar to the ones in $t\bar{t}$ processes, are vetoed. The Standard Model processes which have a detector signature that is similar to the signal signature are mainly $t\bar{t}$, $Z/\gamma^* + jets$, ZV, ZZ and WW. Their contributions to the event yield in the signal regions are estimated with Monte Carlo simulated samples which are normalised to data in control regions. The background due to non-prompt leptons is given by the application of the data-driven Matrix Method.

In general, only events which pass the trigger requirement are used - this means that depending on the flavour and the p_T of the two leptons in the event, a single lepton trigger, a dilepton trigger or at least one of the two must be passed. To each Monte Carlo simulated event a weight equal to the probability that this event passes a trigger in ATLAS data is assigned.

In the scenario of direct slepton production, left-handed slepton masses between 85 and 195 GeV are excluded at 95% confidence level for a 20 GeV neutralino. Masses of the $\tilde{\chi}_1^{\pm}$ between 110 and 340 GeV are excluded at 95% CL when the $\tilde{\chi}_1^0$ has a mass of 10 GeV. The latter exclusion limit is obtained for the scenario $\tilde{\chi}_1^{\pm}\tilde{\chi}_1^{\mp} \rightarrow \tilde{l}^{\pm}\nu(l^{\pm}\tilde{\nu})\tilde{l}^{\mp}\nu(l^{\mp}\tilde{\nu}) \rightarrow (l^{\pm}\nu\tilde{\chi}_1^0)(l^{\mp}\nu\tilde{\chi}_1^0)$. To this decay chain, the signal region which requires a stransverse mass of more than 90 GeV is most sensitive.

In the year of 2012, 20.3 fb^{-1} of data were recorded in ATLAS at $\sqrt{s} = 8$ TeV. In the second analysis presented in this thesis, electroweakly produced supersymmetric particles are assumed to decay into final states with two oppositely charged leptons (electrons or muons), jets and missing transverse energy. The scenario of a pair of charginos which decays via W bosons or sleptons, the scenario of a pair of $\tilde{\chi}_1^{\pm}\tilde{\chi}_2^0$ which decays via W and Z into two leptons, two quarks and two neutralinos as well as the direct slepton production are studied using simplified models. The $\tilde{\chi}_1^{\pm}$ and $\tilde{\chi}_2^0$ are pure wino and mass degenerate.

For the interpretation in the pMSSM, one setting with $\tan\beta = 6$ with intermediate slepton decay and one setting with $\tan\beta = 10$ with very heavy sleptons are used. The supersymmetric μ and M_1 mass parameters are varied.

Three signal regions address the signal processes with two intermediate W bosons, three other signal regions make use of the stransverse mass variable and one signal region is especially designed for the final state with jets. The Standard Model background is estimated by normalising the distribution of Monte Carlo simulated events to data in control regions for $t\bar{t}$, WW, ZW and ZZ processes. In the signal regions with jets, the background due to ZW and ZZ is estimated from control samples with three or four identified leptons in the final state, and the background due to $Z/\gamma^* + jets$ processes is estimated with the data-driven Jet Smearing Method.

Only events which pass one of the dilepton triggers, depending on the p_T of the leptons in the event, are analysed. For the $\mu\mu$ channel, the symmetric and asymmetric dimuon triggers are combined with logical OR when certain requirements on the transverse momenta of the muons are fulfilled. Monte Carlo simulated events are reweighted using the trigger efficiencies measured in ATLAS data.

The expected and observed numbers of events are in agreement in all seven signal regions. The results are used to exclude $\tilde{\chi}_1^{\pm}$ masses between 100 and 105 GeV, 120 and 135 GeV and 145 and 160 GeV at 95% confidence level for $m_{\tilde{\chi}_1^0} = 0$ GeV in the simplified model where $\tilde{\chi}_1^+\tilde{\chi}_1^- \rightarrow W^+\tilde{\chi}_1^0 W^-\tilde{\chi}_1^0 \rightarrow l^+\nu\tilde{\chi}_1^0 l^-\bar{\nu}\tilde{\chi}_1^0$. Slepton masses between 90 and 325 GeV can be excluded at 95% CL for a massless neutralino in the context of direct slepton production.

After the discovery of the Higgs boson in 2012 it became meaningful to include the decay chains with this particle in the search for Supersymmetry. The ATLAS data recorded in 2012 is therefore analysed relating to a scenario where a pair of $\tilde{\chi}_1^{\pm}\tilde{\chi}_2^0$ decays into WH and then into a final state with two same-sign leptons, two quarks and two neutralinos. Six signal regions depending on the flavour of the leptons and the number of jets in the event are designed. The Supersymmetry signal simulated in a simplified model is used to optimise the signal regions. To distinguish the signal from Standard Model background, cuts on the effective mass, the maximum of the transverse masses and the variable which reconstructs the invariant mass of the Higgs boson are important. The Standard Model background in the signal regions consists mainly of events with non-prompt leptons. This contribution is estimated with the data-driven Matrix Method. Diboson processes are also dominating and are - as well as all other background processes - estimated from Monte Carlo simulated samples. A veto on events with so-called third leptons suppresses contributions from WZ. The analysis is still blinded in the signal regions. It is expected that in the simplified model, three mass points with neutralino masses of less than 10 GeV and chargino masses of less than 10 GeV can be excluded at 95% confidence level.

As of this writing, Supersymmetry was not observed. E.g. a sparticle mass range up to 1.34 TeV could be excluded for gluinos in a simplified model. In 2015, ATLAS is going to start to record data at $\sqrt{s}$ =13 TeV. The ongoing data taking will increase the integrated luminosity and therefore provide higher statistics for rare events. The higher centre-of-mass energies mean higher production cross sections of heavy supersymmetric particles. Since the SM background processes are now well understood, the chance to discover sparticles with high masses will be raised.

A. SR Optimisation

A.1. $SR^{ee}_{1\text{jet}}$ and $SR^{ee}_{2,3\text{jet}}$

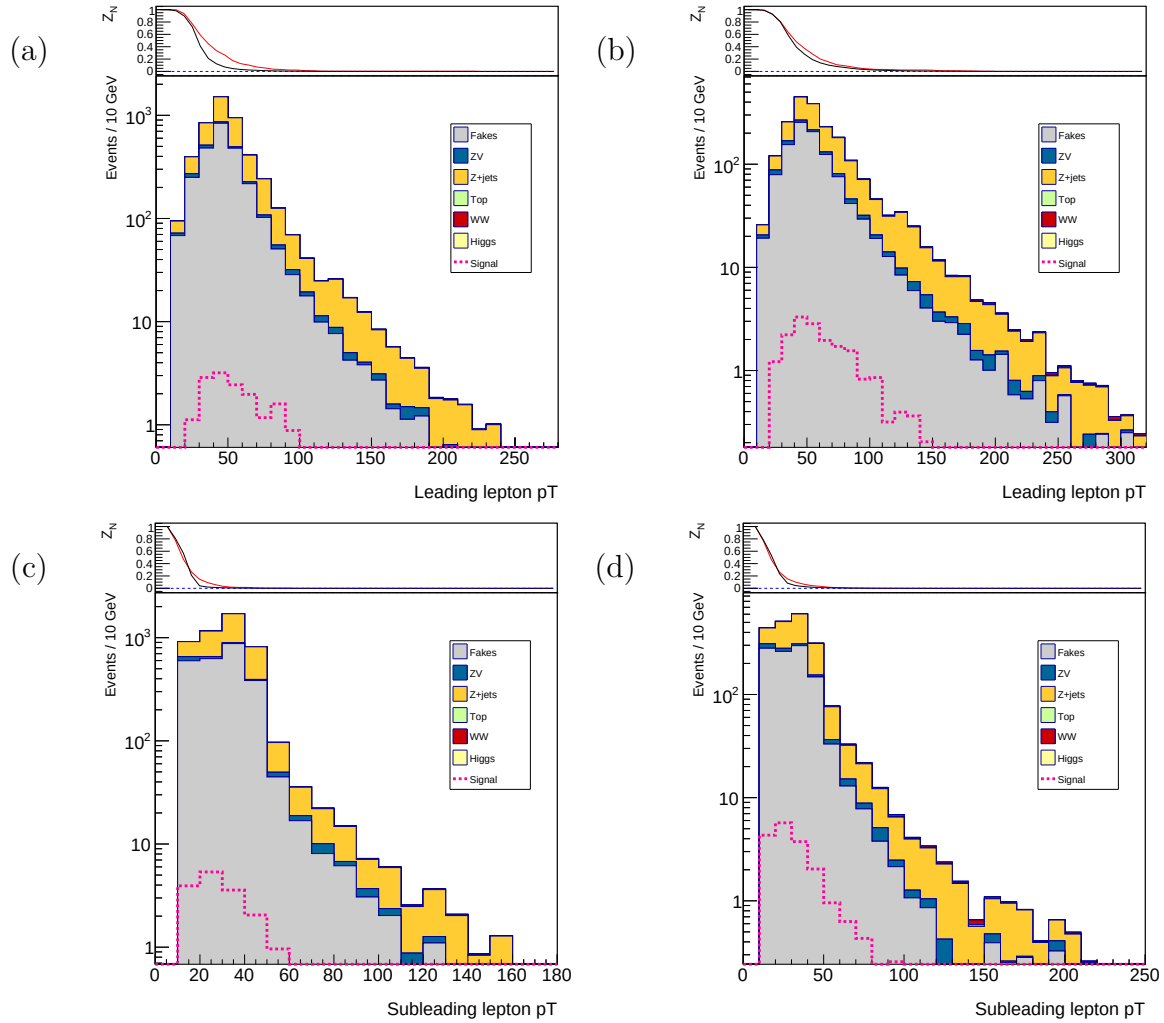

FIGURE A.1.: *The lower plots show the distributions for the variables which motivate the cuts for the SR definition. The events are not selected due to the full SR definition but the cuts are applied in the order which is given in the Table 8.4. The expected SM background consists of 'Fakes' (grey colour), ZV (blue), $Z+jets$ (orange), Top (light green), WW (red) and Higgs (yellow). The predicted SUSY signal for the mass point with $(m_{\tilde{\chi}_2^0}, m_{\tilde{\chi}_1^\pm, \tilde{\chi}_1^0}) = (130, 0)$ GeV is superimposed (pink dashed line). The upper plots show the cut efficiency for increasing cut values (decreasing cut values for m_{lj}, m_{ljj}) for the SM background expectation (black line) and for the predicted SUSY signal (red line). The event yield is used which results from the cut on the value indicated by the particular bin. The blue stacked line shows the significance. (a) shows the distribution for the p_T of the leading electron in $SR^{ee}_{1\,jet}$, (b) shows it for $SR^{ee}_{2,3\,jet}$. (c) shows the distribution of p_T of the subleading electron in $SR^{ee}_{1\,jet}$ and (d) shows it for $SR^{ee}_{2,3\,jet}$.*

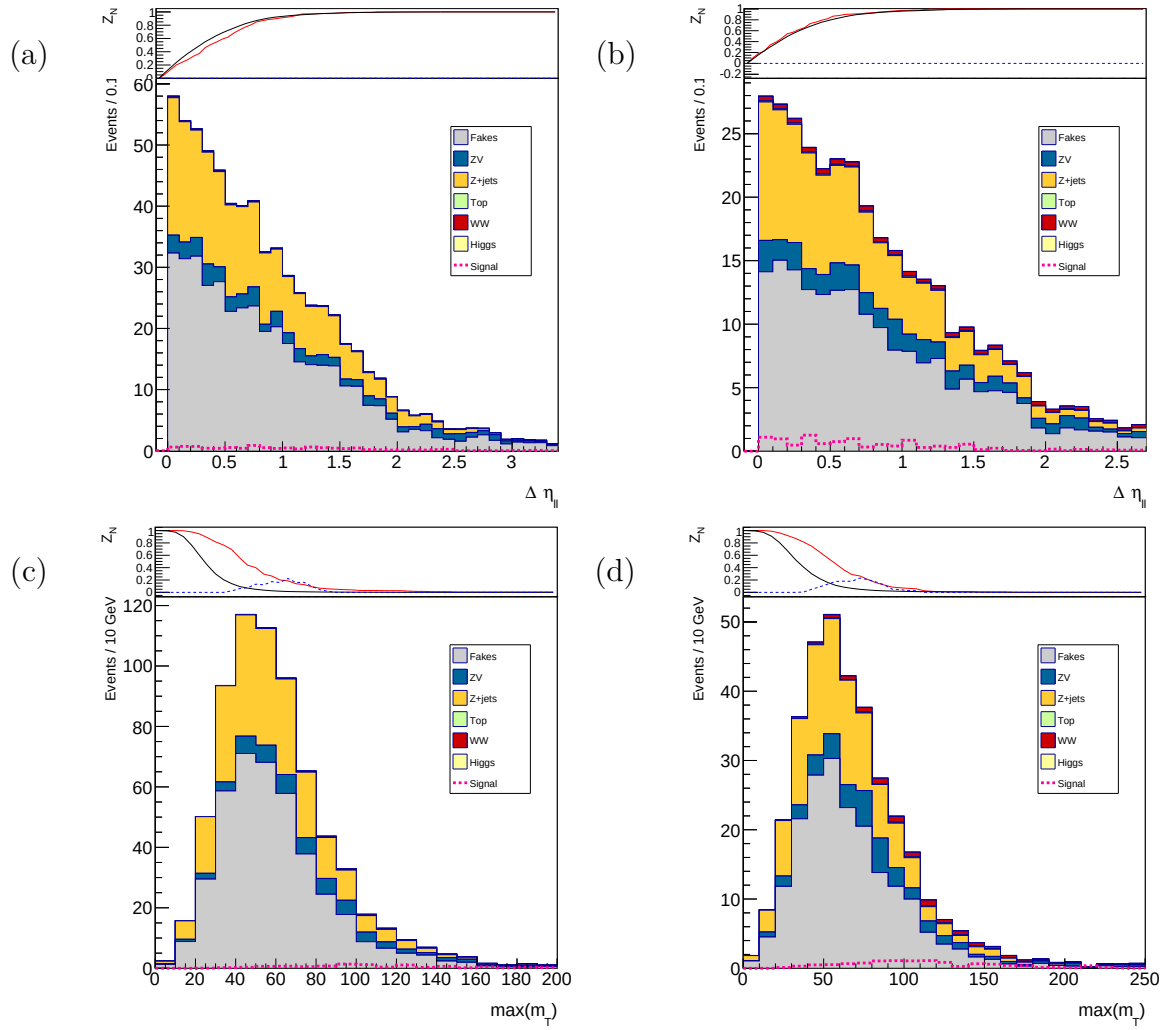

FIGURE A.2.: *The lower plots show the distributions for the variables which motivate the cuts for the SR definition. The events are not selected due to the full SR definition but the cuts are applied in the order which is given in the Table 8.4. The expected SM background consists of 'Fakes' (grey colour), ZV (blue), $Z+jets$ (orange), Top (light green), WW (red) and Higgs (yellow). The predicted SUSY signal for the mass point with $(m_{\tilde{\chi}^0_2}, m_{\tilde{\chi}^\pm_1,\tilde{\chi}^0_1}) = (130, 0)$ GeV is superimposed (pink dashed line). The upper plots show the cut efficiency for increasing cut values (decreasing cut values for m_{lj}, m_{ljj}) for the SM background expectation (black line) and for the predicted SUSY signal (red line). The event yield is used which results from the cut on the value indicated by the particular bin. The blue stacked line shows the significance Z_N. (a) shows the distribution of the difference of the pseudorapidites of the two electrons in $SR^{ee}_{1\,\mathrm{jet}}$ and (b) in $SR^{ee}_{2,3\,\mathrm{jet}}$. (c) shows the distribution of the the maximum of the transverse masses for the leading lepton and E_T^{mmiss} and the subleading lepton and E_T^{miss} in $SR^{ee}_{1\,\mathrm{jet}}$ and (d) shows it for $SR^{ee}_{2,3\,\mathrm{jet}}$*

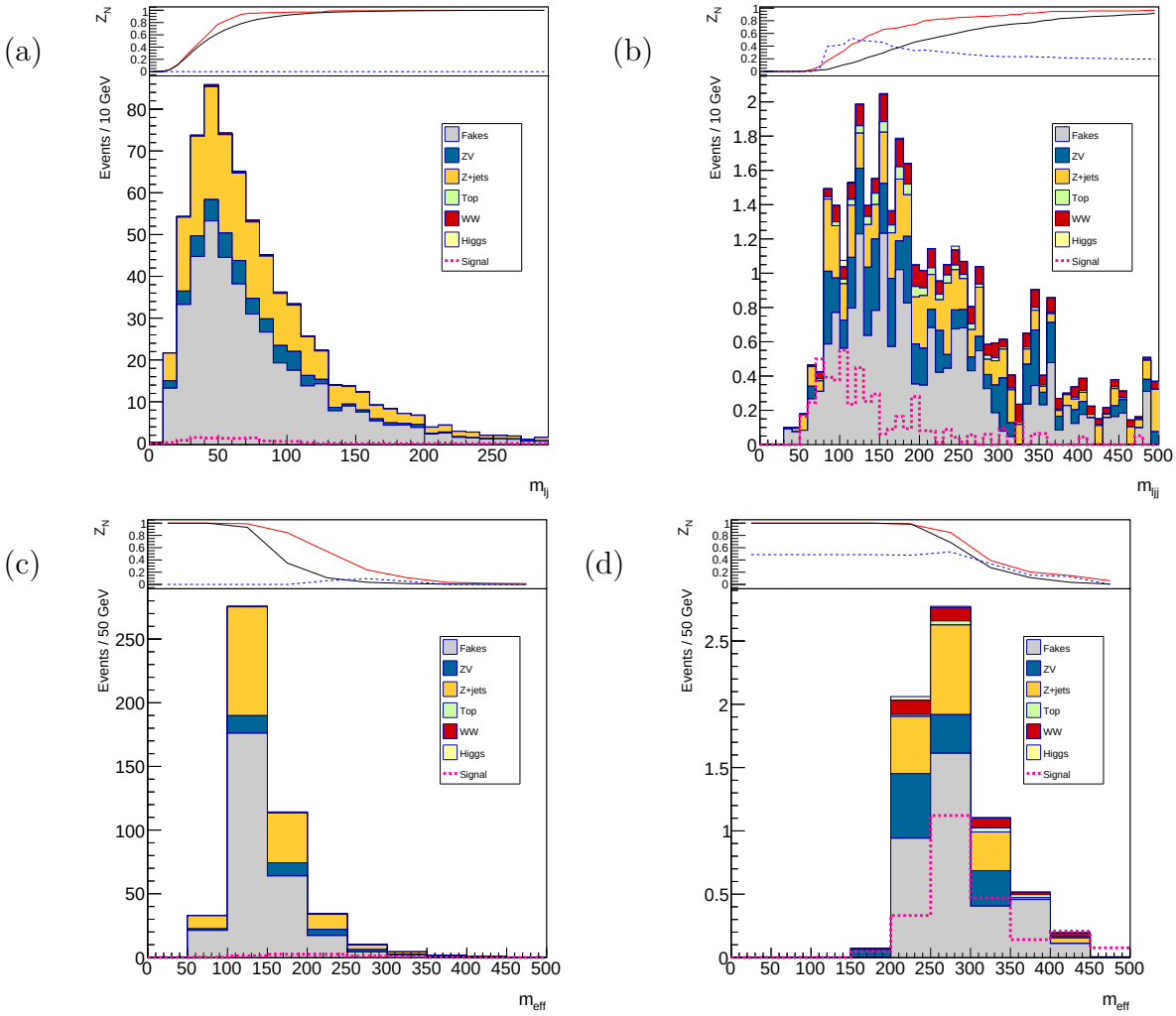

FIGURE A.3.: *The lower plots show the distributions for the variables which motivate the cuts for the SR definition. The events are not selected due to the full SR definition but the cuts are applied in the order which is given in the Table 8.4. The expected SM background consists of 'Fakes' (grey colour), ZV (blue), $Z+jets$ (orange), Top (light green), WW (red) and Higgs (yellow). The predicted SUSY signal for the mass point with $(m_{\tilde{\chi}_2^0}, m_{\tilde{\chi}_1^\pm, \tilde{\chi}_1^0}) = (130, 0)$ GeV is superimposed (pink dashed line). The upper plots show the cut efficiency for increasing cut values (decreasing cut values for m_{lj}, m_{ljj}) for the SM background expectation (black line) and for the predicted SUSY signal (red line). The event yield is used which results from the cut on the value indicated by the particular bin. The blue stacked line shows the significance Z_N. (a) shows the distribution for m_{lj} in $SR^{ee}_{1\,jet}$, (b) shows m_{ljj} for $SR^{ee}_{2,3\,jet}$. (c) shows the distribution of the effective mass in $SR^{ee}_{1\,jet}$ and (d) shows it for $SR^{ee}_{2,3\,jet}$.*

A.2. $SR^{\mu\mu}_{1\,jet}$ AND $SR^{\mu\mu}_{2,3\,jet}$

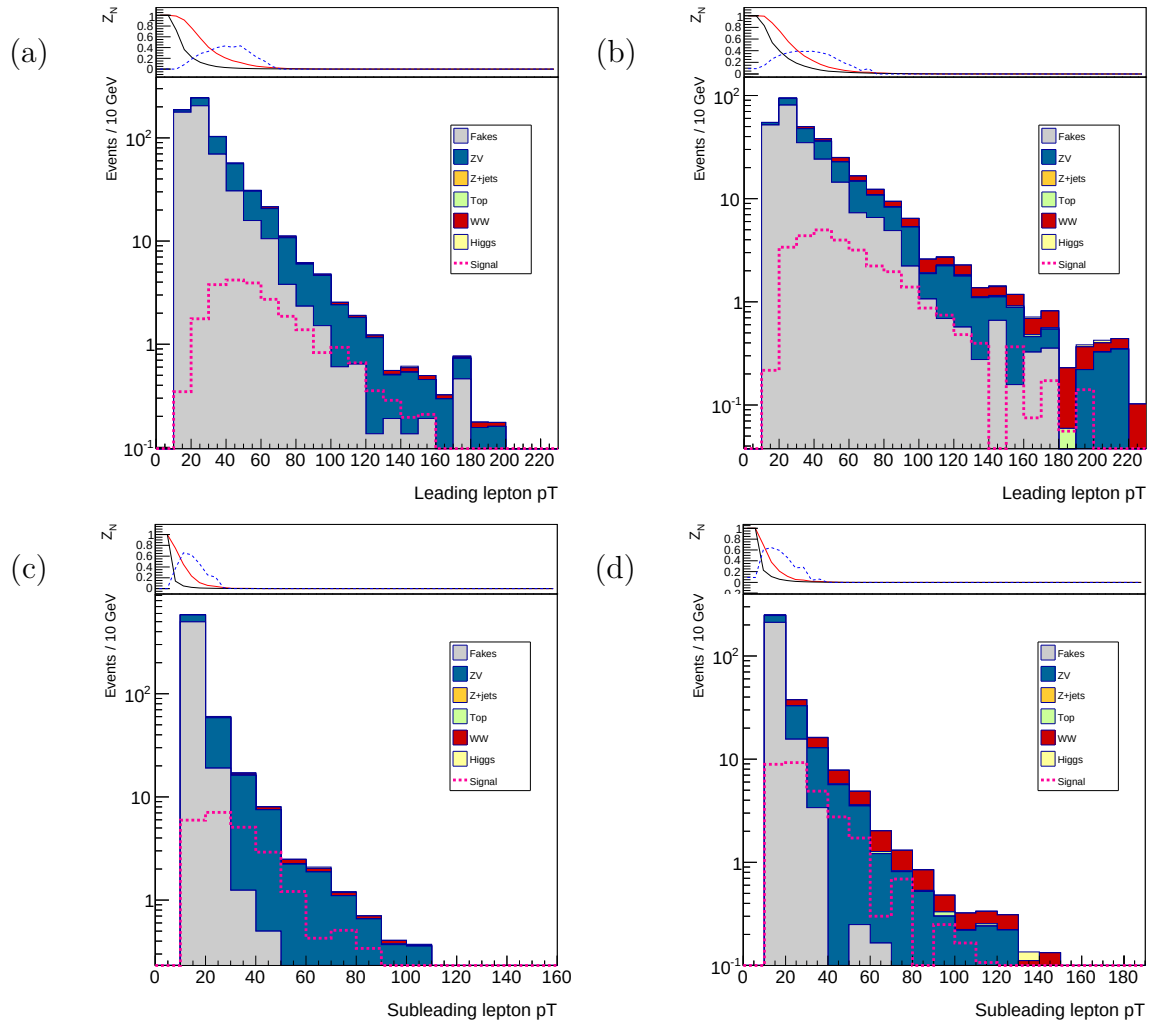

FIGURE A.4.: *The lower plots show the distributions for the variables which motivate the cuts for the SR definition. The events are not selected due to the full SR definition but the cuts are applied in the order which is given in the Table 8.4. The expected SM background consists of 'Fakes' (grey colour), ZV (blue), $Z+jets$ (orange), Top (light green), WW (red) and Higgs (yellow). The predicted SUSY signal for the mass point with $(m_{\tilde{\chi}_2^0}, m_{\tilde{\chi}_1^\pm, \tilde{\chi}_1^0}) = (130, 0)$ GeV is superimposed (pink dashed line). The upper plots show the cut efficiency for increasing cut values (decreasing cut values for m_{lj}, m_{ljj}) for the SM background expectation (black line) and for the predicted SUSY signal (red line). The event yield is used which results from the cut on the value indicated by the particular bin. The blue stacked line shows the significance Z_N. (a) shows the distribution of the transverse momentum of the leading muon in $SR^{\mu\mu}_{1\,jet}$, (b) shows it for $SR^{\mu\mu}_{2,3\,jet}$. (c) shows the distribution of momentum of the subleading muon in $SR^{\mu\mu}_{1\,jet}$ and (d) shows it for $SR^{\mu\mu}_{2,3\,jet}$.*

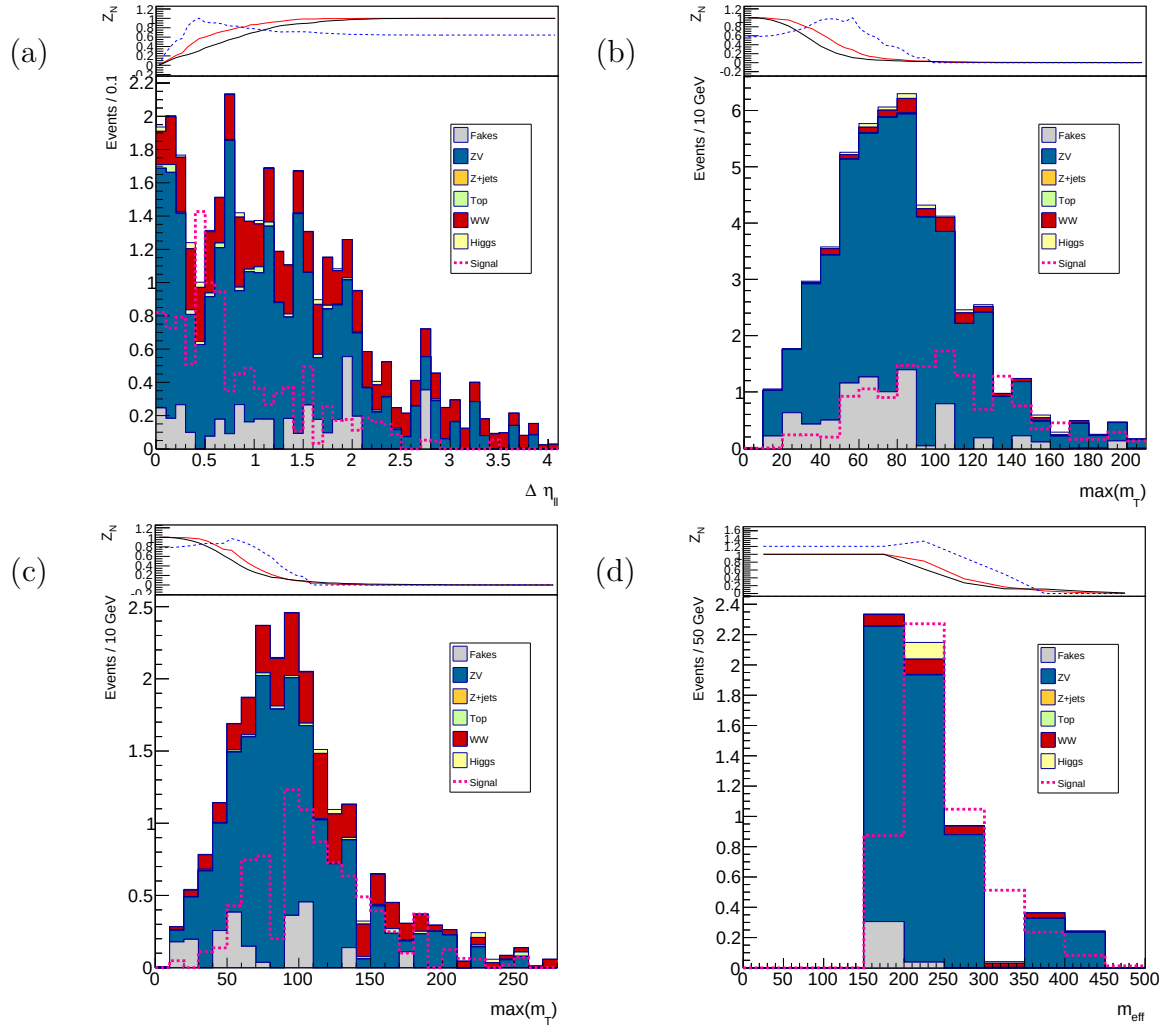

FIGURE A.5.: *The lower plots show the distributions for the variables which motivate the cuts for the SR definition. The events are not selected due to the full SR definition but the cuts are applied in the order which is given in the Table 8.4. The expected SM background consists of 'Fakes' (grey colour), ZV (blue), $Z+jets$ (orange), Top (light green), WW (red) and Higgs (yellow). The predicted SUSY signal for the mass point with $(m_{\tilde{\chi}_2^0}, m_{\tilde{\chi}_1^\pm, \tilde{\chi}_1^0}) = (130, 0)$ GeV is superimposed (pink dashed line). The upper plots show the cut efficiency for increasing cut values (decreasing cut values for m_{lj}, m_{ljj}) for the SM background expectation (black line) and for the predicted SUSY signal (red line). The event yield is used which results from the cut on the value indicated by the particular bin. The blue stacked line shows the significance Z_N. (a) shows the distribution for $\Delta\eta_{ll}$ in $SR^{\mu\mu}_{1\,\mathrm{jet}}$, (b) shows $max(m_T)$ for $SR^{\mu\mu}_{2,3\,\mathrm{jet}}$. (c) shows the distribution of $max(m_T)$ in $SR^{\mu\mu}_{1\,\mathrm{jet}}$ and (d) shows the effective mass for $SR^{\mu\mu}_{2,3\,\mathrm{jet}}$.*

A.3. $\mathbf{SR}^{e\mu}_{1\mathrm{jet}}$ AND $\mathbf{SR}^{e\mu}_{2,3\mathrm{jet}}$

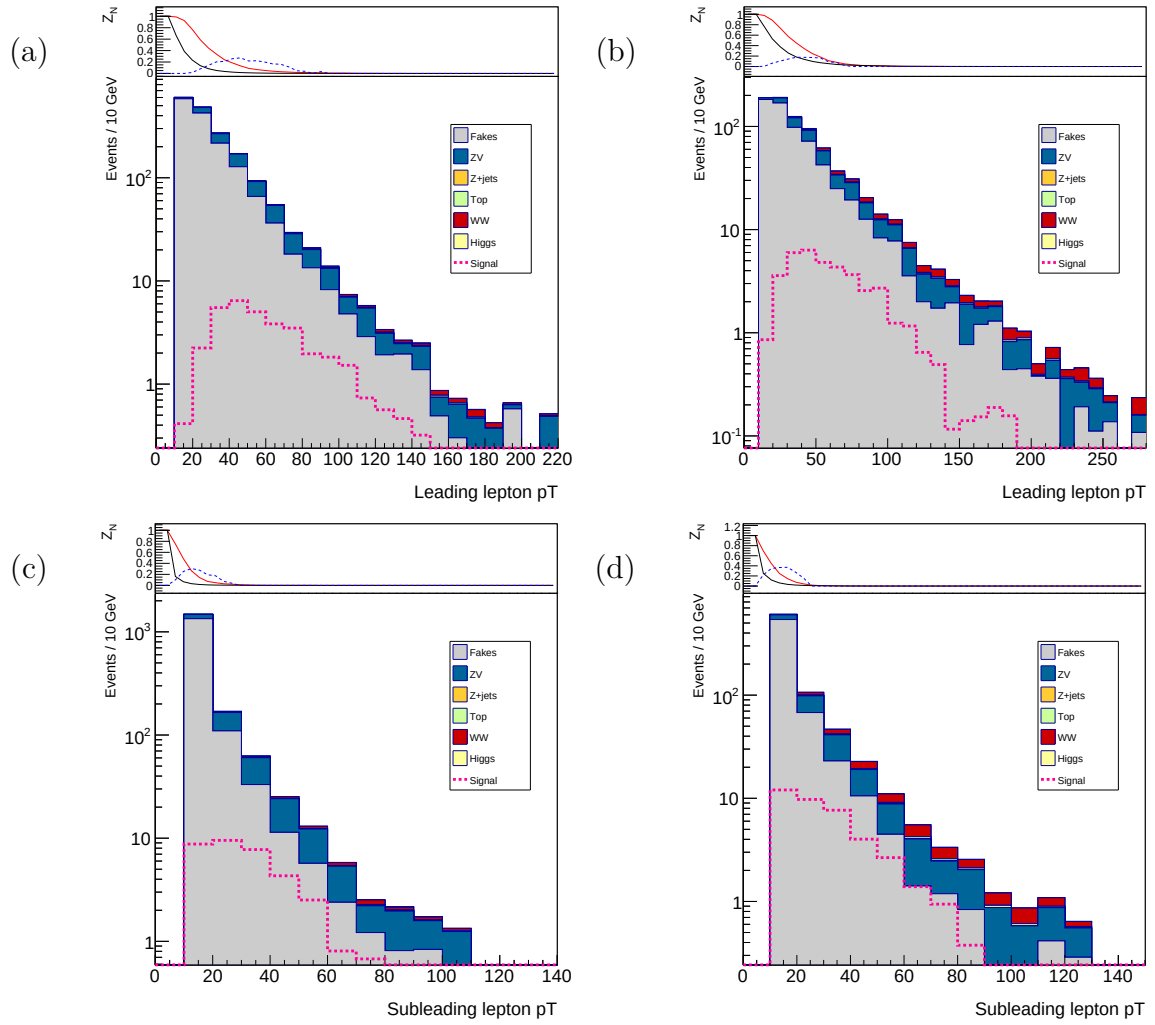

FIGURE A.6.: *The lower plots show the distributions for the variables which motivate the cuts for the SR definition. The events are not selected due to the full SR definition but the cuts are applied in the order which is given in the Table 8.4. he expected SM background consists of 'Fakes' (grey colour), ZV (blue), $Z+jets$ (orange), Top (light green), WW (red) and Higgs (yellow). The predicted SUSY signal for the mass point with $(m_{\tilde{\chi}_2^0}, m_{\tilde{\chi}_1^\pm, \tilde{\chi}_1^0}) = (130, 0)$ GeV is superimposed (pink dashed line). The upper plots show the cut efficiency for increasing cut values (decreasing cut values for m_{lj}, m_{ljj}) for the SM background expectation (black line) and for the predicted SUSY signal (red line). The event yield is used which results from the cut on the value indicated by the particular bin. The blue stacked line shows the significance Z_N. (a) shows the distribution for the transverse momentum of the leading lepton in $SR^{e\mu}_{1\,\mathrm{jet}}$, (b) shows it for $SR^{e\mu}_{2,3\,\mathrm{jet}}$. (c) shows the distribution o the transverse momentum of the subleading leptons in $SR^{e\mu}_{1\,\mathrm{jet}}$ and (d) shows it for $SR^{e\mu}_{2,3\,\mathrm{jet}}$.*

.

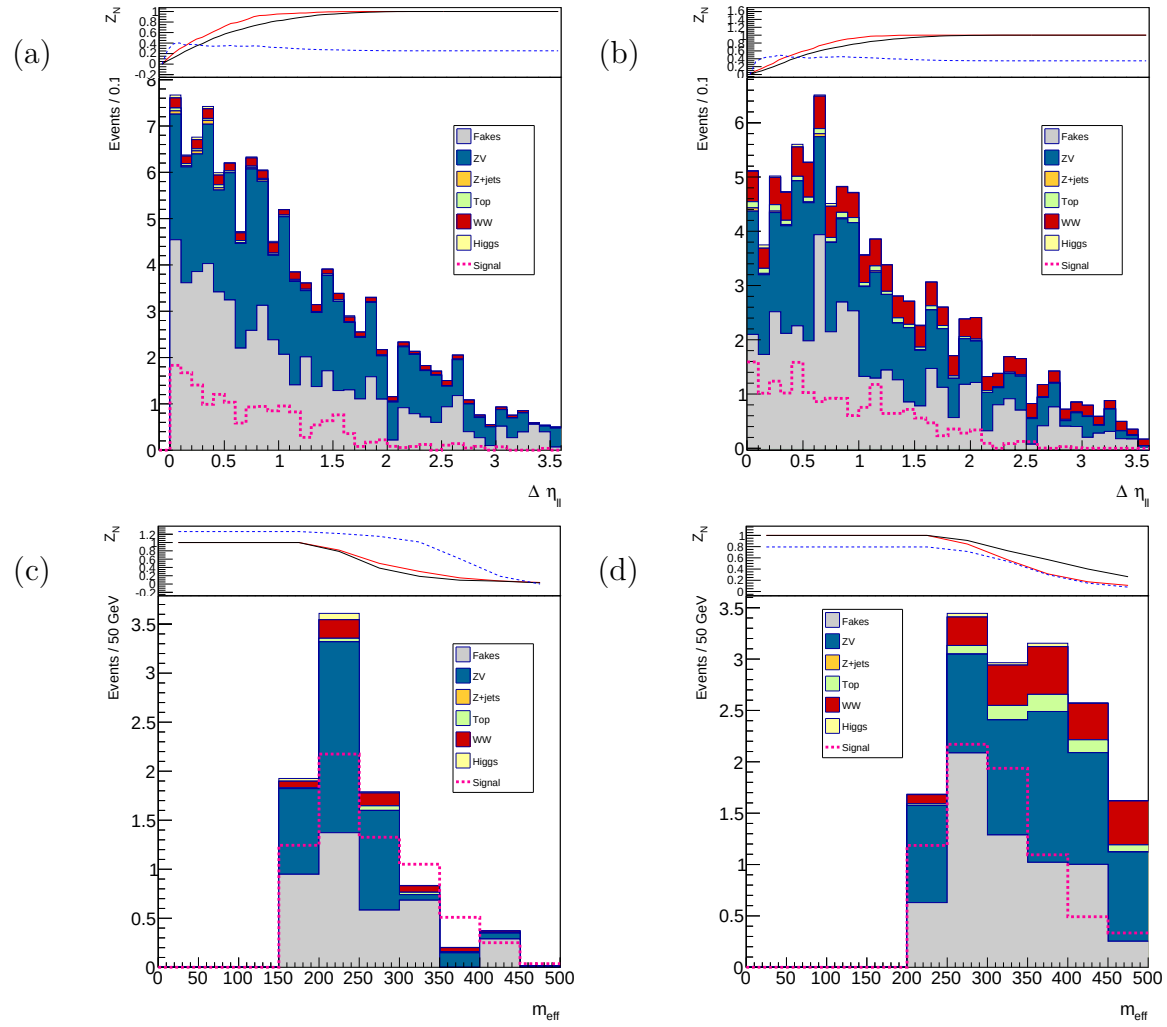

FIGURE A.7.: *The lower plots show the distributions for the variables which motivate the cuts for the SR definition. The events are not selected due to the full SR definition but the cuts are applied in the order which is given in the Table 8.4.T he expected SM background consists of 'Fakes' (grey colour), ZV (blue), $Z+jets$ (orange), Top (light green), WW (red) and Higgs (yellow). The predicted SUSY signal for the mass point with $(m_{\tilde{\chi}^0_2}, m_{\tilde{\chi}^\pm_1,\tilde{\chi}^0_1}) = (130, 0)$ GeV is superimposed (pink dashed line). The upper plots show the cut efficiency for increasing cut values (decreasing cut values for m_{lj}, m_{ljj}) for the SM background expectation (black line) and for the predicted SUSY signal (red line). The event yield is used which results from the cut on the value indicated by the particular bin. The blue stacked line shows the significance Z_N. (a) shows the distribution for $\Delta\eta_{ll}$ in $SR^{e\mu}_{1\,\mathrm{jet}}$, (b) shows it for $SR^{e\mu}_{2,3\,\mathrm{jet}}$. (c) shows the distribution of the effective mass in $SR^{e\mu}_{1\,\mathrm{jet}}$ and (d) shows it for $SR^{e\mu}_{2,3\,\mathrm{jet}}$.*

BIBLIOGRAPHY

[1] HIGGS, P. W.: *Broken Symmetries and the Masses of Gauge Bosons*. Phys. Rev. Lett. 13, 508 - Published 19 October 1964

[2] GRIFFITHS, D.: *Introduction to Elementary Particles*. 2008, Wiley-VCH

[3] LANGACKER, P.: *The Standard Model and Beyond (Series in High Energy Physics, Cosmology and Gravitation)*. CRC Press (December 1, 2009)

[4] SCHAILE, D.: *Advanced Particle Physics*. Lecture LMU München SoSe 2010

[5] J. BERINGER ET AL. (PARTICLE DATA GROUP): *Particle Physics Booklet July 2012*. from Review of Particle Physics, Phys. Rev. D 86, 010001 (2012)

[6] www.quantumdiaries.org (URL last visited at September 16th, 2014)

[7] THE ATLAS COLLABORATION: *Observation of a new particle in the search for the Standard Model Higgs boson with the ATLAS detector at the LHC*. Phys.Lett. B716 (2012) 1-29, arXiv:1207.7214 [hep-ex]

[8] THE CMS COLLABORATION: *Observation of a new boson at a mass of 125 GeV with the CMS experiment at the LHC*. Phys. Lett. B 716 (2012) 30, arXiv:1207.7235 [hep-ex]

[9] CARENA, M. ET AL.: *STATUS OF HIGGS BOSON PHYSICS*. http://pdg.lbl.gov/2013/reviews/rpp2013-rev-higgs-boson.pdf

[10] BERINGER, J. ET AL.: *Review of particle physics*. (2012) PHYSICAL REVIEW D. 86(1)

[11] MARTIN, S.: *A Supersymmetry Primer*. 1997, hep-ph/9709356, arXiv:hep-ph/9709356

[12] ELLIS, J. ET AL.: *Beyond the Standard Model for Montaneros*. CERN-PH-TH/2009-225, arXiv:0911.4409 [hep-ph]

[13] ZWICKY, F.: *Die Rotverschiebung von extragalaktischen Nebeln*. Helvetica Physica Acta, Vol. 6, p. 110-127

[14] MSSM Working Group Collaboration, A. Djouadi et al.: The Minimal Supersymmetric Standard Model: Group Summary Report. Report of the MSSM working group for the Workshop "GDR-Supersymétrie", France. Rep. PM/98-45, arXiv:hep-ph/9901246

[15] Alves, D. et al.: *Simplified Models for LHC New Physics Searches*. 2012 J. Phys. G: Nucl. Part. Phys. 39 105005, arXiv:1105.2838 [hep-ph]

[16] Alwall, J., Schuster,P. , Toro, N.: *Simplified Models for a First Characterization of New Physics at the LHC*. Phys.Rev.D79:075020, 2009, arXiv:0810.3921 [hep-ph]

[17] Plehn, T. *Prospino2* http://www.thphys.uni-heidelberg.de/∼plehn/index.php?show=prospino&visible=tools (URL last visited at September 16th, 2014)

[18] The ATLAS Collaboration: *Search for strong production of supersymmetric particles in final states with missing transverse momentum and at least three b-jets at sqrt(s) = 8 TeV proton-proton collisions with the ATLAS detector*. Submitted to JHEP, arXiv:1407.0600 [hep-ex]

[19] Feng, J.L., Matchev, K.T., Moroi, T.: *Focus Points and Naturalness in Supersymmetry*. Phys.Rev.D61:075005,2000, arXiv:hep-ph/9909334

[20] Drees, M., Godbole, R. M. , Roy, P. : *Theory and Phenomenology of Sparticles*. World Scientific, 2005

[21] *ATLAS EXPERIMENT Public Results, ATLAS Supersymmetry searches*. https://twiki.cern.ch/twiki/bin/view/AtlasPublic/SupersymmetryPublicResults

[22] Cowan, G., Gross, E.: *Discovery significance with statistical uncertainty in the background estimate*. ATLAS Statistics Forum May 8th, 2008, http://www.pp.rhul.ac.uk/∼cowan/stat/notes/SigCalcNote.pdf

[23] Cowan, G., Cranmer, K., Gross, E., Vitells, O.: *Asymptotic formulae for likelihood-based tests of new physics*. Eur.Phys.J.C71:1554, 2011, arXiv:1007.1727 [physics.data-an]

[24] Cousins, R.D., Linnemann, J.T., Tucker, J.: *Evaluation of three methods for calculating statistical significance when incorporating a systematic uncertainty into a test of the background-only hypothesis for a Poisson process*. Nuclear Instruments and Methods in Physics Research A 595 (2008) 480-501, arXiv:physics/0702156 [physics.data-an]

[25] Cranmer, K.: *Statistical Challenges for Searches for New Physics at the LHC*. Proceedings of978 Phystat05, Oxford University Press, Editors Louis Lyons,Muge Karagoz Unel, pages pp.979 112-124, 2005.980., arXiv:physics/0511028 [physics.data-an]

[26] LINNEMANN, J.T.: *Measures of Significance in HEP and Astrophysics*. Talk from PhyStat2003, Stanford, Ca, USA, September 2003, arXiv:physics/0312059 [physics.data-an]

[27] *RooStats::NumberCountingUtils*. http://root.cern.ch/root/html/RooStats__-NumberCountingUtils.html

[28] READ, A.L.: *Modified frequentist analysis of search results (the CL_s method)*. CERN-OPEN-2000-205 (2000), http://cds.cern.ch/record/451614

[29] *CERN website*. http://home.web.cern.ch/

[30] http://te-epc-lpc.web.cern.ch/te-epc-lpc/machines/linac4/general.stm

[31] EVANS, L. AND BRYANT, P.: *LHC Machine*. Journal of Instrumentation 3 no. 08, (2008) S08001.

[32] THE ATLAS COLLABORATION: *ATLAS Detector and Physics Performance Technical Design Report*. 1999, CERN/LHCC 99-14, http://atlas.web.cern.ch/Atlas/GROUPS/PHYSICS/TDR/access.html

[33] THE ATLAS COLLABORATION: *ATLAS Experiment at the CERN Large Hadron Collider*. JINST 3 (2008) S08003, http://iopscience.iop.org/1748-0221/3/08/S08003

[34] THE ATLAS EXPERIMENT: *Official Website*. `http://www.atlas.ch/` (URL last visited: September 16th, 2014)

[35] LAMPRECHT, M.: *Studien zu Effizienz und Akzeptanz des ATLAS-Myontriggers mit simulierten Messdaten*. 2007, Diploma Thesis LMU München

[36] THE ATLAS COLLABORATION *ATLAS TDAQ System Phase-I Upgrade-Technical Design Report*. CERN-LHCC-2013-018, ATLAS-TDR-023, 2013, https://cds.cern.ch/record/1602235/files/ATLAS-TDR-023.pdf

[37] MELLO, A. G. ON BEHALF OF THE ATLAS HIGH LEVEL TRIGGER GROUP: *Overview of the High-Level Trigger Electron and Photon Selection for the ATLAS Experiment at the LHC*. http://inspirehep.net/record/1197235/files/posterP8-6_vImpresso.pdf

[38] D.A. SCANNICCHIO *ATLAS Trigger and Data Acquisition: Capabilities and commissioning*. Nuclear Instruments and Methods in Physics Research A 617 (2010) 306 - 30

[39] THE ATLAS COLLABORATION: *Expected Performance of the ATLAS Experiment*. December 2008, CERN-OPEN-2008-020, http://cds.cern.ch/record/1125884

[40] ANDREA VENTURA FOR THE ATLAS COLLABORATION *The Muon High Level Trigger of the ATLAS experiment*. ATL-DAQ-PROC-2009-010, 2009, http://cds.cern.ch/record/1226759/files/ATL-DAQ-PROC-2009-041.pdf

[41] *ATLAS EXPERIMENT - Public Results. Public Tau Trigger Plots for Collision Data*. https://twiki.cern.ch/twiki/bin/view/AtlasPublic/TauTriggerPublicResults

[42] DUCKECK, G. ET AL.: *ATLAS Computing Technical Design Report*. ATLAS TDR–017, CERN-LHCC-2005-022, http://cds.cern.ch/record/837738/files/lhcc-2005-022.pdf

[43] BRUN, R., RADEMAKERS, F.: *ROOT - An object oriented data analysis framework*. Nuclear Instruments and Methods in Physics Research Section A, Volume 389, Issues 1-2, 11 April 1997, Pages 81-86

[44] DOBBS M., ET AL.: *Les Houches Guidebook to Monte Carlo Generators for Hadron Collider Physics*. arXiv:hep-ph/0403045

[45] SJOSTRAND, T. ET AL.: *PYTHIA 6.4 Physics and Manual*. JHEP 0605:026, 2006, arXiv:hep-ph/0603175

[46] CORCELLA, G. ET AL.: *HERWIG 6.5: an event generator for Hadron Emission Reactions With Interfering Gluons (including supersymmetric processes)*. JHEP 0101:010, 2001, arXiv:hep-ph/0011363

[47] BUTTERWORTH, J.M., FORSHAW, J.R., SEYMOUR, M.H.: *Multiparton Interactions in Photoproduction at HERA*. Z.Phys.C72:637-646, 1996, arXiv:hep-ph/9601371

[48] GLEISBERG, T. ET AL.: *Event generation with SHERPA 1.1*. JHEP 0902:007, 2009, arXiv:0811.4622 [hep-ph]

[49] FRIXIONE, S., WEBBER, B.R.: *The MC@NLO Event Generator*. Cavendish-HEP-02/09, LAPTH-922/02, GEF-th-09/2002, arXiv:hep-ph/0207182

[50] FRIXIONE, S., NASON, B., WEBBER, B.R.: *Matching NLO QCD and parton showers in heavy flavour production*. JHEP 0308 (2003) 007, arXiv:hep-ph/0305252

[51] FRIXIONE, S., LAENEN, E., MOTYLINSKI, P., WEBBER, B.R.: *Single-top production in MC@NLO*. JHEP0603:092, 2006, arXiv:hep-ph/0512250

[52] MANGANO, M. L., MORETTI, M., PICCININI, F., PITTAU, R., POLOSA, A.D.: *ALPGEN, a generator for hard multiparton processes in hadronic collisions*. JHEP 0307 (2003) 001, arXiv:hep-ph/0206293

[53] ALWALL, J. ET AL.: *MadGraph/MadEvent v4: The New Web Generation*. JHEP0709:028, 2007, arXiv:0706.2334 [hep-ph]

[54] ALLISON, J. ET AL.: *Geant4 developments and applications*. Nuclear Science, IEEE Transactions on 53 no. 1, (2006), p. 270 - 278.

[55] CACCIARI, M., SALAM, G.P., SOYEZ, G.: *The anti-k_t jet clustering algorithm*. JHEP 0804:063, 2008, arXiv:0802.1189 [hep-ph]

[56] THE ATLAS COLLABORATION: *Jet energy measurement with the ATLAS detector in proton-proton collisions at sqrt(s) = 7 TeV*. Eur. Phys. J. C, 73 3 (2013) 2304, arXiv:1112.6426 [hep-ex]

[57] THE ATLAS COLLABORATION: *Jet energy resolution in proton-proton collisions at sqrt(s)=7TeV recorded in 2010 with the ATLAS detector*. Eur. Phys. J. C, 73 3 (2013) 2306, arXiv:1210.6210v1 [hep-ex]

[58] THE ATLAS COLLABORATION: *Pile-up subtraction and suppression for jets in ATLAS*. ATLAS-CONF-2013-083, https://cds.cern.ch/record/1570994

[59] THE ATLAS COLLABORATION: *Commissioning of the ATLAS high-performance b-tagging algorithms in the 7 TeV collision data*. ATLAS-CONF-2011-102, http://cds.cern.ch/record/1369219

[60] THE ATLAS COLLABORATION: *Electron efficiency measurements with the ATLAS detector using the 2012 LHC proton-proton collision data*. ATLAS-CONF-2014-032, 2014, https://cds.cern.ch/record/1706245

[61] THE ATLAS COLLABORATION *Performance of the Reconstruction and Identification of Hadronic τ Decays in ATLAS with 2011 Data*. ATLAS-CONF-2012-142, 2012, https://cds.cern.ch/record/1485531

[62] THE ATLAS COLLABORATION: *Performance of Missing Transverse Momentum Reconstruction in ATLAS studied in Proton-Proton Collisions recorded in 2012 at sqrt(s) = 8 TeV*.

[63] THE ATLAS COLLABORATION: *Search for direct slepton and gaugino production in final states with two leptons and missing transverse momentum with the ATLAS detector in pp collisions at sqrt(s) = 7 TeV*. Physics Letters B, Volume 718, Issue 3, 8 January 2013, Pages 879-901, ISSN 0370-2693, http://dx.doi.org/10.1016/j.physletb.2012.11.058

[64] H. BAER, ET AL.: *Detecting sleptons at hadron colliders and supercolliders*. Phys. Rev. D 49 (1994) 3283, arXiv:hep-ph/9311248

[65] M. BAHR: *Herwig++ Physics and Manual*. Eur. Phys. J. C 58 (2008) 639, arXiv:0803.0883 [hep-ph]

[66] FRIXIONE, S., NASON, P., OLEARI, C.: *Matching NLO QCD computations with Parton Shower simulations: the POWHEG method*. JHEP 0711 (2007) 070, arXiv:0709.2092 [hep-ph]

[67] Barr, A., Lester, C., Stephens, P.: *m_T2 : the truth behind the glamour*. J.Phys.G29:2343-2363, 2003, arXiv:hep-ph/0304226

[68] D. Tovey: *On measuring the masses of pair-produced semi-invisibly decaying particles at hadron colliders*. JHEP 04 (2008) 034, arXiv:0802.2879 [hep-ph]

[69] Hamer, M.: *Search for Supersymmetry in Final States with Leptons with the ATLAS Detector at the Large Hadron Collider*. CERN-THESIS-2013-310, 2013, cds.cern.ch/record/1599139

[70] The ATLAS Collaboration: *Search for direct production of charginos, neutralinos and sleptons in final states with two leptons and missing transverse momentum in pp collisions at $\sqrt{s}$ = 8TeV with the ATLAS detector*. JHEP 05 (2014) 071, arXiv:1403.5294 [hep-ex]

[71] Kersevan, B.P. , Richter-Was, E.: *The Monte Carlo event generator AcerMC versions 2.0 to 3.8 with interfaces to PYTHIA 6.4, HERWIG 6.5 and ARIADNE 4.1*. Comput. Phys. Commun. 184 (2013) 919, http://inspirehep.net/record/650986

[72] The ATLAS Collaboration: *Search for direct production of charginos and neutralinos in events with three leptons and missing transverse momentum in $\sqrt{s}$ = 8TeV pp collisions with the ATLAS detector*. JHEP04(2014)169, arXiv:1402.7029 [hep-ex]

[73] The ATLAS Collaboration: *Search for direct production of charginos and neutralinos in events with three leptons and missing transverse momentum in sqrt(s) = 7 TeV pp collisions with the ATLAS detector*. Phys.Lett. B718 (2013) 841-859, arXiv:1208.3144 [hep-ex]

[74] LEP SUSY Working Group, ALEPH, DELPHI, L3 and OPAL: *Combined LEP chargino results, up to 208GeV, note LEPSUSYWG/01-03.1*. CERN, 2001, http://lepsusy.web.cern.ch/lepsusy/Welcome.html

[75] LEP SUSY Working Group, ALEPH, DELPHI, L3 and OPAL: *Combined LEP selectron/smuon/stau results, 183 - 208GeV, note LEPSUSYWG/04-01.1*. CERN, 2004, http://lepsusy.web.cern.ch/lepsusy/Welcome.html

[76] Vujaklija, J.: Electron Identification in Dilepton Searches for Supersymmetry. Diploma Thesis LMU München, Juli 2011

Acknowledgements

Hier erwähnt werden sollte auf jeden Fall:

- Prof. Dr. Dorothee Schaile hat mich an ihrem Lehrstuhl aufgenommen und es mir ermöglicht, die Bachelorarbeit, die Masterarbeit und nun die Doktorarbeit dort zu verfassen. Ihre Tür stand wie angekündigt tatsächlich immer offen und sie erteilte mir guten Rat.
- Prof. Dr. Martin Faessler gebührt Dank für das Verfassen des Zweitgutachtens.
- Dr. Federica Legger is the best technical supervisor I can think of. She was always very professional, patient and positive. She did a great job in advising me, discussing my results and proofreading all my writings. Mille grazie!
- I want to thank the Californian crew Prof. Dr. Anyes Taffard, Dr. Davide Gerbaudo, Suneet Upadhyay, Dr. Steven Farrell and Dr. Alaettin Serhan Mete for the excellent team work for the WH analysis.
- Die LMU SUSY Leute: Dr. Jeanette Lorenz, Dr. Alexander Mann, Dr. (Johannes) Sebastian Becker, Dr. Julien (de) Graat, Christopher Bock, Jasmin Israeli, Fabian Rücker, Balthasar Schachtner und Luis Escobar Sawa.
- Furthermore I want to thank Prof. Dr. Otmar Biebel, Dr. Philippe Calfayan, Dr. Jonas Will, Friedrich Hönig, Bonnie Chow and (Clyde) Christian Meineck for being awesome.
- Meine liebste Frauke Alexander, die einfach weiß, was ich meine.
- Meine liebste Theres(it)a Weis, die mich einfach versteht.
- Monika Schuster, wegen der langen Freundschaft.
- Christopher Unverdorben, der bis zum Schluss mein Bürobuddy war und Michael Bender wegen *PewPew*.
- Michèle van Wezep for her good English knowledge.
- Mama, Papa und Lari und Maxi - weil ihr wirklich immer für mich da seid. Und natürlich meine Großeltern!
- Bas van Nugteren ♡.